Scaling of cytoskeletal organization with cell size in *Drosophila*

by

Alison Kate Laine Spencer

A Dissertation

Presented to the Faculty of the Louis V. Gerstner, Jr.

Graduate School of Biomedical Sciences,

Memorial Sloan-Kettering Cancer Center

in Partial Fulfillment of the Requirements for the Degree of

Doctor of Philosophy

New York, NY

February, 2017

Jennifer A. Zallen, PhD
Dissertation Mentor

Date

Dedication

To my parents, Anita and David Spencer, who fostered my curiosity, instilled my love for science, and without whom none of this would have been possible.

Abstract

Understanding how cells build and organize dynamic subcellular structures is an important challenge in biology. Of particular interest is how micron-scale molecular assemblies become spatially organized. Spatially localized macromolecular complexes are essential for cell and tissue function, but the mechanisms that control this organization process within cells are not well understood. Microtubule-based structures such as mitotic spindles scale with cell size, but less is known about mechanisms of actin scaling within cells. The ventral surface of the *Drosophila* embryo and larva are covered in micron-scale actin-rich denticle precursors. These actin protrusions serve as templates for a series of structures in the cuticle that aid in larval locomotion. Denticle cells change shape and align their edges to form distinct columns, and each cell produces denticles at its posterior cortex. The alignment of the denticle cells and the uniformly posterior placement of denticle structures creates a linear arrangement of denticles that spans the width of the tissue. This arrangement of actin structures is initially established in the embryo, and is maintained in the larvae despite significant changes to cell shape and size that occur during growth. However, the mechanisms that direct the organization of these macromolecular actin structures, and how these patterns are maintained during dramatic changes in cell size, have not been characterized.

I have taken several distinct genetic and cell biological approaches to elucidate the mechanisms by which these intracellular patterns of actin and microtubule organization are generated. To identify regulators of actin structure organization in the denticle system, I performed a germline mosaic screen on the *Drosophila* X chromosome for mutants with defects in denticle formation, denticle organization, and segment patterning and polarity. To establish the denticle cells as a model system for actin organization, I developed computational methods to quantify spatial and temporal patterns of denticle organization and to compare these properties across genotypes. Using this quantitative imaging and statistical modeling approach, I demonstrate that the organization of denticle precursors within cells is not random. Instead, denticle number

and spacing scale with cell length over an order-of-magnitude increase in cell size during larval growth, and are correspondingly reduced under space-limited conditions in embryos. I show that denticle spacing is captured by specific mathematical equations that highlight the robustness of denticle organization. Furthermore, accurate denticle spacing requires an intact microtubule network and the microtubule minus-end binding protein, Patronin. These results identify a novel mechanism of actin cytoskeletal scaling that maintains consistent patterns of actin organization despite a substantial increase in cell size during tissue growth. Moreover, they establish the denticle cells as a system for investigating questions regarding the spatial organization of actin-based structures.

Biographical Sketch

Alison Spencer got her start in biomedical research as a high school student in the clinical immunology lab of Dr. David Dorsky at the University of Connecticut Health Center. In 2005, she began her undergraduate degree at the University of Rochester. During her summers, she continued to work as an undergraduate researcher in the labs of David Dorsky, Donald Kreutzer, Uli Klueh, and Bijay Mukherji at the University of Connecticut. She also participated in several undergraduate research programs, including the Summer Undergraduate Program at Cold Spring Harbor Laboratory, where she studied tumor vascularization in the lab of Dr. Vivek Mittal, and the Gerstner Sloan-Kettering Summer Undergraduate Research Program, where she worked in the lab of Dr. Johanna Joyce investigating the function of cystein cathepsins in tumorigenesis. In 2009, after graduating with a Bachelor of Science in Biochemistry, she joined the doctoral program at the Gerstner Sloan Kettering Graduate School of Biomedical Sciences at Memorial Sloan Kettering Cancer Center. In 2010, after several rotations, she joined the lab of Dr. Jennifer Zallen, where she carried out her dissertation research.

Acknowledgements

There is no way that this work could have been completed without the support of a large number of people. I would first like to thank my advisor, Dr. Jennifer Zallen, for all her guidance and support over the years. Her encouragement, her constant attention to detail, and her willingness to support me as I dove into subjects well beyond the range of 'usual' within the lab, have been unmatched throughout my time in the lab. I also have to thank my thesis committee, Kathryn Anderson and Kat Hadjantonakis, for their critical questions, suggestions and insights over the years. Their interest in this project and their suggestions for its advancement have been instrumental in pushing it forward. I would also like to thank Zhirong Bao, for agreeing to chair my defense committee. Finally, I am extremely grateful to Diana Bratu for agreeing to serve as my external advisor.

I absolutely could not have gotten through this process without the encouragement, support, and distractions provided by my awesome labmates, past and present. I would like to thank Masako Tamada, for being an awesome bay mate, the other half of many late-night conversations, and the source of great genetics and lab-related wisdom, Will Razzell, for always being enthusiastic and excited by everything in lab and out of it, and Karen Kasza, for all the encouragement and quantitative-minded suggestions over the course of this project. To Maria Bustillo and Eric Brooks, thank you for all the scientific, statistical, and off-the-wall conversations, and for the shenanigans inside lab and out - you've made this process infinitely more enjoyable and fulfilling. Thanks to Emily Marcinkevicius, Athea Vichas, Leah Greenspan, Gillian Siegal, Dene Farrell, Rodrigo Fernandez-Gonzalez, Sergio Simões, Chris Fincher, and Zack Mirman, for being amazing colleagues and teachers over the years. To my current labmates, German Sabio, Pooja Naik, Adam Paré, Kia Bourdot, Marissa Gredler, Tarek Islam, Sara Supriyatno, Omar Gutierrez Ruiz, Huapeng Yu, and Jay Shi, it's been great working with and learning from all of you.

I would like to thank my friends and classmates in the Gerstner Sloan Kettering program, who have been awesome from the very beginning. I've learned so much from you all, and I am so grateful for your friendship. I also have to thank all those in the GSK office for all their assistance over the years, especially in getting everything together for this dissertation.

Finally, I have to thank my friends and family for their constant reminders that life is more than just lab. Thank you to my parents Anita and David, my sister Cheryl, and my brother Eric, for your love, support, encouragement, and confidence in me. Thanks also to Katrina Sliwa, Maria Bustillo, and Tawsy Lamech, for uncountably many adventures and laughs. Finally, thanks to my boyfriend Prashant Monian, your constant support, patience and encouragement throughout the graduate school process has been incredible.

Table of Contents

List of Figures

List of Tables

Chapter 1

Introduction

1.1 Epithelial morphogenesis and the spatial control of cell and tissue organization

The question of how diverse cellular patterns and ordered tissues are created from initially unstructured groups of cells has long fascinated scientists from many fields, developmental biologists in particular. This fundamental process by which individual cells are able to transform into complex, coordinated multicellular tissues with specific functions is generally known as epithelial morphogenesis. This process can be broken down into three key steps. First, a cell must know its identity, and find out who it is, and who it must become; in other words, it must undergo cell fate specification. Second, the cell needs to coordinate with and 'talk' to neighboring cells to determine what it must do and where it must be. This is typically accomplished via both long- and short - range extracellular signaling, and the end result is often visible in the polarization of molecules, for instance the establishment of polarity in the plane of the tissue (planar cell polarity, or PCP), or in the localization of subcellular structures such as hairs or cilia. Finally, the cell must integrate the information it has received in these first two processes,

and execute the cell biological mechanisms necessary to move, change shape, or produce specific types of subcellular structures. These three steps allow cells in all types of multicellular organisms to receive a variety of developmental cues in order to carry out the diverse array of processes required to build, evolve, and repair biological tissues.

Understanding how these processes work and which molecular and cellular players are required to carry out each step is essential both for advancing research and technology pertaining to human health and to increase understanding of general developmental principles. Failure to successfully complete these morphogenetic processes can cause a wide range of congenital defects, including failures in neural tube closure (Eom et al., 2013), defective tubulogenesis in many other organs (Lubarsky & Krasnow, 2003; Iruela-Arispe & Beitel, 2013), and ciliopathies (Wallingford & Mitchell, 2011). In adults, wound healing has a number of striking similarities to epithelial morphogenesis processes (Martin & Parkhurst, 2004; Gurtner et al., 2008; Razzell et al., 2011), and mis-regulation of epithelial tissues is linked to cancer (Wodarz & Näthke, 2007; Hanahan & Weinberg, 2011).

Many of the molecular and cellular players required for these morphogenetic processes have been identified over the past several decades through work conducted in model organisms and cultured cells. These studies have also demonstrated that most of the general principles and many of the molecules are conserved across species, making the study of model organisms a valuable resource for understanding human health and disease. However, the morphogenetic process is far from being completely understood. While many molecules that determine the final shapes and functions of various tissue types have been identified, neither their specific roles nor how they collaborate with each other are entirely understood. In particular, while the cell fate determinants driving transcription, production, and localization of specific effector molecules has been reasonably well studied, how these effectors interact to form macromolecular, intracellular structures and subcellular organization patterns is not well understood. Consequently, much work remains to be done before it is truly well understood how all the known molecular players and overarching dynamic processes are leveraged to form sophisticated structures and establish

tissue-wide organization patterns. Continuing advances in imaging live and fixed tissues (Denk et al., 1990; Huisken et al., 2004; Höckendorf et al., 2012; Follain et al., 2016), and in genome sequencing (Metzker, 2010; Gawad et al., 2016), genome editing (Peng et al., 2014; Port et al., 2014), and sequence analysis (Doitsidou et al., 2010; Minevich et al., 2012; Obholzer et al., 2012) technologies make it increasingly feasible not only to identify and characterize new elements required for pattern establishment and morphogenesis, but also to examine how these effectors work singly and in concert within cells to produce fully functional tissues. As a result, the gaps between the developmental signaling cues and the cell biological results are slowly being closed.

1.2 Organization patterns in the *Drosophila* denticle cells: a model system for studing subcellular actin organization

The multitude of hairs, bristles, and other organized subcellular and multicellular structures present at all different stages in *Drosophila* have long attracted scientists seeking to understand how subcellular and tissue-wide patterns are generated. One such tissue is the ventral epidermis of the late-stage embryo and the larvae. Cells in this tissue produce an organized, planar polarized array of actin rich denticle precursors, micron-scale protrusions that provide templates for cuticular structures involved in larval locomotion (Lohs-Schardin et al., 1979; Dickinson & Thatcher, 1997; Colosimo & Tolwinski, 2006; Price et al., 2006; Walters et al., 2006; Dixit et al., 2008; Dilks & DiNardo, 2010; Saavedra et al., 2014). These structures are distributed in a segmentally repeating pattern (**Figure 1.1**). Columns of cells, guided by a variety of striped patterning factors, produce alternating stripes of smooth and decorated cuticle that align with the eight segments of the larval body plan. Cells that will secrete smooth, undecorated cuticle remain relatively static and generally hexagonally-shaped (Lohs-Schardin et al., 1979; Walters et al., 2005, 2006). Cells within stripes fated to produce denticles, in contrast, undergo a series of specific morphological changes after the retraction of the germband (stages 13-16), guided

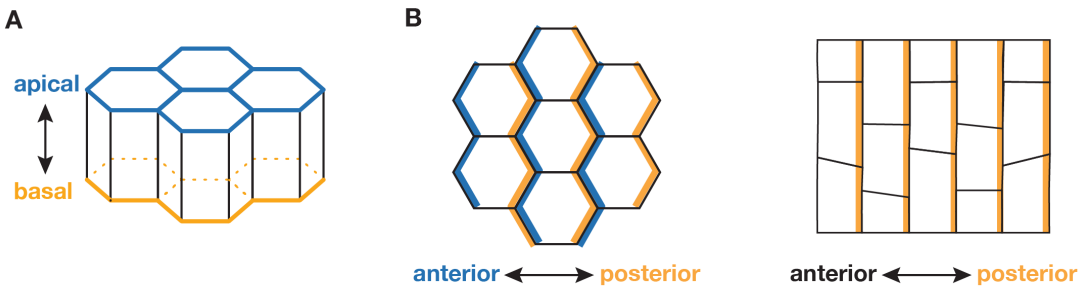

Figure 1.1: Different types of polarity. A. Apical-basal polarity is the differential location of proteins along the apical-basal cell axis. **B.** Planar cell polarity is the asymmetric distribution of proteins orthagonal to the apical-basal axis, in the plane of the tissue.

by the zinc-finger transcription factor *shavenbaby* (*svb*), which is both necessary and sufficient for the creation of denticles (Lohs-Schardin et al., 1979; Mével-Ninio et al., 1991; Szüts et al., 1998). Ultimately, these morphogenetic processes generate eight denticle bands consisting of six well-defined columns of hooked protrusions (the denticles) each. The denticles produced by each column have distinct morphological characteristics, including their size and shape, and the orientation of the hooked tip (**Figure 1.2**). The highly reproducible gross appearance of the denticle belts has served as a readout for the correct establishment of the body axis in genetic screens for many years (Nüsslein-Volhard & Wieschaus, 1980; Perrimon et al., 1989). However, these structures are also an excellent system in which to study cell biological questions pertaining to subcellular structure localization and the organization and regulation of both the actin and microtubule cytoskeleton, as well as the establishment of planar polarity and planar polarized structures, cell fate determination and tissue morphogenesis. In the following section, I will discuss in greater detail the genetic and cell biological events required for the establishment of the precise pattern of actin based denticles, and how the denticle system is an ideal place to examine the mechanisms required for subcellular structure organization.

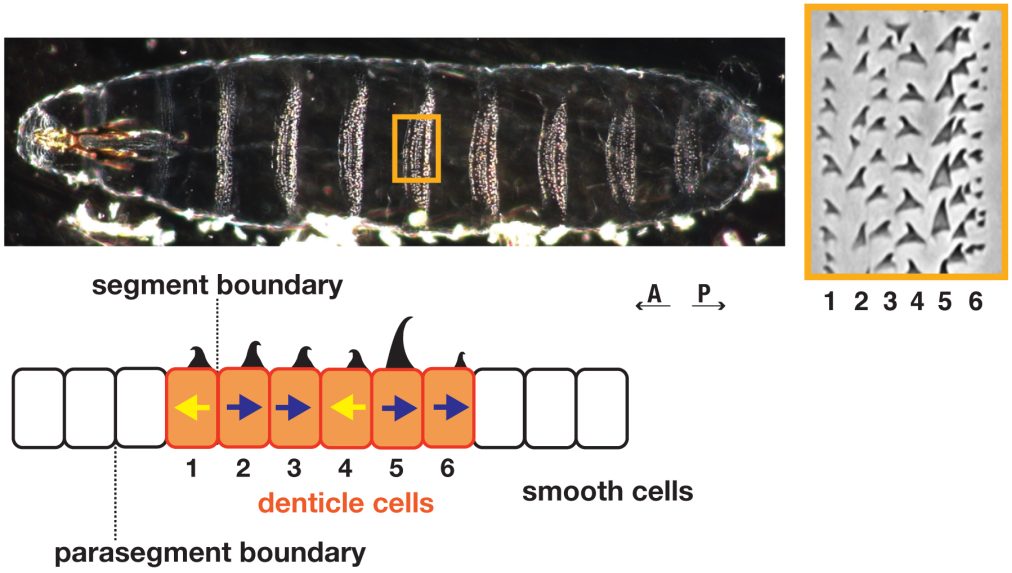

Figure 1.2: The larval denticle belts. A. Larval cuticle preparation showing the 8 alternating bands of denticles and smooth cell regions. Boxed region shows portion of a single denticle belt and highlights the different morphologies of denticles in each column. **B.** Cartoon depicting one full parasegment (approximately 13 columns of cells) and the hook orientation of each denticle column.

1.2.1 Establishing the denticle pattern

The formation of the denticle organization pattern begins early in embryogenesis. As part of the specification of the anterior-posterior body axis, maternal, then pair-rule, then segment polarity genes divide the embryo into 14 parasegments of approximately 12 cells each (DiNardo et al., 1994; Sanson, 2001). Within each parasegment, cells adopt one of two possible fates: smooth cells, which produce naked, undecorated cuticle, or denticle cells, which elaborate hook-shaped structures from their apical domain. The decision of whether to produce a denticle or smooth cuticle is regulated by a cascade of signaling molecules that have been studied in great detail (DiNardo et al., 1994; Hatini & DiNardo, 2001b; Sanson, 2001; Payre, 2004); the expression patterns and interactions of these signaling molecules are summarized in **Figure 1.3**.

In each parasegment, the anterior-most column of cells expresses both the transcription factor engrailed (en) and the secreted signaling molecule hedgehog (hh), while the posterior-most

column of cells express the secreted signaling molecule wingless (wg) (DiNardo et al., 1994). Hh signaling maintains *wg* expression in the posterior cell column. Meanwhile, secretion of wg drives the expression of *en* in the anterior, and these *en*-expressing cells secrete hh (DiNardo et al., 1988; Martínez-Arias et al., 1988; Hidalgo & Ingham, 1990; Sanson, 2001). The initially interdependent expression of these three molecules across the parasegmental boundary eventually stabilizes, and *en* expression becomes independent of wg signaling (DiNardo et al., 1988; Martínez-Arias et al., 1988; Bejsovec & Arias, 1991; Heemskerk et al., 1991; Dougan & DiNardo, 1992; Tabata et al., 1992; Bejsovec & Wieschaus, 1993; Heemskerk & DiNardo, 1994; O'Keefe et al., 1997; Gritzan et al., 1999). This stabilization process both requires the expression of *patched* (*ptc*), as mutations in *wg*, *en*, and *hh* all alter the *ptc* expression pattern (Hidalgo & Ingham, 1990). *wg* expression becomes restricted to the posterior portion of each parasegmental compartment, as it is repressed on the posterior side of the parasegmental boundary by *en/hh* (in cells 0 and 1). Embryos lacking *wg* expression do not create alternating bands of smooth cuticle and denticles; instead, they generate a lawn of denicles that spans the entire ventral epithelium, demonstrating that wg promotes the smooth cell fate (Noordermeer et al., 1992; Szüts et al., 1997; Gritzan et al., 1999; Sanson et al., 1999; Hatini & DiNardo, 2001a; Alexandre, 2008).

The *hh* receptor, *patched* (*ptc*), is initially ubiquitously expressed throughout the ventral epidermis, but its expression is ultimately restricted to two two-cell-wide stripes on either side of the parasegment boundary (denticle columns 2 and 3, and naked cell columns -1 and -2) (Hidalgo & Ingham, 1990; Dickinson et al., 1993; Lawrence et al., 1999; Thérond et al., 1999). Overexpression assays and genetic removal of *hh* and *wg* demonstrate that repressive activity by hh in the anterior and by wg in the posterior of the parasegment leads to the formation of a single stripe of cells expressing *Serrate* (*Ser*), a membrane-bound activator of the Notch signaling pathway, in what will become denticle columns 5 and 6 (Alexandre et al., 1999; Wiellette & McGinnis, 1999). *Ser* and *hh* together activate a single stripe of *rhomboid* (*rho*) expression in what will become denticle columns 2, 3, and 4 (Alexandre et al., 1999). Serrate is required for

the expression of *rho* in column 4, and in its absence results in one fewer column of denticle cells being produced (Wiellette & McGinnis, 1999). However, excess Ser activity causes the formation of ectopic denticles, and the Notch antagonist fringe (fng) is required to restrict Ser activity (Walters et al., 2005) (**Figure 1.3**).

Rho is responsible for cleaving and activating the EGFR ligand spitz (spi), which is ubiquitously expressed in an inactive form through the tissue (Schweitzer et al., 1995; Golembo et al., 1996; Lee et al., 2001; Tsruya et al., 2002, 2007). Spi activation and release in these three cell columns then activates the EGFR pathway specifically within the presumptive denticle field. Spi, wg, and hh, which are each expressed in different subdomains of the parasegment, induce expression of the transcription factor *Stripe* (*Sr*) in three cell columns (columns 2, 5, and -2) at the boundaries of these regions (Hatini & DiNardo, 2001a) (see **Figure 1.3**). Sr is required later for tendon cell specification and muscle attachment to the larval cuticle, as well as for the specification of denticle structure (Dilks & DiNardo, 2010). Thus, in summary, there are two molecular gradients of short-range signaling peptides in addition to hh active in each parasegment, one of spi and one of wg, that overlap across the parasegmental boundary (Hatini & DiNardo, 2001b; Sanson, 2001). These molecules divide each parasegment into four distinct segments, each of which expresses and responds to a unique combination of signals (**Figure 1.3**).

1.2.2 shavenbaby is the key transcriptional regulator of denticle formation

Activation of spitz and the EGFR pathway via hh and Ser leads to the expression of the zinc-finger transcription factor *ovo/shavenbaby* (*svb*) (Mével-Ninio et al., 1991). *svb* mutants make no denticles, and ectopic expression of *svb* in smooth cells is sufficient to induce denticle formation, indicating that *svb* is necessary and sufficient for denticle formation (Payre et al., 1999). Overexpression of activated spitz in wild type results in a lawn of denticles in embryonic cuticles and an increase in the width of *svb* stripes in *in situ* hybridization assays; conversely, expressing

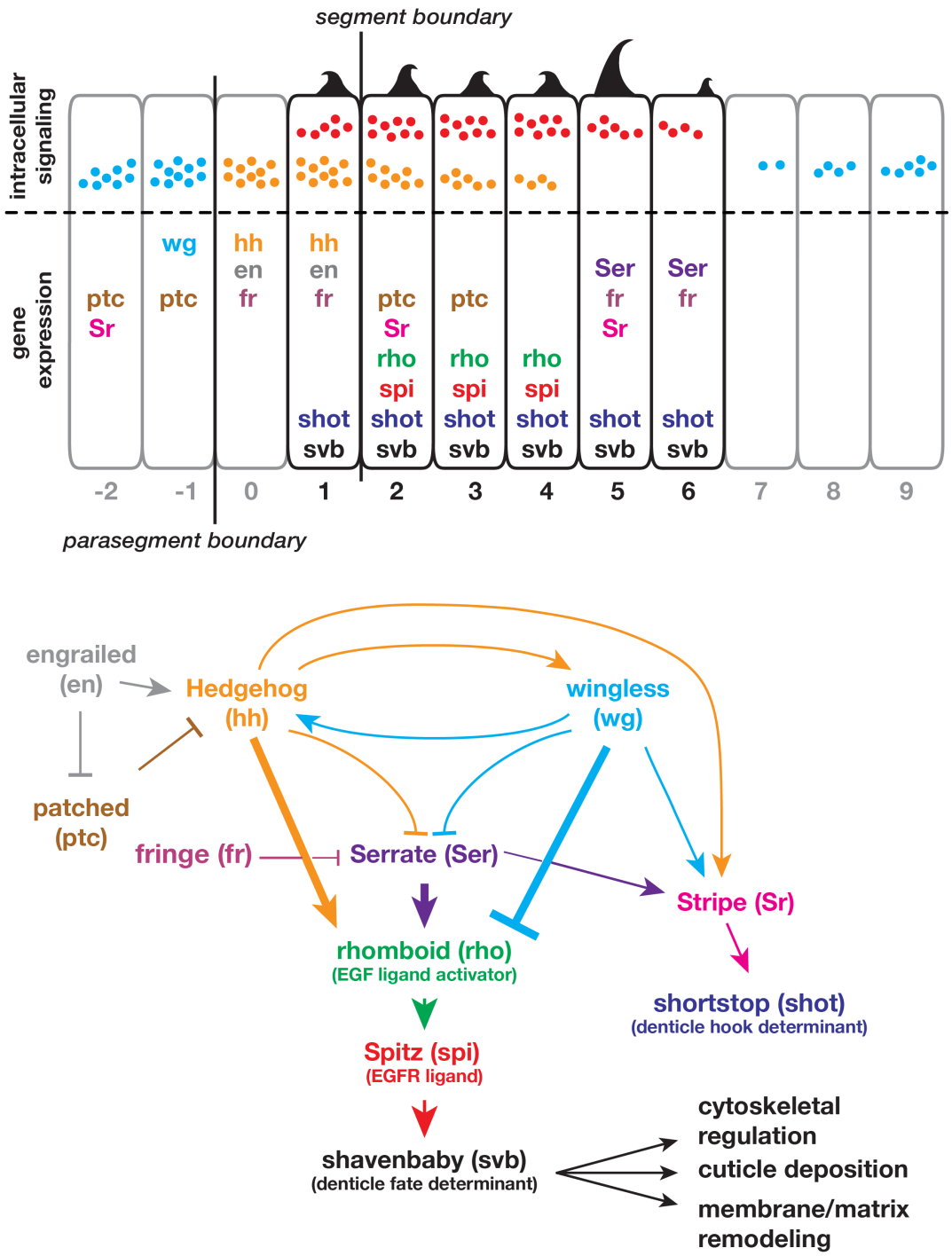

Figure 1.3: Signaling in the *Drosophila* ventral epidermis. Summary of gene expression and signaling within the denticle belts. One parasegment is shown. The signaling cascade, converging on the shavenbaby transcriptional regulator of denticle cell fate, is depicted below.

dominant negative EGFR reduces the size of the denticle belts and *svb* stripes. Therefore, activation of the EGFR pathway promotes denticle cell fate in the embryonic epidermis. Wg signaling, in contrast, restricts this domain of *svb* expression to approximately one half of the parasegment, the six cell columns of the putative denticle field (Payre et al., 1999). As previously indicated, *wg* mutations produce a lawn of denticles and express *svb* across the entire ventral epidermis. Furthermore, constitutive activation of the wg pathway via the overexpression of *armadillo*, a downstream effector of wg signaling, results in naked cuticles and an absence of *svb* expression throughout the epidermis (Payre et al., 1999). Thus, wg and the EGFR pathway act antagonistically to induce *svb* expression in distinct regions of the parasegment, and the expression of *svb* is sufficient to promote denticle formation.

Svb, in turn, triggers expression of a variety of cellular effectors controlling actin nucleation and remodeling, membrane and matrix remodeling, and cuticle deposition; these are discussed in further detail below (Roch, 2003; Chanut-Delalande et al., 2006; Andrew & Baker, 2008; Fernandes et al., 2010). Important to note is the fact that svb controls not only the formation of denticles, but other similar cellular protrusions such as the dorsal hairs in the embryo and various other trichomes, including bristles in the scutum and scutellum, wing hairs, and aristae, in the adult (Delon et al., 2003; Chanut-Delalande et al., 2006). Furthermore, svb's role in regulating the production of actin based structures is conserved across *Drosophilidae*. The *svb* expression pattern is markedly different in *D. sechellia* than in *D. melanogaster*, *D. simulans* or *D. mauritiana*, resulting in a different pattern of dorsal and ventral trichomes. Sequence analysis has identified a number of alterations to the *cis*-regulatory sequences of *svb*, and modification of these regions in *D. melanogaster* is sufficient to alter the *svb* expression pattern and the final trichome pattern, suggesting that differential regulation of *svb* is responsible for the differences in trichome patterns between these species (McGregor et al., 2007; Frankel et al., 2011). Similarly, loss of the mouse homologue of *svb*, *movo1*, causes defects in hair and sperm production in mice (Dai et al., 1998). These data indicate that *svb* is a major player in regulating the production of actin based cellular protrusions. Finally, *svb* is particularly notable because of its ability to

integrate the signals from several different pathways (the above-mentioned cascades through wg, hh, Notch, and EGFR) and translate these inputs into a tangible output (formation of denticles and hairs). Thus, the identification and characterization of *svb* answers a long-unsolved question of how complex patterning events required for cell fate determination are connected to the tissue and cytoskeletal remodeling events required to generate complex intracellular structures (Delon et al., 2003; Delon & Payre, 2004; Chanut-Delalande et al., 2006).

Although *shavenbaby* provides an answer to the question of how cells link cell fate to tissue morphogenetic events, it may not tell the entire story. While it is sufficient to induce actin remodeling in the *Drosophila* epidermis, it is likely that additional factors are required for the formation of fully-differentiated denticles. This is supported by two lines of evidence. First, ectopic expression of *svb* in smooth cells results in the creation of protruding actin bundles, but these structures do not resemble the denticle structures present in the denticle belts, or their subcellular distribution (Payre et al., 1999; Delon et al., 2003; Walters et al., 2006). Second, the known differences in gene expression in each of the six denticle columns cannot yet fully account for the unique denticle morphologies observed across the different denticle columns. Therefore, additional elements controlling patterns of denticle organization and morphology remain to be discovered.

1.2.3 The cell biology of denticle belt formation

Once cell fates are established, denticle cells execute a series of tissue remodeling steps that reshape the apical compartment to create the final denticle pattern. These morphogenetic events, which require a diverse series of cellular effectors to act in concert, can be divided into two major categories; cell alignment and junctional rearrangement, and denticle formation and organization.

1.2.3.1 Junctional rearrangements and cell shape changes

Before denticles are produced, the cells in the denticle belts undergo a series of shape changes and junctional rearrangements that transform them into the elongated, rectilinear cells characteristic of the denticle belts (Price et al., 2006; Walters et al., 2006; Simone & DiNardo, 2010; Marcinkevicius & Zallen, 2013). At the conclusion of germband retraction in stage 13, the epithelium consists of cells with a range of topologies and a range of internal angles (**Figure 1.4**). In contrast, in the final denticle belt configuration cells are elongated along the dorsal-ventral (DV) axis, and their anterior-posterior (AP) edges align to form clearly defined columns of cells (**Figure 1.4**). In this thesis, AP edges are defined as the cell interfaces oriented perpendicular to the AP axis, while DV (dorsal-ventral) edges refer to the cell interfaces oriented parallel to the AP axis. This transition to rectilinear cells, which is specific to the denticle field and does not occur in smooth cells, is achieved mainly through junctional rearrangements and cell elongation. These processes require myosin II, as well as the polarity proteins discs large (dlg) and fat (Simone & DiNardo, 2010; Marcinkevicius & Zallen, 2013). Beginning at stage 13, AP edges of prospective denticle-field cells accumulate myosin II (Walters et al., 2006). This accumulation is particularly enriched at the boundaries between columns 1 and 2 and between columns 4 and 5, and these cells are the first to begin aligning (Simone & DiNardo, 2010).

Alignment occurs through a process that is akin to the neighbor exchange events observed during germband extension (Irvine & Wieschaus, 1994; Bertet et al., 2004; Zallen & Wieschaus, 2004; Blankenship et al., 2006; Fernandez-Gonzalez et al., 2009). AP edges accumulate myosin and the polarity protein discs large (dlg) and begin to shrink (Simone & DiNardo, 2010). Afterwards, the edge may then re-form as a new AP edge (most commonly), or a new DV edge (occasionally); a small fraction of DV edges also undergo this rearrangement process (Marcinkevicius & Zallen, 2013). Depending on the orientations of the original and newly-formed edges, this process may result in a simple junctional shift to increase alignment, or an intercalation event that shifts the position of one or more cells within the denticle columns, and such junctional rearrangements

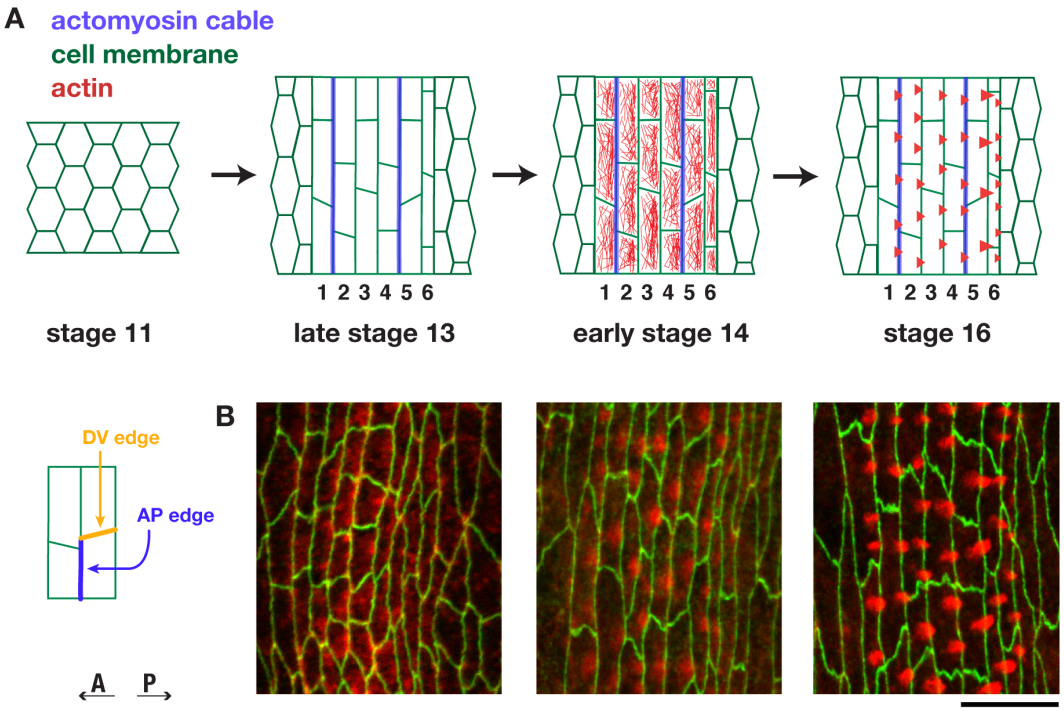

Figure 1.4: Denticles form from an apical actin meshwork. A. Cells (outlined in green) within the prospective denticle fields progress from a field of hexagonal cells to a highly ordered array of rectilinear cells. This process is driven in part by the formation of an actomyosin cable (magenta) between denticle columns 1 and 2 and 4 and 5. After cells have begun to align their edges, the denticles emerge from an apical actomyosin meshwork (red), and elongate apically to deform the plasma membrane (not shown). **B.** Confocal images of denticle belts in embryos of the indicated stages during denticle development, corresponding to the schematized views in F. F-actin (phalloidin, red), E-cadherin (green).

are most common in the middle columns (columns 3 and 4) (Marcinkevicius & Zallen, 2013). The alignment process actively requires myosin activity, as well as dlg and several components of the planar cell polarity pathway mediated by the atypical cadherin fat (Simone & DiNardo, 2010; Marcinkevicius & Zallen, 2013). Cell elongation occurs concomitantly with cell alignment. However, as cell alignment proceeds normally in *u-shaped* embryos, which have reduced cell elongation due to defects in germband retraction and dorsal closure, elongation is not thought to be a major driver of the cell alignment process in denticle cells (Simone & DiNardo, 2010).

1.2.3.2 Denticles are formed from an apical actin meshwork

As cell elongation and rearrangement are progressing, the cells of the prospective denticle field accumulate an apical pool of F-actin and associated cofactors, in anticipation of forming the unipolar, actin based denticle precursors (**Figure 1.4**). This accumulation begins after the germband has retracted, approximately 9 hours AEL (stage 13). Analysis of actin localization in fixed tissue and in live imaging experiments that make use fluorescently-tagged molecules that associate with denticle structures, such as myosin II, have revealed that the initiation of denticle structures begins with the condensation of small actin foci from this apical actin meshwork beginning in stage 14 (approximately 10 hours AEL) (Price et al., 2006; Walters et al., 2006). During the earliest stages of denticle formation, these actin foci are uniformly distributed across the anterior-posterior face of the cell (Walters et al., 2006). Prior to cell elongation and in response to both the activity of the Fat/Daschous and Frizzled planar polarity systems and to activation of the Notch pathway, these foci become planar polarized and accumulate at the posterior edge of the cell (mid-stage 14) (Walters et al., 2006; Price et al., 2006; Donoughe & DiNardo, 2011; Marcinkevicius & Zallen, 2013; Lawlor et al., 2013). Foci then coalesce into larger actin condensations; at this early stage, denticles are rounded 'bumps' at the apical posterior surface. Over the next several hours, denticles elongate form the final pointed, conical actin based denticle precursors (Price et al., 2006), although the directional hook that is obvious in the cuticle is not visible in the embryonic epidermis. While many cells contain a single actin structure, a nearly half of all embryonic cells have multiple denticles, and this number varies by cell and by denticle column (Price et al., 2006; Dilks & DiNardo, 2010, see Chapter 3). This is a critical point, as it requires that cytoskeletal and membrane/matrix reorganization must occur simultaneously at multiple points within a single cell. In contrast, other cells that produce trichomes, such as the wing hairs , create a single structure in which all of the components required are targeted to a single location.

Once established, actin condensations in denticle-forming cells elongate into conical structures protruding from the apical cell surface, templating the denticle structures in the cuticle (Uv & Moussian, 2010; Hillman & Lesnik, 1970; Payre, 2004; Chanut-Delalande et al., 2012). The precise details surrounding the initiation and elongation steps are unclear, although a number of cytoskeletal regulators are involved in this process (see following paragraphs). Once cells have completed neighbor exchange, elongation and actin reorganization, the extracellular cuticle is secreted from the apical cell surface, over the actin precursors. Because the muscles begin to contract at this stage, imaging is technically extremely difficult and little is known about the dynamics of this process. Since denticle hooks are visible only in the cuticle and cannot be seen when observing the localization of cytoskeletal proteins, additional factors aside from actin and myosin are likely necessary to establish the characteristic denticle hooks observed only in the cuticle. Once the cuticle deposition and hardening process has been completed, the cytoskeletal protrusions are dismantled, and reassembled only when new cuticle is being made, just prior to each larval molt (AKLS, unpublished results); (Saavedra et al., 2014).

1.2.3.3 A variety of cytoskeletal regulators associate with denticles

Building each denticle requires a wide variety of cytoskeletal regulators and actin associated proteins. F-actin forms the core of the denticle structure. Myosin II colocalizes with the nascent denticles from the earliest stages. A wide variety of additional actin associated molecules have been shown to have expression and/or localization patterns around the denticles and in the denticle field. Furthermore, the microtubule cytoskeleton and microtubule regulators, have been shown to have associated with denticles. The interplay between these molecules is of great importance to understand how denticles may be formed *in vivo*. These molecules fall into three general classes: actin related molecules with striped expression patterns coinciding with *svb* expression, actin related molecules with ubiquitous epidermal expression or whose expression patterns have not been observed, and microtubules and their associated proteins.

1.2.3.4 Actin associated proteins expressed in *svb* stripes

Several actin regulators, those that are targets of shavenbaby, have been shown to be expressed in stripes in the ventral epidermis through both immunofluorescence and *in situ* hybridization assays (Chanut-Delalande et al., 2006). These include forked, the putative *Drosophila* homologue of the actin bundling protein espin, which is most frequently associated with the creation of straight actin bundes (Bartles et al., 1998; Revenu et al., 2004); singed, a homologue of fascin, another actin crosslinking protein which promotes a tightly packed, hexagonal lattice structure of straight actin bundles (Bryan et al., 1993; Cant, 1994; Revenu et al., 2004); WASP, an actin nucleator that associates with the Arp2/3 complex to promote the formation of branched actin assemblies (Machesky & Insall, 1998; Revenu et al., 2004); and shavenoid, a novel actin binding protein with additional roles in wing hair formation (Ren et al., 2006; Chanut-Delalande et al., 2006). The striped expression of all four of these molecules is strongly reduced in *svb* mutants, indicating that svb is necessary for their expression. Furthermore, mutations in these molecules result in the creation of deformed denticle structures (Chanut-Delalande et al., 2006). These data suggests that these four proteins may be important in creating denticles. Most of these regulators have been well studied in the context of other actin based structures. Many of these studies have also examined their interactions with other regulators, as multiple crosslinking proteins are often required to form properly assembled actin structures.

Forked (espin) and singed (fascin): In the *Drosophila* bristle, forked, an espin - related actin bundling protein, and singed, an actin cross linker, cooperate to form the lattice of actin filaments that makes up the bristle structure (Tilney, 1995, 1996; Tilney et al., 1998; DeRosier & Tilney, 2000). Electron micrographs of cross - sections of the bristle reveal that forked acts at the growing tip of the bristle to promote aggregation of actin into small, loosely packed, disorganized bundles (Tilney, 1995, 1996; Tilney et al., 1998; DeRosier & Tilney, 2000). Singed acts on these bundles to create a tightly packed, hexagonal lattice structure with a highly regular, 12-nm periodicity (Tilney, 1995, 1996; Tilney et al., 1998; DeRosier & Tilney, 2000). During the formation of the

bristles, forked and singed occupy overlapping but slightly different domains; forked, acting first, is more concentrated in the bristle tip, while singed, acting on the bundles already created by forked, is distributed more throughout the base and lower regions of the growing bristle (Tilney, 1995, 1996; Tilney et al., 1998; DeRosier & Tilney, 2000). Zygotic loss of either *forked* or *singed* results in bristles that are deformed; *singed* mutant bristles are less rigid and appear wavy, while *forked* mutant bristles are quite short (Tilney, 1995). These data indicate that both forked and singed are required for correct actin filament assembly in the developing bristle. However, double zygotic *forked/singed* mutants also produce bristles, although they also appear stubby and deformed (Tilney, 1995; Tilney et al., 1998), suggesting that these may not be the only molecules involved in aggregating actin during bristle production, although they are necessary for the correct shaping of the structure.

Consistent with these essential roles in the structural integrity of the actin bundles within the *Drosophila* bristles, both forked and singed affect denticle development. Various alleles of both *forked* and *singed* mutants create recognizable denticles in cuticle preparations, although they are malformed (Dickinson & Thatcher, 1997; Chanut-Delalande et al., 2006). Denticles in *forked* mutants are long and slender, without a pronounced hook (Dickinson & Thatcher, 1997). *singed* mutant denticles are thin, with small hooks, although this phenotype is reportedly slightly less severe than that of *forked* mutants (Dickinson & Thatcher, 1997). Both forked and singed also colocalize with denticle actin in immunofluorescence images (Chanut-Delalande et al., 2006; Dilks, 2010). Forked localizes almost exclusively to denticles, and appears to be enriched at the denticle tip, while singed appears to be distributed throughout the length of the denticle and spreads into the cytoplasm (Chanut-Delalande et al., 2006; Dilks, 2010). Consequently, both forked and singed have roles in the developing denticle, suggesting that at least a portion of the denticle structure is likely to originate from parallel bundles of actin microfilaments. The details, particularly of the dynamics and timing of forked and singed involvement during denticle development have not been tested, however.

Wiskott-Aldrich syndrome protein (WASp): The Wiskott-Aldrich syndrome protein (WASp), is an actin nucleating factor that functions with the Arp2/3 complex to produce branched actin networks, and promote actin polymerization (Goley & Welch, 2006). WASp, along with the rest of the Arp2/3 complex, has crucial roles in cell migration and cell adhesion, axon development, and cytoplasmic organization, as well as many other functions requiring branched actin networks (Goley & Welch, 2006). Most relevantly, Arp2/3 and WASp have been implicated in protein trafficking and intracellular transport, including in phagocytosis and endocytosis (Goley & Welch, 2006). In the *Drosophila* embryo, animals with zygotic mutations in *Wasp* have denticles that are thinner and bent compared to wild-type, indicating that WASp is required for correct denticle morphology. However, although *Drosophila WASp* has a distinctly striped expression pattern in the ventral epidermis in *in situ* hybridization assays, (Chanut-Delalande et al., 2006), the localization of the WASp protein relative to the denticles has not been tested. Additional characterization of WASp in denticle cells will be required to determine what role WASp plays in producing the correct denticle structure.

Shavenoid: The final actin related *svb* target expressed in stripes through the ventral epidermis is *shavenoid* (*sha*) (Chanut-Delalande et al., 2006), which encodes a novel, insect-specific protein predicted to interact with the actin cytoskeleton. In the wing, loss of *shavenoid* causes delays and defects in wing hair formation, resulting in adult flies that generate no hairs or several small or split protrusions (Ren et al., 2006). Similar results with loss-of-function mutants have been reported during formation of the aristae laterals (He & Adler, 2002). Co-immunoprecipitation assays in wing disc cells suggest that shavenoid and actin may interact directly, and sha-GFP accumulates in wing hairs and bristles (Ren et al., 2006), and genetic complementation tests indicate that sha interacts with the frizzled planar polarity pathway, as mutations in *fz* pathway components enhance the hair loss phenotype of *sha* mutants (Ren et al., 2006). Finally, temperature shift experiments during development of the aristae produce results consistent with the hypothesis that sha functions during the initiation of actin based structures (He & Adler, 2002; Ren et al., 2006).

Notably, mutations in *shavenoid* significantly alter the appearance of the denticles. While embryos with mutations in *forked*, *singed*, or *WASp* produce denticles that are thinner, longer, and poorly hooked, they are generally recognizable as denticles (Dickinson & Thatcher, 1997; Chanut-Delalande et al., 2006). In contrast, mutations in *shavenoid* reduce both the size and number of denticles, and the denticles that are formed are severely stunted, frequently appearing only as slight bumps in the cuticle but without any defined structure (Chanut-Delalande et al., 2006; Ren et al., 2006). The localization of shavenoid relative to the denticle plays during denticle development have not been investigated, and precisely how shavenoid interacts with the cytoskeleton to regulate the formation of actin protrusions, including the denticles, hairs, and aristae, has yet to be determined.

1.2.3.5 Ubiquitously expressed actin regulators

In addition to the *svb*-dependent, striped expression of *forked*, *singed*, *WASp* and *shavenoid*, several additional actin related genes show ubiquitous expression throughout the *Drosophila* epidermis, and may have roles in establishing the denticle structure and organization pattern. These include members of the Arp1/2/3 family (aside from WASp), *diaphanous*, *enabled*, and *dAPC* (the (Chanut-Delalande et al., 2006). Arp3, diaphanous, enabled, and dAPC have been shown to co-localize with denticle actin (Delon et al., 2003; Price et al., 2006). In addition, dAPC and diaphanous both associate with microtubules as well as with actin, and will be discussed in that context below.

The Arp2/3 complex: The Arp2/3 complex is an actin nucleating factor that promotes the creation of branched actin networks (Goley & Welch, 2006). Electron micrographs show that these 'Y'-shaped branches occur at regular 70° intervals (Mullins et al., 1998; Amann & Pollard, 2001). On its own, Arp2/3 has no significant effect on actin polymerization. However, associate of Arp2/3 with a nucleation-promoting factors (NPF) protein such as WASP (Higgs et al., 1999) increases its nucleation and polymerization abilities, and regulation of these NPFs allows for

fine spatiotemporal control of actin polymerization within cells (Goley & Welch, 2006). In the denticle cells, Arp3 is observed throughout the length of the elongating denticle (Price et al., 2006), but the effect of Arp3 mutation on denticle formation is unknown. The localization patterns in denticle cells, and the effects of removing them from the ventral epithelium, of the remaining family members have not been described.

Enabled (VASP): Enabled (VASP) Enabled (ena) is the *Drosophila* homologue of the VASP (vasodilator-stimulated phosphoprotein) family of actin polymerizing factors, which promote elongation of actin filaments (Bear et al., 2002). Ena/VASP are generally agreed to promote actin polymerization in the presence of capping factors. *In vitro* studies measuring F-actin incorporation rate (Bear et al., 2002; Barzik et al., 2005) and polymer growth via TIRF (total internal reflection fluorescence) microscopy (Breitsprecher et al., 2008; Pasic et al., 2008; Winkelman et al., 2014) demonstrate that the addition of ena/VASP greatly enhances the actin polymerization rate, although the exact mechanism by which ena/VASP antagonizes capping proteins these studies suggest differs. Ena/VASP is well known for its role in forming and regulating filopodia, along with formins and fascins !cite(Gupton & Gertler, 2007; Yang & Svitkina, 2011). Ena can gather multiple filaments and promote their simultaneous elongation, as demonstrated by tracking of *in vivo* actin assembly by TIRF microscopy (Winkelman et al., 2014). Addition of fascin enhances the processivity of ena's bundling and elongation effects (Winkelman et al., 2014). Thus, ena promotes the assembly of bundled actin filaments, such as those found in filopodia (Winkelman et al., 2014). One possibility raised by this study is that ena/VASP may remodel small domains of the branched actin networks created by the Arp2/3 complex, preventing capping and enhancing polymerization with fascin, although this hypothesis remains to be tested. If true, it would help to explain how branched actin networks and bundled actin filaments co-exist, and are created *in vitro* and *in vivo*. In the denticle cells, ena localizes throughout the denticle protrusion (Price et al., 2006). The effect of *ena* mutation has not been studied specifically in the context of denticle cells; however, zygotic mutants do not have any reported defects in the cuticular structures (Gertler et al., 1990),

1.2.3.6 Microtubule associated proteins in the denticle field

Although the denticles are primarily actin based structures, the microtubule cytoskeleton displays distinct organization in denticle cells, and is associated with sites of denticle formation. Microtubules are aligned with the cell long axis, parallel to the dorsal-ventral axis in denticle cells (Dickinson & Thatcher, 1997; Price et al., 2006; Marcinkevicius & Zallen, 2013). This planar polarized alignment requires activity of the Fat planar cell polarity pathway; in the absence of Fat, microtuble alignment is significantly reduced (Marcinkevicius & Zallen, 2013). Microtubules have also been shown to be enriched at the base of the denticles during the elongation phase, although how or whether these microtubule accumulations contribute to the process of denticle formation has never been directly tested (Price et al., 2006).

APC (adenomatous polyposis coli protein) and diaphanous: The cytoskeletal proteins APC and diaphanous both accumulate in and around forming denticles (Price et al., 2006). Diaphanous (dia), one of the *Drosophila* formin homologues, has been shown to act as both an actin nucleating factor and an actin polymerization promoter in *in vitro* TIRF microscopy and actin polymerization assays (Chesarone et al., 2010; Goode & Eck, 2007; Kühn & Geyer, 2014). This activity results in the creation of unbranched actin filaments. Formins are also able to bind directly to microtubules and stabilize them. Dia associates with microtubules in *in vitro* pulldown and microscopy assasys (Palazzo et al., 2001), and microinjection of dia fragments into cells induces formation of Glu-tubulin, a marker of stabilized tubulin (Palazzo et al., 2001). This microtubule stabilizing functionality of dia is independent of its actin nucleation and polymerization function, as point mutants defective for actin polymerization retained microtubule stabilization functionality (Bartolini et al., 2008). In myoblasts, dia appears to regulate the Arp2/3 complex during myoblast fusion by localizing WASP and SCAR, both of which are Arp2/3 regulators (Deng et al., 2015). These results demonstrate dia's ability to promote actin assembly, while simultaneously generating connections to a stabilized microtubule cytoskeleton.

Electron microscopy data suggests that APC associates with microtubule plus ends (Mogensen et al., 2002), and, in live imaging of *Xenopus* embryos, has been shown to move along the microtubule filament. Pulldown assays show that APC can interact with KAP3, a kinesin linker protein, suggesting that this may be one way in which APC is transported along the microtubule. In addition to interacting with the microtubule cytoskeleton, immunofluorescence data indicates that APC colocalizes with actin in MDCK cells. As this pattern is disrupted in cells treated with latrunculin-B (a drug which induces actin depolymerization) this placement is believed to be actin dependent (Rosin-Arbesfeld et al., 2001; Näthke, 2004). However, the nature of this interaction and its implications for the cell, have not been well characterized.

Dia and APC can interact genetically and physically (Chesarone et al., 2010). During cellularization in the *Drosophila* embryo, APC colocalizes with dia in the cleavage furrow. The localization of APC to the furrow is dia-dependent; mutations in *dia* causes defects similar to those of APC mutants (Webb et al., 2009). This interaction is direct, as demonstrated by co-immunoprecipitation assays (Webb et al., 2009). Although both dia and APC localize to the denticles (Price et al., 2006), the effects of mutating either molecule has not been studied in this tissue. Based on their functions in other tissues, both proteins could have a variety of effects on the creation of the denticle structure or the denticle organization pattern.

Short stop: A third actin microtubule linker protein, the spectraplakin short stop (shot), also co-localizes with actin during denticle formation (Dilks & DiNardo, 2010). Spectraplakins are large proteins that can interact with both the actin and microtubule cytoskeletons and act as cross linkers between actin, microtubules, and the cell membrane (Roper, 2002). Shot is present in all cells through the epithelium, although it is enriched in the tendon cells (denticle columns 2 and 5, and smooth cell column -2) (Gregory & Brown, 1998; Röper & Brown, 2004; Dilks & DiNardo, 2010). Depleting *shot* in denticle cells produces grossly misshapen denticles that are thinner, poorly shaped, and have defects in the directionality of the denticle hook (Dilks & DiNardo, 2010). In particular, shot is required for the anterior-facing hooks of column 1 and column 4 denticles (Dilks & DiNardo, 2010). These data indicate that microtubules may be required for

denticle shape, and suggest that there may be additional, critical roles for microtubules, as well as yet-to-be-identified roles for actin in forming and distributing denticles within the cell.

1.2.3.7 Column-specific differences and the determination of denticle shape

The final hooked shape of the denticles at the level of the cuticle is dependent on apical extension of the actin bundle, coupled with remodeling of the apical membrane domain. Due mainly to the technical difficulties of analyzing embryos at these late stages, comparatively little work has been done to elucidate how the denticles are shaped. Currently, there are just three known categories of effectors that are responsible for orchestrating the creation of the final denticle shape.

One set of downstream targets of *svb* is a family of eight membrane-anchored zona pellucida domain-containing (ZPD) matrix proteins, seven of which localize to the ventral epidermis in stripes coinciding with the denticle-forming cells (Chanut-Delalande et al., 2006; Fernandes et al., 2010). Each of these proteins are localized to a different region of the membrane surrounding the elongating denticle, and each has a distinct role in shaping the nascent protrusion, as the denticle phenotypes of mutants range from normal-looking but small denticles to denticles that are twisted, spit, broken, or otherwise misshapen (Fernandes et al., 2010). Furthermore, ultrastructural analysis demonstrates that these embryos have defects in the connection between the apical plasma membrane and the extracellular cuticle (Fernandes et al., 2010). These data suggest, therefore, that this family of proteins acts to link the actin cytoskeleton remodeling events and the extracellular membrane, promoting denticle formation.

A second requirement for producing correctly-shaped denticles is the *Drosophila* atypical myosin VIIA heavy chain, crinkled (ck) (Kiehart, 2004; Bejsovec & Chao, 2012). Unlike the ZPD proteins, ck does not appear to directly shape actin or the membrane. Mutations in *ck* alone do not alter denticle morphology; however, when *ck* is mutated in a *wg* background, actin accumulates apically in the denticle pattern, but does not elongate into the correct final denticle structures (Bejsovec & Chao, 2012). Ck-GFP accumulates in the denticle punctae, and genetically

modulating the levels of either wg or svb target genes such as *miniature* and *forked* in *ck* mutants modifies the final shape of *ck* mutant denticles, although these changes in protein levels have no effect in otherwise wild-type embryos. Intriguingly, overexpressing *svb* ubiquitously not only induced denticle formation in what should have been naked cuticle, it also altered the morphology of denticle across the denticle field. Thus, precise regulation of *svb* target components, not just their presence, is essential for proper denticle formation. As denticle defects due to *svb* misregulation are enhanced by mutations in *ck*, ck may be required to ensure that components required for actin remodeling and membrane shaping are correctly distributed throughout the elongating denticle (Bejsovec & Chao, 2012).

Finally, the spectraplakin short stop is specifically required in a subset of columns to reverse the hook polarity of column 1 and column 4 denticles (Dilks & DiNardo, 2010). *shot* is a target of the transcription factor Stripe (Sr), which is specifically expressed in columns 2 and 5 of the denticle belt (Hatini & DiNardo, 2001a; Dilks & DiNardo, 2010). Shot is visible across the denticle belt and co-localizes with the incipient denticles at early stages. However, during late stages (the time that cuticle deposition and, presumably, hook orientation is determined) shot seems to become more diffuse, and localized across the 1/2 and 4/5 cell interface rather than in denticle punctae (Dilks & DiNardo, 2010). Embryos lacking *shot* ubiquitously have mis-oriented denticles in columns 1 and 4 at a far higher frequency than wild type embryos. Removing shot via RNAi in either columns 0 and 1 or in columns 2 and 3 causes hook orientation defects in column 1 denticles, suggesting that shot is required both intrinsically and non-cell-autonomously to produce anterior denticle hooks. Finally, depletion of microtubules recapitulates the mis-orientation phenotypes, indicating that shot may interact with microtubules to generate denticle hooks. How precisely shot promotes anterior denticle hooking is unclear. However, its roles in other tissues raise the possibility that shot-cytoskeleton complexes might affect the secretion or deposition of membrane components, the attachment of the cytoskeleton to the membrane, or the induction of additional cytoskeletal remodeling (Becker et al., 1997; Gregory & Brown, 1998; Subramanian et al., 2003; Lee & Kolodziej, 2002; Lee et al., 2000; Dilks & DiNardo, 2010).

1.3 Using the denticle system to explore the formation and organization of subcellular structures

Although a great deal is known about the genetic instructions that lead to the overall segmental pattern of the *Drosophila* embryo, particularly those that result in the formation of the denticle belts, relatively little is understood about how these complex patterns of actin structures are established at the cell biological level. Cytoskeletal components have been studied in great detail *in vitro* and in cell culture systems, but how these molecules act together in the epithelium is not well understood. At least two major questions exist. First, how are very specific cytoskeletal rearrangement events, such as those occurring in the denticle cells, specified by the genetic patterning events occurring upstream, and what are the molecular effectors that carry out these instructions? In this system, these questions have been partially answered by the study and characterization of the transcription factor shavenbaby and the identification of some of its downstream targets. However, much still remains to be discovered about how the genetic pathways that result in shavenbaby expression and the activities of shavenbaby's molecular effectors converge to produce denticles of diverse morphologies. For instance, overexpression of *svb* in smooth cells results in the formation of actin based protrusions, but these structures lack many of the morphological and organizational characteristics of denticles within the denticle field (Payre et al., 1999; Delon et al., 2003), indicating that additional factors are necessary to refine the shape and distribution of denticle structures. Understanding what makes the denticle cells unique and competent to produce these morphologically distinct structures will lend insight into how cytoskeletal structures are sculpted *in vivo*. The second question is, how are cytoskeletal structures arranged *in vivo*? Although the distribution and scaling patterns of microtubule based structures have been studied in some detail, the mechanisms that direct the organization of macromolecular actin structures, and how actin organization is maintained during dramatic changes in cell size during the growth, are not well understood.

One particularly striking feature of the denticle system is the apparent regularity of denticle distribution across the cell column, a pattern which persists despite a several-hundred-fold increase in organism size through the embryonic and larval stages. While the alignment of the AP edges of the denticle cells and the posterior placement of the denticle structures accounts for the alignment of denticles observed in the cuticle, it is unclear how a regular distribution of denticles is maintained within each column. It has been shown that multiple denticles are formed per cell (Price et al., 2006; Dilks & DiNardo, 2010). Therefore, to attain this apparently regular arrangement, there must be mechanisms controlling the planar polarized distribution of denticles along the long axis of the cell. How this organization pattern is generated and maintained is entirely unknown. Given the highly organized patterns of actin organization, the well studied genetic pathways controlling the specification of this pattern, and the accessibility of the system to genetic and live imaging approaches, I believe that the cells of the *Drosophila* denticle belts provide an excellent tissue in which to ask questions about the molecules and mechanisms required to generate complex cytoskeletal patterns.

1.4 Genetic screening in the *Drosophila* embryo

The process of isolating and characterizing mutant organisms with phenotypic defects in a particular tissue or process, known as forward genetics, allows researchers to identify the genes involved in a particular process (St Johnston, 2002). The unbiased nature of this approach makes it extremely powerful, as it allows researchers to connect both known and novel genes to a particular process without making prior assumptions about the genes or pathways required. As a result, forward genetic screens have been essential for elucidating the genetic pathways and molecular mechanisms that underly a multitude of critical processes in a wide range of tissues and developmental stages, for nearly 40 years (St Johnston, 2002).

One of the major advantages to using the fruit fly *Drosophila* melanogaster as a model organism is that genetically it is extremely malleable, and that many tools have been developed over the

past century to allow researchers to capitalize on this feature. As such, the fly is especially well suited to forward genetic screening. It has a rapid life cycle, and a long history of genetic practices, accompanied by a large suite of available tool and techniques for identifying and characterizing new genes (St Johnston, 2002; Rubin & Lewis, 2000), including the ability to maintain and characterize lethal mutations over many generations using defined balancer chromosomes (Muller, 1918; Lindsley & Zimm, 1992). The genome, which consists of only four chromosomes (Lindsley & Zimm, 1992), has now been sequenced and has been shown to be relatively small and non-redundant, with a predicted 13,601 protein-coding genes at an average density of one gene per 9 kb of DNA (Adams et al., 2000), smaller even than the number of predicted *C. elegans* protein coding genes (Adams et al., 2000). Approximately 98% of these genes, which make up the approximately 120 Mb of euchromatic DNA (out of a total of 180 Mb), are distributed over just three chromosomes, the two larger autosomes and the X chromosome (Adams et al., 2000; Celniker & Rubin, 2003). Notably, the *Drosophila* genome has a high degree of homology to mammalian genomes. At least 50-70% of the genes involved in human disease have *Drosophila* homologues (Fortini et al., 2000; Rubin et al., 2000; Reiter et al., 2001; Pandey & Nichols, 2011), with more such genes continuously being identified (Yamamoto et al., 2014; Neely et al., 2010; Bayat et al., 2012). As a result, genetic screens in the fly are not only valuable to the basic research community, but also essential for the identification of human disease related alleles, and advancement of research relating to human development and disease.

Although the isolation and characterization of visible mutations - both naturally occurring mutations and those induced in the laboratory - has been a staple of fly genetics research since the early 1900's when Thomas Hunt Morgan first began his research, the true power of forward genetics was not fully understood until the 1980's. Christiane Nüsslein-Volhard and Eric Wieschaus, who would later win the Nobel Prize for their work, realized that by screening many thousands of flies with embryonic lethal mutations and isolating those with morphological defects in the larval cuticle, they would be able to identify the majority of genes required for embryonic development, as well as the effect on pattern formation that each would have

(Nüsslein-Volhard & Wieschaus, 1980; Wieschaus, 1996b; Nüsslein-Volhard, 1996; Wieschaus & Nüsslein-Volhard, 2016). In their famous Heidelberg screen, they amassed a collection of more than 25,000 mutant stocks on the 2nd, 3rd, 4th, and X chromosomes, 4,000 of which were embryonic lethal. They then isolated and mapped 580 genes in 139 unique complementation groups that caused defects in the well-documented, stereotyped pattern of denticle bands and other trichomes in the larval cuticle (Lohs-Schardin et al., 1979; Wieschaus et al., 1984; Jürgens et al., 1984; Nüsslein-Volhard et al., 1984). Many of these genes are essential for early embryonic development, the establishment of segment patterning, and for specifying the embryonic body plan. A large fraction also have significant roles throughout the lifecycle of flies and vertebrates alike. Among the mutants uncovered in this screen, were alleles in fundamental pathways, include *hedgehog*, *wingless*, *engrailed*, and *Notch* (Nüsslein-Volhard & Wieschaus, 1980; Wieschaus et al., 1984; Nüsslein-Volhard et al., 1984; Jürgens et al., 1984; Wieschaus & Nüsslein-Volhard, 2016). In short, this revolutionary work, and the many other screens that followed it, have opened up entirely new fields of research and have provided a great deal of information about embryonic development and cellular and tissue function.

However, no screen can find every gene required for a particular process (due to redundancy, timing of requirement, necessity prior to the stage in question, among many other reasons), and much still remains to be discovered in how cells are able to organize, internally and externally, into the complex tissues that eventually coordinate and assemble to form a fully functional animal. In particular, there are significant gaps between what is known of the transcription factors and signaling cascades necessary for pattern and cell fate determination - the majority of the genes identified in the Heidelberg screens - and the cell biological effectors that execute the details of this pattern. Consequently, although the fly genetics and developmental biology communities may one day find that forward genetic screens are no longer useful due to the advent of new methods and techniques (St Johnston, 2002), as of today today they remain one of the most effective means of identifying which genetic components control specific aspects of

tissue development, provided that there is a visible phenotypic outcome that may be screened for.

1.4.1 Designing forward genetic screens

1.4.1.1 The embryonic cuticle provides a readout for defects in embryonic epithelial patterning and integrity

One major consideration in designing a forward genetic screen lies in choosing a tissue that will answer the question being addressed. The epidermis of the *Drosophila* embryo, specifically the larval cuticle, is a commonly used when screening for genes that contribute to the patterning of the embryo, including in the Heidelberg screens. Two major factors make the larval cuticle an ideal location for studying both body patterning and subcellular structure organization. First, the cuticle pattern is rich in detail, consisting of stereotyped arrangements of denticles, hairs, sensory organs, and other features, each of which has morphological differences as a function of position relative to the body axes that is highly stereotyped and which has been well described (Lohs-Schardin et al., 1979). Many of these structures, particularly the ventral denticles, are actin based protrusions that display multiple types of high-degree organization patterns. These patterns range from the distribution of denticles across the body plan of the embryo in belts or bands (segment patterning) to the very precise subcellular localization of each structure (planar polarity and other features), and defects or alterations to this organization pattern in the underlying epithelium is typically reflected clearly in the cuticle. This makes it possible and relatively straightforward to screen for phenotypes ranging from gross morphological defects (missing or fused segments, gaping holes) (Nüsslein-Volhard & Wieschaus, 1980; Perrimon et al., 1989, 1996; Wieschaus & Nüsslein-Volhard, 2016) to more subtle abnormalities (change in denticle column number, changes in denticle appearance). Second, the cuticle is the larval exoskeleton, a tough, waterproof, secreted extracellular matrix consisting mainly of chitin, which is deposited at the end of embryonic development to provide protection and structural

support to the larva when it hatches (Hillman & Lesnik, 1970; Moussian et al., 2006; Moussian, 2010). Cuticle secretion marks the transition between the conclusion of embryonic development and larval stages, and therefore reflects the cellular organization, arrangement of subcellular structures, and epithelial integrity of the underlying embryonic epidermis at the end stages of development. However, unlike the soft tissues which degrade quickly upon the death of the animal, the cuticle persists and resists immediate degradation. This makes it possible to collect many more mutant embryos over a relatively long period of time and analyze their endpoint phenotypes at leisure, rather than being restricted to a narrow window in a live animal. The combination of ease of access, tissue perdurance, richly detailed patterns, and density of actin based structures makes the larval cuticle an ideal location to screen for mutants with defects in building and organizing actin based structures.

1.4.1.2 Screening methods in the embryo must take into account both maternal and zygotic gene effects

For forward genetic screens in embryos, it is necessary to be aware that the genotype of the mother may have as much of an effect on the phenotypes observed as the embryonic genotype. This phenomenon is known as maternal effect. Embryonic development is controlled by two sets of gene products, zygotic and maternal (Wieschaus, 1996a; Tadros & Lipshitz, 2009). The zygotic contribution is produced by the embryo and fulfills a number of highly specialized functions, although these genes compose a relative minority of the gene products required for development (Lécuyer et al., 2007). Importantly, these zygotic genes are not immediately transcribed after fertilization and egg - laying. Instead, the earliest stages of embryonic development are controlled by proteins and RNAs deposited by the maternal germline cells. These maternally contributed RNAs and proteins comprise an estimated 30-65% of the protein coding genome of the embryo (Arbeitman et al., 2002; Lécuyer et al., 2007; Tadros & Lipshitz, 2005), and control a significant portion of the earliest developmental stages, including polarity establishment, cell fate determination, and patterning (Schüpbach & Wieschaus, 1986b;

Nüsslein-Volhard et al., 1987; Winslow et al., 1988). The maternal - to - zygotic transition regulates the destabilization and degradation of the maternally - provided proteins and RNAs, and allows zygotic transcription to dictate the remainder of the developmental process. However, the rate at which these maternally provided materials are degraded varies (Tadros & Lipshitz, 2009), and many embryonic processes involve both maternal and zygotic components (Wieschaus, 1996a). As a result, even in zygotic screens, the presence of maternally - contributed protein can compensate for the lack of zygotic protein and minimize the mutant phenotype.

Early efforts to identify maternally contributed genes were labor - intensive and were limited in the number of genes that could be identified, as examination of mutant embryos required the generation of homozygous mutant females (Schüpbach & Wieschaus, 1989, 1986a; Nüsslein-Volhard et al., 1987). Therefore, genes required outside of early embryonic development could not readily be identified. Clonal screens using a dominant female sterile (DFS) mutation circumvent this problem neatly (St Johnston, 2002). This technique uses a dominant female sterile mutation in the *ovo* gene to prevent the formation of fertile eggs. Initially, clones were created by irradiating female flies with X-ray radiation to induce homologous recombination (Perrimon, 1984; Perrimon et al., 1986). Clone generation was made much more efficient with the discovery of the yeast Flp/FRT system in 1989; expression of the Flp recombinase in *Drosophila* allows for efficient recombination between FRT sites (Golic & Lindquist, 1989). Combining these two techniques led to the generation of the FLP-DFS technique, and it is now possible to generate germline clones on the autosomes as well as the X chromosome (Chou & Perrimon, 1992, 1996). This technique has made it possible to identify a wide variety of genes required for but not specific to early embryogenesis (St Johnston, 2002).

1.4.1.3 EMS mutagenesis is a common method of generating mutants in saturation screens

Forward genetic screens require the creation of collections of mutations randomly distributed throughout the genome, followed by the phenotypic characterization of each using a particular assay in the system of interest and the identification of the causal mutation in mutants with the desired phenotype(s). Random mutations are typically generated by inducing DNA damage using chemicals or radiation, or through the insertion of disruptive DNA elements into the genome. One commonly used chemical mutagen in flies is EMS (ethylmethysulfonate), an alkylating agent that creates single point mutations (and occasionally small deletions or other rearrangements) by causing mispairing of alkylated guanine with thymine (Pastink et al., 1991; St Johnston, 2002; Greenspan, 2004; Ashburner et al., 2005). Treating males with low doses of EMS allows for the generation of a collection of mutations distributed relatively uniformly across the genome with, on average, a single lethal hit per chromosome arm (Lewis & Bacher, 1968; Greenspan, 2004; Ashburner et al., 2005). The relatively unbiased nature of EMS mutagenesis allows saturating screens to be performed, which increases the odds of identifying all the relevant players in the pathway of interest. Furthermore, it allows the creation of allelic series, or mutations in a single gene of varying severity (ranging from completely null alleles to subtle missense mutations). The range of phenotypes obtained from these differing mutations are often essential for gene identification and the characterization of gene function (St Johnston, 2002).

1.4.1.4 Recent advances allow for the efficient identification of randomly-induced, X-chromosome mutations

Upon selecting mutants with relevant phenotypes, each mutation must be mapped to a region of the chromosome before the causal gene can be identified. Common mapping strategies include meiotic mapping, which requires tracking the recombination events between the mutated chromosome and a chromosome marked with visible markers (Lindsley & Zimm, 1992; Ashburner

et al., 2005), marked P-elements (Zhai et al., 2011), or SNPs (Berger et al., 2001; Martin et al., 2001; Chen et al., 2008; Schnorrer et al., 2008) to determine which markers are most closely linked to the mutation in question; deletion or deficiency mapping, where one searches for a known chromosomal deletion that fails to complement the mutated chromosome (Greenspan, 2004; Parks et al., 2004; Ryder, 2004); and duplication mapping, which tests for complementation or rescue of the mutant phenotype between the mutant chromosome and a chromosome carrying a duplication of the mutated gene (Greenspan, 2004; Cook et al., 2010; Venken et al., 2010). In addition, complementation testing between the mutant lines isolated from the screen is often performed. Recently, whole genome sequencing approaches have been combined with recombination mapping strategies (Obholzer et al., 2012; Doitsidou et al., 2010; Chen et al., 2008; Schnorrer et al., 2008), making what was traditionally a very tedious and labor-intensive strategy somewhat less so. However, whole genome sequencing frequently reveals multiple differences between the wild-type and the mutagenized chromosome. Therefore, these methods are most effective when many recombinant chromosomes can be generated and their sequences compared, to eliminate mutations that do not track with the desired phenotype. In contrast, deficiency and duplication mapping can be completed with a single cross between the mutant of interest and each deficiency/duplication. Until recently, recombination mapping and deficiency mapping were the dominant techniques with the largest collection of reagents available for determining the location of a newly isolated mutation, while the reagents available for duplication mapping were relatively limited (Cook et al., 2010; Venken et al., 2010).

Many saturating screens for viable mutations have been conducted on all of the major chromosomes (X, 2nd and 3rd) in *Drosophila* (Venken et al., 2010). However, although the X chromosome in *Drosophila* contains nearly 20% of the total euchromatic DNA equalling nearly 15% or approximately 2300 protein coding genes (Rubin & Lewis, 2000; Celniker & Rubin, 2003; Venken et al., 2010), most saturating screens seeking to identify lethal mutations affecting *Drosophila* development have been conducted on the second and third chromosomes, and have avoided the X chromosome. The main reason for this is that in *Drosophila*, as in many

species, males have only a single copy of the X chromosome. Therefore, techniques for gene identification that require the passage of mutant chromosomes from the male, such as deficiency or complementation mapping, are impossible. While recombination mapping techniques are feasible on the X, they are poorly suited to high-throughput applications, as is required for large-scale, chemical mutagenesis screens. Additionally, recombination mapping often fails to provide the fine-grain mapping information that facilitates gene identification. On the autosomes, this is not a serious problem, as using deficiency mapping in parallel or in series can make up for this lack of information. For the X chromosome, in contrast, most classically available duplications are also very large and poorly suited to fine-grained mapping (Venken et al., 2010; Lindsley & Zimm, 1992). As a result, despite accounting for a fifth of *Drosophila* genes, relatively few screens have been performed on the X chromosome.

1.4.1.5 Creation of duplication collections facilitate X-linked gene identification

Two groups have recently undertaken to correct the deficit of reagents that can be used to map sex-linked, lethal mutations. In an ongoing project at the Bloomington *Drosophila* Stock Center, Cook et al. have created a set of large Y-linked X-chromosome duplication stocks (Cook et al., 2010). Their approach, using FLP-FRT site-specific recombination technology to create *attached-XY* chromosomes, followed by repeated irradiation to induce internal deletions of the X-chromosome genetic material, produced 19 'parent' Y-linked duplications. The irradiation-induced deletion process was repeated for each of these 19 parent duplication, creating 19 sets of nested duplications. The endpoints of each duplication were then cytologically and molecularly mapped. The 19 'parent' duplications for each nested set range from 0.32 to 1.68 Mb, with smaller 'child' duplications ranging from a few kb up to 1.68 Mb (Cook et al., 2010). At the time of publication, the 221 publicly-available duplication stocks covered approximately 78% of X euchromatin and at least 78% of X-linked gene; as this work has been ongoing this collection now totals 328 nested stocks at 97-98% coverage of the chromosome (Bloomington Stock Center). This collection of large Y-linked duplications allows for rapid identification of the

broad genomic region in which a mutation of interest lies. However, 40% of these duplications are still estimated to contain 10 or more genes apiece, with a median size of 9 genes, making them most appropriate for medium resolution mapping.

The inability to obtain fine resolution mapping information from these Y-linked duplication stocks due to their large size and nested, rather than tiling, structure might have posed a problem for the future of X-chromosome mapping efforts, had a second group not also been creating an alternate type of duplication stocks. At the same time as the Cook *et al* study, Venken *et al* in the Bellen lab at Baylor College of Medicine used P[acman] BAC clones (Venken et al., 2006) to create an initial series of 408 molecularly defined small duplications inserted onto the third chromosome (Venken et al., 2010). These insertions range in size from 70 to 120 kb, with an average length of 88 kb, and cover approximately 96% of the X euchromatin. Furthermore, they are highly overlapping, making them ideal for fine resolution mapping. Of the duplication stocks created in the initial Venken *et al* study, 22 coverage gaps are reported. 5 of these had no corresponding mapped clones in the BAC libraries used to generate these duplications. The remaining 17 had corresponding mapped BACs, but no duplication stock containing the BAC was recovered in the initial screen; these were marked by the authors for future re-testing. The authors predicted that these gaps were likely to be covered in part by the large Y-chromosome duplications generated by Cook *et al*. As with the Dp(1;Y) collection, work on the Dp(1;3) and P[acman] BAC collections has been ongoing, and the coverage gaps in the initial collection have now been almost completely filled in, bringing the size of this publicly-available collection up to 455 stocks (Bloomington Stock Center; FlyBase Consortium, 2016). In conclusion, as a result of the efforts by these two groups, the entirety of the X-chromosome can now be mapped efficiently and with nearly full coverage using a mere 60 duplication stocks (Bloomington Stock Center). As a result, the technical barrier to mapping X-chromosome mutations, such as those resulting from high-throughput chemical mutagenesis screens, has been virtually eliminated, and the X chromosome is now open to the large-scale screening efforts that have previously

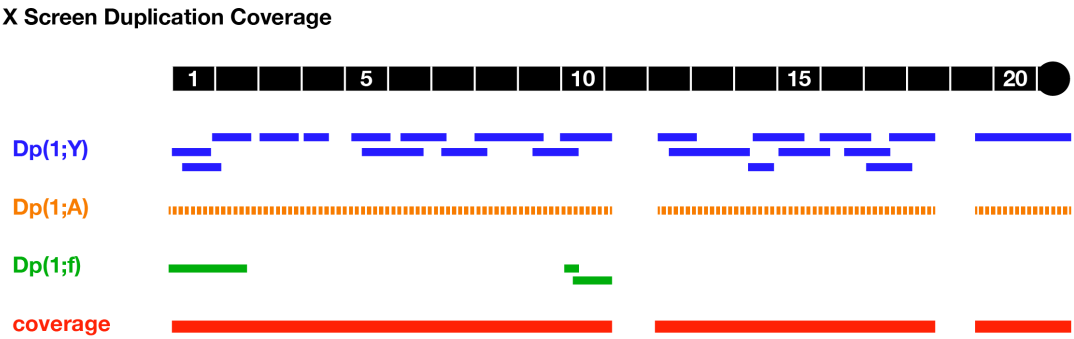

Figure 1.5: X-chromosome duplication coverage. Schematized representation of the X-chromosome duplication coverage during the time this screen was performed (2010-2012). Three types of duplications exist, covering approximately 90% of the X-chromosome (chromosome, black line; coordinates in Mb, white lines/text). Dp(1:Y) (Cook et al., 2010) (top, blue) are large ($\geq$100kb) Y-linked deficiencies generated through chromosomal inversion; Dp(1;A) (Venken et al., 2010) (middle, orange) are smaller (70-120kb) molecularly defined deficiencies generated on the autosomes using the P[acman] BAC library; and Df(1:f) (Lindsley & Zimm, 1992) (bottom, green), several pre-existing 'free' extrachromosomal duplications. Total coverage is indicated in red at the bottom. At the time this screen was performed, three large coverage gaps (at 13A - 13F (approx. 1 Mb), 16D7 - 16F4 (approx. 0.3 Mb), and 18A - 18F (approx. 0.8 Mb)) and assorted smaller gaps existed. A number of these coverage gaps have since been filled by additional molecularly defined duplications attached to the autosomes (Bloomington Stock Center).

been restricted to the autosomes. An illustration of X chromosome duplication coverage as of 2010 can be seen in **Figure 1.5**.

1.5 Organization of subcellular structures

Controlling the size, number, and subcellular distribution of intracellular organelles is critically important to developing functional cells and tissues (Chan & Marshall, 2012). The ER and mitochondrial network, for instance, must attain a certain minimum size in order to meet the biosynthetic or energy requirements of the cell, while the ability of flagella and cilia to generate and sense the mechanical forces required for cell motility, organ development, and organ function is dependent on their length (Ishikawa & Marshall, 2011, 2014). Loss of control of structure

size is a hallmark of disease; changes to nuclear size and morphology and centriole number are commonly used as a diagnostic tool in oncology (Cunha-Ferreira et al., 2009; Zink et al., 2004), and changes in centriole number or incorrect sizing of the mitotic spindle can lead to defects in chromosomal segregation (Goshima & Scholey, 2010). Of equal importance is the distribution and placement of both molecules and of macromolecular structures within the cell. The establishment of cell polarity, for instance, which is one of the hallmarks of epithelia, requires the precise distribution of junctional components to distinct cellular locations. Other precise patterns of organized subcellular structures are found in diverse tissue types, including branching and tiling patterns generated by neurons (Grueber & Sagasti, 2010), the periodic distribution of proteins observed in axons (Taylor, 2006; Xu et al., 2013), the complex positioning and scaling of centrosomes and spindles required for oriented cell divisions (Bergstralh et al., 2013a), and the regular spacing of nuclei in the cytoplasm of multinucleate cells (Bruusgaard, 2006; Metzger et al., 2012; Anderson et al., 2013; Gundersen & Worman, 2013). Despite the differences in the nature of these subcellular structures and the varied cell types, many of these examples use similar methods to generate subcellular organization.

Of course, length, size, and organization is not actively controlled for all subcellular structures (Rafelski & Marshall, 2008; Marshall, 2016). While the nucleus, centrioles, and a number of other structures have clearly defined, if not entirely understood, control mechanisms that restrict copy number, other structures, such as the vacuoles, Golgi, and peroxisomes in yeast, fluctuate in a manner which suggest a stochastic copy number determination without feedback controls (Mukherji & O'Shea, 2014). Similar caveats apply to the lengths or sizes of structures. Determining whether these active feedback mechanisms apply to a given system requires testing whether the distributions of the features possessed by these subcellular structures is markedly different from a null hypothesis of what the pattern would look like in the absence of a control mechanism. For instance, when considering the regulation of subcellular structure size, a limiting component model can be viewed as such a null hypothesis (Marshall, 2015a,b, 2016). In this model, the only restriction to structure nucleation and growth is the concentration or quantity

of molecular building blocks available, and there is no feedback pathway to sense and modify structure size. For questions of subcellular structure positioning or placement, one possible null hypothesis is that structures are randomly distributed. Alternatively, the null hypothesis might be that structures are be clustered together and/or fail to separate. Distinguishing between these active and passive mechanisms of organization is essential for accurate characterization of organization phenotypes. Given the diversity of these order-generating mechanisms and the distinctive patterns that can be observed, studying subcellular scaling and organization mechanisms can provide insight into how cells function in healthy and damaged cells.

In the following sections, I will discuss the mechanisms used by cells to establish and maintain the size and organization patterns of their intracellular structures throughout growth and development. These fall into three broad sections: First, how do cells measure length? Second, how do they count structure number? Finally, how does organization follow from these measuring and counting mechanisms? Although they are separated for simplicity, it is important to note that interplay between these broad categories of mechanisms regulating subcellular structure organization is not only possible but quite likely.

1.5.1 How do cells measure size/length?

The first step to generating organization at the subcellular level is through mechanisms by which cells can measure size, including the total size of the cell itself, the size of individual subcellular structures, and the distances separating those structures. Of course, not all of these mechanisms require a feedback mechanism in the form of an activated protein or pathway to report the current size or state of an intracellular structure. In the most simplistic models to limit organelle growth, maximum organelle size might be determined simply by temporal or spatial constraints. Given an unlimited supply of building materials and an incorporation rate dependent only on concentration, organelle size would be expected to increase linearly with time. In this case, an organelle that has had more time to grow, or has a higher growth rate, will end up larger

than an organelle that has had less time to grow or has a slower growth rate. However, many structures show patterns of size scaling that eliminate this simplistic view of size control. These mechanisms of size control fall into four general classes, which can work independently or in concert to produce appropriately sized structures: molecular ruler models, limiting component or limiting pool models, concentration-dependent phase transition mechanisms, and dynamic balance models. Examples of each model can be found in Figures 1.6 - 1.9.

1.5.1.1 Molecular ruler models

Molecular ruler mechanisms use the length of a protein scaffold or a protein gradient to establish the length or size of a target structure. One classic example of length control by a protein scaffold is the tail length of the bacteriophage λ, which is determined by the product of gene *H*; changes to the length of *H* directly correlate with changes to the length of the tail (Katsura, 1987). A second example of a molecular ruler is in neurons, where actin and spectrin form a periodic banding pattern that is repeated at a distance equal to the length of a tetrameric assembly of spectrin (Xu et al., 2013), although whether this periodic pattern is truly controlled by spectrin has yet to be determined (**Figure 1.6**). The limitation of such a scaffolded molecular ruler model is that the scaffold protein must be equal to the size of the target organelle; this makes it difficult to see how the size of very large structures could be regulated using this mechanism. Furthermore, such a ruler mechanism is scalable only in fixed length units, which do not necessarily relate to the size of the cell, and are not dynamically adjustable. Therefore, such molecular rulers are useful for systems where the generation of highly periodic structures are required, but do not do well to explain how macromolecular structures might scale in proportion to cell size: for instance, how the same organelle might be large in a large cell, but small in a small cell (Rafelski & Marshall, 2008; Chan & Marshall, 2012; Goehring & Hyman, 2012; Marshall, 2015a,b; Reber & Goehring, 2015).

The formation of the actomyosin contractile rings during cytokinesis in early *C. elegans* development is also thought to be guided by a molecular ruler model that produces 'contractile units' of fixed size. Cells in the early *C. elegans* embryo undergo numerous cell divisions within the confines of a fixed-size egg shell. Since the total embryo size remains constant, the size of each individual cell is reduced significantly with each subsequent cell division cycle. Surprisingly however, the time that is needed to complete each division is constant, raising the question of how the rate of actomyosin contraction in the contractile ring is controlled. Careful monitoring of contractile ring size over time in the developing embryo revealed that contractile ring closure occurs in two steps: an initial, constant phase, in which constriction procedes at a fixed rate independent of initial ring diameter, and a second phase in which constriction rate decreases linearly with cell perimeter (Carvalho et al., 2009). This observation is consistent across cells of different developmental ages, and thus, different sizes, and neither the embryonic stage, nor genetic alteration of embryo size disrupted proportionality between cell size and constriction rate. Work done in sea urchins and *S. pombe* suggests that as the ring closes, the volume of actin in the ring decreases, implying that actin filaments are removed from the ring as it constricts. In *C. elegans*, cells treated with LatrunculinB, a drug that sequesters G-actin, are largely able to complete cytokinesis in a normal manner, suggesting that actin turnover is not required for constriction. Furthermore, live imaging studies of contractile ring components (myosin, septin, and anillin) demonstrate that the concentration of these proteins is directly proportional to ring size. These data suggest the contractile ring, whose initial size is directly proportional to cell size, may be composed of fixed-length 'contractile units', and that this number remains constant as constriction progresses. As the number of contractile units that will assemble in the ring will be proportional to the diameter of the cell, and each contractile unit disassembles at a set rate, the overall constriction rate will be equal to the number of units times the disassembly rate, and will therefore scale with cell size. As a result, total time from the beginning to the end of cytokinesis will be independent of the initial size of the cell (Carvalho et al., 2009). This model offers the benefits of a fixed ruler model in that constriction proceeds at a fixed rate, with the added flexibility to adjust to the size of the cell as needed.

A molecular ruler that is even more responsive to changes in cell size has been proposed for the scaling of spindle length in the *C. elegans* embryo. In *Xenopus* and *C. elegant*, the size of mitotic spindles is consistent within a particular cell type, but can vary dramatically between different species (Karsenti & Vernos, 2001; Brown et al., 2007; Wühr et al., 2008). Cell mixing experiments in *Xenopus* suggest that this is due to a cytoplasmic factor (Brown et al., 2007). Careful quantification of intracellular structures in wild-type embryos has demonstrated that spindle length directly correlates with centrosome size. Decreasing the levels of centrosomal proteins via RNAi reduces centrosome size, and also produces a corresponding decrease in spindle length (Greenan et al., 2010). A series of RNAi knockdown experiments demonstrates that centrosome size determines the length of the gradient of TPXL-1, a protein that interacts with AuroraA during spindle assembly. Decreasing the amount of TPXL-1 via RNAi knockdown decreases spindle length, demonstrating that the gradient of TPXL-1 acts as a molecular ruler to set spindle length, although it is not known how this gradient is established (Bird & Hyman, 2008; Greenan et al., 2010) (**Figure 1.6**).

1.5.1.2 Limiting component models

Limiting component models, which link organelle size to total cell volume, have been proposed for controlling the size of a wide range of intracellular structures, including the size of the mitotic spindle (Hara & Kimura, 2009; Good et al., 2013; Hazel et al., 2013), centrosomes (Decker et al., 2011), nuclei (Jevtic et al., 2015; Edens et al., 2013; Hara & Merten, 2015; Conklin, 1912), and nucleoli (Brangwynne et al., 2011; Weber & Brangwynne, 2015). A very common mechanism for limiting the size of intracellular structures in direct proportion to cell size, the limiting component hypothesis relies on there being one critical component that is required to build the organelle, but that is strictly rationed in number or ratio to the other necessary materials. This limited material is the so-called ‘rate limiting’ component. Concentration of this critical subunit decreases as the size or total number of the organelle increases, limiting the ability for growth or for new structures to form. This is balanced by disassembly of the organelle, which

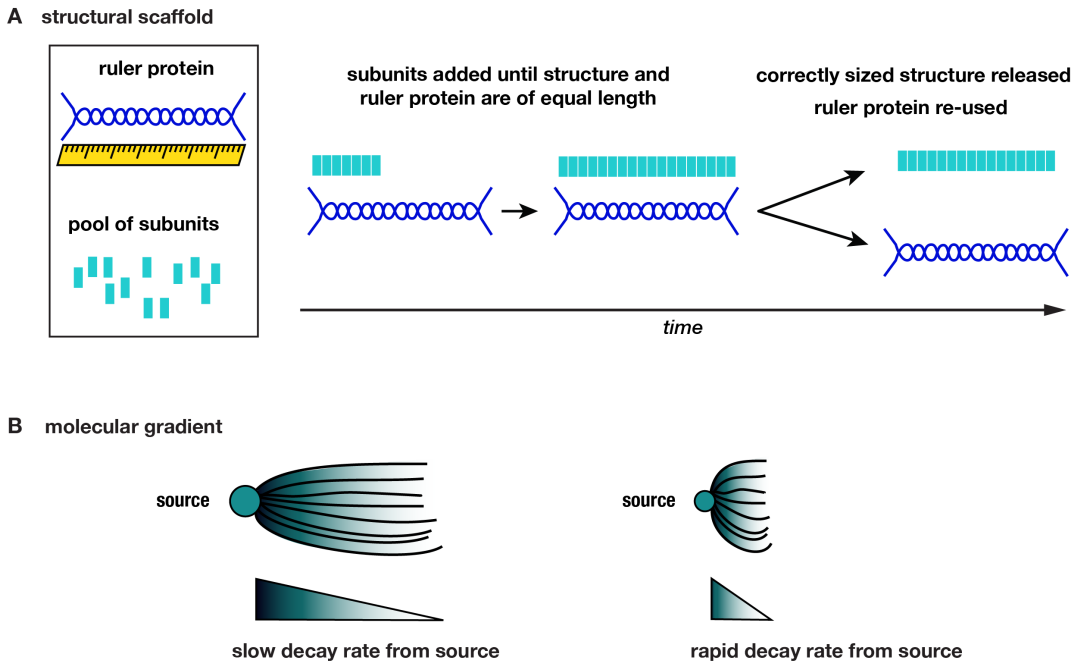

Figure 1.6: Molecular rulers can take the form of either a protein or other physical scaffold structure or a molecular gradient A. A protein (blue) of a given size provides the length template for the final organelle as individual molecular components (cyan) assemble into a macromolecular complex (progression from left to right). **B.** A protein gradient controls the length of astral microtubules between the chromosomes and the centrosome. Proteins with a slow decay rate (left) produce longer gradients, and thus, longer structures, than do those with a rapid decay rate.

releases the rate-limiting component back to the larger pool. As a result, limiting component mechanisms are self-adjusting and will ultimately, if there are no external agents that alter the pool (more below), reach and maintain an equilibrium state. Importantly, this equilibrium does not require the cell to actively adjust assembly rate or measure structure size; instead, this dynamic equilibrium is reached naturally, and self-adjusts to fluctuations in cell size. Furthermore, this size scaling can occur in the absence of a dedicated size sensor, as entire cell acts as a yardstick (Goehring & Hyman, 2012; Reber & Goehring, 2015; Chan & Marshall, 2012; Marshall, 2015b). The limiting component hypothesis makes several important predictions. First, there should be a constant, linear relationship between total organelle volume and cell volume; this is the basic tenet of the limiting component model. Second, for this linear relationship to hold true, the combined total volume of all organelles in a single cell must be independent of the

organelle number. This means that in cells of a given size range, those with a greater organelle number will have smaller organelles, while in those with fewer, each structure will be larger (i.e., $V_{organelle} = \frac{V_{organelle-total}}{N}$, where N is the number of organelles in the cell and V is the indicated volume) (**Figure 1.7**).

The limiting component mechanism is well illustrated in the case of centrosome size control (Decker et al., 2011). The *C. elegans* embryo begins its life at a constant size, with a fixed quantity of maternally delivered molecular components. Over time, cell divisions occur in the absence of cell growth, and the maternally supplied components are distributed to each of these smaller cells. Through this process, the size of the centrosomes (and the mitotic spindle, whose length is at least partially based on centrosome size (Greenan et al., 2010)) in each daughter cell decrease noticeably, and in proportion to the decrease in cell volume. However, the sum of the sizes of all centrosomes in the embryo remains constant. Mutation of ZYG-1, a gene known to control centrosome number, was sufficient to alter centrosome number, but did not affect total centrosome volume. This study also identified a protein required during centrosome development, SPD-2, that acts as a limiting component in determining centrosome size. Modulating the amount of SPD-2 expression via overexpression in embryos altered centrosome size, suggesting that the control of centrosome size is indeed being dictated by a limiting component model responsive to cell volume (Decker et al., 2011). Studies of centrosome regulation in *Drosophila* embryos have reached similar, supporting conclusions (Conduit et al., 2010; Conduit & Raff, 2010). Further work will be required to test the specifics of how SPD-2 affects centrosome size. In particular, measuring the concentration dependence of proteins throughout the cell has been difficult technically, and very little is know about how the tight regulation of protein concentration necessary for such a limiting component model might be regulated (Decker et al., 2011).

Limiting component models have also been proposed to explain the scaling observed in the creation of the mitotic spindle. Spindle size scales with cell size in a variety of systems, including in frogs (Hara & Kimura, 2009) and worms (Greenan et al., 2010). In *Xenopus* extracts, altering cytoplasmic volume produces a corresponding change in spindle length (Good et al., 2013;

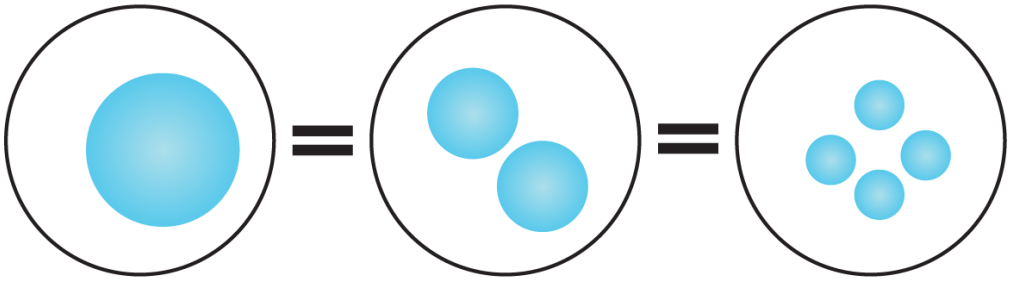

Figure 1.7: Limiting component mechanisms maintain a constant structure volume
In a limiting component model, cells of the same size will produce the same total volume of subcellular structure, regardless of the total number of structures.

Hazel et al., 2013); in contrast, changing the shape of droplets through compression (Good et al., 2013) or using microfluidics chambers of different shapes (Hazel et al., 2013) does not. Furthermore, these cues do not require the cortical signals, as scaling is recapitulated in membraneless droplets of differing sizes (Good et al., 2013). These data indicate that scaling is most likely due to size, not geometry, and suggest that scaling may be regulated by limiting some cytoplasmic factor or factors. Scaling is uncoupled from cell size in the earliest stages of *Xenopus* development (Wühr et al., 2008; Good et al., 2013), when the cell is at its maximum size, further supporting the idea that cytoplasmic components may dictate spindle length. However, what factors contribute to this size-dependent scaling have yet to be uncovered.

1.5.1.3 Concentration-dependent and phase transition mechanisms

An alternative interpretation or addition to the limiting component hypotheses posed for the scaling of centrosomes and spindles is a phase transition mechanism. In physics, phase transitions are the point at which matter shifts between solid, liquid, and gaseous forms. While a common initial perception is that these transitions occur relative to temperature (e.g., liquid water become solid ice as it cools) or pressure (e.g., CO_2 in a can of soda being released as

gas when the can is opened), molecular concentration, as well as many other features, can modulate the point at which phase transitions occur (Brangwynne, 2013). In cells, the cytoplasm is not simply a solution of soluble proteins, but a complex fluid that undergoes phase separations to create multiple sub-domains of concentrated proteins and RNAs (Walter & Brooks, 1995). Examples of such structures include P-granules, processing bodies, stress granules, Cajal bodies, nucleoli, and, potentially, centrosomes and purinosomes (Brangwynne, 2013). Several types of these subdomains, including P-granules and nucleoli, have been shown to behave as liquid-like droplets within the larger semi-colloidal solution of the cytoplasm (Brangwynne et al., 2009, 2011; Li et al., 2012; Aggarwal et al., 2013; Feric & Brangwynne, 2013; Brangwynne, 2013; Wippich et al., 2013). These highly dynamic, membrane-less, cytoplasmic organelles are thought to concentrate relevant molecules within a small region, and are therefore believed to be able to control the rate of reaction between these various components (Brangwynne, 2013). In addition, these phase-transition mechanisms are thought to play a key role in establishing order within the cytoplasm (Walter & Brooks, 1995; Lee et al., 2013).

These membrane-less subcellular structures, like droplets *in vitro*, only aggregate once the concentration of proteins/RNAs reaches a certain threshold (the phase transition point), can only continue accumulating additional molecules until equilibrium with the surrounding cytoplasm is reached, and dissolve when the concentration of components falls below the condensation threshold (Brangwynne et al., 2009; Li et al., 2012; Kato et al., 2012; Lee et al., 2013). Concentration depends entirely on cell size, meaning that the size of the structure, as well as its assembly kinetics in certain cases (Knowles et al., 2011), also depends on cell size (Brangwynne, 2013). Like limiting component models, phase transition models predict that larger cells should contain larger or more numerous subcellular structures, assuming that starting concentration is maintained across cells of different sizes. Of course, this prediction is invalid if cells grow in size without making additional components (Brangwynne, 2013). However, this model is appealing in addition to or in place of a strict limiting component hypothesis, particularly

for the regulation of centrosome and spindle size, as it would allow for multiple components, rather than a single molecule, to simultaneously limit growth (Brangwynne, 2013).

The dynamics of nucleoli formation in the *C. elegans* embryo demonstrate the principles behind phase-transition-mediated structure assembly well (Weber & Brangwynne, 2015). During normal development in *C. elegans* embryos, nucleolar size scales directly with cell and nuclear volume. However, disruption of cell size produces the opposite effect on nucleolar size than would be predicted by a limiting component model; decrease of cell size resulted in larger nucleoli, while increased cell size reduced nucleolar size. Furthermore, nucleoli naturally do not form at the earliest stages of development, when cells are largest. These studies suggest that while nucleoli assemble in a cell-size dependent manner, this process is mediated by a concentration-dependent phase transition, rather than by the presence of a single limiting factor (Weber & Brangwynne, 2015).

1.5.1.4 Dynamic balance of assembly/disassembly rates

Balancing the assembly and disassembly rates of protein complexes is yet another way to regulate the size of subcellular structures. Most structures undergo some degree of turnover, and thus the ideal size is reached only when the rate of assembly equals the rate of disassembly. If the assembly or disassembly rate is dependent of the size of the structure, then this equilibrium can only be attained when the structure reaches a certain size. This is particularly evident in microtubule based structures, as the treadmilling behavior of microtubules is well known, however, similar mechanisms are believed to act for actin structures as well (**Figure 1.8**).

The flagella of the unicellular, biflagellate green algae *Chlamydomonas reinhardtii* is a common system for studying how cells control organelle size. Flagellae are dynamic, microtubule based structures, and undergo constant turnover. Experiments in which the incorporation of HA-tagged tubulin into the flagellae was tracked demonstrates that both addition and removal of subunits occurs predominantly at the distal, plus-end tip (Marshall & Rosenbaum, 2001). Blocking the

kinesin-based intraflagellar transport (IFT) system prevents this cycling (Marshall & Rosenbaum, 2001). Two kinases, LF4 and CNK2, control the balance between assembly and disassembly rate in this system (Hilton et al., 2013). Null mutations in *cnk2* produce algae with exceptionally long flagellae, which are not absorbed when the algae are transfered from liquid to solid media, as occurs in the wild type (Hilton et al., 2013). These data suggest that CNK2 is required to regulate flagella disassembly. Co-mutation of *lf4*, a gene controlling flagellar assembly rate, further increases flagella length (Hilton et al., 2013). Thus, CNK2 and LF4 appear to act in concert to regulate flagellar assembly and disassembly. As evidenced by the length change in teh *Chlamydomonas* flagellae, controlling structure assembly and disassembly rates can have a significant effect on overall structure length.

Similar assembly-rate-control mechanisms have been proposed to control the lengths of certain actin based structures, such as microvilli (Tyska & Mooseker, 2002) or the inner-ear stereocilia (Rzadzinska et al., 2004); here, treadmilling is thought to depend on various atypical myosin motors and the capping protein espin. More recently, work in budding yeast has proposed a novel mechanism to regulate actin cable length through the delivery of a formin-inhibiting protein, Smy1, to the growing actin tip (Mohapatra et al., 2015). Smy1 is a kinesin-like protein that associates with and increases the processivity of type-V myosins (Beningo et al., 2000; Lillie & Brown, 1998; Eskin et al., 2016; Lillie & Brown, 1994; Hodges et al., 2009; Schott et al., 1999; Lillie & Brown, 1992), and which has been shown to control actin cable dynamics by binding to and inhibiting formins (Chesarone-Cataldo et al., 2011; Eskin et al., 2016). This activity may be necessary to maintain organized actin networks and the actin cables required for myosin-based transport (Chesarone-Cataldo et al., 2011).

In contrast to these assembly-rate-controlled systems, control of microtubule length in the mitotic spindle in yeast is regulated by the kinesin-8 family of destabilizing kinesins, the so-called ‘antenna’ model. These highly processive motors promote microtubule disassembly specifically at the plus-end (Varga et al., 2006; Gupta et al., 2006; Hough et al., 2009; Varga et al., 2009). As kinesin-8 proteins bind uniformly along the length of microtubules, the amount of protein

recruited is directly proportional to the length of the microtubule (Varga et al., 2006; Stumpff et al., 2008). Kinesin-8 pauses at the end of its walk, only dissociating from the microtuble plus-end when the next motor arrives. Removal of each motor protein removes only one or two subunits, but the length-dependent recruitment results in the formation of a concentration gradient of motors along the microtubule length (Varga et al., 2006; Stumpff et al., 2008; Varga et al., 2009). As a result, the longer the microtubule is, the greater the rate of dissociation. Assembly rate is length-independent, therefore, narrow range of lengths is eventually achieved at steady-state (Varga et al., 2006, 2009). This regulation is required for correctly sized mitotic spindles and succesful completion of mitosis , and it is proposed that this is the mechanism by which the lengths of overlapping microtubules at the spindle mid-zone are regulated (Burbank et al., 2007; Bieling et al., 2010; Kimura & Kimura, 2011a; Subramanian et al., 2013).

In addition to providing fine control of length, mechanisms that balance the rates of structure assembly and disassembly could be used to control the volume or surface area of an organelle such as the ER, Golgi, or nucleus through the regulation of vesicle fusion/budding rates instead of polymerization/depolymerization (Rafelski & Marshall, 2008), making them highly versatile. Like molecular ruler models, such dynamic balance mechanisms do not precisely create a direct link between structure size and the size of the cell (Reber & Goehring, 2015). Instead, these mechanisms rely on some amount of predetermined component assembly/disassembly rates, which are not easily altered on the fly. However, when coupled with additional mechanisms, dynamic control of assembly/disassembly rates do provide an excellent means by which cells may scale distances relative to their size, for example, in the force-balance mechanisms thought to control spindle and nuclear subcellular localization (see following sections).

1.5.2 How do cells count number of structures?

Also important for generating intracellular organization is the ability of cells to ‘count’, or to control structure number. There is a great deal of overlap, both conceptual and mechanistic,

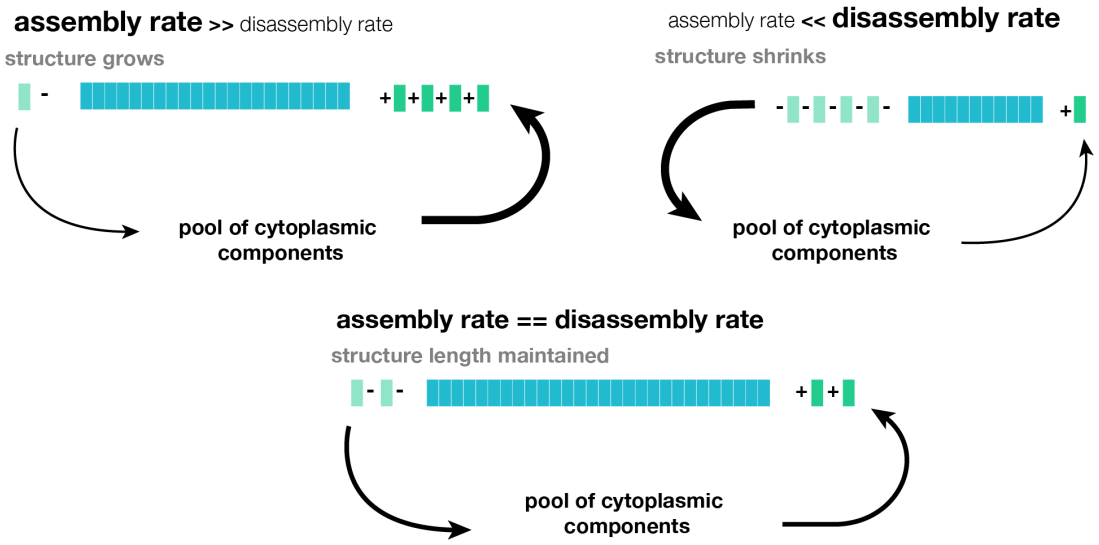

Figure 1.8: Dynamic balance mechanisms equalize assembly and disassembly rates. Maintaining the length of a subcellular structure through a dynamic balance mechanism requires equalizing the rates of assembly and disassembly. When the assembly rate is greater than the disassembly rate, the structure grows; when disassembly proceeds more quickly than assembly, the structure shrinks. Only when rates are balanced is length maintained. When either assembly or disassembly rate is controlled in a length-dependent manner, structures of a particular size may be reproducibly generated.

with the mechanisms and means by which structure length is determined discussed above. The number-control mechanisms fall into two major categories: balance and localization-based mechanisms.

1.5.2.1 Dynamic balance control of structure number

As in determining length, structure number can be controlled by balancing the rate of structure formation with the rate of structure destruction. One way that cells can determine structure number is to employ a sensor mechanism; this sensor could be attuned to the concentration of building component(s), or each organelle could produce a molecular signal that the cell can sense. This signal is capable of regulating a feedback loop that can promote the assembly of new organelles as the signal drops below a given threshold, or induce the destruction of existing ones when the signal increases above the threshold.

Several such systems have been identified in controlling plasmid copy number, which are inherited at each cell division with extremely high fidelity in bacteria. Each relies on the presence of a negative regulatory molecule, or molecular complex, that is encoded directly by the plasmid (del Solar & Espinosa, 2000). For instance, the class of plasmids that includes ColE1 and pT181 expresses a counter-transcribed antisense RNA (ctRNA), which hybridizes to and inhibits the transcription of a required RNA, thus restricting plasmid replication (del Solar & Espinosa, 2000). Mutation of these elements abrogates copy number control and can lead to plasmid loss (Tomizawa & Itoh, 1981; Brantl et al., 1993; del Solar & Espinosa, 2000). In this way, signals generated by the plasmid form a feedback mechanism by which plasmid copy number is controlled.

1.5.2.2 Structure number control by stochastic partitioning

Structure number may also be controlled by a stochastic partitioning mechanism that helps ensure organelle inheritance. In dividing cells, distribution of structures between mother and daughter can modulate number, in either a targeted ratio with cell size or other parameter, or relatively randomly via a partitioning mechanism. In yeast, mitochondrial inheritance in the bud is actively controlled through a scaling mechanism that accounts for bud size, but which frequently reduces the mitochondria to cell volume ratio in the mother (Rafelski et al., 2012). Overall, total mitochondria volume correlates strongly with total cell volume, but this scaling is observed most strongly in the bud rather than the mother (Rafelski et al., 2012). Delaying mitochondrial appearance in the bud via genetic mutation of $\triangle$ypt11 does not alter the mitochondria to cell volume ratio, although it slows growth and increases the time to division. Thus, an active feedback mechanism that senses the volume ratio is favored over a passive scaling mechanism in these cells. The mechanism through which this target volume in the bud is achieved remains unclear. However, increased mitochondrial volume ratio resulted in increased lifetime of the mother cells, suggesting that controlling mitochondrial volume can increase the replicative lifespan of the mother (Rafelski et al., 2012).

Some structures, such as endosomes and lysosomes (Bergeland et al., 2001) appear to associate with the spindle for distribution. Imaging of vesicle localization in cells undergoing mitosis shows that both endosomes and lysosomes accumulate in the perinuclear regions during cell division (Bergeland et al., 2001). This movement is dependent on the microtubule cytoskeleton, as treatment of cells with microtubule disrupting drugs such as nocodazole or taxol inhibits organelle movement (Herman & Albertini, 1984). The actual distribution process is largely a stochastic process, as measured by comparing the fractional inheritance of endosomes and lysosomes in daughters to a binomial random distribution (Bergeland et al., 2001). However, the accumulation may aid in ensuring that each daughter inherits at least some number of vesicles.

Additional work will be required to fully elucidate this distribution process and the mechanisms by which endosomes and lysosomes are inherited by daughter cells following cell division.

Inheritance of the Golgi is assured in some animals via a fragmentation method (Lucocq & Warren, 1987; Rafelski & Marshall, 2008). Quantification of Golgi-body number in electron microscopy images of HeLa cells during interphase and mitosis revealed that the number of Golgi fragments increased dramatically during mitosis (Lucocq & Warren, 1987). Upon completion of division, these fragments then re-fused to create interphase-sized Golgi bodies. Increasing the number of organelle fragments in this way, assuming that the fragments are distributed evenly throughout the cytoplasm or, as above, in the perinuclear region, ensures that daughter cells will inherit approximately half at random. This is because the partitioning of organelles into two daughter cells by random chance can be modeled by the binomial distribution, as there are two simple outcomes (a given organelle is inherited by daughter #1, or daughter #2). According to the binomial distribution, as the number of organelles or organelle fragments increases, so does the probability that both daughters will inherit an equal number increases (Lucocq & Warren, 1987). Therefore, this fragmentation method ensures that each daughter cell inherits approximately half of the Golgi volume of the mother cell. In general, this stochastic mechanism would be sufficient to control the distribution or inheritance of any structure that is present in sufficient number (in the case of the Golgi, 100 structures is estimated to be sufficient to reduce the probability that a daughter inherits no organelles to less than 10^{30} (Lucocq & Warren, 1987). Thus, these stochastic methods are a simple, but powerful, means of ensuring that the next cell generation receives the organelles required for continued existence without the need for complex feedback or control mechanisms. Furthermore, such control methods can be easily tested by quantifying number and applying simple probabilistic models.

1.5.2.3 Regulation of structure number by positional feedback

The intended subcellular localization of structures can be a powerful force in regulating their number. A wide range of cell types display some form of polarization, which establishes directional cues and creates a set of axes along which structures may be distributed. In the *Drosophila* wing, a positionally-based negative feedback mechanism regulates the production of wing hairs. The wing is planar polarized by the *frizzled* (*fz*)/*starry night* (*stan*) PCP pathway, and this polarity is required for the production of a single actin based hair at the distal vertex of each cell in the wing (Gubb & García-Bellido, 1982; Wong & Adler, 1993).

The protein *multiple wing hairs* (*mwh*) is a downstream effector of the *fz/stan* pathway that inhibits actin polymerization through antagonistic interaction with diaphanous, a *Drosophila* formin homologue (Wong & Adler, 1993; Lu & Adler, 2015). Its effects are best studied in the wing, where, in wild type, each cell produces a single, planar polarized hair at the distal vertex. In contrast, wing cells in *mwh* mutant flies form multiple short, mispolarized hairs, indicating that mwh plays an important role in hair formation. Genetic and epistasis experiments comparing the phenotypes of wing hair defects have shown that *mwh* is the most downstream of the known effectors of the *frizzled* pathway, and therefore the most likely to be involved in regulating actin during the determination of planar polarity in the wing (Wong & Adler, 1993).

Several lines of evidence point to mwh as a negative regulator of the actin cytoskeleton during the formation of the actin based wing hair. First, mwh localizes to the proximal side of each wing cell, opposite to where the wing hair will be formed (Strutt & Warrington, 2008; Yan et al., 2008). This proximal localization is dependent on the activity of the frizzled planar cell polarity pathway, as mutation of frizzled pathway effectors, including *inturned*, *fuzzy*, and *fritz*, results in mislocalization of the mwh protein and the formation of multiple wing hairs (Wong & Adler, 1993; Strutt & Warrington, 2008). Second, *mwh* mutants create additional hairs, increase the length of time during which hair initiation occurs, and form ectopic actin bundles which are more numerous than in wild type, and fail to fuse into a single structure (Strutt & Warrington, 2008; Lu

et al., 2015). Conversely, overexpression of *mwh* suppresses wing hair formation, delaying the initiation of the prehair (Strutt & Warrington, 2008). *In vitro* pulldown and actin polymerization experiments confirm that mwh is able to interact directly with the actin cytoskeleton, and inhibit actin polymerization (Lu et al., 2015).

The negative regulation of the actin cytoskeleton by mwh is thought to be mediated in part via its interaction with the formin diaphanous. Mwh and diaphanous interact directly *in vitro*, as demonstrated by co-immunoprecipitation experiments, and they co-localize to the developing hair (Lu & Adler, 2015). They also interact genetically, as expression of a constitutively active diaphanous construct recapitulates the *mwh* wing hair phenotype, and removing *mwh* in wings expressing constitutively active diaphanous enhances this phenotype (Lu & Adler, 2015). These results demonstrate that mwh is a negative regulator of the actin cytoskeleton, and functions downstream of the frizzled planar polarity pathway to regulate the initiation of the actin based wing hair. The localization of mwh along the proximal side of the cell restricts the formation of wing hairs to the distal vertex and promotes the formation of a single hair. Localization of mwh is controlled via the frizzled planar cell polarity pathway, which establishes the tissue asymmetries that provide positional feedback that allow for the coordination of cell behaviors, including the creation of subcellular structures (Zallen, 2007). Thus, the proximal localization of mwh, a negative regulator of the actin cytoskeleton, in response to activity of the frizzled planar polarity pathway, is an example of how positional feedback allows for the creation of structures with specific subcellular localization patterns (**Figure 1.9**).

1.5.2.4 Limiting component and limiting nucleation

Although they do not provide precise control, the limiting component and phase transition models could be applied to the regulation and control of structure number, as well as structure size. Limiting the amount of component materials available to nucleate new structures would be a simple way for the cell to restrict the number of organelles that could be built. *In vitro*

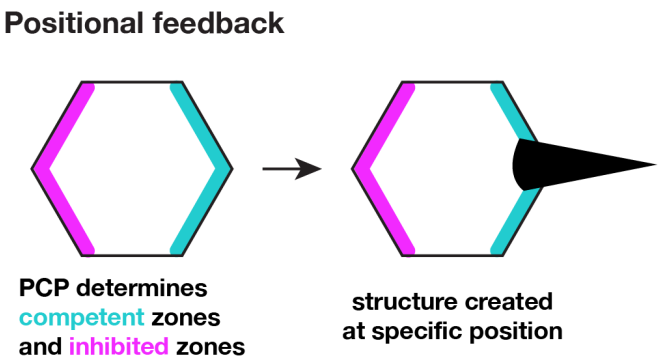

Figure 1.9: Positional feedback mechanisms. Planar cell polarity (PCP) molecules may be used to give positional feedback during the making of subcellular structures. Establishment of PCP (blue) includes the placement of an inhibitory signal (purple), which limits the competency of the one portion of the cell.

studies examining the dynamics of actomyosin contractile structures have demonstrated that a multistage process of coarsening of the F-actin network is sufficient to reorganize actin into distinct condensations (Soares e Silva et al., 2011; Thoresen et al., 2011). This process is stochastic, but live imaging of actomyosin foci creation *in vitro* suggest that aggregation is limited only by the quantity of other nearby foci, with a maximum distance for attraction between foci of approximately 25 µm. This suggests that to some extent, random capture and aggregation, combined with the diffusion, transport, and dimensional constraints imposed by the cell, could serve to limit the number of structures generated, as well as to establish a quasi-distributed localization pattern.

1.5.3 How are the positions of subcellular structures determined?

The final aspect of generating intracellular order is integration of these length control and number control systems to establish an ordered series of structures. Many of these mechanisms build on of the principles established to control structure size and number to generate reproducible, scalable organization patterns. For instance, the determination of structure number via positional feedback inherently results in structures with specific subcellular localization patterns, as occurs

during wing hair formation (Wong & Adler, 1993; Strutt & Warrington, 2008; Yan et al., 2008; Lu & Adler, 2015; Lu et al., 2015). Limiting component and phase-transition type models can also inherently limit the distribution pattern of structures in a way that will scale with the diffusion or transport patterns of components, as neighboring structures may aggregate, as occurs during the formation of actomyosin foci (Soares e Silva et al., 2011; Thoresen et al., 2011). This is particularly apparent if the distribution of molecular building blocks throughout the cytoplasm is somehow regulated, as occurs during centriole biogenesis. However, while controlling the localization of subcellular structures as they are created is a powerful method for regulating intracellular organization, it is also often necessary to move previously-generated structures to new subcellular locations to accommodate processes such as cell growth and division.

1.5.3.1 Force balance mechanisms

The most obvious example of precise positioning of an intracellular structure is the localization of the mitotic spindle and the centrosomes. Centrosome positioning is required for a number of functions, including the positioning of the nucleus, various organelles, and the cell division plane, and can be central or asymmetrically localized. Both pushing and pulling positioning mechanisms (discussed below) have been proposed for centrosome localization in different biological systems (Dogterom et al., 2005; Grill & Hyman, 2005; Kimura & Kimura, 2011a; McNally, 2013; Wühr et al., 2014), and these may act singly or in concert. The demonstrated examples of these two classes of positioning mechanisms both rely primarily on the microtubule cytoskeleton (Strome & Wood, 1983; Minc et al., 2011) to generate cellular symmetry.

1.5.3.1.1 Organization based on pushing forces

In the fission yeast *S. pombe*, centration of the nucleus and its associated centrosome is achieved through a simple microtubule based pushing mechanism (Tran et al., 2001). Live imaging of GFP-tagged tubulin in yeast cells revealed that microtubules emanate from the region

surrounding the nucleus and project outward towards the cell cortex (Tran et al., 2001). The forces that individual microtubules can exert on a substrate has been measured by anchoring one end of microtubule filaments to a fixed surface and analyzing the buckling that occurs as they push against a rigid substrate at the other (Dogterom & Yurke, 1997; Dogterom et al., 2005). These experiments show that microtubule buckling occurs at a force that is inversely proportional to filament length; therefore, shorter microtubules are able to exert a greater force on the cortex without buckling than can longer microtubules (Reinsch & Gönczy, 1998; Dogterom & Yurke, 1997; Dogterom et al., 2005; Kimura & Kimura, 2011a; Kimura & Onami, 2005). Thus, in *S. pombe*, microtubules extend in all directions from the nucleus, and microtubule growth results in pushing against the cell cortex. Since shorter microtubules are able to exert more force before buckling than longer ones, the nucleus will move towards the cell center; only when microtubule lengths equalize in all directions do these forces balance out. This type of passive, polymerization-driven pushing mechanism is sufficient for centration in yeasts (Shaw et al., 1997; Tran et al., 2001). Due to the significantly larger size of animal cells, it is thought to be unlikely that pushing mechanisms promote nuclear movement in this context (Kimura & Kimura, 2011a). However, it seems plausible that such pushing forces could be capable of acting within smaller domains in large cells, though this has not been demonstrated.

In contrast to the passive, polymerization-driven positioning mechanism described above, pushing forces actively generated by plus-end-directed motors may also be employed to localize subcellular structures. The mammalian spindle is a highly dynamic, microtubule based structure, and the sliding of antiparallel microtubules, microtubule polymerization at the spindle midzone, and microtubule depolymerization at the spindle poles all play crucial roles in chromosome segregation and cell division. In particular, the bipolar, plus-end-directed spindle kinesin Eg5 (kinesin-5) appears to be responsible for driving microtubule flux of the *Xenopus* spindle. Immunofluorescence and electron microscopy studies of the *Drosophila* kinesin-5 family member Klp-61F demonstrate that this kinesin can crosslink anti-parallel microtubule bundles, and that it associates with the mitotic spindle (Sharp et al., 1999b,a). Genetic and pharmacologic

depletion of Eg5 in *Xenopus* oocyte extracts causes a dose-dependent loss of microtuble turnover (Miyamoto et al., 2004), and Eg5 has been shown in *in vivo* motility assays in to crosslink and slide antiparallel microtubule bundles (Kapitein et al., 2005). Finally, kinesin-5 overexpression modulates the scaling of spindle length in cultured cells (Yang et al., 2016) and in *Xenopus* extracts (Mitchison et al., 2005), and a recent report has linked the overexpression of kinesin-5 to spindle lengthening in cancer cells *in vitro* (Yang et al., 2016). These data support a model in which kinesin-5 acts at the spindle midzone to crosslink and slide arrays of antiparallel microtubules apart, contributing to microtubule flux, promoting the separation of the spindle poles and localizing the centromeres and attached chromosomes away from the division plane. These kinesin-induced pushing forces could eventually be balanced by pushing forces against microtubules at the cortex to establish structural symmetry. Thus, kinesin-generated pushing forces can also be employed to localize subcellular structures.

1.5.3.1.2 Organization based on pulling forces

Cells may also employ pulling forces to position their organelles. These are often generated by the minus-end-motor dynein proteins, which move along microtubules which may be anchored at the cell cortex, to unknown structures in the cytoplasm, or to cytoplasmic organelles (Kimura & Kimura, 2011b,a; Kimura & Onami, 2005). Centration of the centrosomes in animal cells is thought be achieved through pulling mechanisms (Burakov et al., 2003; Gönczy et al., 1999). When microtubules were depolymerized locally in response to a photoactivatable version of the drug combrestatin4 in zebrafish embryos, centrosomes moved away from the depolymerized zone, supporting the hypothesis that centrosomes are moved towards the cortex by pulling forces, not pushing forces (Wühr et al., 2010). Similar experiments in the sand dollar using the microtubule depolymerizing drug colcemid reached equivalent conclusions (Hamaguchi & Hiramoto, 1986). Centrosome movement is inhibited by the introduction of a dominant-negative dynein in both *Xenopus* and zebrafish embryos, suggesting that their movement may be dynein-dependent (Wühr et al., 2010). Intriguingly, this centration does not appear to be

dependent on dynein anchored at the cortex. Microtubules in large *Xenopus* cells do not reach the cortex (Wühr et al., 2014), and close examination of sand dollar egg during fertilization suggests that no direct contact is required between microtubules and the cell cortex to achieve centration (Hamaguchi & Hiramoto, 1986). Therefore, a mutual-pulling mechanism, in which centrosomes and intracellular organelles pull on each other to attain the proper intracellular localization, has been proposed (Kimura & Kimura, 2011b). Knockdown of the dynein light chain subunit DYRB-1 in *C. elegans* embryos impedes centrosome centration, and similarly abrogates the movement of early endosomes, yolk granules, and lysosomes (Kimura & Kimura, 2011b). Tracking how organelle position changes in conjunction with centrosome movement in these cells shows that these organelles move in the opposite direction to the centrosomes, and this movement is arrested in embryos expressing DYRB-1 RNAi (Kimura & Kimura, 2011b). These experiments support a model in which centrosomes and intracellular organelles pull on each other to correctly position themselves, and demonstrate one way in which pulling forces may position intracellular structures. Thus, dynein-dependent pulling mechanisms are an additional means by which cells are able to generate patterns of symmetrically-distributed structures.

1.6 Thesis objective

The goal of my thesis project has been to use the genetically well-established *Drosophila* denticle system to identify how organization of subcellular structures is achieved, and to better understand the cell biological mechanisms controlling how micron-scale actin based structures are generated and distributed into regular but adaptable patterns. To this end, in Chapter 2 I will first describe in detail the organization pattern of the actin based denticles observed within denticle cells, and demonstrate that this robust pattern scales over a wide range of length scales as a result of dynamic microtubule activity. In Chapter 3 I will discuss the roles played by a number of additional actin and microtuble-interacting proteins in establishing the denticle pattern. In Chapter 4 I will document a forward genetic screen designed to identify new factors involved in creating denticle

structures and establishing this organization pattern, describe the phenotypes and identification of several specific targets, and discuss potential roles for how these contribute to the formation and organization of the denticles. Finally, in Chapter 5, I will discuss the intersection of work done in Chapters 2, 3, and 4, and the implications for future work in the field. The materials and methods used in this work are recorded in Chapter 6.

Chapter 2

Scaling of cytoskeletal structures with cell size in *Drosophila*

2.1 Introduction

The organization of macromolecular structures within cells is essential for many cell functions, and precise patterns of subcellular organization are observed in cells of vastly different types, origins, and dimensions. Examples include the stereotyped branching patterns of neurons and bronchial tissues (Taylor, 2006; Metzger et al., 2008; Grueber & Sagasti, 2010), the positioning of centrosomes and spindles within cells to direct oriented cell division (Bergstralh et al., 2013a), and the regular spacing of synapses and nuclei in multinucleate muscle fibers (Atwood et al., 1993; Bruusgaard, 2006; Metzger et al., 2012; Anderson et al., 2013; Gundersen & Worman, 2013). The discovery of highly ordered subcellular patterns in diverse cell types suggests that subcellular organization is fundamental to cell function. However, how cells regulate the organization of subcellular structures that are larger than individual molecules, yet smaller than the size of a single cell, is not well understood.

The distributions of macromolecular structures within cells are established during development and in many cases must be actively maintained as cells change in size and shape during cell and tissue growth. One mechanism that maintains cellular organization is the scaling of macromolecular structures with cell size. Diverse cellular structures have been shown to scale with cell size, including spindles (Wühr et al., 2008; Carvalho et al., 2009; Hara & Kimura, 2009; Good et al., 2013; Hazel et al., 2013), centrosomes (Greenan et al., 2010; Decker et al., 2011), mitochondria (Rafelski et al., 2012), nuclei (Conklin, 1912; Edens et al., 2013; Hara & Merten, 2015; Jevtic et al., 2015), and nucleoli (Brangwynne et al., 2011; Weber & Brangwynne, 2015). Several classes of models have been proposed to explain macromolecular scaling. These include models in which the size of a structure is controlled by the intrinsic dimensions of its component proteins (molecular ruler models) (Greenan et al., 2010; Xu et al., 2013), by the concentration or availability of specific molecules (limiting component models) (Decker et al., 2011; Goehring & Hyman, 2012; Good et al., 2013; Hazel et al., 2013), or by phase transitions that separate non-membrane-bound organelles from the surrounding cytoplasm like oil separating from water (Brangwynne et al., 2009, 2011; Hazel et al., 2013). However, the molecular mechanisms that underlie most scaling phenomena are poorly understood.

Significant progress has been made in elucidating the size scaling of microtubule-based structures such as mitotic spindles (Levy & Heald, 2016; Marshall, 2015a; Reber & Goehring, 2015). Much less is known about the scaling of actin structures, which have crucial roles in cell shape and tissue organization. Cells in the *Drosophila* embryo and larva produce an array of actin-rich denticle precursors that are distributed across the ventral surface of the embryonic epidermis (Dickinson & Thatcher, 1997; Dixit et al., 2008; Saavedra et al., 2014) . These micron-scale protrusions provide templates for protrusions in the overlying cuticle that are proposed to facilitate larval locomotion. Eight bands of cells on the ventral surface of the embryo, guided by segmental patterning factors, organize into columns of rectangular cells that form denticles at their posterior surface (Colosimo & Tolwinski, 2006; Price et al., 2006; Walters et al., 2006; Simone & DiNardo, 2010), a process that requires the activity of the Fat/Dachsous

planar cell polarity pathway (Repiso et al., 2010; Donoughe & DiNardo, 2011; Lawlor et al., 2013; Marcinkevicius & Zallen, 2013). Individual cells can produce as many as six denticles, which form through the coalescence of actin filaments from an initially diffuse apical actomyosin network (Price et al., 2006; Walters et al., 2006; Dilks & DiNardo, 2010). How denticles are distributed along the length of the cell so that they efficiently cover the ventral surface of the animal is not known.

Here I investigate how micron-scale actin-based denticle structures are organized within cells, and how this organization is maintained as cells grow and change shape during development. Using quantitative imaging and statistical modeling, I show that the organization of denticle precursors within cells is not random. Instead, denticle number and spacing scale with cell length over a ten-fold increase in cell size during larval growth. We demonstrate that denticle spacing is captured by specific mathematical equations and that accurate spacing requires an intact microtubule network and the microtubule minus-end binding protein, Patronin. These results identify a novel mechanism of cytoskeletal scaling that maintains spatial patterns of actin organization despite variations in cell shape and size during tissue growth.

2.2 Results

2.2.1 Denticle number and spacing scale with cell length in the *Drosophila* embryo

Actin-based denticle precursors (referred to here as denticles) are distributed throughout the ventral epidermis of the *Drosophila* embryo in an apparently regular pattern, prefiguring the placement of protrusions in the larval cuticle (**Figure 2.1 A,B**). This pattern could arise through several mechanisms. Denticles could form at a fixed distance from their neighbors (a constant spacing model), denticles could be randomly positioned within cells (a random spacing model), or the distance between denticles could scale with cell size (a scaled spacing model) (**Figure 2.1 C**).

To distinguish between these possibilities, I developed semi-automated tools in ImageJ, MATLAB, and Python to analyze denticle organization in epithelial cells (available as open source software, Materials and Methods). With these tools, the user manually delineates markers for denticle position and cell length and the software automatically generates measurements detailing multiple quantitative properties of each cell. These measurements can be plotted within the toolset or imported into other graphing software for plotting and analysis. Using this toolset, I performed a systematic analysis of denticle organization in a large number of cells in a wide range of genetic backgrounds.

Each denticle belt contains six columns of cells that express distinct combinations of cell fate determinants and display column-specific differences in cell shape, denticle number, and denticle spacing (**Figure 2.9 A-E**) (Alexandre et al., 1999; Walters et al., 2005, 2006; Dilks & DiNardo, 2010; Chanut-Delalande et al., 2012). Despite these differences, consistent patterns were observed across the entire denticle field (**Table 2.1, Table 2.2, and Table 2.3**). Denticles tended to be further apart in cells with fewer denticles and closer together in cells with more denticles (**Figure 2.9 F**). For cells with the same number of denticles, denticles in longer cells tended to be further apart than denticles in shorter cells (**Figure 2.1 D, Figure 2.9 G**). These results are inconsistent with a constant spacing model. As an alternative, I tested if denticles are randomly distributed within cells. In contrast to random distributions generated using Monte Carlo simulations, denticles in embryos were preferentially located at specific positions along the length of the cell (**Figure 2.1 E, Figure 2.9 H, Figure 2.10 H, Table 2.4**). These results demonstrate that denticles are neither uniformly nor randomly distributed in the *Drosophila* embryo. As denticle organization in embryos was not consistent with uniform or random spacing models, I next tested the possibility that denticle organization scales with cell length. Denticle spacing was positively correlated with cell length over a broad range of values, consistent with a scaled spacing model (**Figure 2.1 D**). In addition, the number of denticles per cell also increased with cell length. Shorter cells generated one denticle, whereas longer cells generated as many as six, with a new denticle added for every approximately 2 μm increase above a minimum cell

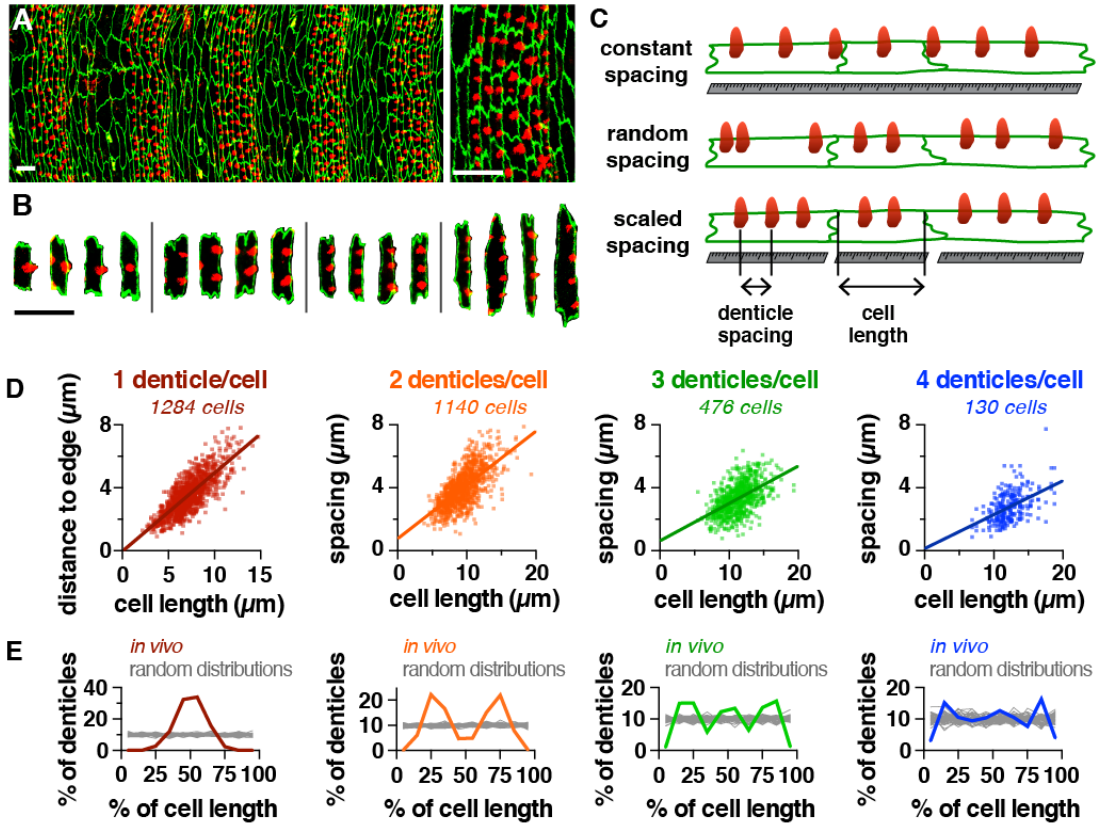

Figure 2.1: Organization of actin based denticles in the *Drosophila* embryo. A. Denticles localize to the posterior margins of ventral epidermal cells in a regular pattern. Ventral epidermis of a wild-type stage 16 embryo (left), single denticle belt (right). F-actin (phalloidin, red), E-cadherin (green). Ventral views, anterior left. **B.** Examples of cells with 1 to 4 denticles. Bars, 10 µm. **C.** Models of denticle organization. **D.** Denticle spacing vs. cell length (length of the posterior cell border, parallel to the dorsal-ventral axis) for cells with 2 to 4 denticles. Denticle-to-edge distances plotted for cells with 1 denticle (distance to the closest dorsal or ventral edge). Lines, best-fit linear regressions. Each dot represents a single denticle-denticle or denticle-edge pair. Measurements falling outside the x and y axis ranges (max. 2% of the total data in each plot) are not shown. **E.** Denticle positions *in vivo* (colored lines) were significantly different from random distributions generated by Monte Carlo simulations (grey lines) for cells with 1 to 3 denticles ($p < 0.05$ in 100% of 10,000 Monte Carlo simulations, Kolmogorov-Smirnov test). Cell length was normalized to 100%, 50 simulations/plot shown (n = 130-1,284 cells in 12 embryos (Table 2.2)).
See supplemental tables for mean $\pm$ standard deviation (SD) values (**Table 2.1**), n values (**Table 2.2**), best-fit linear regression equations and R^2 values (**Table 2.3**), and Monte Carlo simulations (**Table 2.4**).

length (**Figure 2.9 K**). These results demonstrate that two properties of cells, denticle number and spacing, scale isometrically with cell length, demonstrating that denticle cells display a scaled organization of the actin cytoskeleton.

2.2.2 The relationship between denticle spacing and cell length is captured by a single scaling equation in wild-type embryos

We next sought to determine if there is a mathematical scaling relationship between denticle spacing, denticle number, and cell length. Cell length (L) is equal to the sum of the denticle-to-edge (αD) and denticle-to-denticle (D) distances, in which α is the ratio between these distances, defined as the spacing ratio. In a scaled spacing model, the average distance between denticles is represented by the equation $D = \frac{L}{2\alpha+N-1}$ (**Figure 2.2A**). We developed code in MATLAB (MathWorks) to systematically compare *in vivo* denticle distributions to a wide range of predicted scaling patterns using simulations (available as open source software, Materials and Methods). By simulating denticle organization using different values for α (**Figure 2.2A, left**), I could identify spacing ratios that recapitulate the *in vivo* denticle distributions. In order to model the accuracy of denticle spacing, denticle positions were drawn from a normal distribution centered on the distance predicted by the spacing ratio. Varying the width of this distribution using a standard deviation term (σ) alters the size of the region to which denticles are assigned in simulations (**Figure 2.2 A, middle**), providing a measure of how accurately denticles achieve the mean spacing distance. This simulation approach has advantages over solving for single values for α and σ, because it identifies a range of values for α and σ that are consistent with *in vivo* observations, accounting for sample size and variability. This statistical modeling approach represents a generally applicable method for studying the organization of any periodic structure.

We simulated denticle placement for 40 combinations of α and σ, starting with the observed cell length and denticle number measurements in wild-type embryos, and I then predicted the

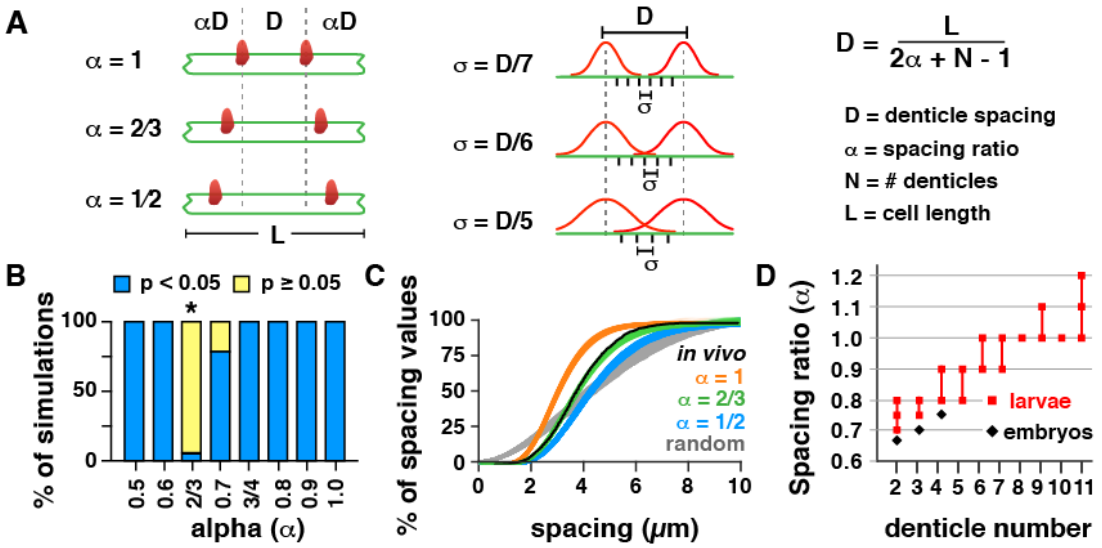

Figure 2.2: A statistical model recapitulates key features of denticle scaling. A. Models for denticle spacing (D) varying the spacing ratio (α) and standard deviation (σ). Cell length (L) and denticle number (N) were measured *in vivo*. **B.** Percentage of simulations that were significantly different from (p $<$ 0.05, blue) or consistent with (p > 0.05, yellow) *in vivo* distributions. Plot varies α for $\sigma = \frac{D}{6}$. The $\alpha = \frac{2}{3}$, $\sigma = \frac{D}{6}$ model (asterisk) most closely fit the data for wild-type (WT) embryos (p > 0.05 in 94.1% of simulations, Kolmogorov-Smirnov test). **C.** Cumulative distribution plot for models varying the spacing ratio (α) for $\sigma = \frac{D}{6}$. 1,000 simulations are shown for each model. Black line, *in vivo* measurements for WT embryos. **D.** The spacing ratio (α) increases with increasing denticle number in embryos (black) and larvae (red).See supplemental tables for a summary of the modeling outcomes in B and C (**Table 2.5**) and D (**Table 2.6**).

distances between denticles using simulations. We performed 10,000 simulations for each combination of α and σ and compared the simulated distributions to the *in vivo* patterns using the Kolmogorov-Smirnov test (**Table 2.5, Figures 2.11 , Figure 2.12**). Comparisons with p $>$ 0.05 indicate that the simulated distribution is not significantly different from, and is therefore consistent with, the *in vivo* distribution. We found that denticle spacing in wild-type embryos most closely fit a model with a spacing ratio of $\alpha = \frac{2}{3}$ and a standard deviation of $\sigma = \frac{D}{6}$ (p $>$ 0.05 in 94.1% of simulations) (**Figure 2.2 B,C, Figure 2.11 A, Figure 2.12 A, Table 2.5**). Therefore, despite substantial variations in cell size, shape, and denticle number across the denticle field, a single mathematical equation fully captures the relationship between cell length and denticle spacing in wild-type embryos. The finding that a spacing ratio of $\alpha = \frac{2}{3}$ recapitulates the distribution of denticles in wild-type embryos is consistent with a mechanism

in which denticles spread out to achieve the maximum separation, with some edge effect. We note that denticle placement *in vivo* was also slightly asymmetric with respect to the dorsal and ventral cell boundaries, with denticles often located closer to the dorsal boundary (**Figure 2.9 I,J**). This dorsal-ventral asymmetry could be present during denticle formation, or it could arise after denticle formation is completed due to cell-shape changes and junctional remodeling in the tissue (Marcinkevicius & Zallen, 2013). This asymmetry did not affect the comparison of denticle spacing between measurements and simulations, as the model only requires that the average of the denticle-to-edge values is equal to αD.

2.2.3 Denticle spacing scales over an order-of-magnitude increase in cell length during larval growth

As denticle spacing scales with cell length in wild-type embryos, I next tested whether denticle organization can accurately scale under space-limited conditions. To reduce cell size, I analyzed denticle organization in two genetic backgrounds that generate aberrantly small cells due to an additional cell division. These were the haploid progeny of *ms(3)k81 males*, which undergo an extra cell division in early embryogenesis, or embryos that overexpress Cyclin E, which have an extra division in mid-embryogenesis (Yasuda et al., 1995; Parker, 2006). The average cell length in *ms(3)k81* and Cyclin E-overexpressing (CycE-OE) embryos was reduced by 35% and 28%, respectively (**Figure 2.3 A, Table 2.1**). The number of denticles per cell was also significantly reduced in both backgrounds, with nearly twice as many cells producing only one denticle compared to wild type, and very few cells producing 3 or more denticles (**Figure 2.3 B**) (cells with no denticles were never observed, even in extremely small cells). In addition, denticle spacing was significantly reduced in *ms(3)k81* and CycE-OE embryos (**Figure 2.10 B,C**). For cells with 2 denticles in *ms(3)k81* and CycE-OE embryos, the mean cell length was reduced by 14-20% and the mean distance between denticles was reduced by 18% compared to wild type (**Figure 2.3 C-F, Table 2.1**). The denticle spacing distribution in *ms(3)k81* and CycE-OE matched the same spacing ratio (α) and standard deviation (σ) values as in wild type ($p > 0.05$ in

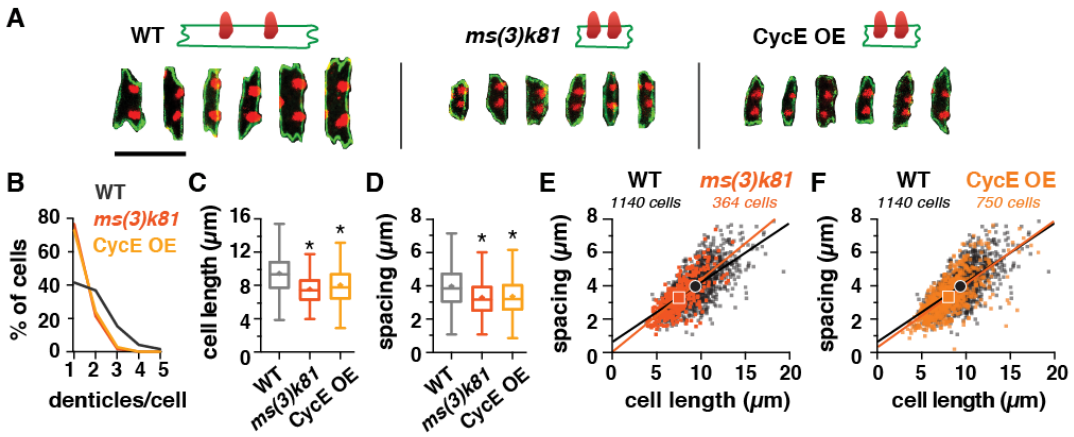

Figure 2.3: Denticle spacing scales with cell length under space-limited conditions in small-cell mutants. A. Examples of cells with 2 denticles in wild type (WT), *ms(3)k81* and CycE OE embryos. F-actin (phalloidin, red), E-cadherin (green). Bar, 10 μm. **B.** Distribution of cells with 1-5 denticles in WT, *ms(3)k81*, CycE-OE embryos. Cells generate fewer denticles in *ms(3)k81* and CycE-OE embryos. **C,D.** Cell length **C** and denticle spacing **D** were significantly reduced in *ms(3)k81* and CycE-OE embryos compared to WT. Data shown for cells with 2 denticles only. Boxes, 25th-75th percentile; whiskers, 1.5 inter-quartile range (IQR); horizontal line, median; +, mean. *, $p < 0.0001$ vs. WT, one-way ANOVA, Tukey's multiple corrections test. **E,F.** Denticle spacing vs. cell length for cells with 2 denticles. Lines, best-fit linear regressions, symbols, means. Measurements falling outside the x and y axis ranges (maximum 1% of the total data in each plot) are not shown. See supplemental tables for mean $\pm$ standard deviation (SD) values (**Table 2.1**), n values (**Table 2.2**), and best-fit linear regression equations and R^2 values (**Table 2.3**).

99.1% and 96.3% of simulations, respectively), although other similar α and σ values also fit the data (**Figure 2.11 B,C, Figure 2.12 B,C, Table 2.5**). These results demonstrate that denticle number and spacing scale with cell length in mutants with unusually small cells, following the same scaling relationship as in wild type.

2.2.4 Denticle spacing in larvae scales over an order-of-magnitude increase in cell length

As denticle number and spacing decrease in extremely small cells, I next tested whether denticle scaling mechanisms can function over long lengthscales in extremely large cells. Cells grow substantially in the *Drosophila* larval stages, and denticle cells were more than three times longer on average in first-instar larvae than in embryos (**Table 2.1**). Denticle-forming cells at embryonic and larval stages encompassed a more than 10-fold difference in length (**Figure 2.4 D**). We analyzed the organization of over 10,000 denticles in first-instar larvae, using fluorescent markers to visualize filamentous actin (F-actin) and cell outlines (**Figure 2.4 A,B**). This analysis showed that denticle number and spacing scale with cell length in larvae, extending the trend observed in embryos over longer lengthscales (**Figure 2.4 F**). For cells with the same number of denticles, denticles were around twice as far apart in larvae as their average separation in embryos (**Table 2.1, Figure 2.4 F**). In addition, the number of denticles per cell also increased with cell length in larvae, with a new denticle added for every approximately 3 μm increase in cell length above a minimum value (**Figure 2.4 C**). Individual cells could have up to 17 denticles in first-instar larvae, nearly triple the maximum number observed in embryos (**Figure 2.4 E**). Denticle spacing plateaued in cells with many denticles, suggesting that there may be an optimal spacing distance for denticles that are far from the cell boundaries (**Figure 2.5A,B**). Together, these results demonstrate that denticle number and spacing scale over an order-of-magnitude increase in cell length during larval growth.

We next asked if the scaling of denticle number and size are consistent with a limiting component model. The simplest prediction of the limiting component model is that the total volume of denticles in a cell should scale with cell volume. However, denticle volume is difficult to measure directly due to the irregular shape of denticle structures. As an approximation of denticle size, I measured the cross-sectional area of denticles and compared this to the apical area of denticle-forming cells. As cells in the epithelial sheet are predicted to have a constant height,

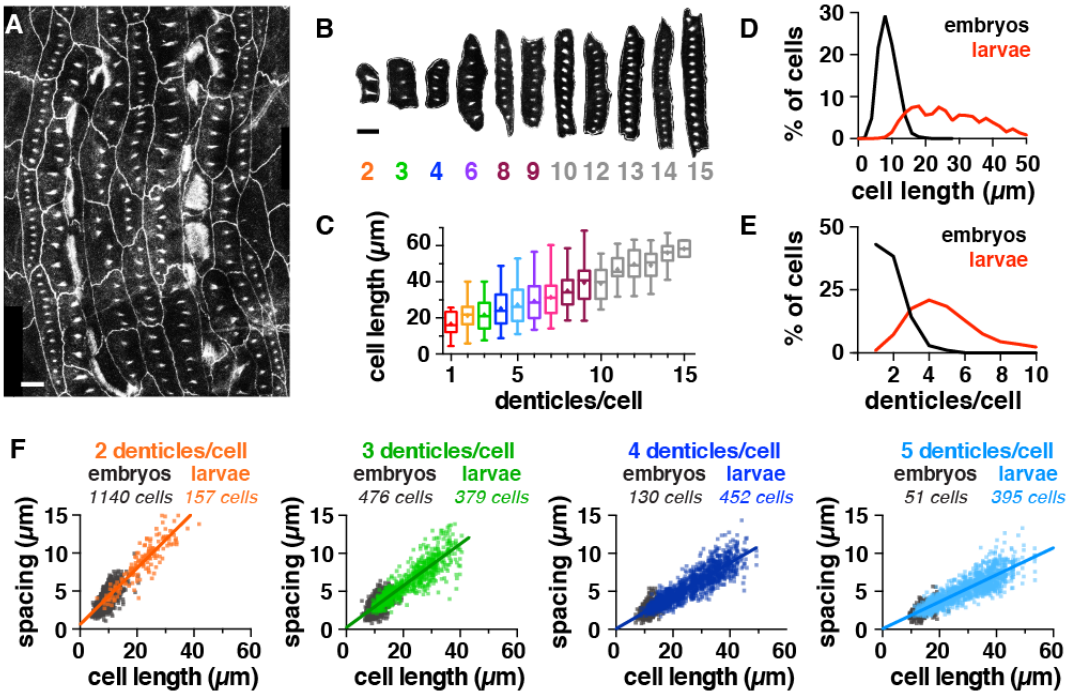

Figure 2.4: Denticle spacing scales over long distances in larvae. A,B. Denticle belt **A** and examples of cells **B** from a first instar wild-type (WT) larva. F-actin (utrophin-GFP), E-cadherin (E-cadherin-GFP). Bars, 10 µm. **C.** Denticle number increases with cell length in larval cells. Bars, 25th-75th percentile; whiskers, 1.5 inter-quartile range (IQR); horizontal line, median; +, mean. **D,E.** Cell length **D** and number of denticles/cell **E** in WT embryos (black) and larvae (red), n = 3,092 cells in 12 embryos, 2,150 cells in 18 larvae ($p < 0.0001$, Student's t-test). **F.** Denticle spacing vs. cell length for cells with 2 to 5 denticles. Embryos (grey), larvae (colors). The lines shown are best-fit linear regressions for the larval data. Measurements falling outside the x and y axis ranges (max 1% of the total data in each plot) are not shown. See supplemental tables for mean $\pm$ standard deviation (SD) values (**Table 2.1**), n values (**Table 2.2**), and best-fit linear regression equations and R^2 values (**Table 2.3**).

apical cell area is predicted to be proportional to cell volume. The total denticle area did not correlate with cell area in larval cells (**Figure 2.5 C**), suggesting that a limiting component model in its simplest form does not accurately describe the scaling of total denticle area in larval cells. However, the summed diameters of all denticles in the cell showed a strong positive correlation with cell length (**Figure 2.5 D**). Denticle diameter was also positively correlated with the distance between denticles: larger denticles tended to be further apart, whereas smaller denticles tended to be closer together (**Figure 2.5 G**). Therefore, a modified limiting component model could theoretically account for the scaling of denticle size and number if this component is proportional to the length of the cell.

We next used our statistical modeling approach to test whether the spacing ratio is a constant value in all denticle cells, or if this ratio varies in different subsets of cells. The simulations that most closely fit the denticle distribution in larvae had a spacing ratio of α = 0.8, which was larger than the spacing ratio of $\frac{2}{3}$ in embryos (p $>$ 0.05 in 95.7% of simulations, Kolmogorov-Smirnov test) (**Table 2.8, Figure 2.11 G, Figure 2.12 G**). As different spacing ratios fit the data in embryos and larvae, this indicates that the spacing ratio is not a constant value. Because larval cells produce more denticles, I postulated that the spacing ratio could vary with denticle number. To test this idea, I performed simulations for cells with different numbers of denticles. These results demonstrate that the spacing ratio was larger for cells with more denticles in both embryos and larvae (**Figure 2.2 D**). For cells with the same number of denticles, larval cells had a larger spacing ratio (**Figure 2.2 D, Table 2.6**). As cells with more denticles also tend to be longer (**Figure 2.9 K,L**), and larval cells are longer than embryonic cells on average (**Figure 2.4 D**), these results are consistent with the idea that the spacing ratio could be a size-dependent parameter.

We next analyzed the accuracy of denticle spacing, or how closely denticles achieve the optimal spacing distance for cells of a given length. To measure the accuracy of spacing, I analyzed the absolute error of denticle spacing, the difference between the observed denticle spacing distance and the distance predicted by the best-fit regression line. We found that the absolute error was

less than 1 μm on average in embryos and larvae (**Figure 2.5 F**). Although the absolute error of denticle spacing was slightly higher in larvae compared to embryos, the error relative to cell length or the predicted spacing distance was lower, despite the increase in the average distance between denticles in larvae (**Figure 2.5 F, Figure 2.9 M,N**). Similarly, the scatter of the residuals distribution, measured as the difference between the observed denticle spacing distance and the best-fit regression lines, did not increase over a several-fold increase in cell length (**Figure 2.5 E, Figure 2.10F,G**). Consistent with these findings, the standard deviation in simulations that best fit the *in vivo* denticle distribution was a smaller fraction of the denticle spacing distance in larvae ($\sigma = \frac{D}{8}$) than in embryos ($\sigma = \frac{D}{6}$) (**Figure 2.9 M,N, Figure 2.11 A,G, Figure 2.12A,G, Table 2.5**). Together, these results demonstrate a remarkably precise control of denticle organization, in which the accuracy of spacing is largely maintained even when denticles are organized over extremely long lengthscales in larval cells.

2.2.5 Denticle spacing is established at the same time as denticle formation

These results suggest the presence of an active mechanism that maintains accurate denticle spacing according to defined mathematical relationships in *Drosophila* embryos and larvae. To gain insight into this mechanism, I first used time-lapse imaging to determine when denticle spacing is established in the embryo. Denticles form through the coalescence of an apical actin meshwork into a single dense structure (Price et al., 2006; Walters et al., 2006; Donoughe & DiNardo, 2011) If denticle spacing mechanisms act before denticles form, then denticles should initiate at the optimal spacing distance from the earliest stages of denticle formation. Alternatively, if denticle spacing mechanisms act during or after denticle formation, then denticles would be predicted to form at a range of positions and then move into the optimal spacing configuration. To determine when denticle spacing is established, I imaged embryos expressing fluorescent markers for F-actin and cell outlines and tracked the localization of F-actin during stages 14 and 15, when denticles form (**Figure 2.6 A-C, Figure 2.13 A-H**). Denticle formation

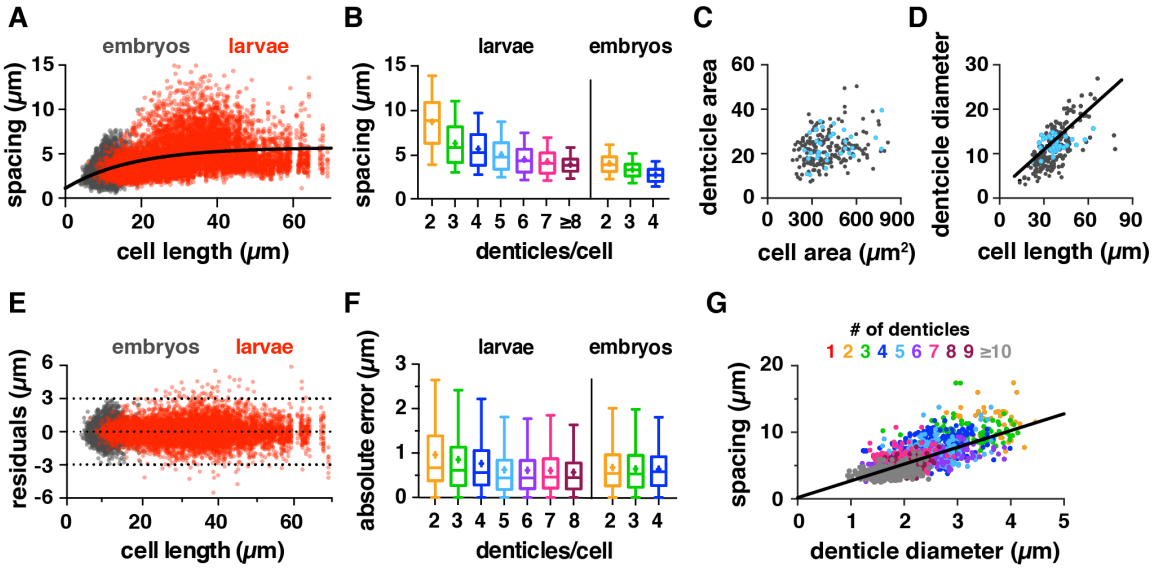

Figure 2.5: The accuracy of denticle spacing is maintained over long lengthscales in larval cells. A. Denticle spacing plateaus over long lengthscales in larvae (red). Grey, data for wild-type (WT) embryos. Best fit curve to all the data, $y = -4.6e^{-0.057x} + 5.730$. **B.** Denticle spacing decreases with denticle number. **C.** The total summed denticle area is not correlated with cell area. $y = 0.01x + 17.2$; R^2 = 0.06. **D.** The total summed denticle diameter correlates with cell length. Best-fit linear regression, $y = 0.3x + 1.9$; R^2 = 0.5. Cells with 5 denticles are highlighted in blue to show the distribution of a representative cell class. **E.** Residuals for the best-fit linear regressions for wild-type embryos (grey) and larvae (red). Dotted lines indicate 3 μm, 0, and -3 μm values. **F.** Absolute error of denticle spacing relative to the best-fit linear regressions for wild-type embryos and larvae. **G.** Denticle spacing increases for larger denticles. Best-fit linear regression (red), $y = 2.5x + 0.2$; R^2 = 0.48. For **A**, **B**, **E**, and **F**, see **Table 2.2** for n values. For **C**, **D**, and **G**, n = 1513 denticles in 223 cells from 3 larvae. Data points in **C** and **D** show summed measurements for all denticles each cell; data points in **G** show individual measurements for each denticle.

occurred as small- to medium-sized mobile foci emerged from the apical actin meshwork and coalesced. In the majority of cells (23/32 cells), the positioning of denticles was concomitant with actin coalescence. At early time points, small- to medium-sized actin foci moved toward each other until they collided to form larger precursors. This aggregation was accompanied by large shift in denticle precursor position. At later time points, as denticle precursors increased in size, adjustments of denticle position declined in frequency and magnitude over time. In a smaller fraction of cells (9/32 cells), only minor adjustments were made to denticle placement over the imaging window. In both cases, denticle position stabilized after the majority of actin had accumulated in denticles. Together, these results suggest that the refinement of denticle spacing occurs during denticle formation as F-actin structures coalesce to form large, stable denticle precursors. Small and intermediate-sized actin foci can display dynamic changes in position, but only small shifts in position occur at later stages, once large precursors have formed.

2.2.6 Denticles colocalize with microtubule minus end-binding proteins

The scaling of denticle number and spacing with cell length in larvae suggests the presence of a molecular mechanism that actively establishes and maintains denticle organization patterns during tissue growth. We speculated that this mechanism could involve microtubules, as microtubules colocalize with actin at the base of each denticle (Price et al., 2006) and apical microtubules are oriented parallel to the long axis of the cell (Dickinson & Thatcher, 1997; Marcinkevicius & Zallen, 2013). To examine the organization of microtubules in denticle cells, I analyzed the localization of three microtubule-associated proteins: Patronin, a microtubule minus-end-binding protein (Goodwin & Vale, 2010), EB1, a microtubule plus-end-binding protein, and Mud/NuMA, which interacts with microtubules and with the minus-end directed Dynein-dynactin motor complex (Merdes et al., 1996; Bowman et al., 2006; Izumi et al., 2006; Siller et al., 2006). Patronin-GFP was enriched at sites of denticle formation (**Figure 2.6 D**), and Mud was concentrated in a circular domain surrounding the nascent denticles (**Figure 2.6 E**), suggesting that denticles colocalize with microtubule minus ends. In contrast, the plus-end marker

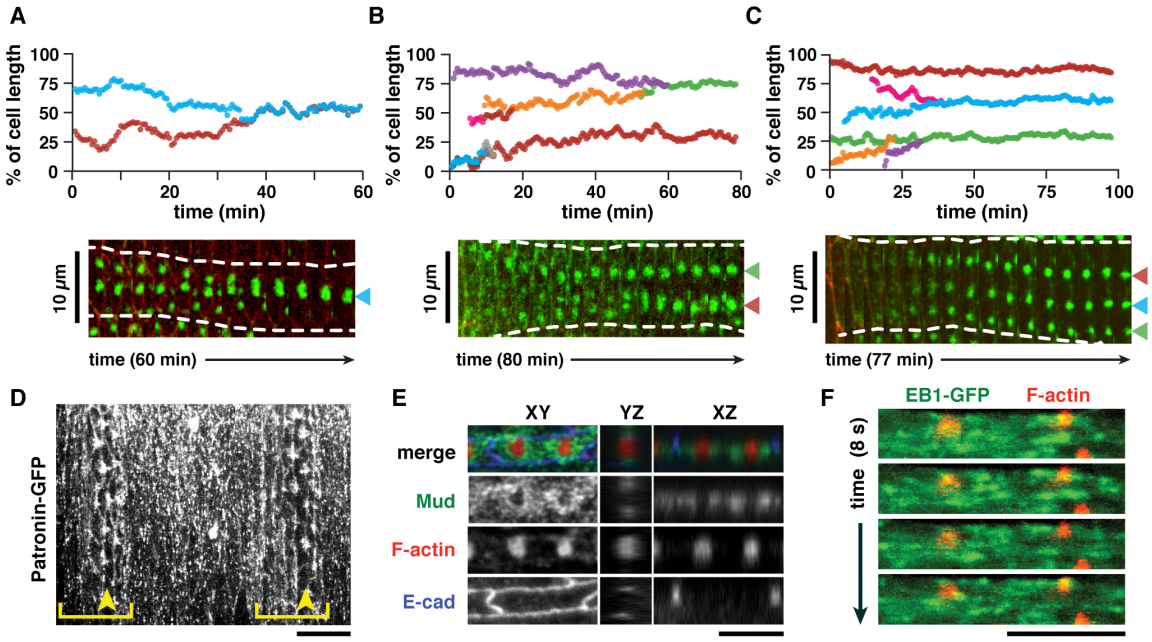

Figure 2.6: Denticles refine their position as they form and colocalize with microtubule minus-end-associated proteins. A-C. Traces of actin foci during denticle formation (mid-to-late stage 14), relative to the total length of the cell (top row) and kymographs (bottom row) of individual denticle cells. Green, F-actin; red, E-cadherin. Each color represents a unique actin focus that has been tracked over time. n = 32 cells analyzed from 6 embryos. **D.** The microtubule minus-end marker Patronin-GFP localizes to sites of denticle formation (stage 15). Brackets, denticle belts; arrowheads, denticle column 5. **E.** Mud is enriched in the regions immediately surrounding sites of denticle formation (late stage 14). Green (anti-Mud), red (F-actin), blue (E-cadherin). **F.** The microtubule plus-end marker EB1-GFP localizes to dynamic puncta that are distributed throughout the apical cellular domain (late stage 14). Green (EB1-GFP) and red (Moesin-mCherry) expressed in column 1 cells with *en*-Gal4. Bars, 10 μm in **A-C**, 5 μm in **D-F**. See also **Figure 2.13**.

EB1-GFP was present throughout the apical cytoplasm (**Figure 2.6 F**). Analysis of microtubule dynamics by imaging EB1-GFP localization in time-lapse movies revealed bidirectional movement of EB1 comets around sites of denticle formation (**Figure 2.6 F**). Together, these results indicate that microtubules are highly dynamic in the denticle field and that microtubules are organized with their minus ends concentrated at sites of denticle formation. Additional information and experiments regarding the roles of Mud and its binding partner Pins within the denticle cells can be found in Chapter 3.

2.2.7 Alterations to the microtubule cytoskeleton disrupt the accuracy of denticle spacing

To ask if microtubules are required for denticle organization, I analyzed denticle patterns in embryos in which microtubules were disrupted. Overexpression of the microtubule severing protein Spastin with the *engrailed*-Gal4 driver strongly reduced the level of cortical microtubules in column one of each denticle belt from stage 14 onwards (**Figure 2.7 B**) (14/14 embryos) (Kammermeier et al., 2003; Dilks & DiNardo, 2010). In addition, I expressed a Patronin shRNA in column 1 cells using *engrailed*-Gal4. Disruption of Patronin, which is predicted to increase microtubule minus-end dynamics (Goodwin & Vale, 2010), did not affect overall microtubule organization (**Figure 2.7 E**) (7/7 embryos). Denticles formed in Spastin-overexpressing (Spastin OE) and Patronin-knockdown (Patronin KD) embryos, but were less uniform in size than in wild type (**Figure 2.7 A**). These embryos displayed a slight increase in cell length, denticle number, and denticle spacing (**Figure 2.7 C,D, Figure 2.10 D,E, Figure 2.14 A-D**). Denticle number increased with cell length in Spastin OE and Patronin KD embryos, although with some differences compared to wild type (**Figure 2.14 G**). The microtubule-depleted cells in denticle column one of Spastin OE embryos most closely fit a model with the same spacing ratio as column one cells in wild type (α = 0.6, p $>$ 0.05 in 99.7% of simulations). In contrast, the best-fit spacing ratio for Patronin KD was smaller (α = 0.5, p $>$ 0.05 in 99% of simulations) (**Figure 2.11 D-F, Figure 2.12 D-F, Table 2.5**). These data demonstrate that knockdown of Patronin, but not an overall depletion of microtubules, alters the spacing ratio of denticle cells. This result suggests that microtubules from stage 14 onwards are not required to establish a wild-type spacing ratio, but an aberrant activity of microtubules at these stages can shift denticle positions closer to the cell boundaries.

Notably, disruption of microtubules in Spastin OE and Patronin KD embryos significantly decreased the accuracy of denticle spacing. Both perturbations caused a marked increase in the scatter of residuals around the best-fit regression line (**Figure 2.7 F**) and a significant increase

in absolute and relative error measurements (**Figure 2.7 G, Figure 2.14 E,F**). Consistent with the reduced accuracy of denticle spacing, the model that best recapitulated the data for Spastin OE had a larger standard deviation than in wild type ($\sigma = \frac{D}{5}$). Similarly, the standard deviation in Patronin KD embryos was larger than in wild type ($\sigma = \frac{D}{6}$, note that the standard deviation is expressed as a fraction of D, which is larger in Patronin KD embryos because of the smaller spacing ratio) (**Figure 2.11 D-F, Figure 2.12 D-F, Table 2.8**). These results demonstrate that two independent perturbations of the microtubule cytoskeleton significantly reduce the accuracy of denticle spacing and show that disruptions of the microtubule cytoskeleton affect distinct aspects of the denticle pattern.

2.3 Discussion

The organization of cytoskeletal structures is essential for cell and tissue function, but the mechanisms that regulate the large-scale organization of actin structures within cells are not well understood. Here, I demonstrate that the regular distribution of actin-rich denticle structures in the *Drosophila* embryo is actively established and maintained during larval growth. Actin organization is dynamically refined as filamentous actin precursors coalesce to form denticles, and both the number of denticles per cell and the distance between them scale with cell length over a broad range. Both properties decrease with reduced cell length in small cells and robustly scale over a ten-fold increase in cell length during larval growth. The relationship between cell length and denticle positioning can be recapitulated by simple mathematical equations, and two independent disruptions of the microtubule cytoskeleton disrupt the accuracy of spacing. These results demonstrate that denticle spacing is not a fixed property of denticle-forming cells, but is actively modulated by the dimensions of the cell, resulting in consistent patterns of actin organization despite substantial changes in cell shape and size during development.

How do cells control the distance between denticles? Several mechanisms of denticle spacing can be evaluated in light of the data presented here. Molecular rulers have been proposed

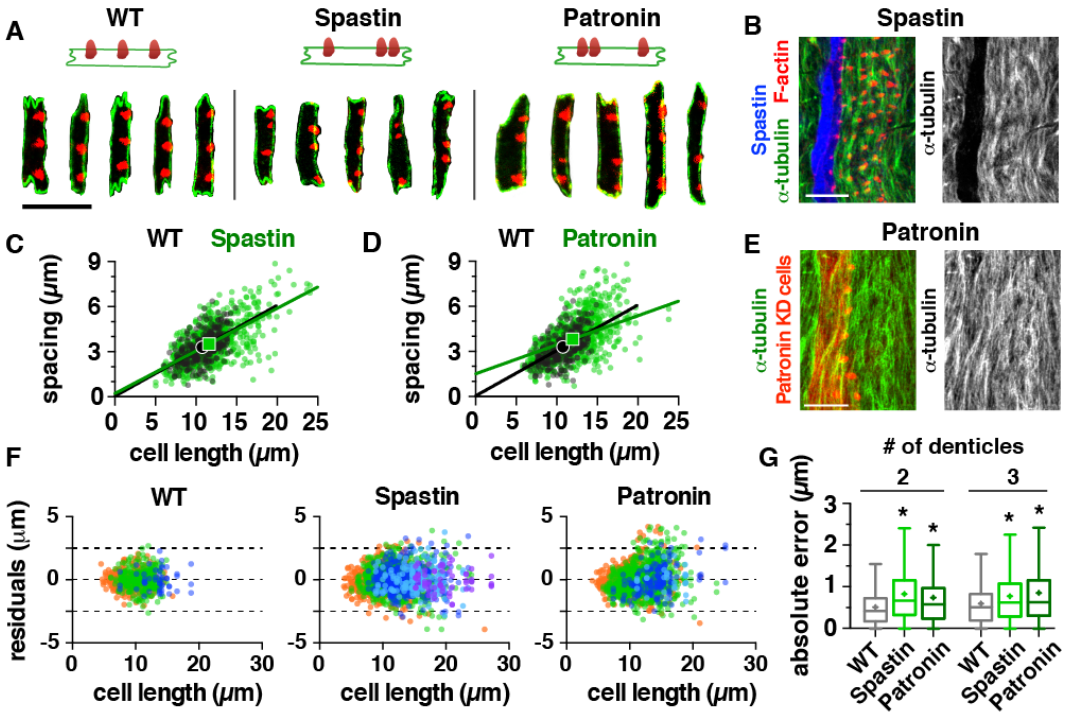

Figure 2.7: Microtubules are required for denticle organization. A. Column 1 cells from wild-type (WT), Spastin-overexpressing (Spastin OE), and Patronin knockdown (Patronin KD) embryos. F-actin (phalloidin, red), E-cadherin (green). **B.** Spastin-GFP overexpression with the *engrailed*-Gal4 driver depletes microtubules in column 1. Green (α-tubulin), red (F-actin), blue (Spastin-GFP). Bar, 10 µm. **C, D.** Denticle spacing vs. cell length for column 1 cells with 3 denticles in WT (black) and Spastin OE or Patronin KD (green) embryos. Lines, best-fit linear regressions. Symbols, means. Measurements falling outside the x and y axis ranges (max 0.3% of the total data in each plot) are not shown. **E.** Expression of a Patronin short hairpin RNA transgene using *engrailed*-Gal4 does not affect the overall organization of column 1 microtubules. Green (α-tubulin), red (Moesin-mCherry labels *engrailed*-Gal4-expressing cells). Bar, 10 µm. **F.** Residuals for the best-fit linear regressions for WT, Spastin OE and Patronin KD. Colors indicate cells with 2 (orange), 3 (green), 4 (dark blue), 5 (light blue), or 6 denticles (purple). **G.** Absolute error of spacing relative to the best-fit linear regressions. *, $p < 0.0001$ compared to WT.See supplemental tables for mean $\pm$ standard deviation (SD) values (**Table 2.1**), n values (**Table 2.2**), and best-fit linear regression equations and R^2 values (**Table 2.3**).

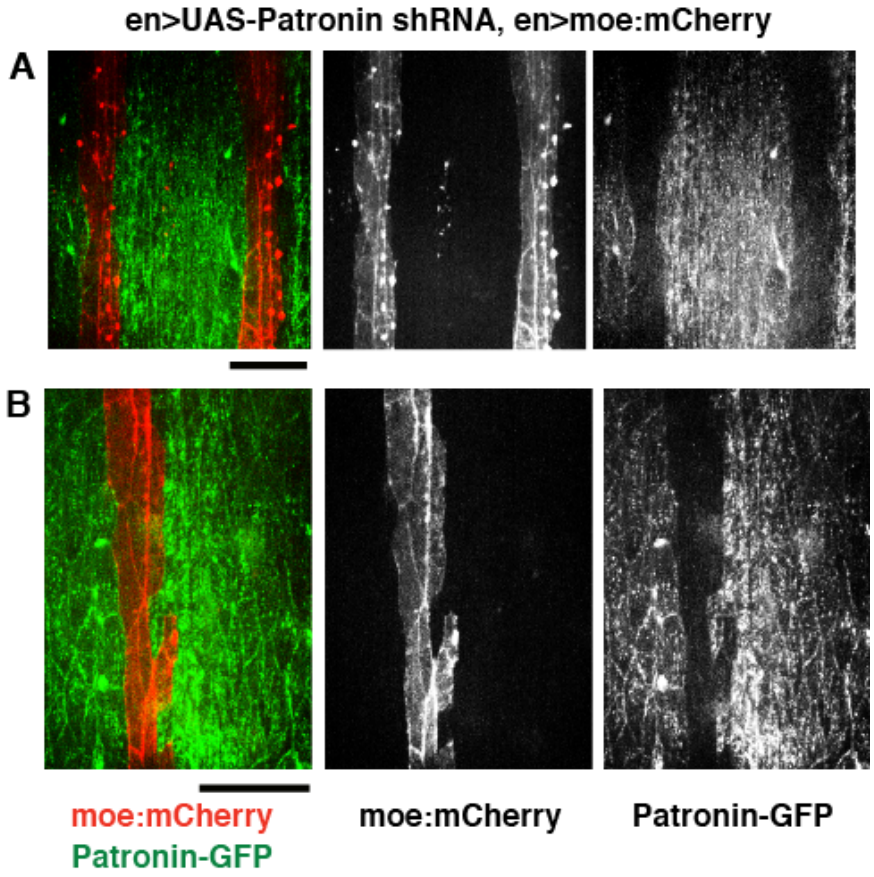

Figure 2.8: Knockdown of Patronin-GFP via RNAi in denticle cells. A,B. Expression of Patronin RNAi in *engrailed*-Gal4 stripes is sufficient to decrease levels of Patronin-GFP. Two independent embryos at approximately stage 15 (**A**) and 14 **B**. Green, ubi-Patronin-GFP; red, *engrailed*-Gal4 > mCherry-Moesin, *engrailed*-Gal4 > Patronin-RNAi.

to determine the spacing of multiple subcellular structures, including actin bands in axons, which are separated by a fixed distance determined by the length of tetrameric spectrin protein complexes (Xu et al., 2013), and the scaling of mitotic spindles, which is determined by a gradient of the microtubule-associated protein TPXL-1 set by the size of the centrosome (Bird & Hyman, 2008; Greenan et al., 2010). The large variation in denticle spacing distances in *Drosophila*, which range from 2-15 µm, is at odds with a molecular ruler model that enforces a strict distance between denticles. These results suggest that different concepts are needed to explain the highly flexible scaling of the number and spacing of denticle actin structures.

The reduced accuracy of denticle spacing in embryos with altered microtubule levels or regulation demonstrate that accurate denticle spacing requires the microtubule cytoskeleton. The mechanisms by which microtubules influence actin organization in the denticle field remain to be determined. The distributions of Patronin, Mud, and EB1 suggest that microtubule minus ends are anchored at sites of denticle formation, with their growing plus ends directed outward, reminiscent of the organization of microtubules at centrosomes and nuclei. These distributions support a model in which denticles could act as noncentrosomal microtubule organizing centers, and this activity could in turn influence their organization within the cell. In this model, growing microtubules originating from denticles could push against the cell cortex and against microtubules emanating from adjacent denticles, stabilizing denticles at sites where these pushing forces are balanced. This model is reminiscent of the force-balance models that have been proposed for nuclear positioning in *S. pombe* (Tran et al., 2001) and the *Drosophila* oocyte (Zhao et al., 2012). Denticle spacing could also be achieved by pushing forces exerted on denticles by plus-end-directed kinesin motors, which could slide apart oppositely oriented microtubules between denticles. This is similar to the activity of the Eg5 kinesin 5 motor, which slides antiparallel microtubules apart at the spindle midzone and maintains spindle length (Sharp et al., 1999b; Shirasu-Hiza et al., 2004; Kapitein et al., 2005; Mitchison et al., 2005), and to the role of kinesin in nuclear positioning (Folker et al., 2014). In both polymerization-driven and kinesin-dependent models, the spacing ratio would result from a balance between microtubule interactions with the cell cortex and with microtubules from neighboring denticles. Other models in which microtubules position denticles indirectly, such as by regulating the trafficking of other proteins, cannot be ruled out, and microtubules present at earlier stages could play additional roles in establishing denticle organization.

Although microtubule-based models could in principle account for the accuracy and scaling of the denticle pattern, the scaling of denticle number is less easily explained by this class of models. Denticle number still scales with cell length when microtubules are disrupted, suggesting that the scaling of denticle number may have a different origin. Limiting component models

propose that the amount of available material sets the size of subcellular structures such as centrosomes (Greenan et al., 2010; Delon et al., 2003; Goehring & Hyman, 2012) and mitotic spindles (Good et al., 2013; Hazel et al., 2013), allowing these structures to scale with cell volume. Although denticle area does not display a consistent relationship with cell area, the summed diameter of denticles correlates with cell length. These results suggest that a limiting component generated along the length of the cell, such as at the posterior cell cortex, could account for the scaling of denticle number. In an alternative model, denticle number could be regulated by an actomyosin-based stochastic capture mechanism. Denticles emerge from an initially diffuse apical actin meshwork through the condensation of small clusters of actin and myosin (Price et al., 2006; Walters et al., 2006; Donoughe & DiNardo, 2011). We show that actin foci are highly mobile and can shift position, disappear, and collide with one another and merge to form larger, stable denticle precursors. This is reminiscent of the behavior of actomyosin networks *in vitro*, in which actin aggregates coalesce into dense foci in the presence of myosin motors (Soares e Silva et al., 2011; Thoresen et al., 2011). An actomyosin-driven capture and clustering mechanism that acts over a defined lengthscale could produce denticle number scaling within cells. In this model, proteins that regulate actin crosslinking, stability, and mobility could determine the number of stable precursors that form denticles from a uniform apical pool of filaments.

The precise organization of denticle structures in the *Drosophila* embryo and larva raise the question of the significance of this actively regulated pattern. Transient actin denticle precursors are translated into permanent protrusions that are distributed across ventral surface of the larval cuticle and contact the underlying substrate as the larva crawls. Although the functions of these structures have not been extensively investigated, the regular placement of denticles may help larvae to gain traction on a wide range of surfaces as they search for food in their environment. In principle, a system that provides regularly distributed contacts with the substrate could provide better traction than a system in which these contacts are irregularly distributed or clustered. Future studies involving the visualization of dynamic scaling processes *in vivo* using live imaging

approaches, combined with genetic methods to determine the molecular basis of actin scaling, will help to uncover the diversity of mechanisms that govern actin organization within cells. An understanding of the molecular control of actin organization may provide insight into the spatial regulation of other periodic structures within cells, such as synapses and neurite branches in neurons (Grueber & Sagasti, 2010), the distribution of organelles involved in carbon fixation in bacteria (Savage et al., 2010), and the organization of lipid homeostasis and oxidative reactions in eukaryotic cells (Lin et al., 2016).

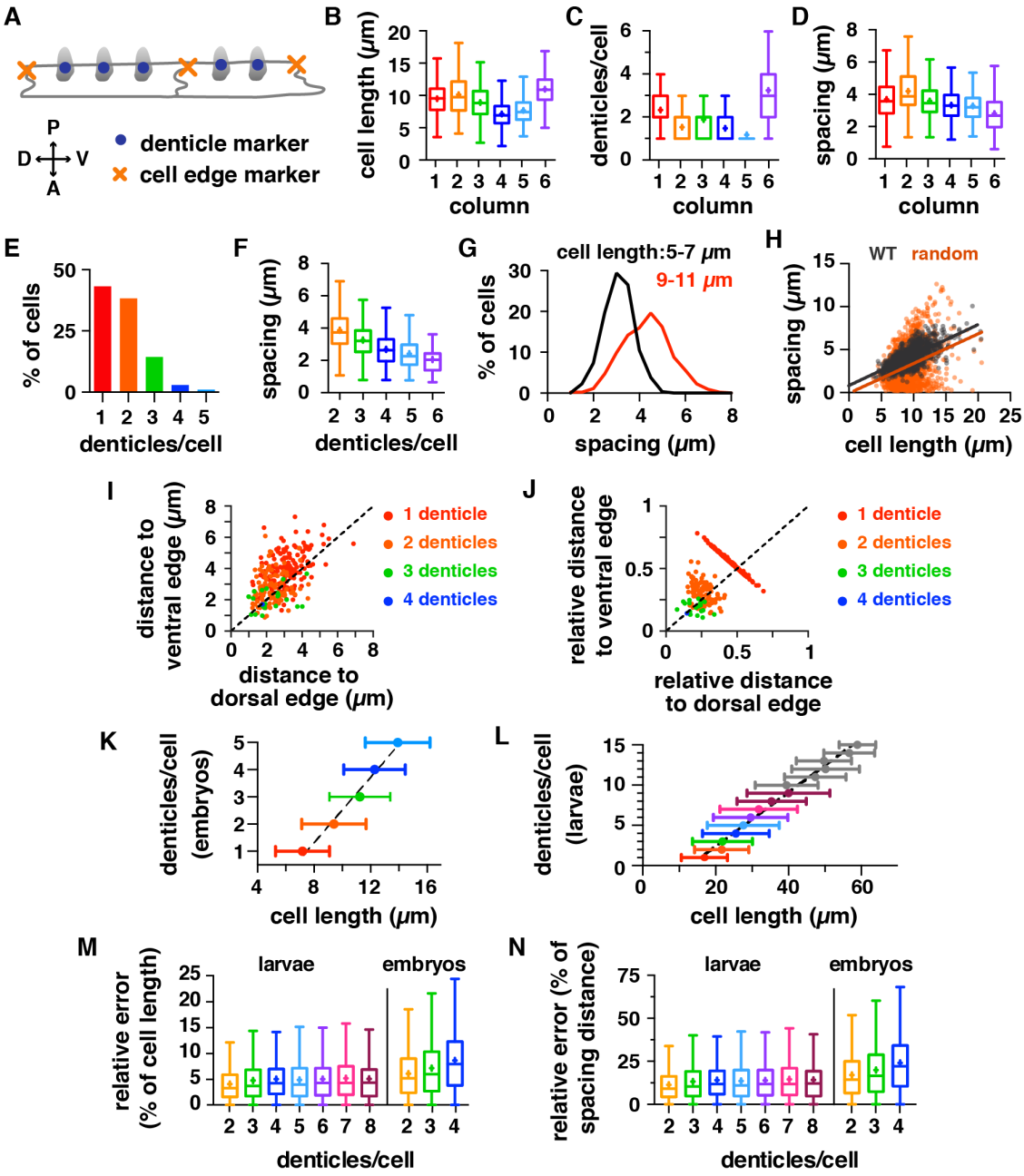
A
P
D
V
A
denticle marker
cell edge marker
B
cell length (μm)
column
C
denticles/cell
column
D
spacing (μm)
column
E
% of cells
denticles/cell
F
spacing (μm)
denticles/cell
G
cell length:5-7 μm
9-11 μm
% of cells
spacing (μm)
H
WT
random
spacing (μm)
cell length (μm)
I
distance to ventral edge (μm)
distance to dorsal edge (μm)
1 denticle
2 denticles
3 denticles
4 denticles
J
relative distance to ventral edge
relative distance to dorsal edge
1 denticle
2 denticles
3 denticles
4 denticles
K
denticles/cell (embryos)
cell length (μm)
L
denticles/cell (larvae)
cell length (μm)
M
relative error (% of cell length)
larvae
embryos
denticles/cell
N
relative error (% of spacing distance)
larvae
embryos
denticles/cell

Figure 2.9: Denticle organization in wild-type and mutant embryos.
A. Denticle and cell edge markers in stage 15-16 *Drosophila* embryos are delineated by the user and several features of the denticle distribution are calculated automatically.
B-D. Cell length along the dorsal-ventral axis (**B**), number of denticles/cell (**C**), and denticle spacing (**D**) plotted by denticle column in wild-type (WT) embryos. One-way ANOVA with Tukey's multiple comparison test. Boxes, 25^{th}-75^{th} percentile; whiskers, 1.5 inter-quartile range (IQR); horizontal line, median; +, mean.

B. $p < 0.01$ for all comparisons.

C. $p < 0.001$ for all comparisons except column 2 vs. column 4.

D. $p < 0.01$ for all comparisons except columns 3 and 4 vs. column 5.

E. Distribution of cells with 1 to 5 denticles in WT embryos.
F. Denticle spacing for WT cells with 2 to 6 denticles. $p < 0.05$ for all comparisons except cells with 5 vs. 6 denticles.
G. Denticle spacing in longer cells (4.2 ± 1.0 μm mean$\pm$SD, red) was larger than denticle spacing in shorter cells (3.1 ± 0.7 μm, black) ($p < 0.0001$, Student's t-test). Data for cells with 2 denticles.
H. Cell length vs. denticle spacing and best-fit linear regression lines for cells with 2 denticles in WT embryos (grey) and Monte Carlo simulations (orange).
I,J. The placement of the outermost denticles relative to the dorsal and ventral boundaries of the cell in WT embryos.

I. Absolute distance of the dorsal-most denticle from the dorsal cell edge (x-axis), absolute distance of the ventral-most denticle from the ventral cell edge (y-axis).

J. Data as in I, but normalized to cell length. n = 153 cells with 1 denticle (red), 94 cells with 2 denticles (orange), and 20 cells with 3 denticles (green).
K,L. Cell length vs. denticle number in WT embryos (**K**) and larvae (**L**) (mean $\pm$ SD). Panel L shows that same data as in Figure 4C, but as mean $\pm$ SD and with the axes reversed for easier comparison with panel K.
M,N. The error relative to cell length (**M**) or relative to the spacing distance predicted by the statistical model (**N**). In both cases, the relative error was slightly decreased for cells with 2, 3, or 4 denticles in larvae compared to embryos ($p < 0.0001$).

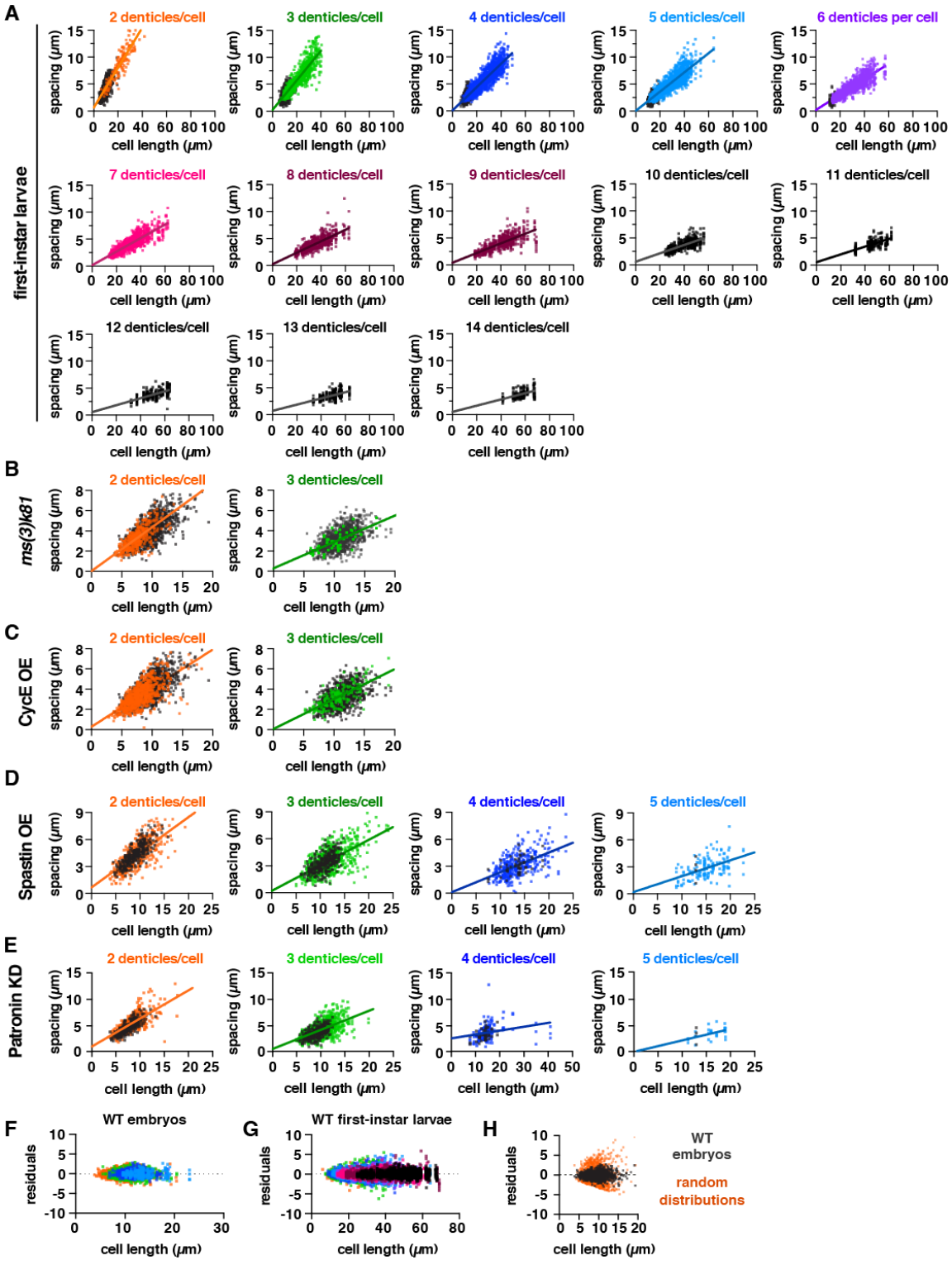
A
first-instar larvae
2 denticles/cell
3 denticles/cell
4 denticles/cell
5 denticles/cell
6 denticles per cell
7 denticles/cell
8 denticles/cell
9 denticles/cell
10 denticles/cell
11 denticles/cell
12 denticles/cell
13 denticles/cell
14 denticles/cell
spacing (μm)
cell length (μm)
B
ms(3)k81
C
CycE OE
D
Spastin OE
E
Patronin KD
F
WT embryos
G
WT first-instar larvae
H
residuals
WT embryos
random distributions

Figure 2.10: Analysis of denticle spacing in multiple genetic backgrounds.
A. Denticle spacing vs. cell length for cells with 2 to 14 denticles in wild-type (WT) embryos (grey dots) and first instar larvae (colored dots). Solid lines, best-fit linear regressions.
B,C. Denticle spacing vs. cell length for cells with 2 or 3 denticles in WT (grey dots), ms(3)k81 (colored dots in **B**) or CycE-OE (colored dots in **C**) embryos. Solid lines, best-fit linear regressions.
D,E. Denticle spacing vs. cell length for cells with 2 to 5 denticles in column 1 cells of WT (grey dots), Spastin-OE (colored dots in **D**) or Patronin-KD (colored dots in **E**). Solid lines, best-fit linear regressions.
F,G. Residuals for the best-fit linear regressions for WT embryos (**F**) and WT larvae (**G**). Colors as in A-E.
H. Residuals for the best-fit linear regressions for WT embryos (grey) and Monte Carlo simulations (orange) for cells with 2 denticles.

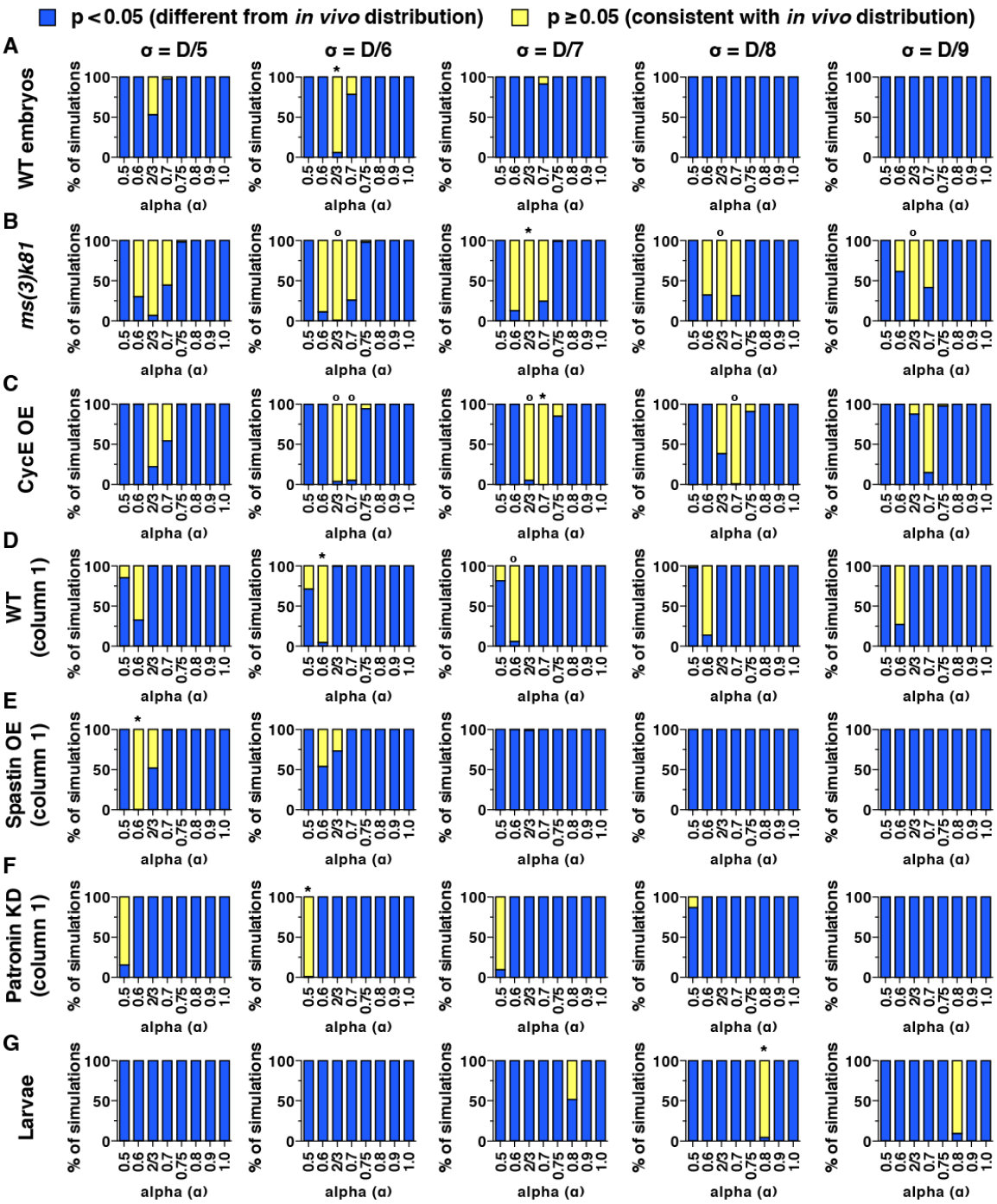

Figure 2.11: Comparison of denticle spacing simulations with *in vivo* measurements. **A-G.** Fraction of simulations that are consistent with ($p \geq 0.05$, yellow) or significantly different from ($p < 0.05$, blue) the *in vivo* distributions for each α, σ pair tested. *, best model tested for each genotype. o, model passes criteria. See **Table 2.5** for a summary of the statistical modeling outcomes.

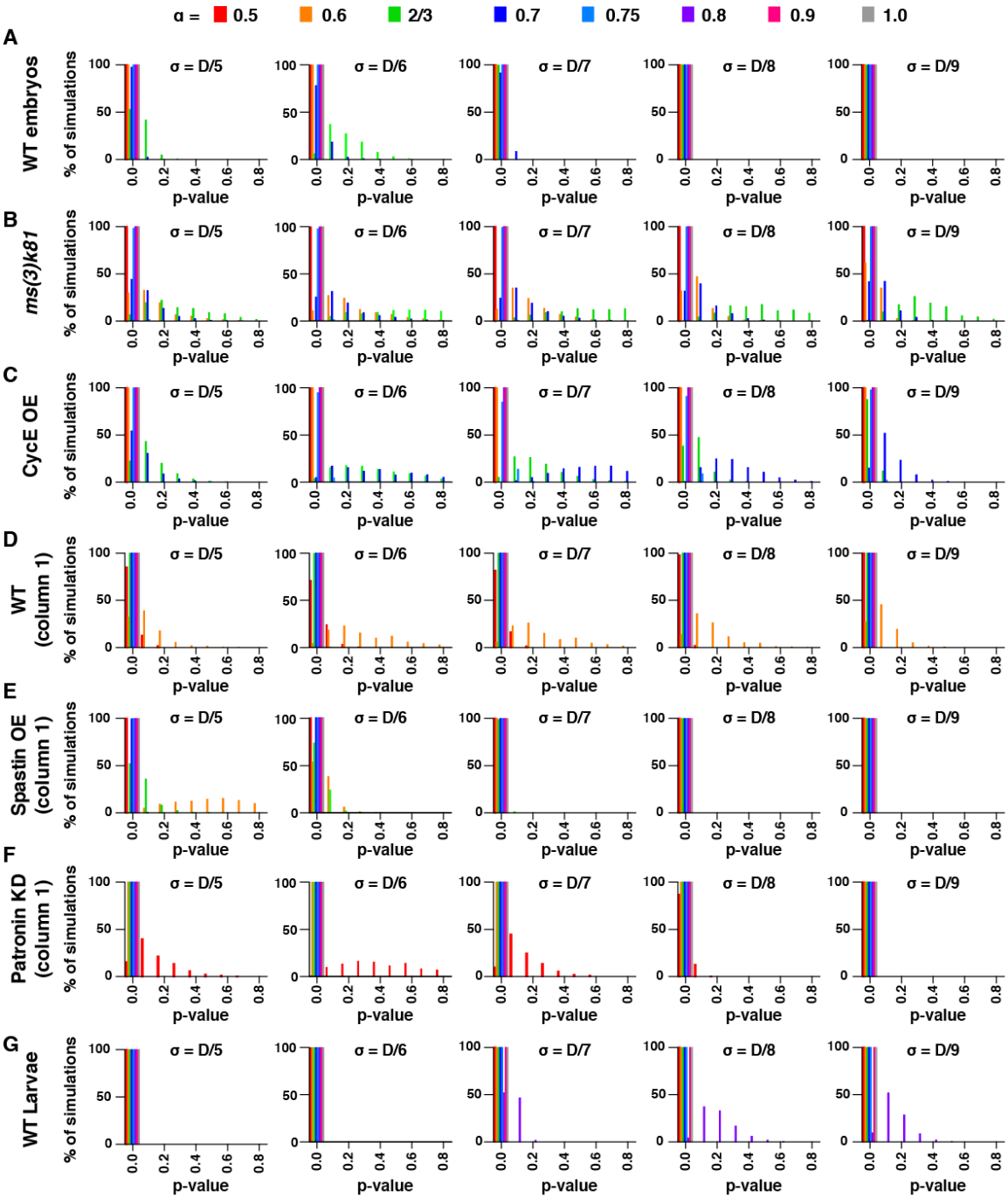

Figure 2.12: p value distributions for denticle spacing simulations compared to *in vivo* measurements. A-G. P value distributions for the indicated models varying α at $\sigma = \frac{D}{5}, \frac{D}{6}, \frac{D}{7}, \frac{D}{8}$, and $\frac{D}{9}$ for embryo and larval data. See **Table 2.5** for a summary of the statistical modeling outcomes.

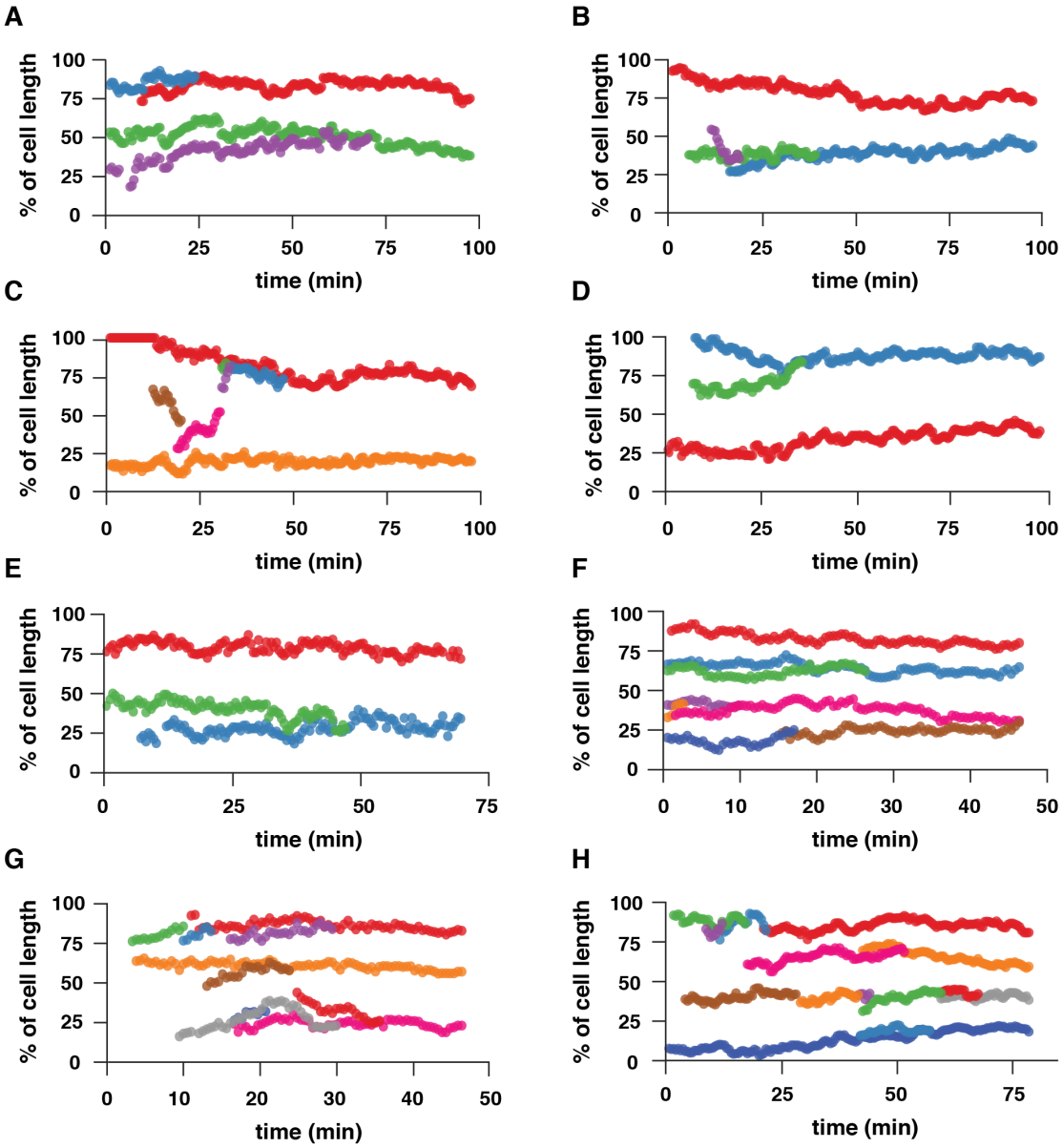

Figure 2.13: Refinement of denticle position during actin coalescence and denticle formation. A-H. Traces of actin foci during denticle formation (mid-to-late stage 14), relative to the total length of the cell for individual cells with 2, 3, or 4 denticles. Green, F-actin; red, E-cadherin. Each color represents a unique actin aggregate that was manually tracked over time. n = 32 cells analyzed from 6 embryos. See also **Figure 2.6**.

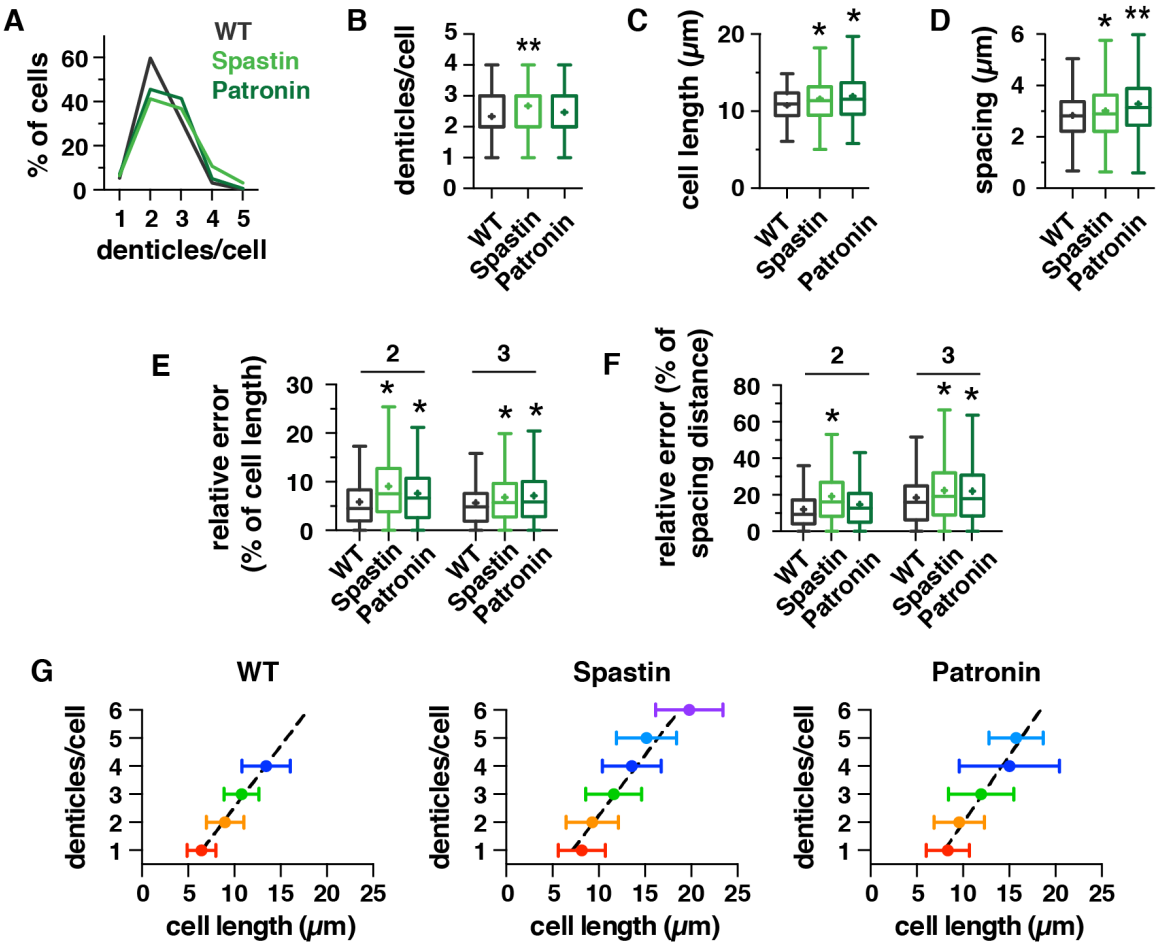

Figure 2.14: Denticle organization in embryos with microtubule defects.
A. Distribution of cells with 1-5 denticles in column 1 cells of WT, Spastin-OE, and Patronin-KD embryos. **B-D.** Number of denticles/cell (**B**), cell length (**C**), and denticle spacing (**D**) in column 1 cells of WT, Spastin-OE, and Patronin-KD embryos. *, $p < 0.05$ and **, $p < 0.0001$ compared to WT, one-way ANOVA with Tukey's multiple comparison test. Data for cells with 3 denticles. **E,F.** The error relative to cell length (**E**) or relative to the spacing distance predicted by the statistical model (**F**) for cells with 2 or 3 denticles in WT, Spastin OE, and Patronin KD embryos. *, $p < 0.0001$ compared to WT, one-way ANOVA with Tukey's multiple comparison test. See supplemental tables for mean $\pm$ standard deviation (SD) values (**Table 2.1**), n values (**Table 2.2**), and best-fit linear regression equations and R^2 values (**Table 2.3**). **G.** Cell length vs. denticle number for column 1 cells in WT, Spastin OE, and Patronin KD embryos (mean $\pm$ SD). Cells with 1, 2, or 3 denticles were significantly longer in Spastin OE and Patronin KD embryos compared to WT ($p < 0.01$), one-way ANOVA with Tukey's multiple comparison test.

Table 2.1: Cell size, denticle number, and denticle spacing measurements. (mean ± SD).

		Genotype						
		WT	**ms(3)k81**	**CycE OE**	**WT col 1**	**Spastin OE col 1**	**Patronin KD col 1**	**Larvae**
Denticles/cell		1.9±1.0	1.3±0.5	1.3±0.5	2.3±0.6	2.7±1.0	2.5±0.7	5.2±2.5
min,max denticles		1,6	1,4	1,5	1,5	1,9	1,5	1,17
Cell length for cells with N denticles	**all**	8.9±2.8	5.8±1.9	6.4±2.4	9.6±2.4	10.9±3.7	10.8±3.6	28.2±11.5
	1	7.2±2.0	5.2±1.5	5.6±1.8	6.4±1.5	8.2±2.5	8.4±2.3	16.9±6.3
	2	9.4± 2.3	7.5±1.8	8.1±2.2	9.0±2.0	9.3±2.8	9.6±2.7	21.7±7.5
	3	11.1±2.2	10.2±2.7	10.8±2.8	10.8±1.9	11.6±3.0	12.0±3.5	21.9±8.2
	4	11.9±2.1	–	–	13.5±2.6	13.6±3.2	15.0±5.4	25.5±9.2
Min cell length		2.2	1.9	1.6	3.6	3.8	3.8	4.6
Max cell length		26.5	17.0	20.3	18.8	33.5	55.0	72.0
Denticle spacing for cells with N denticles	**all**	3.4±1.2	3.3±1.1	3.3±1.2	3.7±1.2	3.6±1.4	4.1±1.5	4.7±2.0
	2	4.0±1.2	3.3±1.1	3.3±1.2	4.3±1.2	4.3±1.5	4.9±1.6	8.7±3.0
	3	3.3±1.0	3.0±0.9	3.2±1.1	3.3±1.0	3.5±1.3	3.8±1.4	6.2±5.6
	4	2.7±0.9	–	–	3.1±0.9	3.1±1.2	3.4±1.4	5.6±2.2
Min spacing		0.6	1.1	0.2	0.8	0.1	0.7	1.1
Max spacing		9.9	7.4	9.6	7.6	9.8	12.2	16.5
Denticle to edge spacing	**all**	2.9±1.4	2.4±1.0	2.5±1.3	2.3±0.9	2.4±1.5	2.3±1.7	4.1±2.8
	1	3.6±1.4	2.6±0.9	2.8±1.1	3.2±1.0	4.1±2.2	4.2±1.7	8.7±3.7
	2	2.7±1.2	2.1±0.8	2.4±1.0	2.4±0.9	2.5±1.4	2.4±1.2	6.7±2.9
	3	2.4±1.0	2.2±0.9	2.2±1.0	2.1±0.7	2.4±1.3	2.2±1.7	5.0±2.5
	4	2.0±0.9	–	–	2.2±0.9	2.2±1.2	2.6±3.1	4.7±2.2
Mean absolute error of spacing	**2**	0.68	0.58	0.68	0.52	0.83	0.75	0.96
	3	0.65	0.51	0.61	0.60	0.78	0.86	0.85
	4	0.64	–	–	0.65	0.79	0.93	0.77
Root mean squared error of spacing	**2**	0.87	0.74	0.90	0.68	1.06	1.05	1.27
	3	0.83	0.64	0.82	0.79	1.01	1.17	1.21
	4	0.79	–	–	0.80	1.03	1.32	1.03

Table 2.2: Number of animals, denticles, and cells analyzed for each genotype. Measurements are in µm

		Genotype						
		WT	**ms(3)k81**	**CycE OE**	**WT col 1**	**Spastin OE col 1**	**Patronin KD col 1**	**Larvae**
Animals		12	10	13	12	36	29	18
Total cells for genotype		3092	1704	3120	497	1103	1054	2150
Total denticles for genotype		5833	2130	4071	1158	2951	2598	11062
Cells/animal, min:max		190 - 370	62 - 245	35 - 350	30 - 70	25842	20 - 60	30 - 240
Denticles/animal, min:max		360 - 700	90 - 300	50 - 460	60 - 150	25 - 165	45 - 140	180 - 1160
Cells with N denticles	1	1284	1310	2274	27	71	76	21
	2	1140	364	750	297	456	480	157
	3	476	28	89	156	407	437	379
	4	130	2	5	16	119	54	452
	5	51	0	2	1	35	7	395
	6	11	0	0	0	12	0	278
	7	0	0	0	0	1	0	164
	8	0	0	0	0	1	0	97
	9	0	0	0	0	1	0	75
	10	0	0	0	0	0	0	51
	11	0	0	0	0	0	0	21
	12	0	0	0	0	0	0	20
	13	0	0	0	0	0	0	18
	14	0	0	0	0	0	0	13
	15	0	0	0	0	0	0	4
	16	0	0	0	0	0	0	2
	17	0	0	0	0	0	0	3

Table 2.3: Best-fit linear regression data for each genotype.

Cells with N denticles		Genotype						
		WT	ms(3)k81	CycE OE	WT column 1	Spastin OE column 1	Patronin KD column 1	Larvae
2	*Equation*	y = 0.36x + 0.63	y = 0.43x + 0.031	y = 0.38x + 0.29	y = 0.47x + 0.10	y = 0.39x + 0.66	y = 0.42x + 0.86	y = 0.37x + 0.63
	R^2	0.48	0.52	0.48	0.66	0.52	0.54	0.82
3	*Equation*	y = 0.24x + 0.64	y = 0.26x + 0.30	y = 0.30x + 0.062	y = 0.30x + 0.03	y = 0.28x + 0.22	y = 0.19x + 1.5	y = 0.27x + 0.23
	R^2	0.28	0.53	0.55	0.34	0.42	0.25	0.78
4	*Equation*	y = 0.21x + 0.21			y = 0.18x + 0.70	y = 0.22x + 0.12	y = 0.069x + 2.4	y = 0.22x + 0.094
	R^2	0.23			0.24	0.31	0.074	0.79
5	*Equation*	y = 0.15x + 0.32				y = 0.18x + 0.19	y = 0.20x-0.13	y = 0.18x + 0.07
	R^2	0.21				0.24	0.28	0.78
6	*Equation*							y = 0.14x + 0.19
	R^2							0.76
7	*Equation*							y = 0.13x + 0.18
	R^2							0.73

Cells with N denticles		Genotype						
		WT	ms(3)k81	CycE OE	WT column 1	Spastin OE column 1	Patronin KD column 1	Larvae
8	*Equation*							y = 0.11x + 0.25
	R^2							0.62
9	*Equation*							y = 0.090x + 0.42
	R^2							0.56
10	*Equation*							y = 0.08x + 0.59
	R^2							0.5
11	*Equation*							Y = 0.072*X+0.53
	R^2							0.41
12	*Equation*							Y = 0.064*X+0.55
	R^2							0.41
13	*Equation*							Y = 0.057*X+0.73
	R^2							0.28
14	*Equation*							Y = 0.058*X+0.51
	R^2							0.24

Cells with N denticles		Genotype						
		WT	ms(3)k81	CycE OE	WT column 1	Spastin OE column 1	Patronin KD column 1	Larvae
15	*Equation*							Y = 0.050*X+0.71
	R^2							0.087

Table 2.4: Summary of Monte Carlo simulations. Models that meet the cutoff criteria are indicated in red.

Cells analyzed	Random model is acceptable ($\geq$ 95% pass) (YES/no)	# of Monte Carlo simulations consistent with in vivo distribution ($p \geq 0.05$) (out of 10,000)	Fraction that pass (% with $p \geq 0.05$)	Fraction that fail (% with $p < 0.05$)
All cells	no	0	0	100
1 denticle	no	0	0	100
2 denticles	no	0	0	100
3 denticles	no	0	0	100
4 denticles	no	5136	51.36	48.64

Table 2.5: Summary of statistical modeling outcomes for 40 combinations of alpha and sigma in all genotypes. Models that meet the cutoff criteria are indicated in red; the best-fit model tested is indicated in bold with an asterisk. 10,000 total simulations

Genotype	Model		Model is acceptable ($\geq$ 94% pass) (YES/no)	# of simulations consistent with in vivo distribution ($p \geq 0.05$) (out of 10,000)	Fraction that pass (% with $p \geq 0.05$)	Fraction that fail (% with $p < 0.05$)
	σ =	α =				
WT						
	D/5	**0.5**	no	0	0.00	100.00
		0.6	no	0	0.00	100.00
		0.667	no	4699	46.99	53.01
		0.7	no	238	2.38	97.62
		0.75	no	0	0.00	100.00
		0.8	no	0	0.00	100.00
		0.9	no	0	0.00	100.00
		1	no	0	0.00	100.00
	D/6	**0.5**	no	0	0.00	100.00
		0.6	no	0	0.00	100.00
		0.667	**YES***	**9413**	**94.13**	**5.87**
		0.7	no	2167	21.67	78.33
		0.75	no	0	0.00	100.00
		0.8	no	0	0.00	100.00
		0.9	no	0	0.00	100.00
		1	no	0	0.00	100.00
	D/7	**0.5**	no	0	0.00	100.00
		0.6	no	0	0.00	100.00
		0.667	no	21	0.21	99.79
		0.7	no	851	8.51	91.49
		0.75	no	0	0.00	100.00
		0.8	no	0	0.00	100.00

Genotype	Model	Model accepted?	# pass	% pass	% fail
	0.9	no	0	0.00	100.00
	1	no	0	0.00	100.00
D/8	**0.5**	no	0	0.00	100.00
	0.6	no	0	0.00	100.00
	0.667	no	0	0.00	100.00
	0.7	no	0	0.00	100.00
	0.75	no	0	0.00	100.00
	0.8	no	0	0.00	100.00
	0.9	no	0	0.00	100.00
	1	no	0	0.00	100.00
D/9	**0.5**	no	0	0.00	100.00
	0.6	no	0	0.00	100.00
	0.667	no	0	0.00	100.00
	0.7	no	0	0.00	100.00
	0.75	no	0	0.00	100.00
	0.8	no	0	0.00	100.00
	0.9	no	0	0.00	100.00
	1	no	0	0.00	100.00
ms(3)k81					
D/5	**0.5**	no	0	0.00	100.00
	0.6	no	6991	69.91	30.09
	0.667	no	9320	93.2	6.8
	0.7	no	5561	55.61	44.39
	0.75	no	189	1.89	98.11
	0.8	no	0	0.00	100.00
	0.9	no	0	0.00	100.00
	1	no	0	0.00	100.00
D/6	**0.5**	no	0	0.00	100.00
	0.6	no	8878	88.78	11.22
	0.667	**YES***	**9908**	**99.08**	**0.92**
	0.7	no	7423	74.23	25.77
	0.75	no	179	1.79	98.21

Genotype	Model	Model accepted?	# pass	% pass	% fail
	0.8	no	0	0.00	100.00
	0.9	no	0	0.00	100.00
	1	no	0	0.00	100.00
D/7	**0.5**	no	0	0.00	100.00
	0.6	no	8731	87.31	12.69
	0.667	YES	9967	99.67	0.33
	0.7	no	7544	75.44	24.56
	0.75	no	83	0.83	99.17
	0.8	no	0	0.00	100.00
	0.9	no	0	0.00	100.00
	1	no	0	0.00	100.00
D/8	**0.5**	no	0	0.00	100.00
	0.6	no	6783	67.83	32.17
	0.667	YES	9957	99.57	0.43
	0.7	no	6813	68.13	31.87
	0.75	no	12	0.12	99.88
	0.8	no	0	0.00	100.00
	0.9	no	0	0.00	100.00
	1	no	0	0.00	100.00
D/9	**0.5**	no	0	0.00	100.00
	0.6	no	3831	38.31	61.69
	0.667	YES	9931	99.31	0.69
	0.7	no	5812	58.12	41.88
	0.75	no	1	0.01	99.99
	0.8	no	0	0.00	100.00
	0.9	no	0	0.00	100.00
	1	no	0	0.00	100.00
CycE OE					
D/5	**0.5**	no	0	0.00	100.00
	0.6	no	2	0.02	99.98
	0.667	no	7761	77.61	22.39
	0.7	no	4559	45.59	54.41

Genotype	Model	Model accepted?	# pass	% pass	% fail
	0.75	no	21	0.21	99.79
	0.8	no	0	0.00	100.00
	0.9	no	0	0.00	100.00
	1	no	0	0.00	100.00
D/6	**0.5**	no	0	0.00	100.00
	0.6	no	0	0.00	100.00
	0.667	YES	9629	96.29	3.71
	0.7	YES	9498	94.98	5.02
	0.75	no	534	5.34	94.66
	0.8	no	0	0.00	100.00
	0.9	no	0	0.00	100.00
	1	no	0	0.00	100.00
D/7	**0.5**	no	0	0.00	100.00
	0.6	no	0	0.00	100.00
	0.667	YES	9484	94.84	5.16
	0.7	**YES***	**9992**	**99.92**	**0.08**
	0.75	no	1499	14.99	85.01
	0.8	no	0	0.00	100.00
	0.9	no	0	0.00	100.00
	1	no	0	0.00	100.00
D/8	**0.5**	no	0	0.00	100.00
	0.6	no	0	0.00	100.00
	0.667	no	6166	61.66	38.34
	0.7	YES	9918	99.18	0.82
	0.75	no	929	9.29	90.71
	0.8	no	0	0.00	100.00
	0.9	no	0	0.00	100.00
	1	no	0	0.00	100.00
D/9	**0.5**	no	0	0.00	100.00
	0.6	no	0	0.00	100.00
	0.667	no	1241	12.41	87.59
	0.7	no	8531	85.31	14.69
	0.75	no	233	2.33	97.67

Genotype	Model	Model accepted?	# pass	% pass	% fail
	0.8	no	0	0.00	100.00
	0.9	no	0	0.00	100.00
	1	no	0	0.00	100.00
WT, column 1 only					
D/5	**0.5**	no	1493	14.93	85.07
	0.6	no	6738	67.38	32.62
	0.667	no	12	0.12	99.88
	0.7	no	0	0.00	100.00
	0.75	no	0	0.00	100.00
	0.8	no	0	0.00	100.00
	0.9	no	0	0.00	100.00
	1	no	0	0.00	100.00
D/6	**0.5**	no	2885	28.85	71.15
	0.6	**YES***	**9547**	**95.47**	**4.53**
	0.667	no	32	0.32	99.68
	0.7	no	0	0.00	100.00
	0.75	no	0	0.00	100.00
	0.8	no	0	0.00	100.00
	0.9	no	0	0.00	100.00
	1	no	0	0.00	100.00
D/7	**0.5**	no	1826	18.26	81.74
	0.6	YES	9419	94.19	5.81
	0.667	no	4	0.04	99.96
	0.7	no	0	0.00	100.00
	0.75	no	0	0.00	100.00
	0.8	no	0	0.00	100.00
	0.9	no	0	0.00	100.00
	1	no	0	0.00	100.00
D/8	**0.5**	no	216	2.16	97.84
	0.6	no	8617	86.17	13.83
	0.667	no	0	0.00	100.00
	0.7	no	0	0.00	100.00

Genotype	Model	Model accepted?	# pass	% pass	% fail
	0.75	no	0	0.00	100.00
	0.8	no	0	0.00	100.00
	0.9	no	0	0.00	100.00
	1	no	0	0.00	100.00
D/9	**0.5**	no	4	0.04	99.96
	0.6	no	7278	72.78	27.22
	0.667	no	0	0.00	100.00
	0.7	no	0	0.00	100.00
	0.75	no	0	0.00	100.00
	0.8	no	0	0.00	100.00
	0.9	no	0	0.00	100.00
	1	no	0	0.00	100.00
Spastin OE					
D/5	**0.5**	no	0	0.00	100.00
	0.6	**YES***	**9969**	**99.69**	**0.31**
	0.667	no	4800	48	52
	0.7	no	30	0.3	99.7
	0.75	no	0	0.00	100.00
	0.8	no	0	0.00	100.00
	0.9	no	0	0.00	100.00
	1	no	0	0.00	100.00
D/6	**0.5**	no	0	0.00	100.00
	0.6	no	4623	46.23	53.77
	0.667	no	2664	26.64	73.36
	0.7	no	0	0.00	100.00
	0.75	no	0	0.00	100.00
	0.8	no	0	0.00	100.00
	0.9	no	0	0.00	100.00
	1	no	0	0.00	100.00
D/7	**0.5**	no	0	0.00	100.00
	0.6	no	1	0.01	99.99
	0.667	no	133	1.33	98.67

Genotype	Model	Model accepted?	# pass	% pass	% fail
	0.7	no	0	0.00	100.00
	0.75	no	0	0.00	100.00
	0.8	no	0	0.00	100.00
	0.9	no	0	0.00	100.00
	1	no	0	0.00	100.00
D/8	**0.5**	no	0	0.00	100.00
	0.6	no	0	0.00	100.00
	0.667	no	0	0.00	100.00
	0.7	no	0	0.00	100.00
	0.75	no	0	0.00	100.00
	0.8	no	0	0.00	100.00
	0.9	no	0	0.00	100.00
	1	no	0	0.00	100.00
D/9	**0.5**	no	0	0.00	100.00
	0.6	no	0	0.00	100.00
	0.667	no	0	0.00	100.00
	0.7	no	0	0.00	100.00
	0.75	no	0	0.00	100.00
	0.8	no	0	0.00	100.00
	0.9	no	0	0.00	100.00
	1	no	0	0.00	100.00
Patronin OE					
D/5	**0.5**	no	8466	84.66	15.34
	0.6	no	0	0.00	100.00
	0.667	no	0	0.00	100.00
	0.7	no	0	0.00	100.00
	0.75	no	0	0.00	100.00
	0.8	no	0	0.00	100.00
	0.9	no	0	0.00	100.00
	1	no	0	0.00	100.00
D/6	**0.5**	**YES***	**9898**	**98.98**	**1.02**
	0.6	no	0	0.00	100.00

Genotype	Model	Model accepted?	# pass	% pass	% fail
	0.667	no	0	0.00	100.00
	0.7	no	0	0.00	100.00
	0.75	no	0	0.00	100.00
	0.8	no	0	0.00	100.00
	0.9	no	0	0.00	100.00
	1	no	0	0.00	100.00
D/7	**0.5**	no	9061	90.61	9.39
	0.6	no	0	0.00	100.00
	0.667	no	0	0.00	100.00
	0.7	no	0	0.00	100.00
	0.75	no	0	0.00	100.00
	0.8	no	0	0.00	100.00
	0.9	no	0	0.00	100.00
	1	no	0	0.00	100.00
D/8	**0.5**	no	1308	13.08	86.92
	0.6	no	0	0.00	100.00
	0.667	no	0	0.00	100.00
	0.7	no	0	0.00	100.00
	0.75	no	0	0.00	100.00
	0.8	no	0	0.00	100.00
	0.9	no	0	0.00	100.00
	1	no	0	0.00	100.00
D/9	**0.5**	no	2	0.02	99.98
	0.6	no	0	0.00	100.00
	0.667	no	0	0.00	100.00
	0.7	no	0	0.00	100.00
	0.75	no	0	0.00	100.00
	0.8	no	0	0.00	100.00
	0.9	no	0	0.00	100.00
	1	no	0	0.00	100.00
Larvae					
D/5	**0.5**	no	0	0.00	100.00

Genotype	Model	Model accepted?	# pass	% pass	% fail
	0.6	no	0	0.00	100.00
	0.667	no	0	0.00	100.00
	0.7	no	0	0.00	100.00
	0.75	no	0	0.00	100.00
	0.8	no	0	0.00	100.00
	0.9	no	0	0.00	100.00
	1	no	0	0.00	100.00
D/6	**0.5**	no	0	0.00	100.00
	0.6	no	0	0.00	100.00
	0.667	no	0	0.00	100.00
	0.7	no	0	0.00	100.00
	0.75	no	0	0.00	100.00
	0.8	no	0	0.00	100.00
	0.9	no	0	0.00	100.00
	1	no	0	0.00	100.00
D/7	**0.5**	no	0	0.00	100.00
	0.6	no	0	0.00	100.00
	0.667	no	0	0.00	100.00
	0.7	no	0	0.00	100.00
	0.75	no	0	0.00	100.00
	0.8	no	4822	48.22	51.78
	0.9	no	0	0.00	100.00
	1	no	0	0.00	100.00
D/8	**0.5**	no	0	0.00	100.00
	0.6	no	0	0.00	100.00
	0.667	no	0	0.00	100.00
	0.7	no	0	0.00	100.00
	0.75	no	0	0.00	100.00
	0.8	**YES***	**9568**	**95.68**	**4.32**
	0.9	no	0	0.00	100.00
	1	no	0	0.00	100.00
D/9	**0.5**	no	0	0.00	100.00
	0.6	no	0	0.00	100.00

Genotype	Model	Model accepted?	# pass	% pass	% fail
	0.667	no	0	0.00	100.00
	0.7	no	0	0.00	100.00
	0.75	no	0	0.00	100.00
	0.8	no	9056	90.56	9.44
	0.9	no	0	0.00	100.00
	1	no	0	0.00	100.00

Table 2.6: Summary of statistical modeling outcomes in embryos and larvae for cells with 2-11 denticles. Models that meet the cutoff criteria are indicated in red. 1,000 total simulations

Genotype	Model	Model is acceptable ($\geq$ 94% pass) (YES/no)	# of simulations consistent with in vivo distribution ($p \geq 0.05$) (out of 1,000)	Fraction that pass (% with $p \geq 0.05$)	Fraction that fail (% with $p < 0.05$)
σ =	α =				
WT, N=2					
D/5	**0.5**	no	0	0.0	100.0
	0.6	no	0	0.0	100.0
	0.667	no	104	10.4	89.6
	0.7	no	6	0.6	99.4
	0.75	no	0	0.0	100.0
	0.8	no	0	0.0	100.0
	0.9	no	0	0.0	100.0
	1	no	0	0.0	100.0
D/6	**0.5**	no	0	0.0	100.0
	0.6	no	0	0.0	100.0
	0.667	no	942	94.2	5.8
	0.7	no	505	50.5	49.5
	0.75	no	1	0.1	99.9
	0.8	no	0	0.0	100.0
	0.9	no	0	0.0	100.0
	1	no	0	0.0	100.0

Genotype	Model	Model accepted?	# pass	% pass	% fail
D/7	0.5	no	0	0.0	100.0
	0.6	no	0	0.0	100.0
	0.667	YES	997	99.7	0.3
	0.7	no	905	90.5	9.5
	0.75	no	0	0.0	100.0
	0.8	no	0	0.0	100.0
	0.9	no	0	0.0	100.0
	1	no	0	0.0	100.0
D/8	0.5	no	0	0.0	100.0
	0.6	no	0	0.0	100.0
	0.667	YES	988	98.8	1.2
	0.7	no	928	92.8	7.2
	0.75	no	0	0.0	100.0
	0.8	no	0	0.0	100.0
	0.9	no	0	0.0	100.0
	1	no	0	0.0	100.0
D/9	0.5	no	0	0.0	100.0
	0.6	no	0	0.0	100.0
	0.667	no	911	91.1	8.9
	0.7	no	886	88.6	11.4
	0.75	no	0	0.0	100.0
	0.8	no	0	0.0	100.0
	0.9	no	0	0.0	100.0
	1	no	0	0.0	100.0
WT, N=3					
D/5	0.5	no	0	0.0	100.0
	0.6	no	0	0.0	100.0
	0.667	no	240	24	76
	0.7	no	890	89	11
	0.75	no	316	31.6	68.4
	0.8	no	0	0.0	100.0
	0.9	no	0	0.0	100.0

Genotype	Model	Model accepted?	# pass	% pass	% fail
	1	no	0	0.0	100.0
D/6	**0.5**	no	0	0.0	100.0
	0.6	no	0	0.0	100.0
	0.667	no	856	85.6	14.4
	0.7	YES	1000	100	0
	0.75	no	585	58.5	41.5
	0.8	no	0	0.0	100.0
	0.9	no	0	0.0	100.0
	1	no	0	0.0	100.0
D/7	**0.5**	no	0	0.0	100.0
	0.6	no	0	0.0	100.0
	0.667	no	261	26.1	73.9
	0.7	no	833	83.3	16.7
	0.75	no	501	50.1	49.9
	0.8	no	0	0.0	100.0
	0.9	no	0	0.0	100.0
	1	no	0	0.0	100.0
D/8	**0.5**	no	0	0.0	100.0
	0.6	no	0	0.0	100.0
	0.667	no	0	0.0	100.0
	0.7	no	83	8.3	91.7
	0.75	no	179	17.9	82.1
	0.8	no	0	0.0	100.0
	0.9	no	0	0.0	100.0
	1	no	0	0.0	100.0
D/9	**0.5**	no	0	0.0	100.0
	0.6	no	0	0.0	100.0
	0.667	no	0	0.0	100.0
	0.7	no	0	0.0	100.0
	0.75	no	6	0.6	99.4
	0.8	no	0	0.0	100.0
	0.9	no	0	0.0	100.0
	1	no	0	0.0	100.0

Genotype	Model	Model accepted?	# pass	% pass	% fail
WT, N=4					
D/5	**0.5**	no	0	0.0	100.0
	0.6	no	50	5	95
	0.667	no	569	56.9	43.1
	0.7	no	830	83	17
	0.75	YES	990	99	1
	0.8	no	931	93.1	6.9
	0.9	no	25	2.5	97.5
	1	no	0	0.0	100.0
D/6	**0.5**	no	0	0.0	100.0
	0.6	no	1	0.1	99.9
	0.667	no	40	4	96
	0.7	no	130	13	87
	0.75	no	570	57	43
	0.8	no	381	38.1	61.9
	0.9	no	0	0.0	100.0
	1	no	0	0.0	100.0
D/7	**0.5**	no	0	0.0	100.0
	0.6	no	0	0.0	100.0
	0.667	no	0	0.0	100.0
	0.7	no	1	0.1	99.9
	0.75	no	32	3.2	96.8
	0.8	no	8	0.8	99.2
	0.9	no	0	0.0	100.0
	1	no	0	0.0	100.0
D/8	**0.5**	no	0	0.0	100.0
	0.6	no	0	0.0	100.0
	0.667	no	0	0.0	100.0
	0.7	no	0	0.0	100.0
	0.75	no	0	0.0	100.0
	0.8	no	0	0.0	100.0

Genotype	Model	Model accepted?	# pass	% pass	% fail
	0.9	no	0	0.0	100.0
	1	no	0	0.0	100.0
D/9	**0.5**	no	0	0.0	100.0
	0.6	no	0	0.0	100.0
	0.667	no	0	0.0	100.0
	0.7	no	0	0.0	100.0
	0.75	no	0	0.0	100.0
	0.8	no	0	0.0	100.0
	0.9	no	0	0.0	100.0
	1	no	0	0.0	100.0
Larvae, N=2					
D/5	**0.5**	no	0	0.0	100.0
	0.6	no	23	2.3	97.7
	0.667	no	432	43.2	56.8
	0.7	no	734	73.4	26.6
	0.75	YES	956	95.6	4.4
	0.8	no	907	90.7	9.3
	0.9	no	197	19.7	80.3
	1	no	3	0.3	99.7
D/6	**0.5**	no	0	0.0	100.0
	0.6	no	26	2.6	97.4
	0.667	no	536	53.6	46.4
	0.7	no	879	87.9	12.1
	0.75	YES	996	99.6	0.4
	0.8	YES	978	97.8	2.2
	0.9	no	330	33	67
	1	no	2	0.2	99.8
D/7	**0.5**	no	0	0.0	100.0
	0.6	no	24	2.4	97.6
	0.667	no	658	65.8	34.2
	0.7	no	943	94.3	5.7

Genotype	Model	Model accepted?	# pass	% pass	% fail
	0.75	YES	999	99.9	0.1
	0.8	YES	994	99.4	0.6
	0.9	no	382	38.2	61.8
	1	no	0	0.0	100.0
D/8	**0.5**	no	0	0.0	100.0
	0.6	no	10	1	99
	0.667	no	692	69.2	30.8
	0.7	YES	959	95.9	4.1
	0.75	YES	1000	100	0
	0.8	YES	999	99.9	0.1
	0.9	no	415	41.5	58.5
	1	no	1	0.1	99.9
D/9	**0.5**	no	0	0.0	100.0
	0.6	no	9	0.9	99.1
	0.667	no	731	73.1	26.9
	0.7	YES	975	97.5	2.5
	0.75	YES	1000	100	0
	0.8	YES	999	99.9	0.1
	0.9	no	457	45.7	54.3
	1	no	0	0.0	100.0
Larvae, N=3					
D/5	**0.5**	no	0	0.0	100.0
	0.6	no	0	0.0	100.0
	0.667	no	5	0.5	99.5
	0.7	no	121	12.1	87.9
	0.75	no	645	64.5	35.5
	0.8	no	332	33.2	66.8
	0.9	no	1	0.1	99.9
	1	no	0	0.0	100.0
D/6	**0.5**	no	0	0.0	100.0

Genotype	Model	Model accepted?	# pass	% pass	% fail
	0.6	no	0	0.0	100.0
	0.667	no	21	2.1	97.9
	0.7	no	339	33.9	66.1
	0.75	YES	978	97.8	2.2
	0.8	YES	968	96.8	3.2
	0.9	no	43	4.3	95.7
	1	no	0	0.0	100.0
D/7	**0.5**	no	0	0.0	100.0
	0.6	no	0	0.0	100.0
	0.667	no	32	3.2	96.8
	0.7	no	520	52	48
	0.75	YES	997	99.7	0.3
	0.8	YES	1000	100	0
	0.9	no	313	31.3	68.7
	1	no	0	0.0	100.0
D/8	**0.5**	no	0	0.0	100.0
	0.6	no	0	0.0	100.0
	0.667	no	9	0.9	99.1
	0.7	no	569	56.9	43.1
	0.75	YES	999	99.9	0.1
	0.8	YES	1000	100	0
	0.9	no	587	58.7	41.3
	1	no	0	0.0	100.0
D/9	**0.5**	no	0	0.0	100.0
	0.6	no	0	0.0	100.0
	0.667	no	2	0.2	99.8
	0.7	no	522	52.2	47.8
	0.75	YES	1000	100	0
	0.8	YES	1000	100	0
	0.9	no	716	71.6	28.4
	1	no	0	0.0	100.0

Larvae, N=4

Genotype	Model	Model accepted?	# pass	% pass	% fail
D/5	0.5	no	0	0.0	100.0
	0.6	no	0	0.0	100.0
	0.667	no	0	0.0	100.0
	0.7	no	0	0.0	100.0
	0.75	no	36	3.6	96.4
	0.8	no	65	6.5	93.5
	0.9	no	0	0.0	100.0
	1	no	0	0.0	100.0
D/6	0.5	no	0	0.0	100.0
	0.6	no	0	0.0	100.0
	0.667	no	0	0.0	100.0
	0.7	no	10	1	99
	0.75	no	721	72.1	27.9
	0.8	YES	985	98.5	1.5
	0.9	no	81	8.1	91.9
	1	no	0	0.0	100.0
D/7	0.5	no	0	0.0	100.0
	0.6	no	0	0.0	100.0
	0.667	no	0	0.0	100.0
	0.7	no	7	0.7	99.3
	0.75	no	938	93.8	6.2
	0.8	YES	1000	100	0
	0.9	no	768	76.8	23.2
	1	no	0	0.0	100.0
D/8	0.5	no	0	0.0	100.0
	0.6	no	0	0.0	100.0
	0.667	no	0	0.0	100.0
	0.7	no	2	0.2	99.8
	0.75	no	847	84.7	15.3
	0.8	YES	1000	100	0
	0.9	YES	984	98.4	1.6
	1	no	0	0.0	100.0

Genotype	Model	Model accepted?	# pass	% pass	% fail
D/9	0.5	no	0	0.0	100.0
	0.6	no	0	0.0	100.0
	0.667	no	0	0.0	100.0
	0.7	no	0	0.0	100.0
	0.75	no	677	67.7	32.3
	0.8	YES	1000	100	0
	0.9	YES	995	99.5	0.5
	1	no	0	0.0	100.0
Larvae, N=5					
D/5	0.5	no	0	0.0	100.0
	0.6	no	0	0.0	100.0
	0.667	no	0	0.0	100.0
	0.7	no	0	0.0	100.0
	0.75	no	0	0.0	100.0
	0.8	no	19	1.9	98.1
	0.9	no	0	0.0	100.0
	1	no	0	0.0	100.0
D/6	0.5	no	0	0.0	100.0
	0.6	no	0	0.0	100.0
	0.667	no	0	0.0	100.0
	0.7	no	0	0.0	100.0
	0.75	no	29	2.9	97.1
	0.8	no	661	66.1	33.9
	0.9	no	477	47.7	52.3
	1	no	0	0.0	100.0
D/7	0.5	no	0	0.0	100.0
	0.6	no	0	0.0	100.0
	0.667	no	0	0.0	100.0
	0.7	no	0	0.0	100.0
	0.75	no	186	18.6	81.4
	0.8	YES	969	96.9	3.1
	0.9	YES	952	95.2	4.8
	1	no	0	0.0	100.0

Genotype	Model	Model accepted?	# pass	% pass	% fail
D/8	0.5	no	0	0.0	100.0
	0.6	no	0	0.0	100.0
	0.667	no	0	0.0	100.0
	0.7	no	0	0.0	100.0
	0.75	no	417	41.7	58.3
	0.8	YES	994	99.4	0.6
	0.9	YES	1000	100	0
	1	no	2	0.2	99.8
D/9	0.5	no	0	0.0	100.0
	0.6	no	0	0.0	100.0
	0.667	no	0	0.0	100.0
	0.7	no	0	0.0	100.0
	0.75	no	414	41.4	58.6
	0.8	YES	995	99.5	0.5
	0.9	YES	1000	100	0
	1	no	14	1.4	98.6
Larvae, N=6					
D/5	0.5	no	0	0.0	100.0
	0.6	no	0	0.0	100.0
	0.667	no	0	0.0	100.0
	0.7	no	0	0.0	100.0
	0.75	no	0	0.0	100.0
	0.8	no	0	0.0	100.0
	0.9	no	34	3.4	96.6
	1	no	0	0.0	100.0
	1.1	no	0	0	100
	1.2	no	0	0	100
	1.3	no	0	0	100
	1.4	no	0	0	100
	1.5	no	0	0	100
	1.6	no	0	0	100
	1.7	no	0	0	100
	1.8	no	0	0	100

Genotype	Model	Model accepted?	# pass	% pass	% fail
	1.9	no	0	0	100
	2	no	0	0	100
D/6	**0.5**	no	0	0.0	100.0
	0.6	no	0	0.0	100.0
	0.667	no	0	0.0	100.0
	0.7	no	0	0.0	100.0
	0.75	no	0	0.0	100.0
	0.8	no	18	1.8	98.2
	0.9	YES	953	95.3	4.7
	1	no	139	13.9	86.1
	1.1	no	0	0	100
	1.2	no	0	0	100
	1.3	no	0	0	100
	1.4	no	0	0	100
	1.5	no	0	0	100
	1.6	no	0	0	100
	1.7	no	0	0	100
	1.8	no	0	0	100
	1.9	no	0	0	100
	2	no	0	0	100
D/7	**0.5**	no	0	0.0	100.0
	0.6	no	0	0.0	100.0
	0.667	no	0	0.0	100.0
	0.7	no	0	0.0	100.0
	0.75	no	0	0.0	100.0
	0.8	no	109	10.9	89.1
	0.9	YES	999	99.9	0.1
	1	no	665	66.5	33.5
	1.1	no	0	0	100
	1.2	no	0	0	100
	1.3	no	0	0	100
	1.4	no	0	0	100
	1.5	no	0	0	100
	1.6	no	0	0	100
	1.7	no	0	0	100
	1.8	no	0	0	100
	1.9	no	0	0	100

Genotype	Model	Model accepted?	# pass	% pass	% fail
	2	no	0	0	100
D/8	**0.5**	no	0	0.0	100.0
	0.6	no	0	0.0	100.0
	0.667	no	0	0.0	100.0
	0.7	no	0	0.0	100.0
	0.75	no	0	0.0	100.0
	0.8	no	244	24.4	75.6
	0.9	YES	1000	100	0
	1	no	927	92.7	7.3
	1.1	no	0	0	100
	1.2	no	0	0	100
	1.3	no	0	0	100
	1.4	no	0	0	100
	1.5	no	0	0	100
	1.6	no	0	0	100
	1.7	no	0	0	100
	1.8	no	0	0	100
	1.9	no	0	0	100
	2	no	0	0	100
D/9	**0.5**	no	0	0.0	100.0
	0.6	no	0	0.0	100.0
	0.667	no	0	0.0	100.0
	0.7	no	0	0.0	100.0
	0.75	no	0	0.0	100.0
	0.8	no	281	28.1	71.9
	0.9	YES	1000	100	0
	1	YES	992	99.2	0.8
	1.1	no	0	0	100
	1.2	no	0	0	100
	1.3	no	0	0	100
	1.4	no	0	0	100
	1.5	no	0	0	100
	1.6	no	0	0	100
	1.7	no	0	0	100
	1.8	no	0	0	100
	1.9	no	0	0	100
	2	no	0	0	100

Genotype	Model	Model accepted?	# pass	% pass	% fail
Larvae, N=7					
D/5	**0.5**	no	0	0.0	100.0
	0.6	no	0	0.0	100.0
	0.667	no	0	0.0	100.0
	0.7	no	4	0.4	99.6
	0.75	no	108	10.8	89.2
	0.8	no	600	60	40
	0.9	no	718	71.8	28.2
	1	no	70	7	93
	1.1	no	0	0	100
	1.2	no	0	0	100
	1.3	no	0	0	100
	1.4	no	0	0	100
	1.5	no	0	0	100
	1.6	no	0	0	100
	1.7	no	0	0	100
	1.8	no	0	0	100
	1.9	no	0	0	100
	2	no	0	0	100
D/6	**0.5**	no	0	0.0	100.0
	0.6	no	0	0.0	100.0
	0.667	no	3	0.3	99.7
	0.7	no	90	9	91
	0.75	no	628	62.8	37.2
	0.8	YES	977	97.7	2.3
	0.9	YES	1000	100	0
	1	no	805	80.5	19.5
	1.1	no	0	0	100
	1.2	no	0	0	100
	1.3	no	0	0	100
	1.4	no	0	0	100
	1.5	no	0	0	100
	1.6	no	0	0	100
	1.7	no	0	0	100
	1.8	no	0	0	100

Genotype	Model	Model accepted?	# pass	% pass	% fail
	1.9	no	0	0	100
	2	no	0	0	100
D/7	**0.5**	no	0	0.0	100.0
	0.6	no	0	0.0	100.0
	0.667	no	8	0.8	99.2
	0.7	no	210	21	79
	0.75	no	873	87.3	12.7
	0.8	YES	998	99.8	0.2
	0.9	YES	1000	100	0
	1	YES	970	97	3
	1.1	no	0	0	100
	1.2	no	0	0	100
	1.3	no	0	0	100
	1.4	no	0	0	100
	1.5	no	0	0	100
	1.6	no	0	0	100
	1.7	no	0	0	100
	1.8	no	0	0	100
	1.9	no	0	0	100
	2	no	0	0	100
D/8	**0.5**	no	0	0.0	100.0
	0.6	no	0	0.0	100.0
	0.667	no	7	0.7	99.3
	0.7	no	182	18.2	81.8
	0.75	no	905	90.5	9.5
	0.8	YES	1000	100	0
	0.9	YES	1000	100	0
	1	YES	994	99.4	0.6
	1.1	no	0	0	100
	1.2	no	0	0	100
	1.3	no	0	0	100
	1.4	no	0	0	100
	1.5	no	0	0	100
	1.6	no	0	0	100
	1.7	no	0	0	100
	1.8	no	0	0	100
	1.9	no	0	0	100

Genotype	Model	Model accepted?	# pass	% pass	% fail
	2	no	0	0	100
D/9	**0.5**	no	0	0.0	100.0
	0.6	no	0	0.0	100.0
	0.667	no	0	0.0	100.0
	0.7	no	84	8.4	91.6
	0.75	no	857	85.7	14.3
	0.8	YES	999	99.9	0.1
	0.9	YES	1000	100	0
	1	YES	1000	100	0
	1.1	no	0	0	100
	1.2	no	0	0	100
	1.3	no	0	0	100
	1.4	no	0	0	100
	1.5	no	0	0	100
	1.6	no	0	0	100
	1.7	no	0	0	100
	1.8	no	0	0	100
	1.9	no	0	0	100
	2	no	0	0	100
Larvae, N=8					
D/5	**0.5**	no	0	0.0	100.0
	0.6	no	0	0.0	100.0
	0.667	no	0	0.0	100.0
	0.7	no	0	0.0	100.0
	0.75	no	0	0.0	100.0
	0.8	no	0	0.0	100.0
	0.9	no	19	1.9	98.1
	1	no	105	10.5	89.5
	1.1	no	0	0	100
	1.2	no	0	0	100
	1.3	no	0	0	100
	1.4	no	0	0	100
	1.5	no	0	0	100
	1.6	no	0	0	100
	1.7	no	0	0	100

Genotype	Model	Model accepted?	# pass	% pass	% fail
	1.8	no	0	0	100
	1.9	no	0	0	100
	2	no	0	0	100
D/6	**0.5**	no	0	0.0	100.0
	0.6	no	0	0.0	100.0
	0.667	no	0	0.0	100.0
	0.7	no	0	0.0	100.0
	0.75	no	0	0.0	100.0
	0.8	no	2	0.2	99.8
	0.9	no	315	31.5	68.5
	1	no	901	90.1	9.9
	1.1	no	30	0.3	99.7
	1.2	no	0	0	100
	1.3	no	0	0	100
	1.4	no	0	0	100
	1.5	no	0	0	100
	1.6	no	0	0	100
	1.7	no	0	0	100
	1.8	no	0	0	100
	1.9	no	0	0	100
	2	no	0	0	100
D/7	**0.5**	no	0	0.0	100.0
	0.6	no	0	0.0	100.0
	0.667	no	0	0.0	100.0
	0.7	no	0	0.0	100.0
	0.75	no	0	0.0	100.0
	0.8	no	10	1	99
	0.9	no	677	67.7	32.3
	1	YES	999	99.9	0.1
	1.1	no	20	2	98
	1.2	no	0	0	100
	1.3	no	0	0	100
	1.4	no	0	0	100
	1.5	no	0	0	100
	1.6	no	0	0	100
	1.7	no	0	0	100
	1.8	no	0	0	100

Genotype	Model	Model accepted?	# pass	% pass	% fail
	1.9	no	0	0	100
	2	no	0	0	100
D/8	**0.5**	no	0	0.0	100.0
	0.6	no	0	0.0	100.0
	0.667	no	0	0.0	100.0
	0.7	no	0	0.0	100.0
	0.75	no	0	0.0	100.0
	0.8	no	22	2.2	97.8
	0.9	no	846	84.6	15.4
	1	YES	1000	100	0
	1.1	no	59	5.9	94.1
	1.2	no	0	0	100
	1.3	no	0	0	100
	1.4	no	0	0	100
	1.5	no	0	0	100
	1.6	no	0	0	100
	1.7	no	0	0	100
	1.8	no	0	0	100
	1.9	no	0	0	100
	2	no	0	0	100
D/9	**0.5**	no	0	0.0	100.0
	0.6	no	0	0.0	100.0
	0.667	no	0	0.0	100.0
	0.7	no	0	0.0	100.0
	0.75	no	0	0.0	100.0
	0.8	no	24	2.4	97.6
	0.9	no	921	92.1	7.9
	1	YES	1000	100	0
	1.1	no	141	14.1	85.9
	1.2	no	0	0	100
	1.3	no	0	0	100
	1.4	no	0	0	100
	1.5	no	0	0	100
	1.6	no	0	0	100
	1.7	no	0	0	100
	1.8	no	0	0	100
	1.9	no	0	0	100

Genotype	Model	Model accepted?	# pass	% pass	% fail
	2	no	0	0	100
Larvae, N=9					
D/5	**0.5**	no	0	0.0	100.0
	0.6	no	0	0.0	100.0
	0.667	no	0	0.0	100.0
	0.7	no	0	0.0	100.0
	0.75	no	0	0.0	100.0
	0.8	no	0	0.0	100.0
	0.9	no	4	0.4	99.6
	1	no	195	19.5	80.5
	1.1	no	130	1.3	98.7
	1.2	no	0	0	100
	1.3	no	0	0	100
	1.4	no	0	0	100
	1.5	no	0	0	100
	1.6	no	0	0	100
	1.7	no	0	0	100
	1.8	no	0	0	100
	1.9	no	0	0	100
	2	no	0	0	100
D/6	**0.5**	no	0	0.0	100.0
	0.6	no	0	0.0	100.0
	0.667	no	0	0.0	100.0
	0.7	no	0	0.0	100.0
	0.75	no	0	0.0	100.0
	0.8	no	0	0.0	100.0
	0.9	no	64	6.4	93.6
	1	no	752	75.2	24.8
	1.1	no	168	16.8	83.2
	1.2	no	40	0.4	99.6
	1.3	no	0	0	100
	1.4	no	0	0	100
	1.5	no	0	0	100
	1.6	no	0	0	100
	1.7	no	0	0	100

Genotype	Model	Model accepted?	# pass	% pass	% fail
	1.8	no	0	0	100
	1.9	no	0	0	100
	2	no	0	0	100
D/7	**0.5**	no	0	0.0	100.0
	0.6	no	0	0.0	100.0
	0.667	no	0	0.0	100.0
	0.7	no	0	0.0	100.0
	0.75	no	0	0.0	100.0
	0.8	no	1	0.1	99.9
	0.9	no	172	17.2	82.8
	1	no	921	92.1	7.9
	1.1	no	542	54.2	45.8
	1.2	no	41	4.1	95.9
	1.3	no	0	0	100
	1.4	no	0	0	100
	1.5	no	0	0	100
	1.6	no	0	0	100
	1.7	no	0	0	100
	1.8	no	0	0	100
	1.9	no	0	0	100
	2	no	0	0	100
D/8	**0.5**	no	0	0.0	100.0
	0.6	no	0	0.0	100.0
	0.667	no	0	0.0	100.0
	0.7	no	0	0.0	100.0
	0.75	no	0	0.0	100.0
	0.8	no	0	0.0	100.0
	0.9	no	200	20	80
	1	YES	965	96.5	3.5
	1.1	no	872	87.2	12.8
	1.2	no	236	23.6	76.4
	1.3	no	30	0.3	99.7
	1.4	no	0	0	100
	1.5	no	0	0	100
	1.6	no	0	0	100
	1.7	no	0	0	100
	1.8	no	0	0	100

Genotype	Model	Model accepted?	# pass	% pass	% fail
	1.9	no	0	0	100
	2	no	0	0	100
D/9	**0.5**	no	0	0.0	100.0
	0.6	no	0	0.0	100.0
	0.667	no	0	0.0	100.0
	0.7	no	0	0.0	100.0
	0.75	no	0	0.0	100.0
	0.8	no	0	0.0	100.0
	0.9	no	124	12.4	87.6
	1	YES	965	96.5	3.5
	1.1	YES	985	98.5	1.5
	1.2	no	545	54.5	45.5
	1.3	no	80	0.8	99.2
	1.4	no	0	0	100
	1.5	no	0	0	100
	1.6	no	0	0	100
	1.7	no	0	0	100
	1.8	no	0	0	100
	1.9	no	0	0	100
	2	no	0	0	100
Larvae, N=10					
D/5	**0.5**	no	0	0.0	100.0
	0.6	no	0	0.0	100.0
	0.667	no	0	0.0	100.0
	0.7	no	0	0.0	100.0
	0.75	no	0	0.0	100.0
	0.8	no	0	0.0	100.0
	0.9	no	2	0.2	99.8
	1	no	13	1.3	98.7
	1.1	no	0	0	100
	1.2	no	0	0	100
	1.3	no	0	0	100
	1.4	no	0	0	100
	1.5	no	0	0	100
	1.6	no	0	0	100

Genotype	Model	Model accepted?	# pass	% pass	% fail
	1.7	no	0	0	100
	1.8	no	0	0	100
	1.9	no	0	0	100
	2	no	0	0	100
D/6	**0.5**	no	0	0.0	100.0
	0.6	no	0	0.0	100.0
	0.667	no	0	0.0	100.0
	0.7	no	0	0.0	100.0
	0.75	no	0	0.0	100.0
	0.8	no	0	0.0	100.0
	0.9	no	50	5	95
	1	no	396	39.6	60.4
	1.1	no	20	0.2	99.8
	1.2	no	0	0	100
	1.3	no	0	0	100
	1.4	no	0	0	100
	1.5	no	0	0	100
	1.6	no	0	0	100
	1.7	no	0	0	100
	1.8	no	0	0	100
	1.9	no	0	0	100
	2	no	0	0	100
D/7	**0.5**	no	0	0.0	100.0
	0.6	no	0	0.0	100.0
	0.667	no	0	0.0	100.0
	0.7	no	0	0.0	100.0
	0.75	no	0	0.0	100.0
	0.8	no	3	0.3	99.7
	0.9	no	293	29.3	70.7
	1	no	885	88.5	11.5
	1.1	no	570	5.7	94.3
	1.2	no	0	0	100
	1.3	no	0	0	100
	1.4	no	0	0	100
	1.5	no	0	0	100
	1.6	no	0	0	100
	1.7	no	0	0	100

Genotype	Model	Model accepted?	# pass	% pass	% fail
	1.8	no	0	0	100
	1.9	no	0	0	100
	2	no	0	0	100
D/8	**0.5**	no	0	0.0	100.0
	0.6	no	0	0.0	100.0
	0.667	no	0	0.0	100.0
	0.7	no	0	0.0	100.0
	0.75	no	0	0.0	100.0
	0.8	no	19	1.9	98.1
	0.9	no	644	64.4	35.6
	1	YES	989	98.9	1.1
	1.1	no	153	15.3	84.7
	1.2	no	10	0.1	99.9
	1.3	no	0	0	100
	1.4	no	0	0	100
	1.5	no	0	0	100
	1.6	no	0	0	100
	1.7	no	0	0	100
	1.8	no	0	0	100
	1.9	no	0	0	100
	2	no	0	0	100
D/9	**0.5**	no	0	0.0	100.0
	0.6	no	0	0.0	100.0
	0.667	no	0	0.0	100.0
	0.7	no	0	0.0	100.0
	0.75	no	0	0.0	100.0
	0.8	no	54	5.4	94.6
	0.9	no	843	84.3	15.7
	1	YES	998	99.8	0.2
	1.1	no	330	33	67
	1.2	no	50	0.5	99.5
	1.3	no	0	0	100
	1.4	no	0	0	100
	1.5	no	0	0	100
	1.6	no	0	0	100
	1.7	no	0	0	100
	1.8	no	0	0	100

Genotype	Model	Model accepted?	# pass	% pass	% fail
	1.9	no	0	0	100
	2	no	0	0	100
Larvae, N=11					
D/5	**0.5**	no	0	0.0	100.0
	0.6	no	0	0.0	100.0
	0.667	no	0	0.0	100.0
	0.7	no	0	0.0	100.0
	0.75	no	1	0.1	99.9
	0.8	no	11	1.1	98.9
	0.9	no	111	11.1	88.9
	1	no	445	44.5	55.5
	1.1	no	505	50.5	49.5
	1.2	no	240	24	76
	1.3	no	62	6.2	93.8
	1.4	no	30	0.3	99.7
	1.5	no	0	0	100
	1.6	no	0	0	100
	1.7	no	0	0	100
	1.8	no	0	0	100
	1.9	no	0	0	100
	2	no	0	0	100
D/6	**0.5**	no	0	0.0	100.0
	0.6	no	0	0.0	100.0
	0.667	no	1	0.1	99.9
	0.7	no	1	0.1	99.9
	0.75	no	24	2.4	97.6
	0.8	no	60	6	94
	0.9	no	428	42.8	57.2
	1	no	868	86.8	13.2
	1.1	no	934	93.4	6.6
	1.2	no	709	70.9	29.1
	1.3	no	298	29.8	70.2
	1.4	no	53	5.3	94.7
	1.5	no	30	0.3	99.7
	1.6	no	0	0	100

Genotype	Model	Model accepted?	# pass	% pass	% fail
	1.7	no	0	0	100
	1.8	no	0	0	100
	1.9	no	0	0	100
	2	no	0	0	100
D/7	**0.5**	no	0	0.0	100.0
	0.6	no	0	0.0	100.0
	0.667	no	3	0.3	99.7
	0.7	no	10	1	99
	0.75	no	44	4.4	95.6
	0.8	no	185	18.5	81.5
	0.9	no	654	65.4	34.6
	1	YES	952	95.2	4.8
	1.1	YES	999	99.9	0.1
	1.2	no	936	93.6	6.4
	1.3	no	563	56.3	43.7
	1.4	no	163	16.3	83.7
	1.5	no	70	0.7	99.3
	1.6	no	0	0	100
	1.7	no	0	0	100
	1.8	no	0	0	100
	1.9	no	0	0	100
	2	no	0	0	100
D/8	**0.5**	no	0	0.0	100.0
	0.6	no	0	0.0	100.0
	0.667	no	2	0.2	99.8
	0.7	no	10	1	99
	0.75	no	60	6	94
	0.8	no	245	24.5	75.5
	0.9	no	791	79.1	20.9
	1	YES	986	98.6	1.4
	1.1	YES	1000	100	0
	1.2	YES	985	98.5	1.5
	1.3	no	748	74.8	25.2
	1.4	no	194	19.4	80.6
	1.5	no	60	0.6	99.4
	1.6	no	0	0	100
	1.7	no	0	0	100

Genotype	Model	Model accepted?	# pass	% pass	% fail
	1.8	no	0	0	100
	1.9	no	0	0	100
	2	no	0	0	100
D/9	**0.5**	no	0	0.0	100.0
	0.6	no	0	0.0	100.0
	0.667	no	0	0.0	100.0
	0.7	no	4	0.4	99.6
	0.75	no	66	6.6	93.4
	0.8	no	283	28.3	71.7
	0.9	no	859	85.9	14.1
	1	YES	998	99.8	0.2
	1.1	YES	1000	100	0
	1.2	YES	986	98.6	1.4
	1.3	no	771	77.1	22.9
	1.4	no	210	21	79
	1.5	no	20	0.2	99.8
	1.6	no	0	0	100
	1.7	no	0	0	100
	1.8	no	0	0	100
	1.9	no	0	0	100
	2	no	0	0	100

Chapter 3

Investigation of additional potential regulators of denticle organization

3.1 Introduction

The *Drosophila* denticles are planar polarized, actin based protrusions arranged in a quantifiable, stereotyped organization pattern. Denticles are formed through the condensation of small clusters of actin and myosin from an initially diffuse apical actin meshwork, which then aggregate to form larger, stable denticle precursors (Chanut-Delalande et al., 2006; Price et al., 2006; Walters et al., 2006; Donoughe & DiNardo, 2011). These structures are distributed linearly and in a unipolar manner along the cell DV axis, and each embryonic cell may create between one and six denticles (Price et al., 2006; Walters et al., 2006; Dilks & DiNardo, 2010). Once established, each precursor then extends apically, reshaping the apical membrane and providing a template for the formation of the larval cuticle. The formation of denticles and the creation of this distribution pattern depend on both the actin and microtubule cytoskeletons, as well as the planar cell polarity pathways (Walters et al., 2006; Repiso et al., 2010; Marcinkevicius &

Zallen, 2013; Lawlor et al., 2013; Saavedra et al., 2016). I have shown that the denticle cells of the *Drosophila* embryo produce a quantifiable, stereotyped organization of actin foci that scales with cell size, and that the generation and fidelity of this pattern requires an intact, dynamic microtubule cytoskeleton. However, it is still not well understood how the number and spatial arrangement of these structures is controlled.

The involvement of microtubules in organizing denticles (see Chapter 3), the presence of a microtubule cluster at the site of denticle formation (Price et al., 2006), and the localization of the minus-end-binding protein Patronin at sites of denticle formation (see Chapter 3), raise the possibility that the denticles may behave as acentrosomal MTOCs, and that this behavior allows for the creation of the spatial organization pattern of denticles. Furthermore, while it is well established that denticles arise at the posterior margin of the denticle cells and that this localization requires activity of both PCP pathways (Repiso et al., 2010; Donoughe & DiNardo, 2011; Marcinkevicius & Zallen, 2013; Lawlor et al., 2013; Saavedra et al., 2016), precisely how this localization is established, or how denticles are anchored at the posterior margin, is unclear. In this chapter, I will introduce some classes and several additional candidate molecules, including additional regulators of the actin and microtubule cytoskeletons, whose localization patterns, molecular characteristics, or roles in similar systems suggested that they may be involved in the formation and / or spatial organization of denticles. For clarity, I will introduce each molecule and provide a discussion of its known roles and activities immediately prior to discussing the specific experiments I conducted during the course of this thesis to evaluate the potential roles for these candidates in the spatial organization of the denticles (Chapter 2). Additionally, I will describe a number of experiments that investigate the dynamics and temporal regulation of the actin cytoskeleton relative to the creation of the denticle organization pattern.

3.2 The conserved spindle-orientation proteins mud and pins have specific localization patterns in the denticle cells

3.2.1 Mud mediates force-dependent microtubule reorganization

The localization within the denticle of microtubules and microtubule regulating proteins such as Patronin raise the possibility that denticles may behave like acentrosomal microtubule organizing centers, and thus be spaced in a microtubule dependent manner. This hypothesis is supported by the defects observed in denticle organization when Spastin overexpression or Patronin knockdown are used to disrupt microtubules in denticle cells (**Figure 2.7**). Therefore, I asked whether either mud or pins, important effectors of microtubule organization and polarity, might have roles in coordinating the microtubule cytoskeleton during denticle formation to achieve denticle spacing, placement, or both. Additional discussion of mud's localization within the denticle cells can be found in Chapter 2.

Mud (mushroom body defect) is a dynein-associated, microtubule binding protein required for spindle organization (Kotak & Gönczy, 2013). Mud is the *Drosophila* homologue of the mammalian protein NuMa (nuclear mitotic apparatus protein 1), which has well defined roles in the organization of centrosomal microtubules and spindle orientation during asymmetric division (Guan et al., 2000; Fant et al., 2004; Bowman et al., 2006; Izumi et al., 2006; Siller et al., 2006; Morin & Bellaïche, 2011). Mud has several distinct roles in organizing microtubules, mainly through its ability to enhance microtubule polymerization (Bowman et al., 2006) and interact with the minus-end-directed motor dynein (Johnston et al., 2009). Correct spindle positioning and orientation, particularly during asymmetric cell division, requires the asymmetric localization of mud. This interaction between mud and the spindle is dependent on the pins (partner of inscuteable; LGN in mammals) - Gαi complex, and involves the association of mud with the dynein / dynactin complex to properly rotate the spindle into the correct division plane (Bowman et al., 2006; Izumi et al., 2006; Siller et al., 2006; Morin & Bellaïche, 2011; Bergstralh et al.,

2013a). Pins is a scaffolding protein containing three GoLoco motifs, which allow it to bind to heterotrimeric G protein α subunits at the membrane, and several tetratricopeptide repeats, which can bind to mud (during spindle orientation) or Inscuteable (which helps to recruit pins in a planar polarized manner) (Bergstralh et al., 2013a; Kotak & Gönczy, 2013). The primary role of pins is in spindle orientation, where it acts as a linker between the membrane-bound Gαi and the cytoplasmic mud at specific locations in the cell, as dictated by insc. Planar polarized localization of pins at the membrane and its subsequent recruitment of mud and the dynein / dynactin complex is required for correct spindle orientation (Bergstralh et al., 2013a). While pins' best-described role is as a molecular scaffold during asymmetric division, mud has several additional, pins-independent roles in organizing centrosomes and centrosomal microtubules.

3.2.2 Pins-dependent roles for mud during mitotic spindle orientation

Mud activity and localization is required for the orientation of the mitotic spindle. This has been particularly well studied in the *Drosophila* neuroblasts, which divide asymmetrically to ensure correct fate determination in the daughter cells. Mud, like its homologue NuMA, provides a direct link between the membrane-associated pins-Gαi complex and the microtubules of the mitotic spindle. Pins mediates spindle orientation through two means. Microtubule attachment to the cortex is mediated through phosphorylation of pins by the spindle-associated kinase aurora A, which promotes the binding of discs large (dlg). Dlg, in turn, recruits the plus-end-directed kinesin Khc73, which is able to partially, but not completely, orient the spindle (Siegrist & Doe, 2005; Johnston et al., 2009; Mauser & Prehoda, 2012; Bergstralh et al., 2013b). In contrast, the pulling force that shifts the centrosome and spindle complex towards the cortex is mediated through its binding to mud, which recruits the dynein / dynactin motor complex (Siller et al., 2006; Siller & Doe, 2009). Recruitment of dynein / dynactin through mud is required to properly align the spindle (Bowman et al., 2006; Izumi et al., 2006; Siller et al., 2006). This pins / mud binding and cortical recruitment also requires the scaffolding protein canoe (afadin in mammals), which

is able to recruit Ran GTPase activity (Wee et al., 2011). Interestingly, the hippo kinase complex may also be involved in the cortical accumulation of mud by acting as a switch to promote the activity of pins / mud (Dewey et al., 2015). Balance between the activity of these two modes is thought to be regulated through binding to the upstream regulator inscuteable (Mauser & Prehoda, 2012), which can bind both to bazooka (baz; Par-3 in mammals) in the PAR polarity complex and to pins / LGN in the spindle orientation complex. Insc, along with dlg, is localized by the frizzled planar polarity system to spindle orientation, thus linking the planar polarity system to spindle alignment (Kaltschmidt et al., 2000; Kraut et al., 1996; Schober et al., 1999; Wodarz et al., 1999; Bellaiche et al., 2001a,b; Segalen et al., 2010; Mauser & Prehoda, 2012; Johnston et al., 2013). The association of mud with pins is further enhanced though interactions with the centriolar protein anastral spindle 2 (Ana2), and the dynein light chain cut up (ctp) (Wang et al., 2011).

3.2.3 Mud has additional, pins-independent roles in microtubule organization

While the best-characterized roles for mud are the pins-dependent mechanisms for spindle organization, mud also has several pins-independent roles in microtubule organization. mud is assumed to share the general ability of NuMA to interact directly with the dynein complex (Johnston et al., 2009; Merdes et al., 1996); mud has been shown to associate with the dynein light chain cut up (Wang et al., 2011), and mutants for dynein / dynactin complex components such as Lis1 and glued show spindle orientation defects similar to those in *mud* mutants (Siller et al., 2005). These data suggest that, like NuMA, mud most likely is able to interact with the dynein-dynactin complex. Mud appears also to have the ability to orient spindles independent of and in addition to the classical pins / Gαi pathway. In the neuroblasts, the late-stage rescue of spindle orientation observed in *pins* mutants is thought to be due to a pins-independent role for mud in telophase, near the end of cell division (Izumi et al., 2006). In the pupal notum, the tricellular junctions may provide some necessary spatial information for spindle orientation.

Mud localizes to the tricellular junctions in wild-type tissues, and this localization is decreased upon loss of its junctional binding partner, discs large, as well as the tricellular junctional protein Gliotactin (Bosveld et al., 2016). This localization appears to regulate the mud-induced dynein pulling forces that orient the spindle, as the rate of centrosome recoil after ablation of the astral microtubules decreased in *mud* and *discs large* mutants as compared to the wild type (Bosveld et al., 2016). Finally, recent work suggests that mud is required in postmitotic neurons for axon guidance, possibly via its ability to rearrange the microtubule cytoskeleton in response to polarity cues (Cate et al., 2016).

Most interestingly, mud also has roles outside of spindle orientation in the general regulation of microtubule organization and dynamics, particularly in the context of microtubule organizing centers (MTOCs). Like NuMA, mud can interact with microtubules independently of pins to promote polymerization (Du et al., 2002; Haren & Merdes, 2002; Bowman et al., 2006). In the *Drosophila* neuroblasts, mud localizes to both the apical cortex and to the centrosomes. In the absence of pins or Gαi, mud is lost from the apical cortex, but remains at centrosomes in a microtubule dependent manner, implying a separate recruitment and function of mud at centrosomes (Izumi et al., 2006). *Mud* mutants frequently have additional centrosomes (Izumi et al., 2006), and although these centrosomes do not induce the formation of multipolar spindles, it has been reported that these supernumerary centrosomes may be the focal points for weak microtubule arrays (Izumi et al., 2006). Together, these data indicate that mud likely has roles in centrosome assembly or maintenance. More generally, it implies that mud may have some regulatory function in microtubule assembly at MTOCs. Therefore, I asked whether either mud or pins, important effectors of microtubule organization and polarity, might have roles in coordinating the microtubule cytoskeleton during denticle formation to achieve denticle spacing, placement, or both.

3.2.4 Localization patterns of mud and pins in the denticle cells

Antibodies are available for both mud and pins (Izumi et al., 2006), therefore I first addressed the question of whether mud or pins are involved in establishing the denticle organization pattern by investigating whether either protein has a specific localization patterns in the denticle cells. During the denticle-forming stages, mud is expressed at elevated levels in denticle cells compared to the smooth cells (**Figure 3.1 A**) (n=13 embryos at stage 14-16, qualitative analysis of expression levels). In the earliest stages (stage 14), it is generally cortical and distributed unevenly throughout the apical regions of the cell, but as denticle formation progresses, it begins to form doughnut-like rings around the nascent denticles and is excluded from the actin 'core' of the denticle (**Figure 2.6 B**). At later stages of denticle formation as the actin bundle elongates, mud also extends apically around the denticle protrusion: in cross-sectional views of stage 16 and later embryos, mud seems to surround the entire denticle, still without being a part of the actin core (**Figure 3.1 B**).

Pins, in contrast, appears by eye to be mildly AP polarized in the denticle cells. Staining of pins is weak and is highly punctate. Nevertheless, pins appears to accumulate along the long edges of denticle cells, though this accumulation appears somewhat fragmented and does not occur evenly within every cell **Figure 3.1 C)** (n=12 embryos at stage 13-16). As with mud, by eye, pins levels appear to be elevated in denticle cells compared to the adjacent smooth cells (data not shown). These data indicate that both mud and pins may have roles in the denticle cells during denticle forming stages, although further analysis will be required to determine what, if any, role they play in denticle organization.

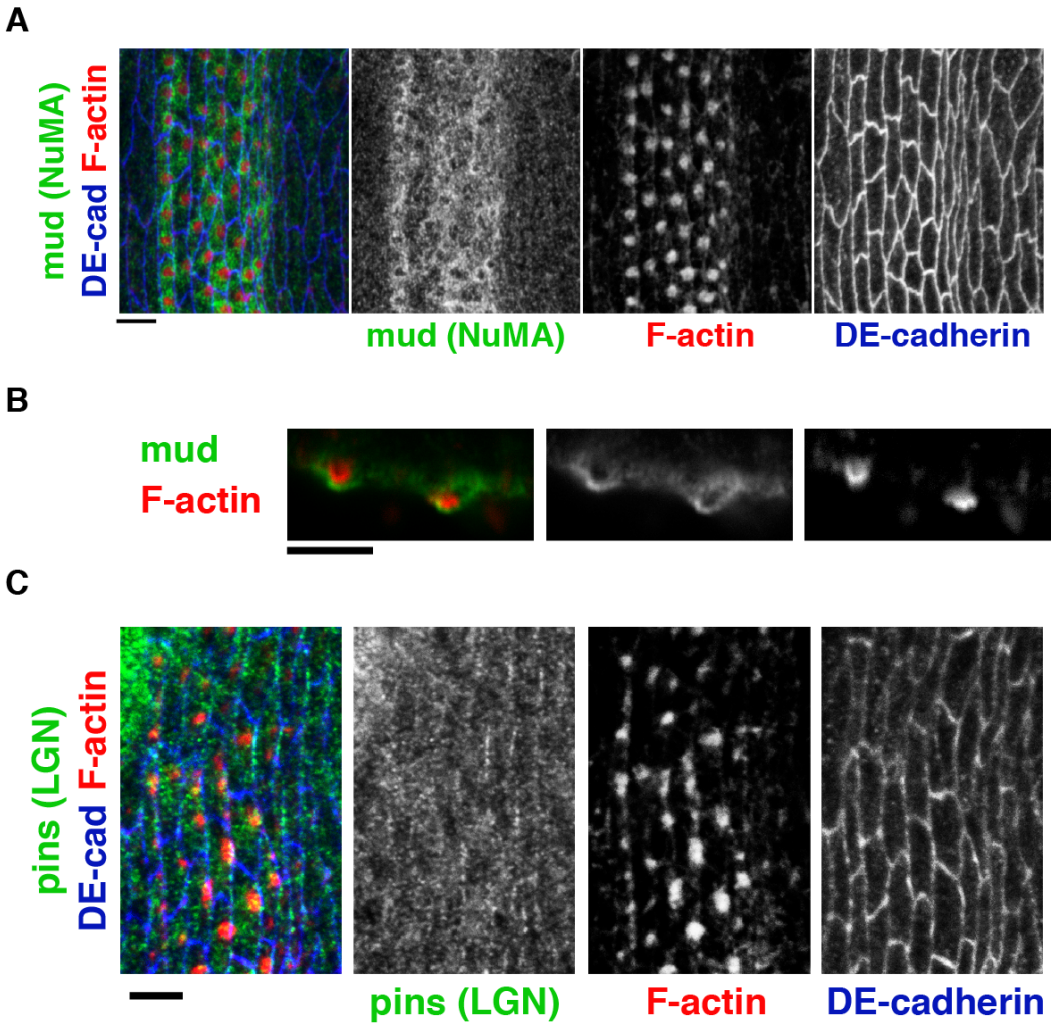

Figure 3.1: Localization patterns of the microtubule associated proteins mud and pins in denticle cells. **A.** mud is enriched in denticle cells, and surrounds the actin protrusions. mud, green; F-actin, red; DE-cadherin, blue. Bar, 5 µm. n = 13 embryos at stages 14-16. **B.** mud surrounds the apical portion of the denticle protrusion in late-stage embryos (stage 16). mud, green; F-actin, red. Bar, 5 µm. **C.** pins is polarized along the AP axis in denticle cells. pins, green; F-actin, red; DE-cadherin, blue. Bar, 5 µm. n = 12 embryos at stages 13-16.

3.2.5 Neither zygotic *mud* mutants nor maternal / zygotic *pins* mutants have a denticle organization phenotype

Next, I tested whether mutation of either *mud* or *pins* affects the organization pattern of the denticles. Mud is required for female meiosis, and for all of the classical alleles of *mud*, females are sterile and do not produce embryos (de Belle & Heisenberg, 1996; Yu et al., 2006). Therefore, I quantified denticle organization patterns in zygotic mud^{F33} mutants. However, these embryos did not show any defects in denticle organization or formation (n=6 stage 14-16 zygotic mud^{F33} mutants imaged, 4 out of 6 quantified for denticle organization). Quite possibly, if mud does have a role in the denticle cells, maternal contribution of *mud* is sufficient, and additional work will be required to test mud's influence on the denticles.

It is possible to recover embryos from mothers bearing germline *pins* mutations, therefore I next attempted to examine denticle organization patterns in the $maternal^{-}$ / $zygotic^{+/-}$ progeny of females bearing $pins^{p62}$ *FRT 82B* germline clones (a null allele of *pins* (Bergstralh et al., 2016)). Curiously, however, I was unable to recover late-stage (stage 14 onward) embryos that were both maternally and zygotically mutant for *pins*, which should have been identifiable by their lack of the Twist::GFP expression from the balancer chromosome. Zygotically rescued *pins* mutants, which were identified by the expression of Twist::GFP provided by the male parent, did not show any defects in denticle organization, formation, or placement (n=16 stage 14-16 embryos imaged, 4 out of 16 quantified for denticle organization).

3.3 Analysis of the spatiotemporal formation of denticle precursors

The large denticle precursors emerge from an initially dispersed actomyosin meshwork through the coalescence of smaller actin foci (Price et al., 2006; Walters et al., 2006). Therefore, denticles

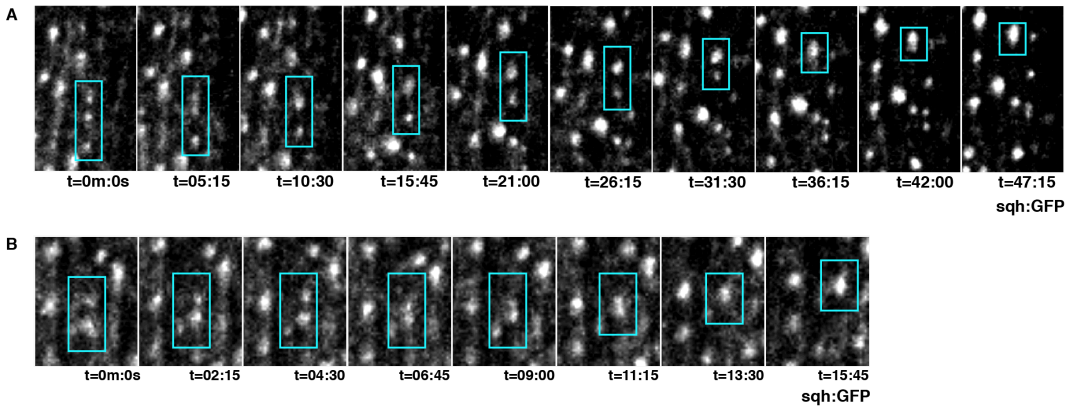

Figure 3.2: Dynamics of actin condensations. A, B. Denticle condensations can shift positions and can merge with other actin foci. Stills from live movie of a stage 14 embryo expressing *spaghetti squash* (myosin RLC)-GFP ubiquitously. n = 7 movies of stage 14-16 embryos expressing various actomyosin markers (including sqh-GFP, moe-mCherry, and utrophin-GFP).

could be initiated at their final location, or they could initiate randomly across the DV axis of the cell and be shifted to form the final denticle distribution pattern later. To test whether the localization of denticle precursors are static or dynamic, I tracked denticle precursor formation live in embryos expressing one of several GFP-tagged actin markers: spaghetti-squash::GFP, moesin::GFP, or utrophin::GFP. In embryos expressing the myosin regulatory light chain *spaghetti-squash-GFP*, I found that actin foci in the denticle cells are highly mobile (n = 7 movies of 2-3 denticle belts each from stage 14-16 embryos). Denticle punctae can shift position, disappear, and occasionally collide with one another and merge to form a larger, single denticle precursor (**Figure 3.2**). In high-magnification movies of embryos expressing the actin binding protein utrophin tagged with GFP, denticle precursors change size and shape during the initial actin accumulation stages. These data suggest that denticle localization is determined through a dynamic process. However, more detailed analysis of this process, particularly with additional markers for microtubule related proteins, will be required to fully understand how and where denticles are initiated, and the dynamics of their spatial distribution.

3.4 Mutation of *multiple wing hairs*, a negative regulator of actin bundle formation, alters denticle number and denticle organization patterns

3.4.1 *multiple wing hairs* is a negative regulator of actin bundle formation

The *Drosophila* wing hairs are another type of planar polarized trichomes that have been studied in great detail. Like the denticles, the wing hairs are actin based, apically protruding structures, and consist of bundled actin and microtubule (Wong & Adler, 1993; Turner & Adler, 1998; Lee & Adler, 2002). However, several key differences exist. First, the wing hairs are nearly an order of magnitude larger than the denticles: wing hairs are reportedly 10-20 µm long (Guild, 2005), while denticles extend only approximately 2 µm beyond the apical cell surface (Chanut-Delalande et al., 2006), suggesting that there are likely to be differences in the formation mechanisms, and in the structural requirements. The second difference, most important for this work, is that unlike the denticle cells, which may form multiple denticle protrusions each (Price et al., 2006; Dilks & DiNardo, 2010) see Chapter 2, each wing cell forms a single, distally-oriented hair at its distal-most vertex (Gubb & García-Bellido, 1982; Wong & Adler, 1993). However, as many of the mutations that cause defects in wing hair formation also alter denticle structure and / or formation, including mutant alleles of forked, fascin (Guild, 2005), zipper (myosin II heavy chain) (Winter et al., 2001), and *crinkled* (Turner & Adler, 1998), it is likely that there is a high degree of overlap between the cytoskeletal regulators required for the formation and organization of both these actin based, apical cuticular extensions (Dickinson & Thatcher, 1997).

One particularly interesting regulator whose mutation causes disorganization phenotypes in the wing and in the denticles is the novel actin cytoskeleton antagonist, *multiple wing hairs* (*mwh*) (Dickinson & Thatcher, 1997; Gubb & García-Bellido, 1982; Strutt & Warrington, 2008; Lu et al., 2015; Lu & Adler, 2015). mwh is a G-protein binding domain-formin homology 3

(GBD-FH3) domain protein that acts downstream of the Frizzled planar polarity pathway to regulate trichome formation (Gubb & García-Bellido, 1982; Strutt & Warrington, 2008; Yan et al., 2008). Structurally, it shows significant similarity to family members of the formin Diaphanous, and acts antagonistically with Diaphanous in the regulation of wing hair formation (Lu et al., 2015; Lu & Adler, 2015). Studies in the wing show that mwh has two temporally separate roles in wing hair formation (Strutt & Warrington, 2008; Yan et al., 2008; Lu & Adler, 2015; Lu et al., 2015). At early stages of development, mwh accumulates at the proximal side, inhibiting actin polymerization everywhere except the distal vertex (Lu et al., 2015). Later, mwh accumulates in the hairs, promoting bundling (possibly in concert with Diaphanous) and inhibiting the formation of new hairs at the base of the elongating primary hair. Thus, mwh acts as a negative regulator of the actin cytoskeleton in the wing, ensuring that a single, distally-positioned wing hair is formed. In larval cuticle preparations, mutation of *mwh* increases the denticle density and general disorder throughout the belt. In column 1 cells, it also generates extra and disorganized denticles (Dickinson & Thatcher, 1997). What this crowding phenotype looks like at the cellular level is unknown. To test how this apparent crowding in the denticle cells affects the spatial organization of the denticles, I quantified denticle organization in *mwh* mutant embryos.

3.4.2 Mutations in *mwh* affect denticle number without altering cell size

Consistent with the phenotypes observed in the cuticle, mutation of *mwh* manifests in two distinct phenotypes in the denticle cells: in the placement of denticles in column 1 cells, and in the density of denticles throughout the belt (**Figure 3.3 A,B, Table 3.1**). Denticles in column 1 cells of *mwh* mutants were frequently misplaced; denticles were no longer restricted to the posterior margin, as occurs in wild type, and a single cell could have have a mixture of denticles placed at the posterior margin, at the anterior margin, and in the middle of the cell (**Figure 3.3 A**). These observations are consistent with a role for the Frizzled PCP pathway in promoting the correct localization of mwh. Notably, however, this phenotype was not uniform across the belt, occuring most often in column 1 denticle cells (**Figure 3.3 B**), and denticle hook polarity was not

reversed in cuticle preparations (Dickinson & Thatcher, 1997), as occurs in embryos mutant for components of the Fat PCP pathway (Marcinkevicius & Zallen, 2013). Denticles in these cells appeared qualitatively to have regular, if decreased, spacing, but were excluded from the spacing analysis due to the additional complexity of integrating the 2-dimensional spacing patterns of these mixed-placement cells with the 1-dimensional spacing pattern observed in all other cells and genotypes.

In cells across the belt where denticle placement was correctly confined to the posterior margin, I quantified the change in denticle spacing. The average number of denticles made per cell did not increase significantly between WT and *mwh* mutants (1.9 $\pm$ 1.0 and 2.0 $\pm$ 0.8 denticles / cell, respectively), possibly because the most affected cells showed placement defects and were removed from the analysis. Similarly, cell size was similar, though slightly decreased in *mwh* mutants compared to the WT (8.9 $\pm$ 2.8 µm in WT vs. 8.5 $\pm$ 2.9 µm in *mwh*^{1}) (**Table 3.1**). However, there was a pronounced upward shift compared to wild-type in the percentage of cells making one denticle versus the percentage of cells making two denticles in the *mwh* mutant embryos (**Figure 3.3 C**). This was most likely due to the fact that cells making one or two denticles in *mwh* mutants were markedly smaller than the corresponding cells in wild type (**Table 3.1**). The mean spacing distance in these cells was also correspondingly smaller (**Figure 3.3 C, Table 3.1**). Despite this, however, spacing scaled in a manner similar to wild type (**Figure 3.3 H**), suggesting that although there is an absolute increase in number, the spacing mechanism scales correctly when denticles are properly distributed along the posterior boundary.

3.5 Testing the limiting component hypothesis

Determining the size of intracellular structures is an important component of achieving optimal intracellular organization, and a wide variety of structures, including centrosomes (Greenan et al., 2010; Decker et al., 2011), mitotic spindles (Wühr et al., 2008; Carvalho et al., 2009;

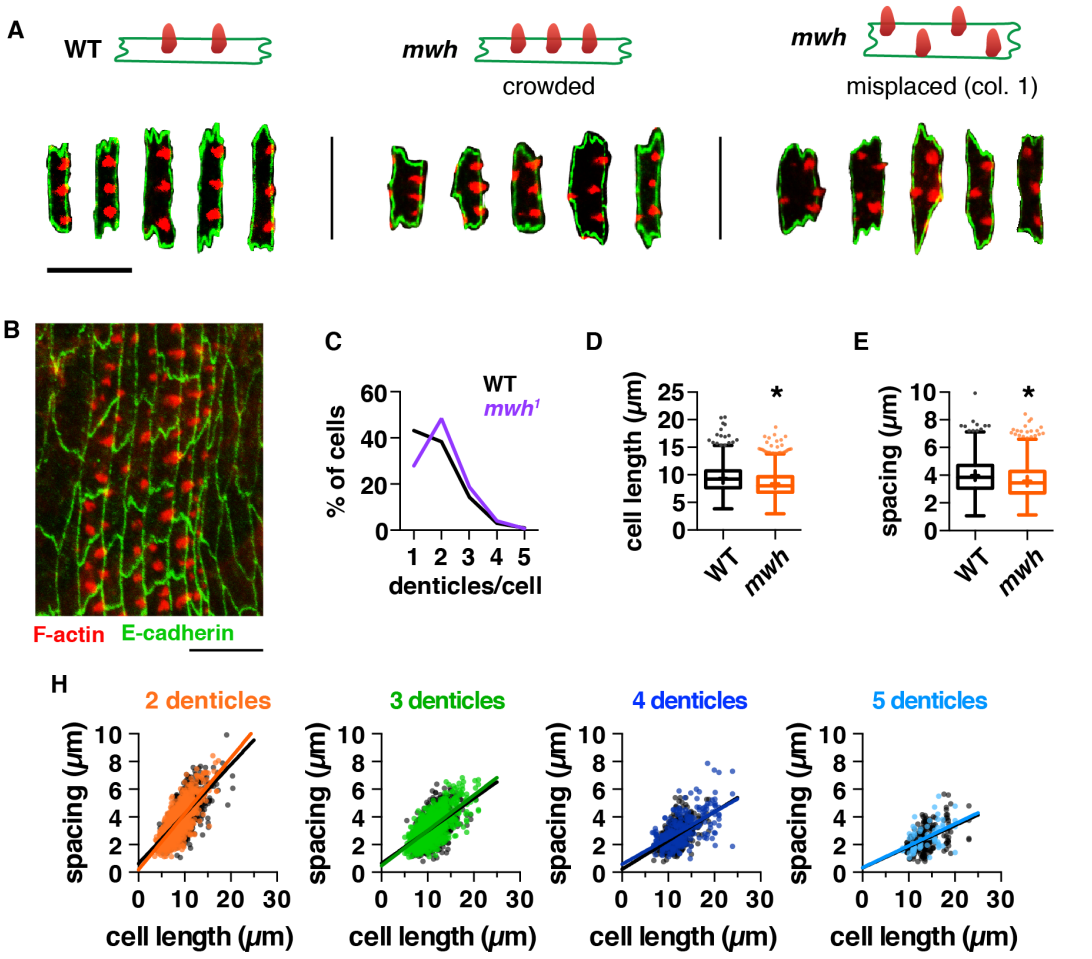

Figure 3.3: Multiple wing hairs affects denticle number and organization. **A.** Examples of denticle cells in wild type (WT) and *mwh*^{1} embryos, showing the two phenotypes in *mwh*^{1} mutants. Left and middle, cells with 3 denticles show the crowding phenotype of *mwh*^{1}. Right, column 1 denticle cells in *mwh*^{1} mutants often produce a mixture of posteriorly and anteriorly positioned denticles; this rarely occurs in the WT. F-actin (phalloidin, red), E-cadherin (green). Bar, 10 μm. **B.** Denticle belt from a *mwh*^{1} mutant showing the two phenotypes, crowding and mis-polarization. **C.** Distribution of cells making 1 to 5 denticles in *mwh*^{1} (purple) vs. WT (black). **D,E.** Cell length (D), denticle spacing (E) for all cells. Boxes, 25th-75th percentile; whiskers, 1.5 inter-quartile range (IQR); horizontal line, median; +, mean. *, $p < 0.0001$ vs. WT, one-way ANOVA, Tukey's multiple corrections test. **F.** Denticle spacing vs. cell length for cells with 2-5 denticles in WT (black) and *mwh*^{1} (colors). Lines, best-fit linear regressions, symbols, means.

Table 3.1: Cell size, denticle number, and denticle spacing measurments for *mwh*[1] (mean ± SD)

Genotype		WT	*mwh*[1]
Number of embryos		12	17
Cells analyzed		3092	2368
Denticles analyzed		833	4755
Denticles/cell		1.9 ± 1.	2.0 ± 0.8
min, max denticles		1, 6	1, 7
Cell length (μm) for cells with N denticles)	**all**	8.9 ± 2.8	8.5 ± 2.9
	1	7.2 ± 2.0	6.5 ± 1.7
	2	9.4 ± 2.3	8.4 ± 2.2
	3	11.1 ± 2.2	10.7 ± 2.9
	4	11.9 ± 2.1	12.9 ± 3.7
Min. cell length (μm)		2.2	1.9
Max. cell length (μm)		26.5	27.8
Denticle spacing (μm) for cells with N denticles)	**all**	3.4 ± 1.2	3.3 ± 1.2
	2	4.0 ± 1.2	3.6 ± 1.2
	3	3.3 ± 1.0	3.2 ± 1.1
	4	2.7 ± 0.9	3.0 ± 1.2
Min. spacing (μm)		0.6	1
Max. spacing (μm)		9.9	8.4
Denticle-to-edge spacing (μm)	**all**	2.9 ± 1.4	2.6 ± 1.1
	1	3.6 ± 1.4	3.3 ± 1.1
	2	2.7 ± 1.2	2.5 ± 1.0
	3	2.4 ± 1.0	2.3 ± 1.0
	4	2.0 ± 0.9	2.2 ± 1.1

Hara & Kimura, 2009; Brugués et al., 2012; Good et al., 2013; Hazel et al., 2013), and nucleoli (Brangwynne et al., 2011; Weber & Brangwynne, 2015), have been demonstrated to scale with cell size. Denticle cells range greatly in size, and each cell may produce a variable number of denticles. These denticles are then spaced along the cell length as a function of number. Importantly, the number of denticles does not seem to be a fixed property of cell length; similarly sized cells may make many denticles, or only a few. Spacing then is a function of both denticle number and of cell size. However, the precise nature of the relationships between denticle number, denticle size, and cell size and how these factors are balanced is unclear. While these questions are evident in the embryo, the increased range of cell sizes, denticle sizes, and denticles per cell counts in larvae provide an ideal opportunity to explore more thoroughly the relationships between the dimensions of the cell, the number of denticles produced, and the size of each denticle. Therefore, this section will provide details for measurements taken in first instar larvae, rather than in embryos.

One way in which denticle size and number may be balanced with cell size is through a limiting component model, in which the concentration of actin or some other critical component is limited in proportion to cell size. According to a limiting component model such as the one proposed for the scaling of centrosomes (Decker et al., 2011; Goehring & Hyman, 2012), there should be a linear relationship between cell size and the amount of material within all subcellular structures of a given type, regardless of the total number of structures in the cell. If such a limiting component model is at work in the rectangular cells of the denticle system, I would expect to see three things. First, cells with a larger total apical area should have a larger total denticle area; second, in cells of similar size, denticle size should decrease as denticle number increases; third, for cells with a given number of denticles, denticle size should increase with cell size. Although evaluation of the limiting component hypothesis typically relates structure volume to cell volume, as the denticle cells are of uniform height, surface area may act as a proxy for volume, and the following experiments test the relationships between cell surface area and denticle area.

I began by testing how cell area might relate to denticle size by quantifying cell and denticle areas in larval images. Increasing cell area did not correspond to an increase in total denticle area (**Figure 3.4 A**), and total denticle area did not show consistent increases in cells with a greater number of denticles (**Figure 3.4 E**). Furthermore, in cells making a specific number of denticles, the area of each individual denticle was similar across cells with a wide range of areas (**Figure 3.4 G**). This led me to conclude that cell area is not the primary determinant of denticle area.

I next tested the possibility that cell length, rather than cell area, might be limiting denticle size. Indeed, although denticle area was only weakly correlated with cell length (R^2 = 0.18) (**Figure 3.4 B**), I found that the total width of all denticles in a cell was highly correlated with cell length (R^2 = 0.5) (**Figure 3.4 C**), as well as with denticle number (R^2 = 0.96) (**Figure 3.4 F**). Additionally, individual denticles decreased in width as denticle number increased (**Figure 3.4 D**). This suggests that the posterior cell length, rather than the total cell area, may determine competency for forming denticles and thus may act as a limiting factor to scale denticles along a single dimension of the cell, controlling both denticle spacing and denticle number.

As it has previously been shown that mitotic spindle length scales with centrosome size (Greenan et al., 2010), I looked at the relationship between spacing and denticle diameter. Consistent with the trends I was able to observe by eye, the spacing distance increases with increasing denticle diameter (R^2 = 0.49) (**Figure 3.4 H**). The denticle separation distance decreased linearly with denticle diameter, such that the largest denticles (produced by the smallest cells) were spaced furthest apart, while the smallest denticles (produced by the largest cells) were spaced closely together. These results indicate that the determination of denticle size and the denticle spacing distance are linked, rather than being a fixed property of cell size.

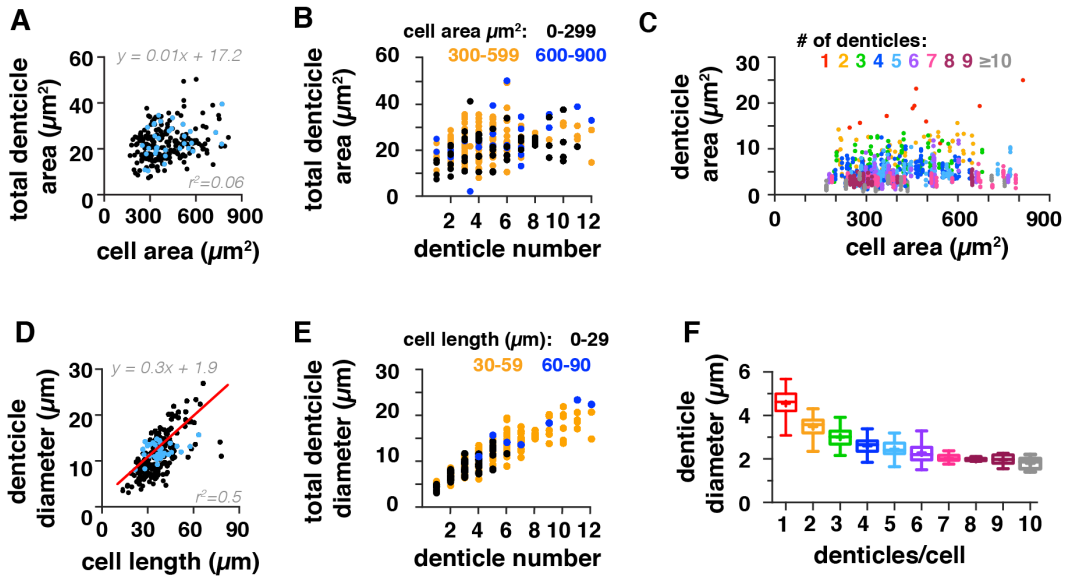

Figure 3.4: Testing the limiting component hypothesis in denticle cells. For **A** and **D**, cells with 5 denticles are highlighted (light blue) to give an idea of the scatter for a single denticle class, in addition to the whole set. **A** and **D** are also shown in 2, and are included here for comparison. n = 223 cells with 1513 denticles from 3 first-instar larvae. **A,B.** Total denticle area is not correlated with cell area (**A**) or denticle number (**B**). **C.** The area of individual denticles does not correlate with cell area. **D, E.** Denticle diameter correlates with cell length (**D**) and denticle number (**E**). **F.** Denticle diameter decreases with increasing denticle number.

3.6 The Fat planar polarity pathway does not influence denticle spacing along the dorsal-ventral axis

As fat has demonstrated roles not only in PCP establishment but also in organizing the actin and microtubule cytoskeletons in the denticle cells (Donoughe & DiNardo, 2011; Marcinkevicius & Zallen, 2013; Lawlor et al., 2013), I asked whether the shift in denticle placement from the posterior to the anterior margin of the cell caused by disruption of the fat atypical cadherin would change the denticle spacing pattern along the DV axis, or whether the denticle spacing mechanism would continue to be active and to correctly distribute denticles even when no longer restricted to the posterior margin of the cell. To test this, I quantified denticle spacing in images obtained from Emily Marcinkevicius of maternal^{-}, zygotic^{-} *fat*^{NY1} and *fat*^{Grv} mutant embryos. To

minimize the possibility of seeing an effect on spacing that was due to mixed placement at both the anterior and posterior faces of the cell, I excluded from my analysis any cell that did not place all of its denticles along the anterior margin. My data indicate that there was no significant difference between the spacing pattern of wild type embryos and *fat*^{NY1} and *fat*^{Grv} embryos in cells that had all of their denticles at the anterior cell boundary (**Figure 3.5**). This indicates that the mechanisms controlling denticle organization along the DV axis are separable from the planar polarity pathways controlling the placement of denticles along the AP axis. Furthermore, it suggests that the spacing machinery exists throughout the cell, could be an inherent property of the denticles, rather than a specific property of the cell margin. or could be inverted in *fat* mutant cells where denticles form anteriorly.

3.7 Shroom-mediated tension does not appear to influence denticle organization

3.7.1 Shroom regulates cortical actomyosin contractility

In the denticle cells, one possible model for how denticle organization is established that there is a molecular ruler that controls the nucleation and / or formation of denticles. Similarly, denticle spacing might be the result of active communication through a tension-sensitive molecular ruler. The cortically localized, actin associated protein Shroom has been shown to be involved in the regulation of actomyosin contractility and cell shape determination (Hildebrand & Soriano, 1999; Haigo et al., 2003; Hildebrand, 2005; Nishimura & Takeichi, 2008; Bolinger et al., 2010; Simoes et al., 2014). Our lab has shown that in the early embryo, loss of Shroom results in reduced Rho-kinase and myosin planar polarity, decreased junctional tension, and defects in germband extension (Simoes et al., 2014). Conversely, ectopic Shroom has been shown to promote apical constriction of epithelial cells (Haigo et al., 2003; Hildebrand, 2005; Nishimura & Takeichi, 2008). These results implicate Shroom as an important regulator of actomyosin

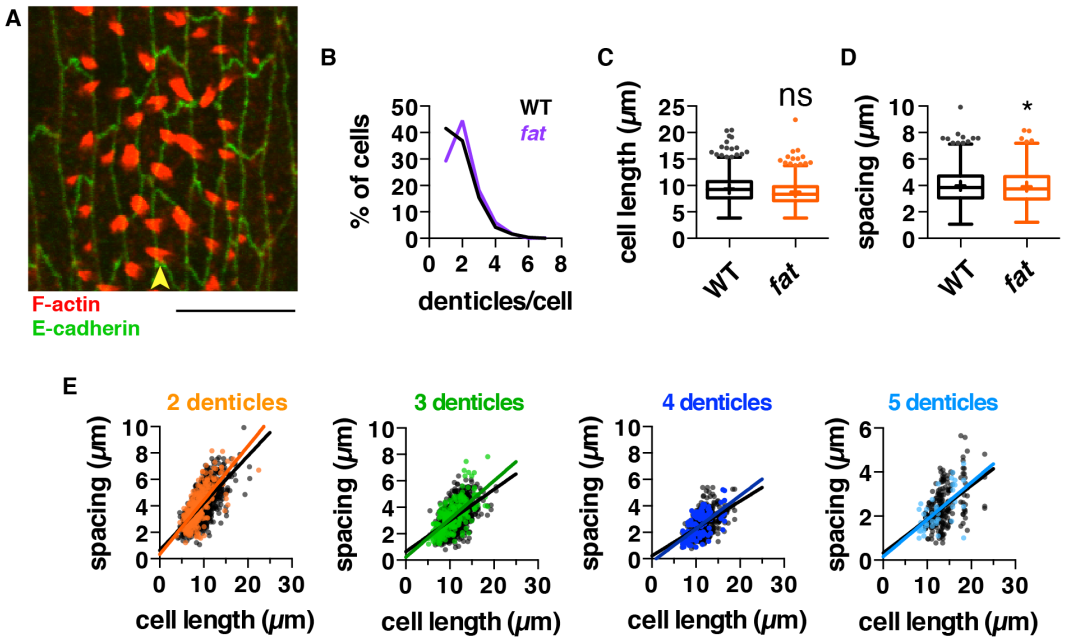

Figure 3.5: Disruption of planar polarity in *fat* mutants does not affect the denticle organization pattern. A. *fat* mutant embryo. Yellow arrows indicated cells with mispolarized denticles. Red, F-actin (phalloidin); green, DE-cadherin. *fat*^{NY1} and *fat*^{Grv} were both used, and the results combined for these studies. **B.** Distribution of denticles produced per cell in WT (black) and *fat* mutant (blue) embryos. **C,D.** Cell length of (C) and denticle spacing (D) for cells with 2 denticles. Boxes, 25th-75th percentile; whiskers, 1.5 inter-quartile range (IQR); horizontal line, median; +, mean. *, $p < 0.0001$ vs. WT, one-way ANOVA, Tukey's multiple corrections test. ns, not significant. **E.** Denticle spacing vs. cell length for cells with 2, 3, 4, or 5 denticles in WT (black) and *fat*^{NY1} or *fat*^{Grv} mutant embryos (colors). Lines, best-fit linear regressions, symbols, means. n = 6 embryos with 700 cells and 1448 denticles.

tension in the epithelium. One way Shroom regulates tension is through its interaction with Rho-kinase (ROCK) (Hildebrand, 2005; Nishimura & Takeichi, 2008; Mohan et al., 2012). The N-terminal and C-terminal domains of ROCK are separated by a long, rigid coiled-coil domain. Truncation mutants in this coiled-coil domain have kinase activity *in vitro*, but are nonfunctional *in vivo*, suggesting that the length of the coiled-coil region is essential for ROCK activity *in vivo* and that ROCK may therefore act as a molecular ruler in controlling actin cytoskeleton dynamics (Truebestein et al., 2015). Given the interactions between Shroom, actin, and ROCK, Shroom is an ideal candidate for regulating a tension-sensitive mechanism of denticle spacing. Although most studies have focused on other stages, *in situ* data from the Berkeley *Drosophila* Genome Project suggests that Shroom is expressed during denticle-forming stages in the late embryo (Hammonds et al., 2013). I therefore wondered whether actomyosin tension generated via Shroom activity might be required for the organized pattern of denticle structures in the late epithelium. Conversely, I tested the possibility that mis-regulation of cortical tension via Shroom overexpression would be sufficient to alter the denticle organization pattern.

3.7.2 Tension regulation does not influence denticle organization

I first analyzed denticle organization in the progeny of *Shroom / Df* females and males, both of which are m^-, z^- for *Shroom* (genotype *Shrm* $\triangle$*11 / Df(2R) Exel7131* or *Shrm* $\triangle$*13.6 / Df(2R) Exel7131*). Cell size was largely unaffected (**Figure 3.6 B**). When I quantified denticle spacing in *Shroom* mutant embryos, I saw no significant differences in spacing or organization as compared to the wild-type control (*yw*). These data suggests that Shroom is unlikely to be a required regulator of denticle organization, although it could have other roles in the late embryo.

I next asked whether the increased cortical tension caused by overexpression of Shroom in denticle cells would be sufficient to alter the denticle spacing pattern. I used the ubiquitous driver *daughterless*-Gal4 to overexpress ShroomA in the epithelium in cells of the late embryo. Shroom misexpression was sufficient to distort cell shapes, suggesting that this overexpression caused an

increase in cortical tension in the late embryonic epithelium. Frequently, this resulted in embryos with severe holes and tearing of the epithelium. In the least affected embryos, this manifested as holes or tears, sometimes eliminating several denticle belts. In the most severe embryos, no epithelial tissue was apparent, and the mesodermal tissues were entirely exposed (**Figure 3.6 A**). These severe phenotypes made it difficult to impossible to analyze actin organization within the denticle belts. Visual inspection of denticle cells in the least affected embryos suggested that denticle organization was not strongly, if at all, affected by ShroomA-overexpression. Therefore, I decided that this was unlikely to be a productive series of experiments to pursue further. If Shroom does affect denticle organization directly, alternative methods of altering tension in the late embryo will have to be employed to test this hypothesis.

3.8 RNAi screen

The increased error in denticle spacing caused by depleting microtubules with Spastin overexpression indicates that microtubules play an important role in controlling the accuracy of denticle spacing. To test the roles of candidate regulators of the microtubule cytoskeleton, I used engrailed-Gal4 to express shRNAs created by the Transgenic RNAi Project at Harvard Medical School (Perkins et al., 2015) against the microtubule binding proteins listed in **Table 3.2**. I then screened for disruptions to the denticle organization pattern in the engrailed-expressing, column 1 denticle cells. The majority of RNAi lines tested did not show any denticle phenotypes. The exception was shRNA against γ-tubulin, which appeared to have a somewhat disorganized denticle distribution comparable to embryos overexpressing Spastin. As γ-tubulin is a minus-end associated microtubule nucleator (Kollman et al., 2011), knockdown of γ-tubulin is predicted to have a similar phenotype to Spastin overexpression, and this phenotype was not quantified.

I also tested several GFP-tagged, transgenic microtubule associated proteins, listed in **Table 3.3**, to investigate whether these proteins display distinct localization patterns with respect to the

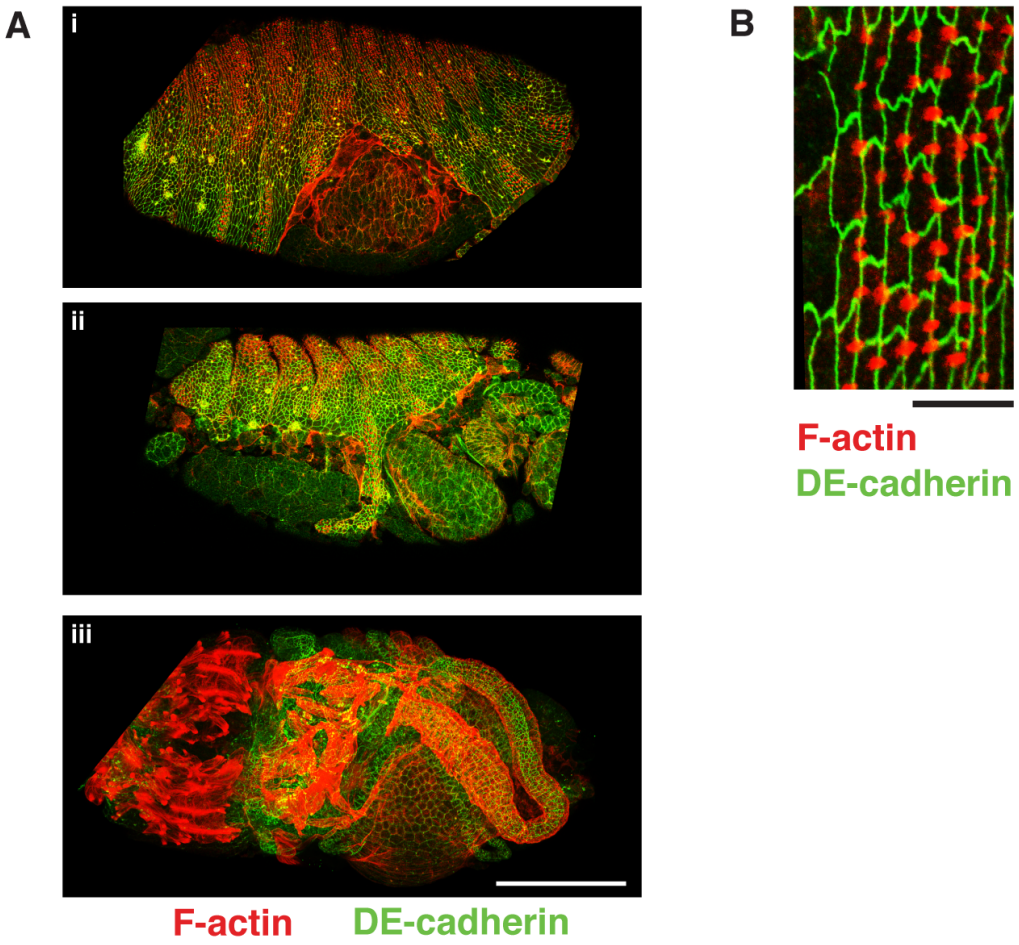

Figure 3.6: Shroom-mediated tension does not influence denticle organization. A. Embryos overexpressing ShroomA using *daughterless-Gal4*, an epidermal driver, show a range of epithelial shearing phenotypes due to increased contractile tension. i) mild tearing exposes the gut, but some denticle belts are still visible; ii) more extreme tearing exposes significant portions of the mesoderm, and only a single denticle belt is visible; iii) the epithelium is essentially nonexistent in most the most extreme cases. Red, F-actin (phalloidin); green, DE-cadherin. Bar, 100 µm. n = 16 embryos. **B.** The progeny of *Shroom / Df* females and males, both of which are m^-, z^- for *Shroom* have phenotypically normal denticle belts. An example of an embryo from the Shroom /Δ13 cross is shown; results for the Shroom /Δ11 cross are similar. Red, F-actin (phalloidin); green, DE-cadherin. Bar, 10 µm. n = 10 embryos

forming denticle structures. Although shRNA-mediated knockdown had no noticeable effect on denticle organization, the GFP-tagged versions of two kinesin-like proteins, Klp61F and Klp10A, were observed to have diffuse localization throughout the ventral epithelium, including in denticle extensions. The ambiguity of these localization results makes it difficult to draw meaningful conclusions from these experiments.

Table 3.2: Genes and stocks used in RNAi candidate screen. Stocks were obtained from the Bloomington *Drosophila* stock center and created by the Transgenic RNAi Project (Ni et al., 2011).

gene	genotype	notes
cut up	P{TRiP.HMS02760} attP2	dynein light chain
fascetto	P{TRiP.GL00393} attP2	antiparallel MT crosslinker; associated with spindle midzone; controls spindle elongation; required for midzone stability (Wang et al., 2015)
Kank	P{TRiP.HMS00319} attP2	EB1-interacting protein (Clohisey et al., 2014)
aurora A	P{TRiP.GL01136} attP2	kinase associated with centrosome maturation; regulation of spindle assembly/stability (Noatynska et al., 2013)
aurora A	P{TRiP.HMS01511} attP40	
aurora A	P{TRiP.HMS02205} attP40	
aurora B	P{TRiP.JF03107} attP2	similar to aurA; localizes to centromeres (Noatynska et al., 2013)
aurora B	P{TRiP.HMJ22415} attP40 / CyO	
aurora B	P{TRiP.GL00202} attP2	
CLIP-190	P{TRiP.JF01206} attP2	end-binding protein; (Folker et al., 2014)

gene	genotype	notes
Dhc64C	P{TRiP.GL00543} attP40	dynein heavy chain
Dhc64C	P{TRiP.HMS01587} attP2	dynein heavy chain
gamma-tubulin	P{TRiP.JF01722} attP2	component of the MTOC, ring complex; MT nucleating factor
gamma-tubulin	P{TRiP.GL01171} attP2	
Kinesin-like protein at 10A	P{TRiP.HMS00920} attP2	kinesin-like, motor activity
Kinesin-like protein at 3A	P{TRiP.HMS02192} attP40	kinesin-like, motor activity; associated with spindle midbody
Kinesin-like protein at 3A	P{TRiP.GLC01416} attP2	kinesin-like, motor activity; associated with spindle midbody
Kinesin-like protein at 59C	P{TRiP.GL00433} attP2	kinesin-like; motor activity
Kinesin-like protein at 61F	P{TRiP.HMS00552} attP2 / TM3, Sb	bipolar mitotic kinesin; associated with spindle midzone (Sharp et al., 1999a; Heck et al., 1993)
Kinesin-like protein at 61F	P{TRiP.GL00441} attP40	bipolar mitotic kinesin; associated with spindle mid zone
Kinesin-like protein at 64D	P{TRiP.HMS02193} attP40	bipolar mitotic kinesin; associated with spindle mid zone

gene	genotype	notes
mini-spindles (XMAP215)	P{TRiP.JF01613} attP2	plus-end associated protein; promotes microtubule instability (Kinoshita et al., 2002; Currie et al., 2011; Reber et al., 2013)
mini-spindles (XMAP215)	P{TRiP.HMS01906} attP40/CyO	
mud (NUMA)	P{TRiP.HMS01458} attP2	associates with dynein/dynactin complex; promotes correct spindle orientation (Bergstralh et al., 2013a)
polo	P{TRiP.GL00014} attP2	
polo	P{TRiP.HMS00530} attP2	

Table 3.3: Genes and stocks used in GFP-tagged candidate screen. Stocks were obtained from the Bloomington *Drosophila* stock center.

gene	genotype	notes
feo-GFP (II)	w; Ubi-p63E-feo.GFP	
feo-GFP (III)	w; Ubi-p63E-feo.GFP / TM3,Sb	
feo-GFP (X)	w, Ubi-p63E-feo.GFP	
feo-mCherry (II)	w; Ubi-p63E-feo.mCherry / CyO	homozygotes present
feo-mCherry (III)	w; Ubi-p63E-feo.mCherry / TM3,Sb	homozygotes present
Klp10A-GFP (II)	w; Ubi-p63E-Klp10A.GFP / CyO	
Klp10A-GFP (III)	w;; Klp10A.GFP	
Klp61F-GFP (II)	w; Ubi-Klp61F.GFP	
Klp61F-GFP (III)	w;; Ubi-Klp61F.GFP	

3.9 Discussion

The data in this chapter demonstrate that the microtubule and dynein / dynactin interacting protein mud and its binding partner pins have specific localization patterns within the denticle cells during denticle-forming stages, although they are insufficient to suggest specific roles that either molecule may play in forming or organizing denticles. However, they do raise the question of exactly how these molecules might interact with the cytoskeleton at sites of denticle formation. In the denticle cells, mud is localized in the immediate vicinity of the emerging denticles but is excluded form the denticle core. Mud is generally recognized for its ability to interact with microtubules and promote their polymerization (Bowman et al., 2006), to interact with pins (Siller et al., 2006) and to interact with the dynein / dynactin complex (Izumi et al., 2006). Consistent with its polarized localization in dividing cells (Kotak & Gönczy, 2013), pins localizes weakly along the AP cell margins in the denticle cells. Although mutation of these two genes does not produce any overt denticle phenotypes, this may be for technical reasons relating to the timing of zygotic gene expression and the degradation rates of maternal protein. Further exploration of mud and pins in the denticle cells, perhaps in the larvae, rather than the embryo, may be required to identify whether either of these molecules are influential in forming denticles or in determining denticle spacing.

Although the Diaphanous antagonist multiple wing hairs is not required for the scaling of denticle organization along the dorsal-ventral axis, it is required for restricting formation of the denticle precursors to the posterior domain and regulating denticle number. The expansion of the cell area competent to produce denticles in *mwh* mutants elevates the normally one-dimensional issue of denticle organization in wild-type to a two-dimensional problem. Additional quantification of this multidimensional pattern of denticle placement may be informative to understand the nature of denticle spacing, and the conditions under which denticles may be spaced. For instance, if denticles in *mwh* mutant cells maintain regular spacing only with neighbors along the dorsal-ventral axis, it would favor a spacing mechanism that is spatially restricted, perhaps with the DV-aligned microtubule cytoskeleton. If denticles are regularly distributed only along the posterior margin and denticles in other regions of the cell are not, it would suggest that the spacing mechanism is only active in the posterior, and it would be most useful to search for spacing regulators in that region. In contrast, if denticles in *mwh* mutant cells are able to maintain a constant spacing distance between all *n* nearest neighbors in both dimensions, it favors a more general mechanism that acts in multiple directions.

Surprisingly, almost none of the microtubule regulating proteins analyzed via RNAi knockdown had an effect on the denticle organization pattern, and the two tagged molecules which were observed apparently within the denticle protrusions had generally diffuse localization throughout the tissue. As such, it is difficult to draw any meaningful conclusions from these experiments. In particular, the partial knockdown often achieved through shRNA experiments makes it difficult to rule out any of these regulators. It is entirely possible that one or more of the regulators listed in Table 3.2 are required for establishment of the denticle organization pattern, and that the shRNA was expressed at insufficient levels, did not actually target the protein in question, there was sufficient maternal protein to compensate for mRNA knockdown, or any number of other reasons. Therefore, a role for these microtubule related molecules in establishing or maintaining the denticle organization pattern cannot be conclusively ruled out, and more information may be gained by testing genetic mutants for these molecules, where available. Alternatively, it may

be useful to move these studies into the larvae, where the longer timeframe and larger cells may provide more chances to see variations, and may make these experiments more fruitful. In addition, several additional transgenic RNAi lines against the dynein / dynactin regulator mud and its binding partner pins exist, but were not tested in this screen. As mud and pins both have suggestive localization patterns relative to the denticles, these should be investigated further.

Chapter 4

Identification of genes required for epithelial morphogenesis in the late *Drosophila* embryo

4.1 Introduction

Forward genetic screens have been successfully used for many years to identify new genes required for the development of a wide variety of tissues at all developmental stages in the fruit fly. In particular, a large number of screens using the embryonic cuticle pattern as a readout for successful body patterning have been performed (St Johnston, 2002). Despite this, several factors make performing additional screens for cuticle defects a continued viable and potentially fruitful option. First, due to technical constraints in identifying sex-linked, embryonic lethal mutations, most screens have focused on the 2nd and 3nd chromosomes and avoided the X chromosome. As the X chromosome contains nearly 20% of the coding genes in *Drosophila*, it is therefore likely that there are a large number of genes existing on the X that have not yet been

assigned roles in tissue development, as well as many other processes. Second, the previously performed screens were primarily interested in identifying mutants with large-scale, tissue-wide patterning defects. Therefore, these screens mainly sought to identify mutants that grossly altered the body plan of the embryo, rather than seeking out more subtle phenotypes relating to structure organization and fine-scale distribution, and, as a result, mutants with these subtle phenotypes could have been overlooked. Third, recent technological advances have been made that make identifying the mutations retrieved from chemical mutagenesis screens significantly more reliable and less labor intensive. Whole-genome sequencing is becoming increasingly more cost-effective, making it possible to sequence large collections of mutants (Sarin et al., 2008; Blumenstiel et al., 2009; Hobert, 2010; Sarin et al., 2010; Haelterman et al., 2014) and reliably identify causal mutations (Obholzer et al., 2012; Doitsidou et al., 2010; Minevich et al., 2012; Haelterman et al., 2014). New tools to map mutations, including a nearly-full-coverage set of X-chromosome duplications, further streamline the gene identification process (Cook et al., 2010; Venken et al., 2010). Combined, these factors make screening the X chromosome a viable and worthwhile endeavor.

4.2 A germline mosaic screen for maternal /zygotic mutants affecting actin structure organization and tissue morphogenesis

Recently, in an effort to identify essential genes required for the formation and maintenance of the *Drosophila* nervous system, Hugo Bellen's laboratory at the Baylor College of Medicine generated a large collection of low-dose, EMS-mutagenized stocks in an isogenized FRT19A background, providing a means to screen the X-chromosome for lethal mutations using a mosaic approach (Yamamoto et al., 2014, 2012; Xiong et al., 2012). Of the 31,530 mutagenized stocks generated, nearly 6,000 carried recessive lethal mutations. The Bellen lab then performed an F3 clonal screen of the wing, thorax and eye to identify lines with a broad range of

phenotypes, including those affecting the nervous system, wing patterning, and pigmentation; at the conclusion of this screen, they retained 2,083 lines with interesting phenotypes for additional characterization. In 2010, our lab was given access to these lines, and I and several additional lab members performed an F3 embryonic mosaic screen on this collection to identify genes relevant to axis elongation and cell polarity in the early embryo (Leah Greenspan, AKLS, Emily Marcinkevicius, and Athea Vichas, unpublished results), and denticle formation and organization in the late embryo (AKLS, with help from Leah Greenspan in processing the cuticle preparations) (**Figure 6.2**). Of the 1,235 recessive lethal lines screened for epithelial morphogenesis defects at early developmental stages. I performed an additional cuticle screen on the embryonic progeny of females bearing homozygous mutant germline clones for 748 of these mutant lines to identify those with cuticle defects relating to denticle formation, denticle organization, and segment patterning and polarity, and identified 5 lines in 3 complementation groups with particularly interesting phenotypes (**Figure 4.1**). In this chapter, I will document the results of our overlapping primary screens using this collection of X-chromosome, recessive lethal mutants to identify new genes involved in denticle organization and formation in the cuticle of the late embryo, and convergent extension and tissue elongation in the early *Drosophila* germband. I will then discuss the phenotypic characterization and gene identification strategies applied to the top five hits to come out of my cuticle screen.

4.3 Identification of maternal and zygotic X-chromosome mutations affecting tissue morphogenesis and the formation of the actin based denticles

4.3.1 Initial categorization of cuticle screen mutant phenotypes

Mutations that cause alterations to the stereotyped patterns of denticles, hairs, and sensory organs in the *Drosophila* epidermis are captured and stored in the tough, apical extracellular

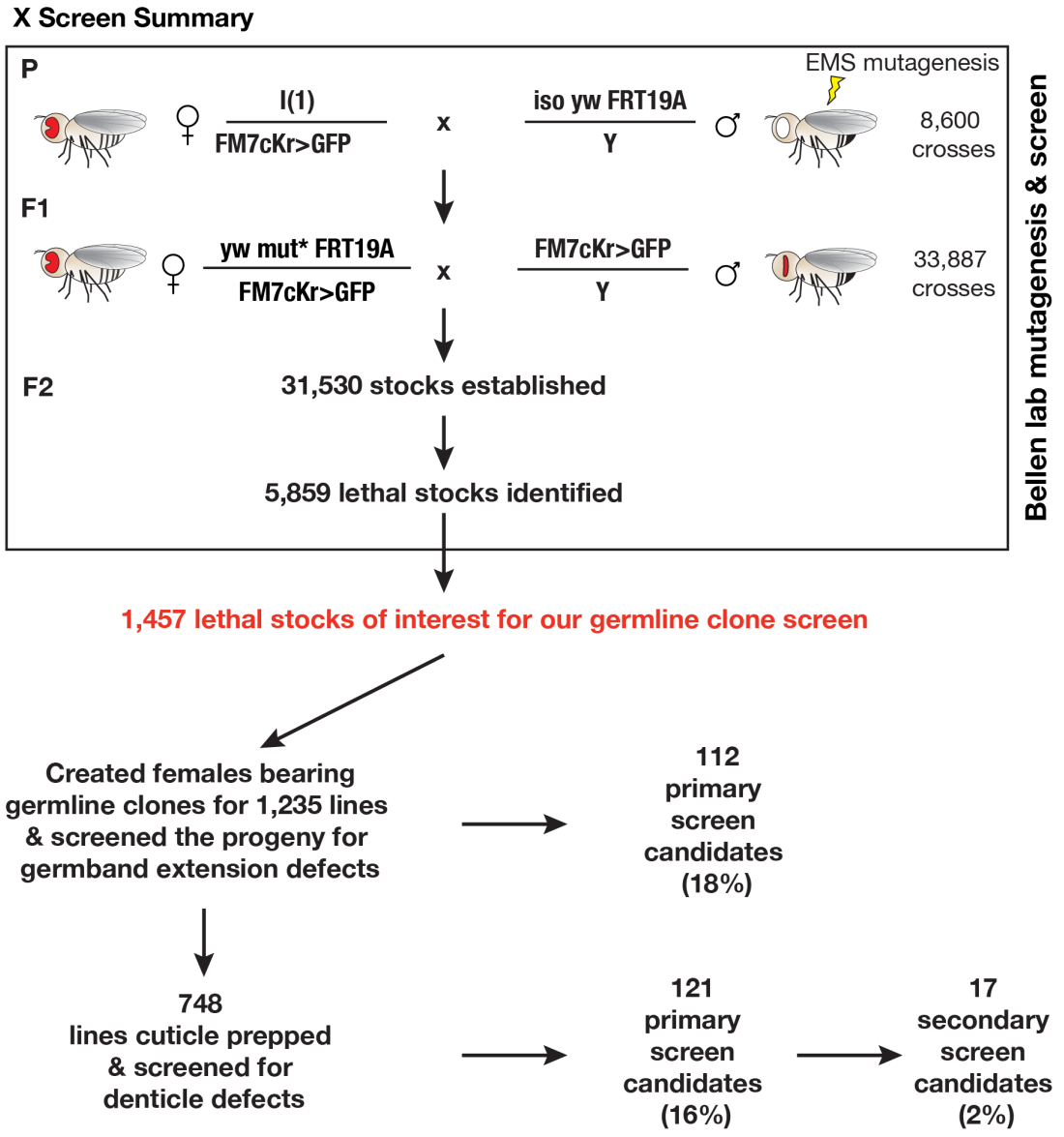

Figure 4.1: Summary of X-chromosome mutant generation and screening outcomes (Yamamoto et al., 2012; Xiong et al., 2012; Haelterman et al., 2014; Yamamoto et al., 2014).

cuticle produced by the embryo just prior to hatching (Nüsslein-Volhard & Wieschaus, 1980). The cuticle, therefore, is durable tissue that acts as a record of the success of the morphogenetic processes occurring in the epidermis throughout development, and screening for embryos with defective cuticle patterns allows for the identification of genes affecting cytoskeletal organization, cell polarity, and tissue organization. I used this tissue to screen for mutations that affect the subcellular organization patterns of the ventral denticles, as well as mutations affecting cell elongation, cell alignment, and denticle morphology.

The phenotypes of the mutants I was most interested in segregate into one of three broad categories: denticle organization, denticle morphology, and A-P patterning (**Figure 4.2**). These categories and examples of known genes with these phenotypes are discussed below, and summarized in **Table 4.1**. During the course of my screen I identified mutants that did not fit into the above categories and were not of interest for my future studies, but which could be grouped together into one of several additional categories. These included mutants with defects in dorsal-ventral patterning, in dorsal closure, in head involution, as well as those that had a loss of epithelial integrity (i.e. holes), or were sufficiently mutilated to preclude further classification. These additional categories are described in **Table 4.2**.

Denticle organization: I expected to identify several subclasses of mutants with defects in denticle organization in this screen. These included mutants with defects in denticle spacing, denticle alignment, denticle placement, and denticle number. I defined spacing mutants as mutant embryos in which the observed denticle spacing distance was consistently greater or smaller than the typical distance in wild-type embryos, or where denticles were distributed in a random or unpredictable manner. These types of effects might be caused by mutations in genes directly involved in the regulation or control of the spacing mechanism, such as actin or microtubule regulators (e.g. *multiple wing hairs* (Dickinson & Thatcher, 1997)), or other molecules serving as a molecular ruler within denticle cells. Alternatively, these could be mutations in genes controlling the size or shape of the denticle cells. Finally, these phenotypes could be caused by misregulation of molecules responsible for determining the number of

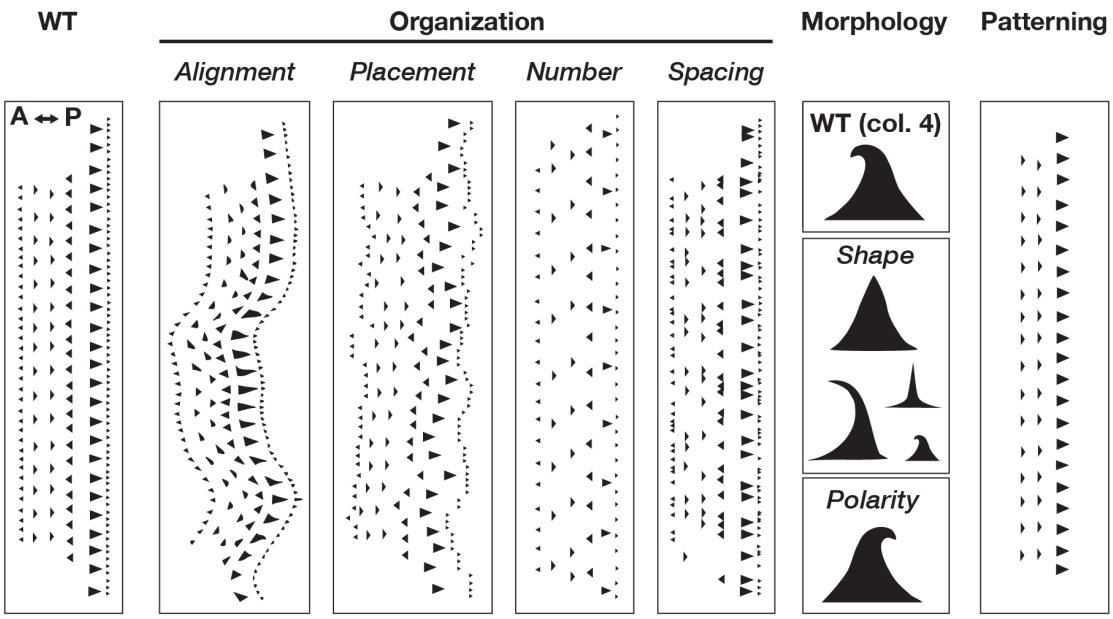

Figure 4.2: Cuticle phenotypes of interest. Cuticle preparations of wild-type denticle belts have 6 distinct columns of denticles (left). I hoped to identify mutants in three categories during my screen of mutant cuticles: Denticle organization (with the subcategories of denticle alignment and denticle spacing) - where the correct number of denticle belts are specified, but denticles are not evenly distributed and/or not aligned into clear columns; Denticle morphology, where the appearance of denticles, including hook direction and denticle size, is incorrect; and AP patterning, where the number or appearance of columns is incorrectly specified.

denticles produced by each cell. Putative mutants with defects in denticle placement or denticle alignment were defined as those whose denticles were mis-localized along the anterior-posterior axis of the cell. These mutants could be identified by an increased disorganization or waviness within each cell column, and might be caused by mutations in effectors of the planar cell polarity pathways (e.g. *Fat* (Marcinkevicius & Zallen, 2013) or *multiple wing hairs* (Dickinson & Thatcher, 1997; Gubb & García-Bellido, 1982)) or mutations in factors required for cell alignment (e.g. myosin II).

Denticle morphology: The morphology category encompassed mutants with alterations to the physical appearance of the denticle structure. The morphology category included two distinct types of pheotypes. The first is denticle shape, where the dimensions of the tip or base are

altered, there is fraying or splitting of the tip, or other changes in shape or size while remaining reasonably true to the wild-type column characteristics. Examples of phenotypes in this category include those that occur when genes that disrupt the cytoskeleton, [e.g. *crinkled* (Bejsovec & Chao, 2012)] or the connection between the epidermis and the cuticle, [e.g. the ZPD proteins *miniature* or *dusky-like* (Fernandes et al., 2010)] is disrupted. The second type of phenotype is denticle polarity, or denticle identity. This subcategory includes mutants where the denticle hooks were ambiguous or incorrectly oriented for the column they appear in, or the denticle belt was missing specific, identifiable rows. These types of phenotypes can occur when genes that regulate denticle formation in specific columns, e.g. *short stop* (Dilks & DiNardo, 2010) or *Serrate* (Walters et al., 2005), are disrupted.

AP patterning: As it is known that there are a number of X-linked genes known to affect segment patterning (including *armadillo* and *Notch*) and cuticle screens have been highly effective in the past at uncovering mutants with patterning defects, I expected to see a large number of mutants with defects in AP body axis patterning. While I did not anticipate that the majority of mutants in this category would be useful to understand how defects in denticle structures are organized at the subcellular level, novel mutants that might have been missed in previous screens could fill in gaps in how the AP patterning system functions. In particular, it is not entirely understood how the diverse morphologies of denticles arise on a per-column basis. Therefore, mutants in this category with particularly striking, novel defects were of interest for further study and were flagged for secondary screening.

4.3.2 Primary screen results

To identify maternal and/or zygotic genes involved controlling the formation of denticles and their particular spatial organization pattern, I characterized the phenotypes of the embryonic progeny of females bearing germline clones from 807 of the lethal lines in the Bellen collection into the aforementioned categories. A small number of crosses were accidentally duplicated

Table 4.1: Screen categories: denticle organization and formation. Categories are not mutually exclusive.

Category	Phenotype
Denticle Organization	
alignment or placement	denticle columns appear wavy or angled, rather than aligned could indicate misplacement of denticles or misalignment of cells
spacing or number	distance between denticles is altered denticle density is altered (more or fewer denticles than normal) examples include *fringe* (Walters et al., 2005), *multiple wing hairs* (Dickinson & Thatcher, 1997)
Denticle Morphology	
morphology	defects in the size, shape, identity or polarity of denticles examples include *forked*, *singed* (Dickinson & Thatcher, 1997), *crinkled* (Bejsovec & Chao, 2012), and *miniature* (Chanut-Delalande et al., 2006)
polarity or identity	sub-category of morphology denticle hooks are incorrectly oriented in one or more rows, or denticle columns are missing from the belt examples include *Serrate* (missing column) (Walters et al., 2005) and *short stop* (hook orientation) (Dilks & DiNardo, 2010)

Table 4.2: Screen categories: Cuticle phenotypes. General categories used during the cuticle screen for defects in denticle organization. Categories are not mutually exclusive.

Category	Phenotype
denticle organization and formation	defects denticle placement, alignment, organization, or morphology see **Table 4.1** for details
anterior-posterior (AP) patterning	denticle belts do not have 8 belts with 6 columns each includes lawns, partial belts, fused belts, or an incorrect number of belts, rows, or body segments
dorsal-ventral (DV) patterning	missing dorsal or ventral tissues 'twisted' or 'corkscrewed' appearance
holes	gaps in the dorsal, lateral, or ventral cuticle includes presumed dorsal closure mutants
other	other interesting and clearly defined phenotypes includes dorsal closure, germband retraction, embryo shape/size defects
roadkill	monsters with no specifically identifiable or unifying phenotypes also noted as 'messy' or 'disaster(ed)'
young dead	poorly differentiated cuticular features, and/or hazy cuticle likely due to developmental arrest in the early stages of denticle formation
unscorable or no embryos	slides containing no embryos slides with only vitaline membrane outlines This was a very common category

during the set up process, therefore, of these 807 crosses, only 748 represented unique lines. One technical challenge that quickly arose during the course of the primary screen was that a number of females bearing germline clones proved inefficient at laying eggs, perhaps due to the nature of the mutations or the limited number of females that could be analyzed per line. Therefore, many of the cuticle preparations that I screened had very few embryos. I discarded those lines which had fewer than 3 scorable embryos, but I chose to advance to the secondary screen a number of lines that had very few embryos but potentially promising denticle-related phenotypes, as I expected that I would be able to generate more embryos in the secondary screen. It should be noted that these categorizations were broad and not uniquely assigned. For instance, embryos have denticle defects falling under both the 'Organization' and 'Morphology' categories simultaneously, and a line could have both a denticle morphology defect, and have holes in the cuticle.

Of the embryos screened from the 807 crosses, 68 had defects in denticle organization, 94 had defects in denticle morphology, and 97 had AP patterning defects. As noted above, these categories were not mutually exclusive. Embryos with head defects (43 lines), holes (50 lines) and DV patterning defects (32 lines) were also identified. In addition to these definitive categories, 85 lines had 'other' defects, including apparent problems with dorsal closure, germband retraction, and other issues that were striking but not common enough to create a new independent category. Finally, 169 lines had no apparent denticle defects, and 271 lines were unscorable, either because they produced either no embryos or only the outline of the vitaline membrane and no other features were visible in the slide. Out of the 242 total unique lines within the denticle organization, denticle morphology, and AP patterning categories, I selected 119 independent lines (16% of the total lines screened) with promising defects in denticle formation or organization phenotypes for further study.

4.3.3 Secondary screening results and choice of mutants

To confirm the presence of a denticle phenotype in each of these stocks, I repeated the germline clone cross and cuticle assay for each of the mutants identified in the primary screen. Of the 121 original stocks, 21 lines re-tested with reproducible phenotypes in the three major categories: 8 lines had defects in denticle organization, 9 lines showed defects in denticle morphology, 5 of which had size or shape defects and 4 of which had defects in denticle polarity, and 5 had A-P patterning type phenotypes (**Figure 4.2**).

Choosing which of these 21 candidates to prioritize for more thorough characterization and gene identification required more information regarding the cellular phenotype of each line than the cuticle assay, which reflects only the end-stage topology of the epidermis, could provide. Therefore, I examined the cellular phenotype of embryos from each germline clone cross. I fixing and stained mutant embryos for DE-cadherin to visualize cell outlines, F-actin to visualize denticles. To determine whether the phenotype was paternally rescued, I also stained for the presence of GFP (provided paternally on the FM7c,Kr>GFP balancer chromosome) and assessed whether the phenotype was present in both maternal^{-}/zygotic^{-} and maternal^{-}/zygotic^{+} embryos. This information was important in both my assessment of how penetrant the phenotype was, and to determine whether future analysis would require me to distinguish between the different phenotypes in maternal^{-}/zygotic^{-} and maternal^{-}/zygotic^{+} embryos. While choosing which candidates to prioritize, I also took advantage of the complementation and cloning data made available to us by the Bellen lab to identify lines with mapping information available. Priority was given to lines that a) had interesting or unique phenotypes that, if applicable, were matching in both the cuticle and in the epithelium; b) were mapped to genes without known AP patterning effects, or no gene.

The mapping information allowed me to immediately eliminate alleles of *shavenbaby/ovo*, which is the key transcriptional regulator promoting denticle fate (Payre et al., 1999), and *ocelliless*, which is required for development of the head and CNS (Finkelstein et al., 1990; Finkelstein &

Perrimon, 1990). A mutation in *Smad-on-X* (*Smox*) had a curious 'paired' denticle localization pattern in the initial cuticle screen where denticle positions were very uneven across the column. However, on further evaluation this phenotype presented at extremely low penetrance and was therefore discarded. Several other lines (1830, 3057, 4271) were simply very sick and produced very few embryos, making them similarly difficult to work with. A mutation in *cacaphony* (*cac*), a voltage-gated calcium channel (Kawasaki et al., 2004), caused severe epithelial disruption phenotypes without any specifically identifiable effects on the denticle cells. A stock that had been mapped to a mutation of *Casein kinaseII-*β (*CKII-*β) became viable; as our screen was based on embryonic lethal phenotypes, this was discarded. As I had alternative and more interesting candidates in the morphology, spacing, and polarity categories, I also discarded as non-priority candidates all the lines with a 'Patterning' phenotype. The exception was a mutant line called 2871, which had a particularly novel and specific loss of column 2 or 3 denticles. Following these eliminations, eight lines were retained for further study: a group of 4 lines which showed hook polarity defects specifically in column 4 (1302/XFVB040/XE10E (Crag), 1912/XHCB028 (Hr4), 812/XESY038, and 1099/XEZK036); 5369/XMHW123, which had defects in denticle morphology and cell alignment; two lines, #1264 and #4422, which had apparent spacing defects; and 2871, a novel patterning mutant.

4.3.4 Phenotypic and molecular characterization and gene identification of mutants with denticle defects

4.3.5 Crag is required for column 4 denticle hook orientation

Of the eight lines I selected to characterize further, a group of four lines showed defects in column 4 hook orientation (**Figure 4.3A**). Column 4 denticles in wild type have an anterior-facing hook. In contrast, column 4 denticles in this group of mutants point in all different directions apparently randomly. Two out of the four lines had been mapped to genes by the Bellen lab screen team - 1302/XFVB040, which had been identified as a member of complementation group XE10, and

an allele of *Crag* (*Calmodulin-binding protein related to a Rab3 GDP/GTP exchange protein*) (Xiong et al., 2012), and 1912/XHCB028, an allele of the nuclear hormone receptor *Hr4*. The other two, 812/XESY038 and 1099/XEZK036, had neither been assigned to a complementation group or mapped to a known gene at the time of my screen, although coarse duplication mapping showed them to be in the same general region of the chromosome. To identify the approximate chromosomal region in which these two unknown mutations were located, I initially performed duplication mapping using the X chromosome duplication kit available from the Bloomington *Drosophila* Stock Center (BDSC) on each of these lines, and looked for rescue of the male lethality phenotype (Cook et al., 2010; Venken et al., 2010). As I was beginning my mapping crosses, I received data from the Bellen lab sequencing results suggesting that that 812/XESY038 was also likely to be Crag. As 1302, 812 and 1099 had all been rescued by the same large duplication in the Bellen lab (a preliminary duplication from the Cook *et. al* study, Dup(5678) (Cook et al., 2010)), it was likely that both the uncharacterized mutants 812 and 1099 were alleles of Crag. To confirm this hypothesis, I crossed in a genomic rescue construct for Crag covering a 12 kb region, including the Crag coding region plus 2 kb of sequence upstream and 1.5 kb of sequence downstream of the open reading frame (Denef et al., 2008), and again looked for rescue of male lethality. Male lethality was rescued in both mutant 812/XESY038 and 1099/XEZK036, confirming that both were *Crag* alleles. While I was confirming lethality rescue via rescue construct, additional sequencing information on the X10/Crag complementation group became available from the Bellen lab (Xiong et al., 2012; Haelterman et al., 2014) (N.Haelterman and S.Yamamoto, personal communication). While the causal mutations for 1302/XFVB040 and 1099/XEZK036 remain unknown, 812/XESY038 is caused by a missense mutation (W1306X) in the C-terminal region of *Crag* (Haelterman et al., 2014), (N. Haelterman and S. Yamamoto, personal communication). The mutation for *Hr4*, in contrast, is unknown and was not pursued any further.

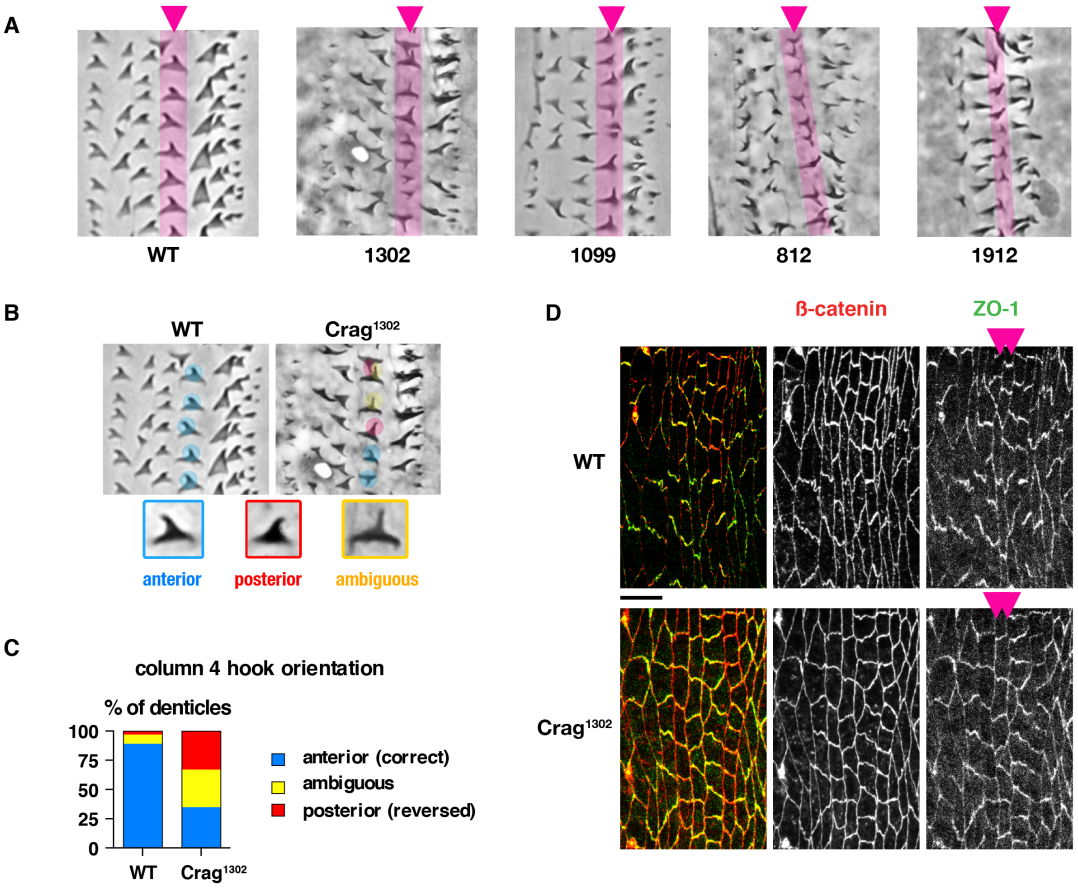

Figure 4.3: *Crag* mutants disrupt column 4 denticle hooking. A. Cuticle phenotypes of the 'Morphology' class of cuticle screen hits. Pink arrows and highlights indicate detnicle column 4. 1302, 812, and 1099 map to Crag; 1912 maps to HR4. The wild type embryo in this figure is OregonR. **B.** Maternal^{-}/zygotic^{-} *Crag* ^{1302} mutants alter the directionality of denticle hooks in column 4 compared to wild type. Column 4 denticles are highlighted to indicate hook directionality. Blue, anterior hooks; red, posterior hooks; orange, hook has an indeterminate/ambiguous direction. **C.** *Crag* ^{1302} mutants randomize the orientation of denticle hooks in column 4 cells compared to wild type. Hook polarity of denticles in *Crag* ^{1302} mutants and wild type were quantified and normalized to the total for each genotype. Blue, anterior hooks; red, posterior hooks; orange, hook has an indeterminate/ambiguous direction. **D.** Polarized junctional molecules are incorrectly localized, suggesting that *Crag* ^{1302} mutants may have junctional remodeling defects. Pink arrows indicate the boundaries between denticle columns 2/3 and 3/4, where the localization defect is most prominent. Green, pyd (polychaetoid, ZO-1); Red, arm (armadillo, β-catenin) . Bar, 10 µm. Embryos at stage 16; wild type in this image is OregonR.

4.3.5.1 Crag is a RabGEF involved in polarized trafficking

Crag is a highly conserved, DENN (differentially expressed in normal and neoplastic cells) domain protein originally initially identified in a screen for calmodulin-binding proteins in the fly retina (Xu et al., 1998; Semova et al., 2003). The functions of DENN domains in proteins are not well understood, but these domains are often found in proteins with roles in vesicular trafficking, particularly Rab GTPases (Levivier et al., 2001). Consistent with this hypothesis, Crag has been shown to have roles in protein trafficking, and to act as a guanine nucleotide exchange factor (GEF) for Rab10, which localizes to exocytic vesicles exiting the Golgi and is believed to be involved in polarized trafficking in various cell types (Schwartz et al., 2007; Stenmark, 2009; Lerner et al., 2013) and Rab11, is associated with recycling endosomes (Denef et al., 2008; Xiong et al., 2012; Lerner et al., 2013).

In the follicular epithelium, mutations in *Crag* disrupt the basal, unipolar localization of basement membrane (BM) proteins, resulting in a loss of epithelial integrity and enhanced cellular invasiveness (Denef et al., 2008). Further analysis revealed that Crag interacts directly with Rab10, which is a regulator of polarized secretion, and Crag is required to target Rab10 to the basal cell surface (Lerner et al., 2013). Crag also colocalizes with two other Rab proteins, the early endosome marker Rab5 (Schwartz et al., 2007; Denef et al., 2008) and the recycling endosome marker Rab11 (Schwartz et al., 2007; Denef et al., 2008), in the follicular epithelium (Denef et al., 2008). No molecular interaction between Rab5 and Crag has been identified. However, mis-targeting of BM components to the apical cell surface in the absence of Crag or Rab10 appears to occur through a Rab11-dependent mechanism (Lerner et al., 2013); this suggests that Crag may be able to interact with multiple trafficking molecules to direct establishment of epithelial architecture and polarity. The idea that Crag may have multiple roles in polarized secretion is bolstered by experiments in the *Drosophila* rhabdomeres. In the original X screen conducted by the Bellen lab, alleles of *Crag* were identified as causing photoreceptor degradation (Xiong et al., 2012). As in the follicle cells, mutations in *Crag* caused defects in

protein trafficking and secretion, leading to degeneration of the photoreceptors (Xiong et al., 2012). This work demonstrates that Crag is required with Rab11 to recycle rhodopsin from the apical photoreceptor membrane upon light stimulation. Furthermore, it indicates through a series of *in vitro* and *in vivo* assays that Crag acts as a GEF for both Rab10 and Rab11. These data demonstrate that Crag is a multifunctional Rab GEF, which likely has roles in the polarized trafficking and secretion of proteins.

4.3.5.2 Mutations in Crag randomize column 4 denticle hook orientation

My initial characterization of the denticle phenotype of the embryonic progeny of females bearing *Crag* germline clones (*Crag* mutants) used the first allele I identified, 1302/XFVB040 (referred to from here on as *Crag*^{1302}). I began by quantifying the column 4 hook polarity phenotype in wild type and *Crag*^{1302} mutant embryos. In wild-type embryos, 89% of column 4 denticle hooks had an anterior orientation, while 8% of denticles had an ambiguous or indeterminately oriented hook, and a mere 3% of denticle hooks faced the posterior of the animal (**Table 4.3**). These data are consistent with previous results (Dilks & DiNardo, 2010). In contrast, *Crag*^{1302} mutants had a nearly-equal distribution of denticle hook orientations, with 33% oriented posteriorly, 35% oriented anteriorly, and 32% where hook direction was ambiguous (**Figure 4.3B,C, Table 4.3**), indicating that without Crag, the orientation of the denticle hook is essentially random. Nearly 100% of Crag^{1320} mutant embryos had some mis-oriented denticles, although not all the denticles in any single embryo were mis-oriented (n = 31 *Crag* mutant embryos). This denticle misorientation phenotype was not observed in zygotic mutants, suggesting that this denticle hook requires maternally-loaded Crag protein. Somewhat curiously, however, this defective hooking phenotype was specific to column 4 denticles. In wild-type embryos, both column 1 and column 4 denticles have an anteriorly-oriented hook (**Figure 1.2**). Mutations in *Stripe* and *short stop*, which alter column 4 denticle hook orientation, also affect column 1 hooks. Curiously mutations in *Crag*, in contrast, do not appear to affect column 1 denticle hook orientation, although this phenotype was not quantified.

Table 4.3: Quantification of *Crag*^{1302} column 4 hooking defects.

	WT (OregonR)		*Crag*^{1302}	
embryos counted	5		31	
denticles counted	490		1240	
# of anterior hooks	437	89%	431	35%
# of ambiguous hooks	38	8%	409	33%
# of posterior hooks	15	3%	400	32%

I next confirmed that the general formation of denticles and overall cellular architecture was normal in *Crag* mutant embryos. The orientation of the denticle hook is not visible in the epidermis, only in the cuticle; therefore, as I expected, *Crag* mutants stained for DE-cadherin and F-actin had no visible defects on the posterior placement of denticles, denticle spacing, or cell shape (n = 6 embryos). However, in preliminary experiments, *Crag* mutants stained for the adherens junction proteins β-catenin (armadillo in *Drosophila*) and ZO-1 (polychaetoid in *Drosophila*), the localization of junctional proteins appeared abnormal (**Figure 4.3 D**). In wild-type embryos, ZO-1 is enriched at DV edges and excluded from AP edges (Marcinkevicius & Zallen, 2013). However, in *Crag* mutants, ZO-1 was uniformly distributed along cell boundaries, particularly in the middle denticle columns (columns 3 and 4) (n=3 embryos). Qualitatively, ZO-1 did appear to be correctly excluded from the 1/2 and 4/5 boundaries in these animals, perhaps reflecting the unique differences between these two boundaries and the rest of the denticle belt cells in establishing and maintaining junctional alignment. Overall, these data suggest that, consistent with its demonstrated roles in protein trafficking, Crag may be required for the planar polarized localization of β-catenin and ZO-1 in the denticle belts.

4.3.6 5369 mutants have defects in cell alignment and denticle placement

4.3.6.1 Phenotypic characterization of 5369/XMHW123

The most interesting candidate mutation with defects in denticle organization and formation to come out of the screen was a stock named 5369/XMHW123 (referred to here as '5369'). This mutant was of particular interest because it was the only mutant to come out of the screen to have strong defects in denticle organization, the primary category of interest at a reasonably high penetrance. The cuticle phenotype of the progeny of females with germline clones homozygous for the 5369 mutation (5369 mutants) shows a clear defect in the morphology of the denticles; where wild-type denticles are shaped like rose thorns, which a clear base and tapered hook, 5369 mutants have stubby, misshapen denticles (**Figure 4.4 A, left panel**). Furthermore, the denticles of 5369 mutant embryos were poorly aligned, and did not form neat columns like the wild-type (**Figure 4.4 A, red lines**). This disorganization phenotype was most obvious in the more posterior denticle belts (belts 5, 6, and 7), though it was noticeable to some degree across all belts (n = 16 stage 14-17 $m^{-}z^{-}$ and $m^{-}z^{+}$ 5369 mutant embryos).

To characterize the phenotype of 5369 mutants, and to look for potential causes for the organization defects, I first stained 5369 mutant embryos for actin to label denticles, DE-cadherin to label cell outlines, and GFP to look for presence or absence of the Kr>GFP balancer chromosome, which defines which embryos have been paternally rescued ($m^{-}z^{+}$) and which have not ($m^{-}z^{-}$). These experiments revealed that cells are poorly aligned in 5369 mutant embryos, particularly in columns 3 and 4 (**Figure 4.4 A, middle panel, yellow arrowheads**). Furthermore, denticle placement was no longer confined to the posterior margin in many cells (**Figure 4.4 A, right panel, white arrows**). Therefore, I concluded that the disorganization phenotype I observed in the cuticle was due to problems in both cell alignment and denticle placement. These defects were present in both the $m^{-}z^{-}$ male and the paternally-rescued $m^{-}z^{+}$ female embryos (n=16 embryos), and removal of the 5369 maternal component caused

embryonic lethality. These phenotypes were not observed in zygotic 5369 mutants (n=7 embryos), suggesting that the gene(s) mutated in 5369 are required maternally, but may be dispensable for denticle organization zygotically.

Gut constriction in wild-type embryos occurs concurrently with denticle formation and organization, and embryonic stage may be determined phenotypically using a combination of the extent of dorsal closure and the degree of complexity of the gut. In stage 13 wild-type embryos, denticle cells begin rearranging to form clear columns, germband retraction has just completed, dorsal closure has not yet begun, and the gut consists of a single, rounded chamber. Dorsal closure progresses through stage 14, such that relative age can be determined by the extent of zippering over the amnioserosa cells, and the gut remains as a single rounded chamber. Dorsal closure is completed at stage 15, though there is a noticeable 'scar' where the zippering process has recently concluded, and the gut begins to constrict to form additional chambers. By stage 16 (the point at which the actin based denticle precursors have finished forming), this dorsal closure 'scar' has mostly healed, the dorsal hairs have formed, and the gut consists of three clearly delineated sections (**Figure 4.4 B, top**). An additional, notable phenotype of 5369 mutants was that these embryos had consistent defects in development of the gut. Although dorsal closure progresses apparently normally in 5369 mutant embryos and dorsal hairs are eventually formed, the gut remains unconstricted and consists of only a single chamber (n=14/14 $m^{-}z^{-}$ embryos) (**Figure 4.4 B, bottom**).

I next examined the cell alignment phenotype of 5369 mutants with the help of a rotation student, Pooja Naik, by live imaging with a GFP-tagged β-catenin, which outlines cells. Previous work done by Emily Marcinkevicius indicates that abnormal cell shape/column alignment at late stage denticle belts could be caused by abnormalities in cell junctional rearrangements earlier in development (Marcinkevicius & Zallen, 2013). Therefore, I asked whether cell rearrangement and junctional alignment proceeded normally in these mutant embryos. Cells in 5369 mutants are generally more static than WT cells, and there appeared to be fewer productive rearrangements in the tissue overall (n=4 movies of embryos stages 14-16). Qualitatively, cells also went through

many contraction-relaxation cycles that failed to change tissue topology, rather than shrinking their junctions and rearranging. Occasionally, these contractions proceeded rapidly along all edges, and the cell would ingress basally, out of the imaging plane. Together, these abnormally unproductive contractile behaviors could be sufficient to account for the lack of cell junction alignment in the fixed tissue (**Figure 4.4 C**).

4.3.6.2 Identification of 5369 candidate genes

The Bellen lab reported that 5369 was rescued by a single duplication, but that it was a single allele that had not been assigned to a complementation group, and no stable rescued stock could be established (S. Yamamoto, personal communication). When I attempted to confirm this finding, I was unable to observe rescue of 5396 male lethality using this same duplication. Initial sequencing by the Bellen lab found no mutation in the region to which lethality was originally mapped (N. Haelterman, personal communication), suggesting that the initial result of rescue was incorrect.

To identify the gene responsible for the 5369 phenotype, I next used the X chromosome duplication kit to perform the duplication mapping crosses for 5369 as with the mutations in the Crag complementation group. However, I was unable to identify a single rescuing duplication. My failure to isolate the lethality to a single region suggested that either there were issues with the duplication mapping, the gene was in one of the regions with no duplication coverage, or that there was possibly a secondary lethal mutation in this line. To overcome this and identify all potential mutations in the 5369 genome, 5369 mutant females were crossed to the isogenized *y,w,FRT19A* starting stock obtained from the Bellen lab and the non-balancer progeny sequenced using HiSeq by the MSKCC sequencing core facility. The sequencing results were aligned to the reference sequence and unique SNPs (small nucleotide polymorphisms) were identified by comparing the 5369 sequence against the publicly-available D.mel reference (D.mel Release 5.5) (Adams et al., 2000), a reference sequence of the original *y,w,FRT19A* isogenized line

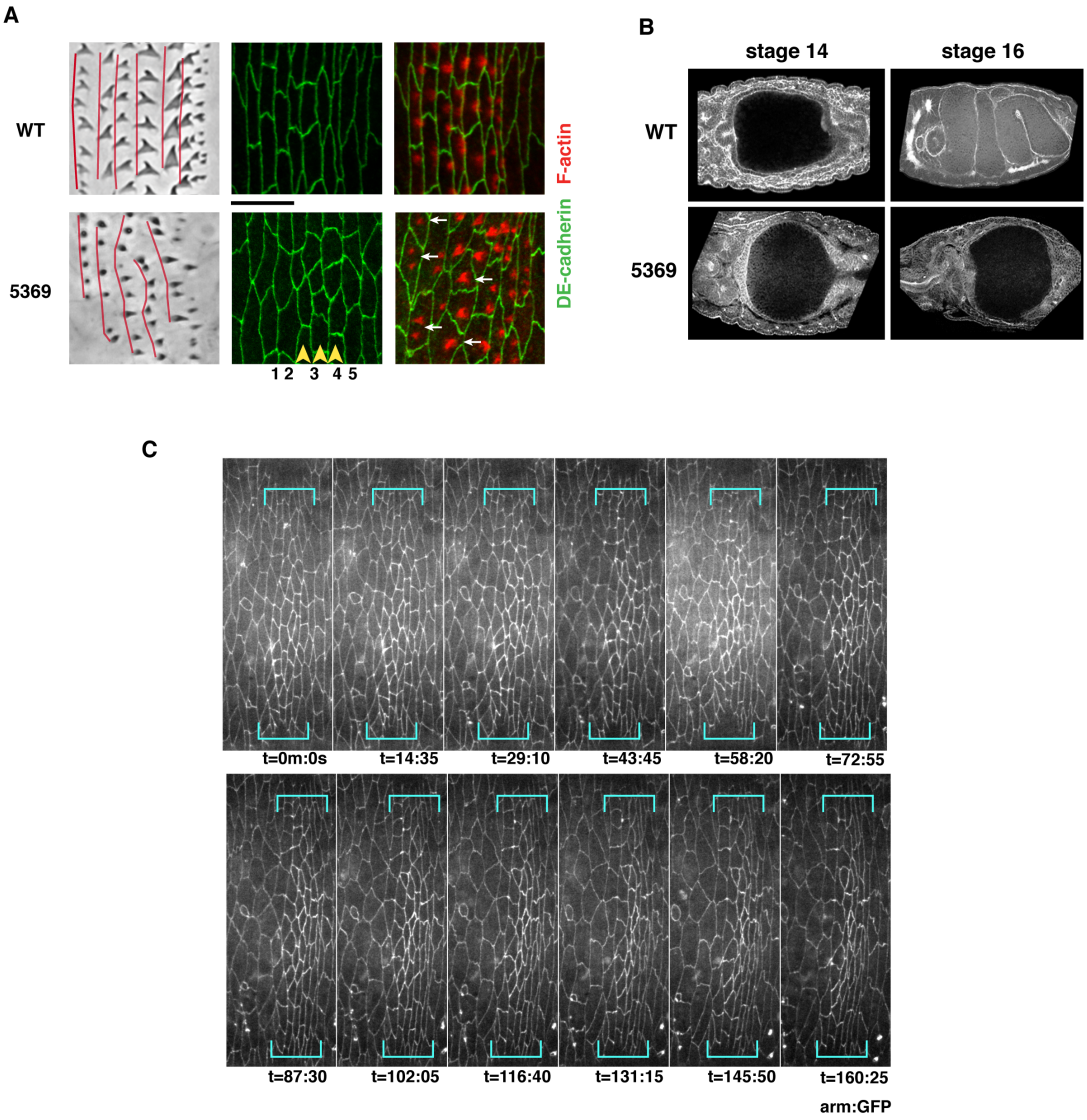

Figure 4.4: 5369 mutants have decreased cell alignment and disorganized denticles. **A.** 5369 mutants produce malformed, mislocalized denticles, in poorly aligned cells. Left, cuticle preparation of WT (OregonR) vs. 5369 mutants; red lines highlight misalignment of the denticle columns. Middle, cells marked by DE-cadherin, (green) are poorly aligned and form disorganized columns in 5369 mutants; yellow arrowheads highlight poorly aligned middle columns. Right, denticles are located away from the posterior edge in 5369 mutants (white arrows); red, F-actin (phalloidin); green, DE-cadherin. n = 16 $m^{-}z^{-}$ 5369 mutant embryos. **B.** 5369 mutants fail to produce a multi-chambered gut, even at late stages. **C.** Cells fail to align and become rectilinear in 5369 mutants, even over the course of several hours. Marker, armadillo (β-catenin) GFP. Blue brackets highlight the denticle belt.

obtained from the Bellen lab, and the screen mutant 2871 (see following section 4.3.7), which was sequenced simultaneously, by Nicholas Socci of the MSKCC Bioinformatics core facility. The core returned to me a list of all the nonsynonomous SNPs occuring in coding regions and in the 5' or 3' UTRs (untranslated regions) of 5369. From this list I manually eliminated any SNPs which occurred in other whole genome sequencing results from the lab (A. Vichas, unpublished results) (Vichas et al., 2015). As these sequence data used for comparison were from a separate project and the flies sequenced had no denticle defects, any mutations shared by these results and the 5369 (or 2871) sequences were unlikely to be causative of my denticle-related phenotypes. This analysis allowed me to eliminate 12 candidates. For each of the remaining 14 candidates, I annotated the results with publicly available expression data and information on known mutants (Attrill et al., 2016), and was able to eliminate two based on lack of maternal or zygotic expression. In total, I was able to identify 10 unique SNPs (9 in open reading frames, 1 in a 3' UTR) in 5369.

4.3.7 2871 mutants are missing denticle column 2 or 3

4.3.7.1 Characterization of 2871/XJBX006

Although many of the genetic requirements for denticle cell fate have been identified, precisely what factors distinguish one denticle column from another remains elusive. In particular, what molecules dictate the size, shape, and orientation of denticles in each column is largely unknown. One such factor is the Notch pathway activator, Serrate, which is required for column 4 denticle fate. Embryos lacking *Serrate* expression generate incomplete denticle belts, in which denticle columns 3 and 4 are replaced with a single column of denticles with an indeterminate morphological type, and Serrate has been demonstrated to extend the field of EGF signaling, thus expanding the region in which *shavenbaby* is active (Walters et al., 2005). Consequently, although the line named 2871/XJBX006 (referred to as '2871' from here onwards) was initially classified among the 'AP patterning' mutants, its phenotype was sufficiently novel to

be considered for further analysis. 2871 mutant embryos have well formed and well organized denticles in most rows, but consistently replace denticle columns 2 and 3 with a single column of indeterminate-type denticles (**Figure 4.5 A**). This suggests that the defective gene in 2871 mutants might be responsible for determining column 2 or column 3 denticle cell fate.

2871 mutant embryos showed loss of column 2/3 denticles at high penetrance, with no other obvious defects in the embryo or denticle morphology (n = 13 embryos). Mutant embryos stained for DE-cadherin and F-actin show no apparent defects in denticle formation or in denticle or cellular organization (**Figure 4.5 B**). However, as is seen in *Serrate* mutants, loss of the denticle column is balanced by gain of a column of smooth cells (Walters et al., 2005) (note gain of cells in smooth cell (bracketed) regions).

To identify the mutation responsible for the denticle column loss in 2871 mutants, I used a combination of duplication mapping and whole genome sequencing. Like 5369, 2871 was a single allele mutant that was not associated with any identified complementation group and had not been rescued by any duplication during the Bellen lab's screen (S. Yamamoto, personal communication). I attempted to map the gene causing male lethality in 2871 mutants using the X chromosome duplication kit, but was unable to identify a single rescuing duplication. Whole genome sequencing of females heterozygous for the mutant chromosome was subsequently performed to identify all potential mutations in 2871 embryos. As I did for 5369 mutants, I filtered the resulting SNP data in coding regions and UTRs against the isogenized reference chromosome, the 5369 mutant sequence, and other available sequencing data, and I annotated the resulting list of genes with publicly available expression data and information on known mutants. This analysis revealed 16 potential SNP mutations that could be the causal mutation. As I was unable to find a single duplication able to rescue the male lethality phenotype in these mutants, it is possible that 2871, like 5369, has a second-site lethal mutation, or that the observed phenotypes are the result of the combined effects of multiple mutations.

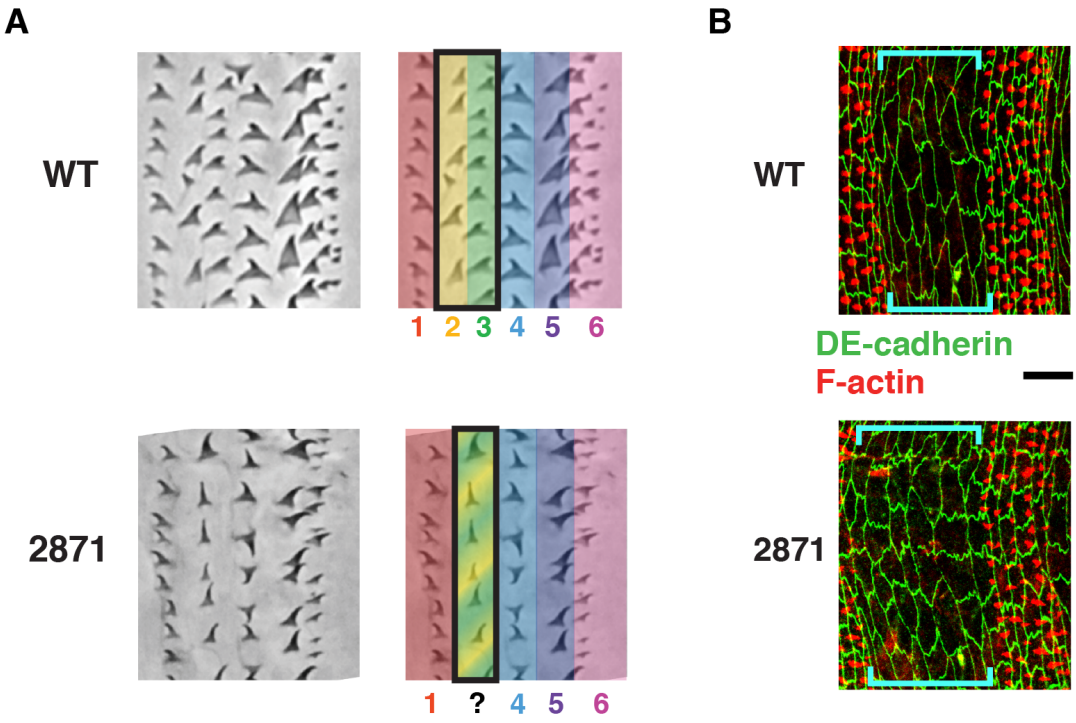

Figure 4.5: 2871 mutants lack denticle column 2 or 3. A. Cuticle preparation of 2871 mutants (right) form morphologically normal denticles, but are missing denticle column 2 or 3 (green/yellow highlighted region) compared to WT (left). **B.** Denticles and denticle cells appear normal in 2871 mutants (bottom) aside from the loss of a denticle column. The smooth cell field expands in 2871 mutants compared to WT (top) (note increased breadth). Red, F-actin; green, DE-cadherin. n = 9 $m^{-}z^{-}$ mutant embryos.

4.3.8 Preliminary characterization and elimination of spacing mutants 4422 and 1264

As the primary goal of the screen was to identify mutants with defective denticle organization, I first quantified the denticle spacing distances in mutant lines #4422 and #1264. My analysis initially revealed that spacing is indeed decreased in this stock, while denticle number is increased. However, on further inspection, I found that there were noticeable baseline differences between embryos of the OregonR wild type strain, which was the control I had been using, and wild-type embryos in a y,w background, which was the starting stock for all the X-chromosome mutants. This alteration in number was sufficient to change the spacing trends when comparing between the OregonR and *y,w* strains. When I compared denticle spacing in mutant #4422 to *y,w* control embryos I found that denticle number and denticle spacing were actually quite similar, suggesting that the initial differences were due to differences between the OregonR and *y,w* backgrounds, rather than any specific denticle defect in this mutant. As neither #4422 or #1264 mutants had additional defects in denticle organization or denticle appearance, this result led me to exclude both mutants from further analysis, leaving me with six candidates. In addition, from this point onward I used *y,w*, rather than OregonR, as a control for my denticle spacing analysis.

4.4 Discussion

Recent advances in sequencing technologies and the creation of new tools for mapping mutations induced via chemical mutagens, including two large collections of molecularly mapped duplications (Cook et al., 2010; Venken et al., 2010), have opened the *Drosophila* X chromosome to large-scale screening for the first time. Our lab received access to a large collection of fly stocks with EMS-induced mutations (Yamamoto et al., 2012, 2014), which we screened in an F3 germline clone screen for mutants with defects in the subcellular organization patterns of the ventral denticles, as well as defects in elongation of the body axis during early embryogenesis.

Of the 748 and 121 mutant cuticles that I examined in the primary and secondary screens, respectively, I identified 21 mutants with reproducible defects affecting the organization, formation, and morphology of the ventral denticles. Of these, I selected five mutants in three different complementation groups as having specific and interesting defects in denticle formation and organization. The three genes in the first of these complementation groups map to the gene Crag, which is involved in Rab10/Rab11-mediated protein trafficking (Denef et al., 2008; Xiong et al., 2012; Lerner et al., 2013). These mutants have column-four-specific defects in denticle hook polarity. The molecular identities of the remaining two mutants are unknown, but whole genome sequencing has identified several candidate SNPs for each. The first of these mutants, named 5369, has defects in cell alignment, denticle formation, and denticle placement. The second mutant, 2871, has a unique patterning defect, in which column 2 and column 3 denticles are specifically lost and replaced with a single column of indeterminate-type denticles.

4.4.1 Challenges of germline clone screening for late embryonic defects

In order to screen for both denticle defects in the late embryo and for germband extension defects in the early embryo, we performed a germline clone screen of the Bellen lab's X chromosome collection. However, this approach has drawbacks. The actin based denticle precursors arise late in embryogenesis (approximately 10.5 hours after the egg is laid), although the genetic program that establishes the denticle cell fate is initiated several hours earlier (approximately 4.5 hours AEL). Consequently, denticle cells are likely influenced by both zygotically transcribed and maternally-derived gene products, and this is likely to complicate the identification of mutants with denticle defects. In this screen, I would have been able to identify two broad classes of genes required for denticle organization: those who are nonessential during early development, and those whose expression is purely zygotic. The removal of the maternal component in this germline clone screen would have excluded those genes whose products are essential earlier during development, as their removal could have caused prior lethality, or produced a phenotype that masked the requirement during the denticle-forming stages. For instance, the myosin heavy

chain, *zipper*, is required for denticle shaping and positioning, as well as denticle cell shape and alignment (Walters et al., 2006); however, germline clones of *zipper* fail to produce eggs (Bloor & Kiehart, 2001). Consequently, it is quite possible that similar regulators of denticle organization were missed in this screen. It is important to note also that the requirements for many genes early in embryogenesis is likely to have contributed to the high percentage of lines classified as 'no embryos/early dead' during the primary screen. As cuticle is not deposited until the end of embryogenesis, genes that cause lethality in early stages could severely disrupt cuticle formation and therefore would be unscorable for my purposes.

Furthermore, such simple screens cannot identify genes whose sole removal causes very subtle defects, or where there is redundancy that can compensate for the removal of a single gene. Homozygous mutants of the *Drosophila* myosin VII, *crinkled*, do not show significant defects in denticle morphology on their own (Bejsovec & Chao, 2012). However, mutating *crinkled* in a *wingless* mutant background results in significant defects in the shaping and elongation of the denticles (Bejsovec & Chao, 2012). Other genes may be required both early and late in such a way that removing the maternal component prevents oogenesis. In addition to performing additional screens in backgrounds that are not wild-type, one alternative method would be to perform more thorough RNAi screens, using a strong epithelial driver such as *engrailed*-Gal4. This could be sufficient to decrease the levels of gene products without entirely preventing early development. Future screens that make use of the larval denticle pattern, rather than the embryo may circumvent this problem. Larvae create denticles twice after hatching, before each larval molt, and, like embryos, produce a cuticle that is readily accessible to screening approaches. More adaptable imaging methods and immobilization techniques have been and continue to be developed, make it increasingly possible to study the larvae at the cellular level in addition to examining cuticles. Screening zygotic mutants in larvae, or generating mutant clones in the epidermis to screen during the larval stages (Saavedra et al., 2014), where maternal contribution is a nonissue, may reveal genes that would otherwise be embryonic lethal. Furthermore, in these large cells, defects in denticle organization, in particular, might be enhanced compared to the

smaller embryonic cells. In summary, while this germline clone screen did identify some mutants with denticle formation and organization defects, screens of multiple types will be necessary to identify additional molecules required for producing and maintaining the complex patterns of organization observed in the denticle cells.

4.4.2 Technical challenges encountered during the X-chromosome screen

Several technical challenges that arose during the course of the screen likely contributed to the limited selection and difficulty in identifying causal mutations.The high-throughput nature of the screen and the limited time allotted for the primary screen phase limited the number of flies in each cross, and likely contributed to the many lines with insufficient or no embryos. In the germband extension phase of the screen, we observed many 'collapsed' embryos, which is characteristic of eggs produced by *ovo*^{D2} females. This could be because the mutated gene is required during oogenesis, but it could also be the result of inefficient recombination during the F_1 generation. We endeavored to choose only non-balancer (germline clone bearing) females and non-balancer *ovo*^{D2}; hs-flp bearing males while establishing our crosses. However, during the height of the screen, the vast quantities of flies and limited time avaliable made it difficult to identify and remove every balancer female, thus potentially reducing the efficiency of the screen. Screening in vials is more cost-effective and physically more practical than screening in bottles, but reduces the number of F_2 progeny. In a very sick stock, this could prove the difference between obtaining a sufficient number of scorable embryos and not. In future screens, even more expansion of necessary *ovo*^{D2} stocks should be conducted prior to screening, and mutant stocks should be expanded as much as possible, as this will make the best use of time and effort.

4.4.3 Conclusion

While I was able to identify several mutants with defects in morphology and alignment, I did not identify any mutants that fell solely within my most interesting category, i.e. those with defects in the fine-scale, subcellular placement of the denticles. While it is entirely possible that such genes are not present on the X chromosome, it is also possible that such subtle defects do not appear strongly at the level of the cuticle, and thus were not identified in the primary screen. The cuticle is a convenient tissue for screening because it arises at the end of embryogenesis, and is semi-permanent, therefore mutant embryos can be accumulated and screened at a later time in bulk. However, as they represent all the accumulated embryos that died prior to hatching, cuticle phenotypes can be extremely messy, and include embryos that died for reasons unrelated to the mutant phenotype. Furthermore, my analysis has indicated that cell boundaries are an important feature of the denticle spacing pattern, but cuticle patterns do not include the outlines of the underlying cells, only the apically projecting structures such as the denticles and hairs. Additionally, mutant phenotypes such as those caused by overexpression of Spastin and knockdown of Patronin, while clearly disorganized at the tissue level, are quite subtle. Thus, these phenotypes may have been overlooked in the primary screen. Alternative approaches might be to screen embryos that have been stained for actin and a cell outline marker, or screen live embryos expressing tagged versions of these proteins, and quantify denticle spacing for a small number. However, while these approaches are significantly more sensitive, they are also significantly more time consuming.

Chapter 5

Future Directions

In this thesis, I have described my work using the actin-based denticle structures created by the *Drosophila* embryo and larvae to investigate how subcellular patterns of organization are generated among macromolecular structures. I have conducted several inter-related projects to understand this process. I have created computational tools and used fixed and live imaging to quantify the denticle organization pattern in embryos and larvae, and to thoroughly characterize the wild type denticle organization pattern. Using genetic approaches, I examined the role of cell size in establishing the denticle pattern, and identified the microtubule cytoskeleton as an important factor in generating a robust organization pattern. In conjunction, I have conducted a forward genetic screen of the X chromosome in order to identify new regulators involved in forming denticles, in aligning denticle cells, and in creating the organization pattern of the denticle structures. In this screen, I identified the RabGTP-related trafficking molecule Crag as an essential player in determining the anterior denticle hook orientation observed in column 4 denticles. I also uncovered two as-yet unknown genes or combinations of genes; the first of which, 5369, disrupts both denticle placement and cell alignment across the denticle belt, while the second, 2871, is a novel AP patterning mutant that eliminates formation of denticle column 2 or 3.

This work establishes the *Drosophila* embryonic and larval ventral epidermis, as a new system in which the mechanisms of subcellular structure organization can be investigated. It further provides a framework through which future studies may identify additional genetic components and cell biological mechanisms necessary for intracellular organization. In this chapter I will discuss potential future directions that could be taken to further understand actin-based structure organization in the denticle system.

5.1 How is denticle number specified?

It is difficult to consider scaling models for the denticle spacing distribution without also reflecting on the ways in which denticle number may scale. In wild-type embryos, denticle number varies from one to six structures per cell, and in larvae, the maximum nearly triples to 17 per cell. We have shown how denticle number influences the spatial organization pattern, but the question of how denticle number is established remains elusive. A major unanswered question that remains is, what determines denticle number? This is an important question that needs to be answered for a full understanding how denticle spacing is regulated, as denticle number greatly influences the denticle organization pattern. My results suggest that a microtuble-based mechanism could control the denticle spacing pattern, as disrupting microtubules causes denticle placement and organization to become less regular. However, these data show that the scaling of denticle number persists even when microtubules are disrupted, implying that the microtuble cytoskeleton is likely not the primary determinant of denticle number. In *in vitro* aggregation assays, actomyosin foci form spontaneously and can grow by condensing these small foci into larger structures (Soares e Silva et al., 2011; Thoresen et al., 2011). In embryonic epidermis, the actin foci that will become denticle precursors condense from a diffuse apical actomyosin meshwork (Chanut-Delalande et al., 2006; Price et al., 2006; Walters et al., 2006; Donoughe & DiNardo, 2011). This work and others demonstrates that these actin punctae are dynamic

and can change position, disperse and vanish, or merge to form larger foci, reminiscent of the behavior of actomyosin foci *in vitro*.

Denticle number could be governed by one of several mechanisms. One possibility is that there is a limiting nucleating factor that regulates precursor formation. This mechanism alone seems unlikely, as the existence of such a limiting nucleator would imply that the denticle creation follows a limiting component hypothesis. My results testing the hypotheses set out by the limiting component model (Chapter 3) indicate that the limiting component hypothesis is not entirely sufficient to explain the scaling of structure number and size with regard to cell size in the denticle system.

One possible alternative model is a stochastic capture mechanism that aggregates transient punctae to form larger, stable denticle precursors and works concurrently with the spatial organization mechanism to balance denticle number and denticle size with the available cell length. Denticle formation initiates with the condensation of actin foci from an apical actin meshwork. These foci subsequently elongate apically to form the final denticle precursor structure. This process requires activity of myosin II, and occurs in the presence of a wide variety of cytoskeletal regulators promoting both straight and branched actin networks (Walters et al., 2006; Price et al., 2006; Chanut-Delalande et al., 2006). During the very early stages of denticle condensation, multiple transient actin foci are distributed uniformly across the anterior-posterior face of the cell; these foci later accumulate at the posterior edge prior to elongating, in response to the activity of the Fat/Daschous and Frizzled planar polarity systems (Walters et al., 2006; Donoughe & DiNardo, 2011; Marcinkevicius & Zallen, 2013; Lawlor et al., 2013). In agreement with this data, I observe that denticle pre-punctae form along the length of the cell, and that these punctae are highly mobile and may shift position, disappear, and occasionally collide with one another and merge to form a larger, single denticle precursor. This is reminiscent of the dynamics of actin aggregation observed in vitro, where highly dynamic actomyosin aggregates form dense foci, may coalesce with other nearby aggregates and accumulate into larger punctae, and stop coalescing only when there were no more nearby structures with which to interact (Soares e

Silva et al., 2011). A similar random initiation-aggregation-capture system in denticle cells would allow stochastic determination of denticle number specifically within the lengthscales actionable on by the microtubule-dependent spacing mechanism. This model is appealing as it would allow denticle number, denticle size and denticle spacing to be balanced along the entire available posterior cell margin, while accounting for the variability in these features seen in vivo. One approach to test whether this stochastic capture model is driven by actomyosin activity would be to examine denticle formation in flies expressing variants of the myosin regulatory light chain (RLC), which is regulated by phosphorylation (Kasza et al., 2014). If actomyosin activity drives actin aggregation, denticle cells in flies expressing a non-phosphorylatable myosin myosin RLC would be expected to have more numerous, smaller denticles. Conversely, activating myosin using a phosphomimetic myosin RLC construct would be predicted to promote foci aggregation, resulting in fewer, larger denticles in each cell.

Alternatively, denticle number might be regulated by a mechanism that suppresses the growth of certain pre-denticle punctae, in conjunction with or independently of a stochastic capture model. Similar to the myosin-based regulation proposed above, these cytoskeletal regulators could act to promote foci fusion. Alternatively, they could act to spatially restrict the region in which foci formation can occur, acting in a manner similar to a positional-feedback mechanism. In the wing, multiple wing hairs (mwh) is a negative regulator of the actin cytoskeleton, and acts downstream of the frizzled planar cell polarity pathway both to specify the location and number of hairs initiated in early wing development (Strutt & Warrington, 2008; Yan et al., 2008; Lu et al., 2010, 2015). It also is able to prevent additional hairs from forming in later stages (Strutt & Warrington, 2008; Yan et al., 2008; Lu et al., 2010, 2015). In the wing, removal of *mwh* results in the formation of ectopic hairs (Wong & Adler, 1993; Strutt & Warrington, 2008; Yan et al., 2008); overexpression suppresses hair formation (Yan et al., 2008). In the denticle cells, my data demonstrate that cells in mwh^{1} mutants have a greater number of denticles, and that these 'extra' denticles are no longer restricted to the posterior margin. These data indicate that mwh is able to limit the region of denticle formation, consistent with its documented roles in regulating

wing hair number (Gubb & García-Bellido, 1982; Strutt & Warrington, 2008; Yan et al., 2008; Lu & Adler, 2015; Lu et al., 2015). If mwh promotes foci coalescence, overexpression of mwh would be predicted to decrease the overall number of denticles. Conversely, if mwh acts solely to restrict the localization of actin foci to specific regions of the cell, overexpression would not be predicted to reduce denticle number. Similar mutation and overexpression experiments could be used to test roles for additional cytoskeletal regulators, such as the formin diaphanous, in regulating actin foci number.

An intriguing additional candidate molecule for regulating denticle number and denticle size is *shavenoid* (*sha*), a novel, insect-specific protein believed to interact with the actin cytoskeleton. Sha is expressed specifically in denticle stripes, downstream of the master transcriptional regulator of denticle fate, shavenbaby (Chanut-Delalande et al., 2006). Denticles in *sha* mutants are severely stunted, have little defined structure, and can often only be seen as slightly raised pimples in the cuticle (Chanut-Delalande et al., 2006; Ren et al., 2006). While it has been known for many years that mutations in *sha* affect trichome formation (Nüsslein-Volhard & Wieschaus, 1980; Ren et al., 2006), very little is known about sha's molecular or cellular functions. Sha's localization in the wing hairs and bristles is consistent with a model in which it interacts with the actin cytoskeleton, and it interacts synergistically with the frizzled pathway during (Ren et al., 2006). However, aside from its potential to interact with actin, its activity is unknown. As shavenoid is the only molecule aside from shavenbaby known to prevent denticle formation to such an extreme extent, it seems like a worthy candidate for further exploration. However, to identify shavenoid's role during denticle formation, a thorough molecular, cellular, and biochemical investigation of its properties will need to be conducted.

5.2 Alternative screening approaches to identify required components for denticle organization and formation

Identifying additional regulators of denticle formation and organization will be a key portion of any future work to understand the denticle spacing process. As discussed in Chapter 4, my cuticle screen of germline clone embryos may have been too simple to identify subtle changes to the denticle pattern, or technical issues arising from removal of essential genes from the developing embryo may have precluded my identification of molecules controlling denticle spacing. Several alternative screening approaches are possible to overcome these issues.

One worthwhile alternative approach may be to use the larval epidermis to screen. Larvae create a new set of denticles just prior to each molt, thus in total, there are three time points at which denticle organization defects may be scored. Like embryonic denticles, larvae create a cuticle record of the structure of the underlying epidermis that is highly amenable to screening, and this work and others has demonstrated that the larval epidermis is accessible to fluorescence imaging modalities. There are several advantages to using the larval denticle system rather than the embryonic denticle system. Removal of genes from the larval epidermis is more likely to be tolerated than in the embryo, as the organism is more thoroughly developed. Despite this, if denticles are created *de novo* just prior to each larval molt, this late removal can still be predicted to have an effect on denticle organization and formation. Larval cells are larger and produce more denticles (see Chapter 2), which may make it easier to observe defects in placement. Additionally, while denticles in the larval cells are aligned along the posterior boundary of each cell the same as in the embryo, cells are not as rectangular and well aligned as in the embryo. This makes it easier at the cuticle level to identify cell boundaries, and thus may facilitate screening for intracellular organization phenotypes, while discarding intercellular denticle relationships. In the embryo, this was not possible, and may have increased the threshold at which a denticle belt was scored as ‘disorganized’.

Several different types of screening approaches could be taken at these stages. A simple zygotic screen may bypass the early requirement for many genes that are essential for embryonic development. Although zygotic screens in the larvae have been conducted in the past (Nüsslein-Volhard & Wieschaus, 1980), the subtlety of the denticle organization defects observed in this work makes it plausible that such mutants would have been overlooked in previous screens. Such a screen could make use of existing collections, such as those available in the Bloomington *Drosophila* Stock Center, or the Kyoto Stock Center. These collections have the advantage of being readily available, and many lines have already been sequenced and otherwise characterized. This avoids one of the major problems encountered during the screen described in this work, which identified two alleles with potential second-site lethal mutations, while still providing the opportunity to conduct a relatively unbiased genetic screen. In any event, future screens should diligently avoid any mutant lines that fail at the complementation testing or other initial verification step, regardless of the attractiveness of the phenotype.

A second type of screen that could be performed in larvae is an RNAi screening approach, using transgenic RNAi fly stocks such as those available from the *Drosophila* RNAi Screening Center/Transgenic RNAi Project at Harvard Medical School (Perkins et al., 2015) and the Vienna Drosophila RNAi Center. Such a screening approach has been successfully employed in the larval epidermis to identify genes required for wound healing (Lesch et al., 2010). Using RNAi lines would circumvent the lethality associated with removing essential genes in the embryo, similar to examining zygotic mutants. However, this approach would require the identification of an appropriate Gal4 driver that 1) drives expression at a sufficient level to obtain strong knockdown; 2) is expressed only during larval stages, or at a sufficiently low level in the late embryonic tissue that the embryo is able to hatch. Thus, it would be necessary to conduct an initial screen of available Gal4 drivers to determine temporal expression and relative expression levels. Possible drivers include the afore-mentioned *engrailed*-Gal4, which is highly expressed in stripes, but may be too strong to obtain larvae; *69B*-Gal4 and *e22c*-Gal4, which are two commonly-used epithelial drivers that express in both the embryo and larvae; and *A58*-Gal4,

which is expressed in the larval epidermis and has been successfully used in RNAi-based wound healing screens (Lesch et al., 2010). Regardless, a thorough evaluation of each driver at the larval stages would be required before such an RNAi screen could be conducted.

This RNAi screening approach could be conducted using cuticle preparations of larvae and/or embryos, using the same procedures as the original X-chromosome screen. However, as expression with Gal4 is not entirely uniform, and several of the above-mentioned drivers are not ubiquitously expressed through the epidermis, a more labor-intensive, though more thorough approach would be to screen live larvae for defects in denticle organization and formation at the cellular level. The advantage of this approach is that it is possible to identify which cells express the shRNA construct, reducing the chance for false negatives due to low or limited expression, and advances in imaging technology and larval immobilization approaches (Füger et al., 2007; Heemskerk & DiNardo, 1994) make this approach a viable option. In addition to identifying an appropriate Gal4 driver, fluorescent reporters for actin and for cell outlines would need to be incorporated. The larval experiments presented in this work used the actin marker utrophin-GFP and the cell outline marker E-cadherin. However, the Gal4 experiments presented herein were most successful when a UAS reporter construct, such as *UAS-moesin-mCherry*, was employed to identify the shRNA-expressing cells. For the best chance of success, these experiments would employ a robust actin reporter such as utrophin-GFP and a similarly robust cell outline marker such as E-cadherin-GFP, and at least one of these would be a Gal4-responsive reporter construct, rather than a ubiquitously-expressed marker. Although this screening approach is highly labor intensive, a live, reporter-based RNAi screen where denticle organization can be assessed on a cellular level is likely to be a more effective approach to identifying molecules required for denticle organization and formation than a cuticle-based screen, as it is more sensitive to subtle phenotypes.

One caveat to these general screening approaches is that it is possible that removal of individual molecules is insufficient to completely prevent the formation of denticles, or the generation of a denticle organization pattern. For instance, zygotic mutation of the *Drosophila* myosin VII,

crinkled alone does not produce significant defects in denticle morphology (Bejsovec & Chao, 2012). However, mutating *crinkled* in a *wingless* mutant background results in severe defects in denticle appearance, suggesting that there is redundancy and a potential dosage-dependence of cytoskeletal components on denticle formation (Bejsovec & Chao, 2012). Similarly, mutation of combinations of the actin bundling proteins *singed* and *forked*, the actin nucleating factor *wasp*, and the membrane remodeling protein *miniature* produces misshapen, but recognizable denticles (Chanut-Delalande et al., 2006), suggesting that there is significant redundancy in the denticle formation process, at least. Therefore, screens in wild-type background that seek isolated molecules affecting denticle organization or formation may be ineffective. One alternative would be to perform one of the screens proposed above in a sensitized background, such as the one that identified crinkled (Bejsovec & Chao, 2012), and look for enhancement of the denticle disorganization phenotype. For instance, screening for increased denticle disorder in a *patronin* mutant background, where denticle placement is subtly disrupted, may be useful to uncover molecules that interact with the microtuble cytoskeleton to promote denticle placement.

5.3 What role might mud have in forming or organizing denticles?

The specificity of the localization patterns of both pins and mud within the denticle belts suggests that both may have roles in building or organizing denticles. However, what these roles might be remains unclear and additional work will be required to identify whether either molecule contributes to denticle formation and organization, and, if so, how. The localization pattern of mud around the sites of denticle formation is particularly intriguing and suggestive of a possible role for mud in denticle formation or organization. However, mud's essential role in early embryogenesis prevents our analysis of embryos from females bearing germline clones, and zygotic mutants may not reduce mud levels sufficiently or at an early enough stage for denticle phenotypes to become apparent. This deficiency may be addressed in several ways.

First, several RNAi lines for mud show potential (Ni et al., 2011), but have yet to be thoroughly tested. Knockdown of mud via shRNA may be enough to bypass its requirement early in embryogenesis, while still reducing protein levels to a sufficient level and at an early enough stage to impact the denticles during their formation. Alternatively, it may be more productive to use the larval denticles, to more thoroughly examine the requirement for mud during denticle development, as removal or mis-expression of the protein in the epidermis may be better tolerated and have fewer side effects on general development in these older animals. Finally, several GFP-tagged mud constructs have recently been generated (Bosveld et al., 2016). A better understanding of the dynamics of the microtubule-associated proteins mud will help to elucidate what role, if any, mud has during denticle formation. For instance, observing how mud accumulates in the space surrounding denticles may reflect how microtubules accumulate or become oriented around denticles. The movement of mud with respect to the denticles could help to support or refute the hypothesis that microtubule minus ends are concentrated at the site of denticle formation, as is suggested by the Patronin-GFP localization experiments. In addition, using these constructs for structure-function analysis in the denticle cells would also help to determine which types of roles mud may have in promoting denticle formation. In the wing, mud constructs lacking the coiled-coil domain correctly localize to junctions, but fail to produce the wild-type astral pulling forces in microtubule ablation experiments (Bosveld et al., 2016). As the function of mud in denticle cells is entirely unknown, such experiments would shed light onto its activity.

If any of these alternative approaches to disrupting mud function are successful, these experiments may start to address potential roles for mud in forming and organizing denticles. In the denticle cells, mud is localized in the immediate vicinity of the emerging denticles but is excluded form the denticle core. Mud localizes in a pins-independent manner to the centrosomes (Izumi et al., 2006), which are well known to be microtubule organizing centers. The centrosomal defects observed in *mud* mutants suggest that mud is involved in the maintenance or assembly of the centrosome (Izumi et al., 2006). The localization of Patronin within denticles (Chapter 2)

suggests that microtubules may be organized around the denticles as if the denticle were an acentrosomal MTOC, with minus ends anchored in or at the denticle structure and plus ends polymerizing outwards. Live imaging of dynamic microtubules using the plus-end-TIP marker EB1 does not rule out this hypothesis (Chapter 2); unfortunately, no conclusive evidence of a role for dynein activity in denticle positioning exists (see following section). In addition, mud has been shown to associate with microtubule plus ends, where it can recruit the dynein/dynactin complex and promote microtubule polymerization (Bowman et al., 2006; Izumi et al., 2006; Siller et al., 2006; Siller & Doe, 2009; Bergstralh et al., 2013a). Given these published data and my preliminary analysis, mud could have one of several potential roles relating to denticle formation and pattern generation. Mud may accumulate at sites of denticle formation to promote correct denticle MTOC formation, consistent with its pins-independent role at the centrosomes. Alternatively, mud may be involved more directly in denticle organization. During spindle formation, mud anchored at the cortex recruits dynein/dynactin and promotes pulling of the spindle pole towards the membrane (Bowman et al., 2006; Izumi et al., 2006; Siller et al., 2006; Siller & Doe, 2009; Bergstralh et al., 2013a). In the oocyte, mud is recruited to the posterior membrane of nuclei during nuclear positioning, which occurs through directed pushing towards the anterior of the cell (Yu et al., 2006). In this case, microtubule plus ends apparently contact the nucleus, and microtubule polymerization from an MTOC located posterior to the nucleus pushes it towards the anterior of the cell. Mud's exact role in this process is unknown (Zhao et al., 2012), although dynein activity is required. If mud is indeed involved in generation of the denticle organization pattern, then these data suggests two potential mechanisms for mud involvement at the denticle sites. First, mud may promote the polymerization of microtubules outward, generating pushing forces on the cytosol, intracellular organelles, or other denticles that might serve to promote regular denticle spacing. Alternatively, mud may recruit dynein/dynactin in the surrounding regions and pull the denticles into an evenly spaced pattern. An alternative possibility that would explain mud's localization pattern and the lack of an organization defect in *mud* mutants is that mud could be required for extension of the membrane or connection with the apical membrane as denticles elongate. The localization of mud above and around the

denticles in late-stage embryos is suggestive of a molecule associated with the membrane as the actin bundle extends upwards. Association of mud with the apical cortex might be associated with the extension of the denticle into the apical space or transport of required components as the denticle is built upwards, similar to the requirement for apical sculpting and molecular transport by the atypical myosin *crinkled* (Bejsovec & Chao, 2012). Additional experiments with mud and proteins of the dynein/dynactin complex will be required to determine if either of these mechanisms are likely to be occurring in the denticle cells.

5.4 What is the role of Crag in denticle formation?

What might Crag's role be in specifying the hook polarity of column 4 denticles? How hook polarity is established in the denticle field is an open and ongoing question. One possible role for Crag might be in regulating the polarized transport and subsequent localization of the spectraplakin short stop (shot) during denticle hooking. Recent work has demonstrated a cell-autonomous and cell-non-autonomous requirement for the transcription factor *Stripe* and one of its downstream effectors *short stop*, in assigning anterior hook polarity in both denticle columns 1 and 4 (Dilks & DiNardo, 2010). Stripe is best known for regulating the epidermal-muscle attachments between the basement membrane and the tendon cells (Becker et al., 1997); in the embryonic denticle belts, tendon cells are also the cells that generate the denticle columns 2 and 5. Spectraplakins function as linkers between the actin and microtubule cytoskeletons and membranes (Roper, 2002). In the denticle cells, *shot* is expressed in two pools, one ubiquitous across the denticle belt, and one specifically in the tendon cells; it localizes both to the denticles and across the 1/2 and 4/5 column interfaces (Dilks & DiNardo, 2010). Interestingly, although its location along the apical-basal axis has not been specifically identified in denticle cells, in the tendon cells, shot is found at both the apical and basal membranes (Gregory & Brown, 1998). This suggests the possibility that shot could be acting as a linker between muscle, the basal cell surface, and apical protrusions such as the denticles to promote larval locomotion. If localization of shot is

required specifically at apical and/or basal surfaces, as it appears to be in the tendon cells, one possible role for Crag might be in regulating the polarized transport and subsequent localization of shot during denticle hooking. This hypothesis could readily be tested with antibodies or fluorescently-tagged transgenes to look at the localizations of each of these molecules. Such molecules might be required apically, in the denticle, or basally to stabilize the linkage with the basement membrane.

A related question is, is Crag required both cell-autonomously and -non-autonomously in column 4 denticle cells, as shot is, or is the requirement limited to one or the other? Shot localization seems to be required in the column that produces the anterior-facing hooked denticle, and in the adjacent posterior column (Dilks & DiNardo, 2010). Identifying where Crag is required in the denticle belt would help to better define its role in establishing denticle hook polarity.

One curious feature of these data is that mutations in *Crag* result in denticle hook defects in column 4 cells, but not in column 1 cells. In contrast, Stripe and shot appear to be required for hooking in both columns. One possibility is that the differential expression of proteins across cells in the denticle belts makes cells of column 4 sensitized to loss of Crag, whereas column 1 cells are able to compensate. Perhaps in column 1 cells, another Rab protein is able to compensate for loss of Crag, somewhat akin to the way in which trafficking balances between Rab10 and Rab11 in the follicle cells. It is clear that, although they both produce denticles with anteriorly-facing hooks, columns 1 and 4 each make distinct types of denticles, and are assigned to the denticle cell fate by a different combination of molecules (Figure 1.3). Elucidating the role that Crag plays in assigning column 4 denticle hook polarity will most likely be required to resolve this conundrum.

Chapter 6

Materials and Methods

6.1 Fly stocks and genetics

6.2 Fly stocks and genetics used in Chapter 2

Embryos were grown at 22-25° C and were analyzed at stages 15-16, except for **Figure 2.6** and **Figure 2.14** as indicated. *y, w* was the wild-type control for embryos, *sqh::GFP-utrophin-ABD; ubi-E-cadherin:GFP* (Rauzi et al., 2010; Oda & Tsukita, 2001) was the wild-type control for larvae. To generate CycE-OE embryos, *UAS-CycE; UAS-p35 or UAS-p35; UAS-CycE* males were crossed to daughterless-Gal4 females and the progeny were analyzed. *UAS-p35* stocks were gifts of B. Edgar and *UAS-CycE* stocks were gifts of B. Edgar and H. Richardson, obtained from the Bloomington *Drosophila* stock center. No significant differences were observed between these genotypes and the results were combined for analysis. To generate *ms(3)k81* embryos, *ms(3)k81*^{1} */Df(3R)ED6255* or *ms(3)k81*^{Z3416} */Df(3R)ED6255* males were crossed to *y, w* females. The *ms(3)k81* stocks were gifts of B. Wakimoto (Yasuda et al., 1995). No significant differences were observed between the progeny of *ms(3)k81*^{1} and *ms(3)k81*^{Z3416} hemizygous

males and the results were combined for analysis. For Spastin-OE, *UAS-Spastin-EGFP /TM3* (Jankovics & Brunner, 2006) or *UAS-CFP-Spastin /TM3* (Du et al., 2010) was crossed to *engrailed-Gal4, UAS-moesin-mCherry* or *engrailed-Gal4*. No significant differences were observed between these genotypes and the results were combined for analysis. For Patronin-KD, *P{y^{1}, sc*, v^{1}; TRiP.HMS01547}attP2* (Ni et al., 2011) was crossed to *engrailed-Gal4, UAS-moesin-mCherry*. Patronin-GFP stocks were *w*; P{Ubi-p63E-Patronin.A.GFP}1M /CyO* or *w*; P{Ubi-p63E-Patronin.A.GFP} 3M /TM3, Sb*, from the Bloomington *Drosophila* stock center. For EB1-GFP experiments, *UAS-EB1-GFP /TM3* (gift of N. Brown) (Bulgakova et al., 2013) was crossed to *engrailed-Gal4, UAS-moesin-mCherry*.

6.3 Fly stocks and genetics used in Chapter 3

Embryos were analyzed at 22-25° C. *y, w* or *OregonR* was the wild-type control, as indicated, for embryonic experiments. *sqh::GFP-utrophin-ABD; ubi-E-cadherin:GFP* (Rauzi et al., 2010; Oda & Tsukita, 2001) was the wild-type control for larvae experiments. *mwh*^{1} flies were obtained from the Bloomington *Drosophila* stock center (BDSC). For analysis of *fat* mutants, images of the embryonic progeny of females bearing *fat*$^{\mathrm{Grv}}$ (Bryant et al., 1988) or *fat*$^{\mathrm{NY1}}$ (Tyler & Baker, 2007) germline clones were obtained from Emily Marcinkevicius (Marcinkevicius & Zallen, 2013). For experiments with *Shroom* mutants, *Shroom* mutant flies were generated by crossing *ShrmΔ11 /Df(2R)Exel7131* or *ShrmΔ13.6 /Df(2R)Exel7131* females and males, as in (Simoes et al., 2014); no significant differences were detected between these genotypes. For Shroom overexpression experiments, *UAS-ShroomA2.3 /FM7c* females (Hildebrand, 2005) was crossed to *daughterless-Gal4* males. To analyze zygotic *mud* mutants, *mud*^{1} */FM7a* flies obtained from the BDSC and rebalanced over *FM7c, Kr>GFP*. For analysis of *pins* mutant embryos (the embryonic progeny of females bearing *pins* germline clones), *pins*$^{\mathrm{p62}}$ *FRT 82B /TM3,Twist>GFP* (Yu et al., 2000) were crossed to *hs-flp; ovo^{D2} FRT 82B /dominant-marker* males. Non-balancer, non-marker virgin females were collected and crossed to *pins^{p62} FRT 82B /TM3, Twist>GFP*

or *armGFP; pins^{p62} FRT 82B /TM3, Twist>GFP* males. Progeny were categorized as zygotic mutant (z) of zygotic rescued (z^+) based on GFP status during imaging.

For candidate genes tested in the RNAi screen, *engrailed-Gal4, UAS-moesin-mCherry* or *engrailed-Gal4, UAS-moesin-mCherry; sqh-GFP* females were crossed to males bearing RNAi transgenes (in stocks where homozygous non-balancer males were present, these were preferentially selected). A complete list of genes and stocks can be found in Tables 3.2 and 3.3.

6.4 Fly stocks and genetics used in Chapter 4

All stocks for the X chromosome screen were generated by the X Screen Team of Hugo Bellen's lab (Baylor College of Medicine, Houston, TX) (Yamamoto et al., 2014, 2012). Stocks had the genotype *y, w, *, FRT19A /FM7c,Kr>GFP*. The original isogenized *y, w,* FRT19A reference stock was obtained from Nele Haeltereman and the X Screen Team in Hugo Bellen's lab. Duplication stocks (Dp(1;Y) and Dp(1;3)) for mapping were obtained from the Bloomington *Drosophila* Stock Center (Bloomington Stock Center). *ovo*^{D2}, *FRT19A* stock was a gift of N. Tolwinski. *ovo*^{D2}*, FRT19A; hs-flp, arm:GFP* and *ovo*^{D2}*, FRT19A; hs-flp, sqh:GFP* stocks were created in the Zallen lab by Leah Greenspan.

Tagged alleles of Crag-PB (*UAS-HA-CragB*), mutant alleles *Crag*^{CJ101} and *Crag*^{CB188}, and rescue constructs *Crag-genomic-88* and *Crag-genomic-98,* (which were generated from a 12.4kb fragment including 1695 bp upstream, and 1561 bp downstream of the Crag gene), were gifts of T. Schüpbach (Denef et al., 2008).

6.4.1 Generation of germline clones

Germline clones were generated using the FLP-DFS system (Chou & Perrimon, 1996). For X-chromosome mutations, mutation/balancer (*FM7c* or *FM7c, Kr>GFP*) virgin females were crossed to *w, ovo^{D2} FRT19A; hs-flp* males. The *hs-flp* chromosome contained either no GFP marker, or was recombined with either *sqh-GFP* or *arm-GFP*. For autosomal mutations, mutation/balancer virgin females were crossed to either *hsflp; ovo^{D2} FRT40A/dominant-marker* or *hsflp; ovo^{D2} FRT82B/dominant-marker* males. Progeny were heat shocked for 1 to 1.5 hours (for crosses in vials and bottles, respectively) in a 37° C water bath on days 2 and 3 after egg laying at room temperature. For X-chromosome crosses, non-balancer females were collected and crossed to sibling males; balancer females were discarded. For third chromosome mutations, non-balancer, non-marker virgin females were collected.

6.5 Immunofluorochemistry

Embryos were dechorionated in 50% bleach for 2 min and washed with water. For immunofluorescence experiments except those with rabbit anti-pTyr, embryos were fixed with vigorous shaking in a 1:1 mix of 37% formaldehyde and heptane for 7 min, transferred to a piece of double-sided tape via a pad of apple juice agar, covered with buffer, and manually devitellinized using a glass needle. For experiments with rabbit anti-pTyr, embryos were fixed in a boiling solution of 0.03% Triton X-11 and 0.4% NaCl for 10 seconds, then cooled on ice for at least 30 minutes, then vortexed in a 1:1 mixture of heptane and methanol to devitilinize. Embryos were stained in 1X PBS or 0.1M Na_2HPO_4, pH 7.2 (for DE-cadherin antibodies) and mounted in Prolong gold (Molecular Probes). Primary antibodies were rat anti-DE-cadherin (1:50, Developmental Studies Hybridoma Bank (DSHB)), rabbit anti-GFP (1:100, Torrey Pines Biolabs, Inc.), mouse anti-α-tubulin (1:500, DSHB), rabbit anti-mud (1:50, gift of F. Matsuzaki (Izumi et al., 2006)), rabbit anti-pins (1:50, gift of F. Matsuzaki (Izumi et al., 2006)), mouse anti-shot

(1:50, DSHB), and rabbit anti-pTyrosine (1:500, Sigma), and were detected with Alexa Fluor 488, 546, 568, and 647-conjugated secondary antibodies (1:500, Molecular Probes). F-actin was visualized with Alexa Fluor 488, 546, 568, or 647-conjugated phalloidin (1:1000, Molecular Probes) or Alexa Fluor 405-conjugated phalloidin (1:1000, Santa Cruz). Guinea pig anti-Bazooka (Par-3) (1:500) (Blankenship et al., 2006) was included with phalloidin in the red channel in **Figure 2.7**, but is not visible at the gain shown.

6.6 Cuticle preparations

Embryos were dechorionated in 50% bleach for 2 min and washed with water. Larvae were washed with water to remove food particulate. Both embryos and larvae were were mounted in Hoyer's medium diluted 1:1 with lactic acid (Alexandre, 2008), then imaged on an AxioImager.Z1 with a PlanNeoFluor 40x/0.75 Ph2 objective (Zeiss).

6.7 Hatch rate

To calculate the hatch rate of mutant embryos, collection plates were aged for for 36 hours at room temperature, and the number of embryos counted. The hatch rate was calculated as the number of empty chorions (egg shells) versus the total number of unhatched embryos plus the number of empty chorions.

6.8 Fixed image acquisition

Images of fixed embryos were single Z-planes acquired with a PlanNeofluor 40x/1.3 NA oil objective (Zeiss) at 1.8x zoom (section of 0.5 µm). Images of larvae were Z-stacks acquired with a PlanNeofluor 40x/1.3 NA oil objective (Zeiss) at 1x or 1.3x zoom (section of 0.5

µm) or a Plan-Apochromat 63x/1.4 oil objective (Zeiss) (section of 0.5 µm). Imaging was performed on an LSM700 or LSM710 confocal microscope (Zeiss). Images were converted from multichannel Zeiss .lsm to composite RGB TIFF in ImageJ, and were projected using a maximum intensity projection in ImageJ (Schneider et al., 2012) where applicable. The PhotoMerge automated algorithm in Photoshop was used to create a single image of each animal for further analysis.

6.9 Time-lapse imaging

For live imaging experiments, dechorionated embryos were oriented dorsal-side-up between thin strips of double-sided tape on a coverslip and mounted between the coverslip and a gas-permeable membrane (YSI, Yellow Springs, OH) in halocarbon 27 oil (Sigma). Time-lapse movies of live embryos were acquired with a Plan-Apochromat 100x/1.4 oil objective (Zeiss) on a Perkin Elmer Ultra-View VOX spinning disk microscope, or a Plan-Apochromat 63x/1.4 or Plan-Apochromat 100x/1.46 oil objective (Zeiss) on an LSM710 confocal microscope. Images were exported as multichannel time series from Volocity or Zeiss .lsm format, projected using a maximum intensity Z-projection in ImageJ, and registered via fiducial markers using SIESTA (Fernandez-Gonzalez & Zallen, 2011).

6.10 Laser ablations and wounding

As for live imaging experiments, dechorionated stage 14-16 embryos were mounted between a coverslip and gas-permeable membrane (YSI, Yellow Springs, OH) in halocarbon 27 oil (Sigma). Time-lapse imaging was performed on a Perkin Elmer RS5 spinning-disk confocal microscope with a Plan Neofluor 63x/1.4 NA oil-immersion objective (Zeiss) or Plan-Apochromat 100x/1.46 oil objective (Zeiss), which was also used to focus the MicroPoint laser (Photonics Instruments). Cuts were made using the MicroPoint laser tuned to either 405 nm or 440 nm dye cells. For

wounding experiments, cuts were made to a single AP boundary, and imaged as the wound expanded and through closure. For denticle ablation experiments, the laser was focused on an apical plane on denticles, or between two denticles in the same cell, and recovery of the cell was imaged.

6.11 Larval imaging

Larvae were rinsed with water, placed on a coverslip in halocarbon 27 oil (Sigma), anesthetized using dry ice or ether, and then selected based on the presence of denticles in the GFP channel. For experiments using cold as an anesthetic, larvae were immobilized by applying dry ice to the underside of the coverslip. Selected larvae were transferred to a fresh coverslip, oriented ventral side down, and gently flattened between the coverslip and a glass slide. Larvae were kept immobile during imaging with direct application of ice. For experiments using ether as an anesthetic, larvae were placed in a Falcon tube containing a cotton ball with several drops of ether for several minutes. Selected larvae were then transferred to a custom built chamber (Füger et al., 2007; Heemskerk & DiNardo, 1994) in halocarbon oil, oriented ventral side down, and flattened between the dish bottom and a coverslip. A drop of ether was added, and the chamber sealed with vacuum grease (Corning) and parafilm.

6.12 Staging

For fixed analyses, embryos were staged based morphological criteria. The two major factors were the degree of dorsal closure completed and the extent of gut formation, while more minor factors included the appearance and alignment of denticle cells. For live analyses, cell appearance (in movies where a cell outline marker was present) or denticle appearance (in movies with an actin marker) were used to approximate the stage. (**Figure 6.1**) shows examples of the relevant stages in fixed embryos and stage-specific traits are described below.

At stage 13 (approximately 9.3-10.3 hours after egg laying (AEL) at 25° C), the germband has fully retracted, but dorsal closure has not yet begun, as evidenced by the rounded edges of the dorsal hole. Cells begin to rearrange and align. At stage 14 (approximately 10.3-11.3 hours AEL), dorsal closure begins, as evidenced by the 'eye' shaped, pinched-oval appearance of the dorsal closure. As stage 14 progresses, the dorsal hole goes through a 'zippering' process from the anterior and the posterior ends of the animal, and the two ends eventually meet in the middle. The relative age of the animal (early-, mid-, or late-stage 14) can be determined by how much of this zippering process has completed. During this time, the gut consists of a single rounded chamber. In late stage 13 and early stage 14, an apical actin meshwork accumulates; denticles begin to become apparent during the middle of this stage; cell rearrangements have completed to form 5 clearly defined columns. Stage 15 (approximately 11.3-13.3 hours AEL) is marked by the completion of dorsal closure, though there is an evident 'scar' where the two edges of the epithelium have met. The gut begins to constrict and form separate chambers. Embryos with fewer than 3 gut chambers were considered to be stage 15. Denticles elongate during this stage. Stage 16 (approximately 13.5-15 hours AEL) embryos have at least three but fewer than five to six gut chambers. Dorsal hairs are present, and the scar from dorsal closure fades. Stage 15 and 16 embryos were analyzed for denticle organization in Chapter 2. Stage 17 (approximately 15-22 hours AEL) is the final stage of embryonic development which ends in the embryo hatching into a first instar larvae. The gut increases in complexity and has 3 to 5 or 6 chambers. In live embryos, muscles begin to contract.

6.13 Quantification of denticle organization

Analysis of denticle cells was conducted on abdominal segments 3-7. The positions of denticles and the dorsal and ventral ends of the posterior cell boundaries were manually identified and recorded using the ImageJ CellCounter plugin. Cell length was measured as the length of a straight line connecting the dorsal and ventral ends of the posterior margin of each cell. Custom

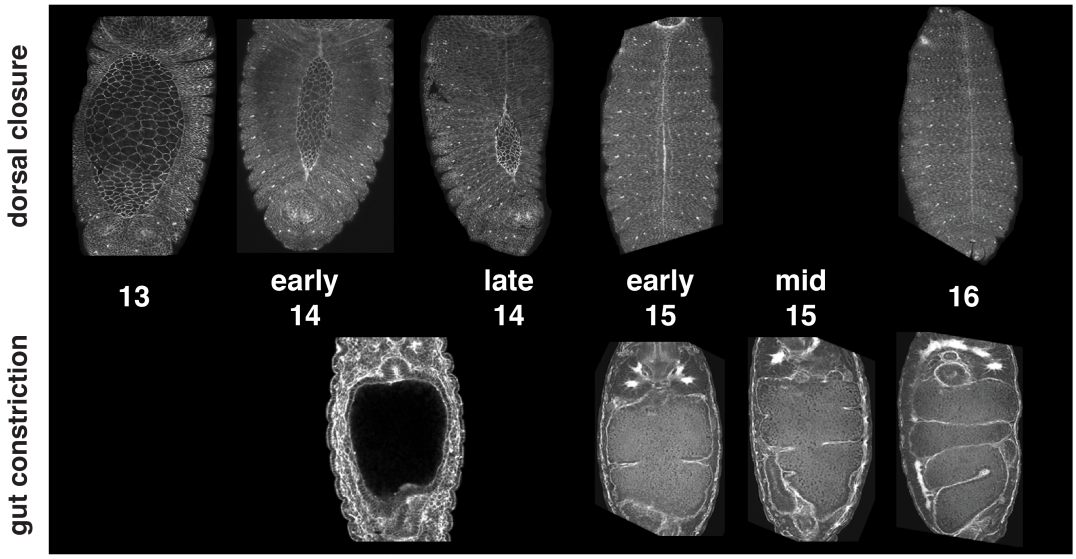

Figure 6.1: Late stage, wild type embryos can be reliably staged based on phenotype. Top, progression of closing of the dorsal hole is a reliable determinant of stage in earlier embryos. Bottom, gut constriction can be used to stage the later embryo.

MATLAB code was used to organize the data based on column and cell of origin, calculate cell length from the dorsal and ventral posterior markers, calculate distances between adjacent denticles, and perform basic measurements and statistics (Mathworks, version R2013). Graphs and statistical tests were generated using Prism (GraphPad) and matplotlib, seaborn, and scipy in Python3. Best-fit linear regressions were generated in Prism or using scipy for each category of denticle cells with more than 5 cells. The spacing error was calculated relative to the best-fit linear regressions for each class of denticle cells for each genotype. Plots show the spacing error (absolute distance from the position predicted by the best-fit linear regression, or this distance normalized to cell length or the predicted denticle spacing for each cell) for each individual denticle spacing measurement in the indicated condition; values in Table 2 are mean values for all spacing error measurements in a given condition.

6.14 Quantification of denticle size

Individual cells were manually identified as regions of interest (ROIs) in ImageJ. Cell length was measured for each cell by drawing a line between the dorsal and ventral ends of the posterior boundary, and cell area was obtained from the specified ROI. The 3DObject counter plugin (Bolte & Cordelieres, 2006) was then used to identify and calculate the area of each denticle in each cell of interest. Denticle diameter was back-calculated from area, under the assumption that ROIs were circular.

6.15 Modeling and statistics

P-values for comparisons for measurements of denticle spacing, cell length, and denticle number were calculated using one-way ANOVA (multiple comparisons, Fisher's LDS), or Student's t-test. Regressions were calculated using a least-squares nonlinear regression analysis. Monte Carlo simulations were performed using custom Python code, and distributions compared using a 2-sample Kolmogorov-Smirnov test in Python (scipy.stats.ks_2samp).

The relationship between the denticle spacing distance (D), cell length (L), and the number of denticles (N) was derived from the following equation, in which α is the ratio between the denticle-cell edge distance and the denticle-denticle distance (the spacing ratio), as follows:

$$L = \alpha D \ + \ D_{d_1,\, d_2} + D_{d_2,\, d_3} + \ldots + D_{d_N - 1,\, d_N} \tag{6.1}$$

We extended this to the general case by assuming that all the denticle separation distances for a single cell are equal, which allowed us to obtain a general equation for calculating D with respect to L, N and α:

$$
\begin{aligned}
L &= \alpha D + \sum_{i=1}^{N-1} D_{i:i+1} + \alpha D \\
&= \alpha D + D(N-1) + \alpha D \\
&= D(2\alpha + N - 1)
\end{aligned}
$$

$$
D = \frac{L}{2\alpha + N - 1} \tag{6.2}
$$

In addition, the relative position R of each denticle n_i with position p may be determined by the following:

$$
\begin{aligned}
R_{n_i} &= \frac{p_{n_i}}{L} \\
&= \frac{\alpha D + D(n_I - 1)}{\alpha D + D(N-1) + \alpha D} \\
&= \frac{\alpha + n_I - 1}{2\alpha + N - 1}
\end{aligned} \tag{6.3}
$$

Andrew Schaumberg, a rotation student in the lab, developed the framework for a statistical modeling method to test which values of α most closely captured the relationship between D, L, and N *in vivo*, which I implemented and validated in Python. For each (L,N) pair in the dataset and each value of α in simulations (where α equals one of [0.5, 0.6, 2/3, 0.7, 0.75. 0.8, 0.9, 1]), we calculated the mean separation distance (D_{mean}) and the positions for each denticle n_i (μ_i). We then sampled from normal distributions with $\mu = \mu_i$ and $\sigma = \{\frac{D_{mean}}{5}, \frac{D_{mean}}{6}, \frac{D_{mean}}{7}, \frac{D_{mean}}{8}, \frac{D_{mean}}{9}\}$ to obtain the positions of each denticle. Data from each simulated model (pair of (α, σ) values) was compared to the *in vivo* data using the Kolmogorov-Smirnov test (scipy.stats.ks_2samp). For each model, 10,000 simulations of 1100-3100 cells each (based on the number of *in vivo* measurements in Tables !table(TableS2)

and !table(TableS5)) were performed. Simulations were considered consistent with the *in vivo* datasets if they were not significantly different ($p \geq 0.05$) from the data. The model with the greatest number of simulations consistent with the *in vivo* data was considered to be the best fitting model. All accepted and best-fitting models had greater than 94% of simulations with $p \geq 0.05$.

For all analyses, the cell length L along the dorsal-ventral axis was defined as the distance between manually defined dorsal and ventral cell edge markers. In some cells, denticles did not fall along a straight line, mainly due to cell or embryo curvature, and therefore this L differed slightly from the summation of the individual distances as in equation 1. Similar α values where obtained when α was directly calculated using a least-squares estimate. The least squares estimate of α using equation 2 was 0.715 in wild-type embryos, 0.715 in CycE-OE embryos, 0.66 in *ms(3)k81* embryos, 0.66 in Spastin-OE embryos, 0.6 in Patronin-KD embryos, and 0.94 in wild-type larvae larvae (V. Seshan, MSKCC Biostatistics Core Facility, personal communication).

6.16 Code and code management

Code used was written and tested in MATLAB version R2013, or the Anaconda distribution (v 2.5.0) of Python3 (Continuum Analytics). Version control maintenance was performed using git.

6.17 X chromosome screen

6.17.1 Screen genetics

To generate flies bearing germline clones, *y, w, * FRT19A/FM7c, Kr>GFP* mutant females were crossed to *ovo*^{D2}, *FRT19A/Y; hs-flp(/CyO)* males at a ratio of approximately 5:1 (F0). Resulting progeny were heatshocked at 37° C twice on consecutive days as larvae, and allowed to mature. Adults were sorted based on sex and presence of Bar eye and curly wing phenotypes. To screen for germband and cuticle defects, non-Bar eyed, non-Curly wing females (half of which were expected to have homozygous mutant germline clones; expected germline genotype either *y, w, * FRT19A/y, w, * FRT19A* or *y, w, * FRT19A/ovo*^{D2}, *FRT19A*) were crossed to sibling males (*FM7c, Kr>GFP/Y*) and placed in multi-chamber screening condos with apple juice agar laying plates. Plates were changed several times daily. Over the course of the screen, crossing either *ovo^{D2} FRT19A /FM7c,Kr>GFP; +/+* or *ovo^{D2} FRT19A /FM7c,Kr>GFP; CyO/+* females to *FM7c, Kr>GFP /Y; +/hs-flp* sibling males and screening the resulting progeny for the presence of viable embryos was the negative control to confirm that oogenesis was blocked in females bearing an *ovo*^{D2} chromosome. Mutants with known and recognizable germline clone phenotypes (such as *bazooka/Par-3*) were included over the course of the screen to provide a positive control for the germline clone crosses. An overview of the crossing schema can be seen in Figure 6.2.

6.17.2 Primary screening of germline clone embryos

6.17.2.1 Screen for cuticle defects

To screen for cuticle defects, flies were allowed to lay at 25° C overnight. Plates were then collected, covered with a half-condo (similar to the screening condo, but shorter and without the mesh screening at the top) to limit the movement of hatched larvae and allowed to age for 36 hours at 25° C (**Figure 6.3**). After 36 hours, plates were removed to 4° C for up to a

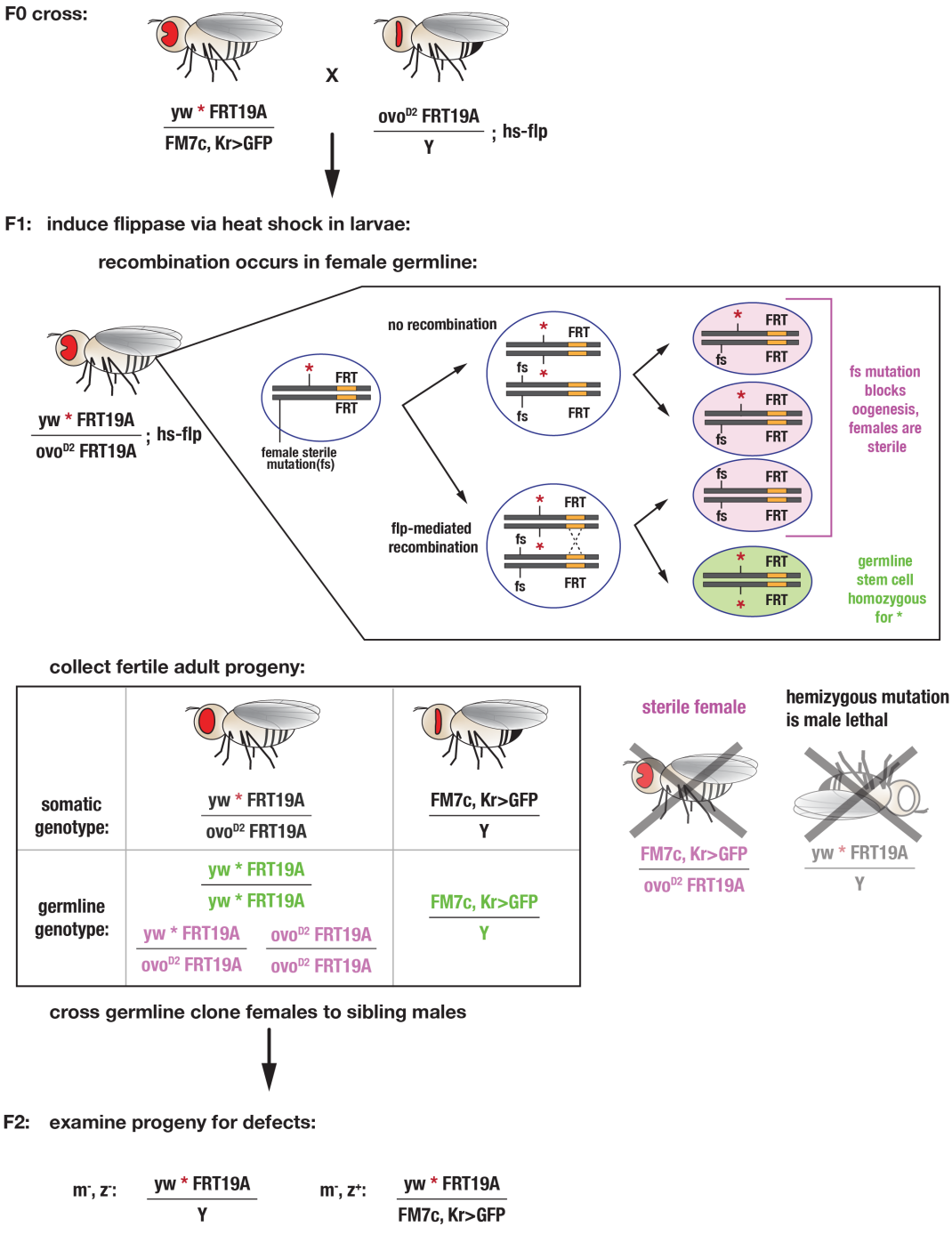

Figure 6.2: Crossing schema for the generation of X-chromosome germline clone mutants.

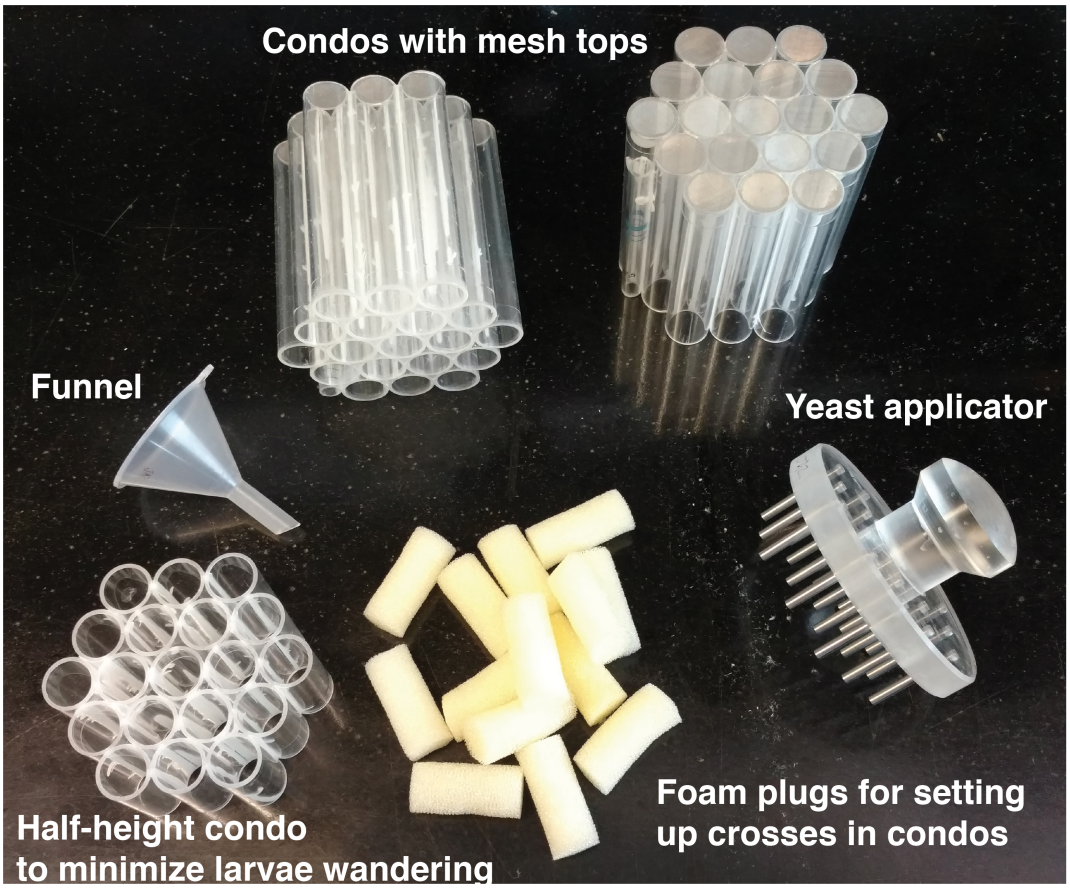

Figure 6.3: Apparatus used during the X chromosome screen.

week. Plates were shipped overnight on ice from Houston, Texas to the lab in New York, where cuticle preparations of embryos and larvae were generated using standard protocols (Alexandre, 2008). These were then examined using phase contrast microscopy on an AxioImager Z.1 microscope with a Plan Neofluor 5x/0.15 objective (Zeiss) or a Plan-Apochromat 40x/0.75 PH2 objective, and the phenotype(s) of each line recorded (see **Table 4.2, Table 4.1**). Candidate lines to include in secondary screening steps were selected on the basis of phenotype, with secondary consideration to penetrance.

6.17.3 Secondary screening of germline clone embryos

The initial phase of secondary screening entailed screening embryonic cuticles to confirm the presence and penetrance of the mutant phenotypes identified in the primary screen. This step was carried out in a similar manner as in the primary screen; the main difference was that crosses were scaled up to include a larger number of flies for each cross, and screened in laying cups as well as the multi-well condos to increase the number of mutant embryos. The second phase of screening and initial mutant characterization entailed examining the cellular phenotypes of stage 14-16 embryos. Embryos were stained for an actin marker, a cell outline marker, and GFP to screen for defects in cell organization and denticle formation and organization in m^-/z^- and m^-/z^+ embryos, respectively. Candidates were selected for further study based on phenotype and penetrance.

6.17.4 Whole-genome sequencing

Genomic DNA was isolated from *y, w, 5369 FRT19A /y, w, FRT19A iso* and *y, w, 2871 FRT19A /y, w, FRT19A iso* and sequenced using Illumina HiSeq (paired-end run with length of ends 2x100, 20x reads per sample) by the MSKCC Genomics Core Laboratory. (In the sequencing reaction, 2871 was accidentally mislabeled as 2971, which is reflected in the WGS data.) Sequenced libraries were mapped to the *Drosophila* genome (*D.mel* Release 5.5 reference sequence) using a custom pipeline developed by Nick Socci of the MSKCC Bioinformatics Core.

6.17.5 Identification of candidate mutations from WGS results

Initial category assignment of mutations uncovered during whole-genome sequencing was performed by Nick Socci in the MSKCC Bioinformatics Core. In/dels & SNPs were then identified based on the *D.mel* Release 5.5 reference sequence. These calls were then filtered to include hits that were unique to either 5369 or 2871, that were mutations in coding regions or nearby

UTRs, and which were non-synonymous. A reference sequence of the original, isogenized *y, w, FRT19A* stock obtained from N. Haelterman and the X Screen team (H. Bellen, Baylor College of Medicine) (Haelterman et al., 2014; Yamamoto et al., 2014) was used to filter out calls from each genotype that were also in the parent stock. Finally, calls were manually screened against sequence data from an unrelated project in the lab to further eliminate any potential non-deleterious polymorphisms not captured in the parent or reference sequences. To eliminate candidates based on temporal and transcript expression, if available, candidates were manually screened against the modENCODE data available from FlyBase (Attrill et al., 2016; modENCODE Consortium et al., 2010). Candidates were further screened based on expression and lethality data available in FlyBase.

6.17.6 Duplication mapping

Duplication stocks in the 'X Chromosome Duplication Kit' (Cook et al., 2010; Venken et al., 2010), as well as additional duplications covering the genes identified through whole genome sequencing, were obtained from the Bloomington *Drosophila* Stock Center (Bloomington Stock Center). To map screen candidate lines, mapping crosses consisting of males bearing duplications crossed to virgin females (genotype *y, w, *, FRT19A /FM7c, Kr>GFP*) were established for each stock of interest. Progeny were then scored for rescue of male lethality. Phenotypes varied slightly depending on the specific duplication in question, but in general, in crosses to Dp(1;3) stocks, these rescued males were identified by dark red eye color and round eye, as they lacked the FM7c X balancer chromosome carrying the visible dominant marker Bar (B^1); sibling non-rescued males bearing the FM7c balancer chromosome had light orange/white eyes with the small, narrow phenotype characteristic of the Bar mutation. In crosses to the Dp(1;Y) stocks, rescued males had white, round (non-Bar) eyes. As nondisjunction can become an issue and XXY females can accumulate in X chromosome stocks kept over FM7 over time, and because the Y chromosome is not required for male viability, to confirm rescue, males

with dark eyes presumed to have been rescued by the duplication were crossed back to virgin females from the original stock to again check for the presence of rescued males.

6.17.7 Outcrossing of X chromosome mutant stocks

To generate outcrossed stocks for X screen mutant lines, heterozygous virgin females from the mutant stock (*y, w, ★, FRT19A /FM7c, Kr>GFP*, where ★ indicates the unknown EMS-induced mutation) were crossed to males from the isogenized parent stock (*y, w, FRT19A iso /Y*). Non-balancer females (*y, w, *, FRT19A /y, w, FRT19A iso*) and balancer males (*FM7c, Kr>GFP /Y*) were recovered in the F1 generation, and crosses with a single male/female pair were established to isolate potential recombination events in the F1 females. In the F2 generation, virgin females (*y, w, *,FRT19A /FM7c, Kr>GFP* or *y, w, FRT19A iso /FM7c, Kr>GFP*) were recovered, and as many isolates as possible (minimum of 50) were crossed back to *FM7c, Kr>GFP /Y* males in single male/female crosses, to establish stable stocks. This process was repeated for several generations.

References

Adams, M. D., Celniker, S. E., Holt, R. A., Evans, C. A., Gocayne, J. D., Amanatides, P. G., Scherer, S. E., Li, P. W., Hoskins, R. A., Galle, R. F., George, R. A., Lewis, S. E., Richards, S., Ashburner, M., Henderson, S. N., Sutton, G. G., Wortman, J. R., Yandell, M. D., Zhang, Q., Chen, L. X., Brandon, R. C., Rogers, Y. H., Blazej, R. G., Champe, M., Pfeiffer, B. D., Wan, K. H., Doyle, C., Baxter, E. G., Helt, G., Nelson, C. R., Gabor, G. L., Abril, J. F., Agbayani, A., An, H. J., Andrews-Pfannkoch, C., Baldwin, D., Ballew, R. M., Basu, A., Baxendale, J., Bayraktaroglu, L., Beasley, E. M., Beeson, K. Y., Benos, P. V., Berman, B. P., Bhandari, D., Bolshakov, S., Borkova, D., Botchan, M. R., Bouck, J., Brokstein, P., Brottier, P., Burtis, K. C., Busam, D. A., Butler, H., Cadieu, E., Center, A., Chandra, I., Cherry, J. M., Cawley, S., Dahlke, C., Davenport, L. B., Davies, P., de Pablos, B., Delcher, A., Deng, Z., Mays, A. D., Dew, I., Dietz, S. M., Dodson, K., Doup, L. E., Downes, M., Dugan-Rocha, S., Dunkov, B. C., Dunn, P., Durbin, K. J., Evangelista, C. C., Ferraz, C., Ferriera, S., Fleischmann, W., Fosler, C., Gabrielian, A. E., Garg, N. S., Gelbart, W. M., Glasser, K., Glodek, A., Gong, F., Gorrell, J. H., Gu, Z., Guan, P., Harris, M., Harris, N. L., Harvey, D., Heiman, T. J., Hernandez, J. R., Houck, J., Hostin, D., Houston, K. A., Howland, T. J., Wei, M. H., Ibegwam, C., Jalali, M., Kalush, F., Karpen, G. H., Ke, Z., Kennison, J. A., Ketchum, K. A., Kimmel, B. E., Kodira, C. D., Kraft, C., Kravitz, S., Kulp, D., Lai, Z., Lasko, P., Lei, Y., Levitsky, A. A., Li, J., Li, Z., Liang, Y., Lin, X., Liu, X., Mattei, B., McIntosh, T. C., McLeod, M. P., McPherson, D., Merkulov, G., Milshina, N. V., Mobarry, C., Morris, J., Moshrefi, A., Mount, S. M., Moy, M., Murphy, B., Murphy, L., Muzny, D. M., Nelson, D. L., Nelson, D. R., Nelson, K. A., Nixon, K., Nusskern, D. R., Pacleb, J. M., Palazzolo, M., Pittman, G. S., Pan, S., Pollard, J., Puri, V., Reese, M. G., Reinert, K., Remington, K., Saunders, R. D., Scheeler, F., Shen, H., Shue, B. C., Sidén-Kiamos, I., Simpson, M., Skupski, M. P., Smith, T., Spier, E., Spradling, A. C., Stapleton, M., Strong, R., Sun, E., Svirskas, R., Tector, C., Turner, R., Venter, E., Wang, A. H., Wang, X., Wang, Z. Y., Wassarman, D. A., Weinstock, G. M., Weissenbach, J., Williams, S. M., WoodageT, Worley, K. C., Wu, D., Yang, S., Yao, Q. A., Ye, J., Yeh, R. F., Zaveri, J. S., Zhan, M., Zhang, G., Zhao, Q., Zheng, L., Zheng, X. H., Zhong, F. N., Zhong, W., Zhou, X., Zhu, S., Zhu, X., Smith, H. O., Gibbs, R. A., Myers, E. W., Rubin, G. M., & Venter, J. C. (2000). The genome sequence of *Drosophila melanogaster*. *Science*, *287*(5461), 2185–2195.

Aggarwal, S., Snaidero, N., Pähler, G., Frey, S., Sánchez, P., Zweckstetter, M., Janshoff, A., Schneider, A., Weil, M.-T., Schaap, I. A. T., Görlich, D., & Simons, M. (2013). Myelin membrane assembly is driven by a phase transition of myelin basic proteins into a cohesive protein meshwork. *PLoS biology*, *11*(6), e1001577.

Alexandre, C. (2008). Cuticle preparation of*Drosophila* embryos and larvae. *Methods in Molecular Biology*, *420*, 197–205.

Alexandre, C., Lecourtois, M., & Vincent, J.-P. (1999). Wingless and Hedgehog pattern*Drosophila* denticle belts by regulating the production of short-range signals. *Development (Cambridge, England)*, *126*(24), 5689–5698.

Amann, K. J., & Pollard, T. D. (2001). Direct real-time observation of actin filament branching mediated by Arp2/3 complex using total internal reflection fluorescence microscopy. *Proceedings of the National Academy of Sciences of the USA*, *98*(26), 15009–15013.

Anderson, C. A., Eser, U., Korndorf, T., Borsuk, M. E., Skotheim, J. M., & Gladfelter, A. S. (2013). Nuclear Repulsion Enables Division Autonomy in a Single Cytoplasm. *Current Biology*, *23*(20), 1999–2010.

Andrew, D. J., & Baker, B. S. (2008). Expression of the*Drosophila* secreted cuticle protein 73 (dsc73) requires Shavenbaby. *Developmental dynamics : an official publication of the American Association of Anatomists*, *237*(4), 1198–1206.

Arbeitman, M. N., Furlong, E. E. M., Imam, F., Johnson, E., Null, B. H., Baker, B. S., Krasnow, M. A., Scott, M. P., Davis, R. W., & White, K. P. (2002). Gene expression during the life cycle of *Drosophila melanogaster*. *Science*, *297*(5590), 2270–2275.

Ashburner, M., Golic, K. G., & Hawley, R. S. (2005). *Drosophila: a laboratory handbook. Second edition.*. Cold Spring Harbor Laboratory Press.

Attrill, H., Falls, K., Goodman, J. L., Millburn, G. H., Antonazzo, G., Rey, A. J., Marygold, S. J., & FlyBase Consortium (2016). FlyBase: establishing a Gene Group resource for *Drosophila melanogaster*. *Nucleic Acids Research*, *44*(D1), D786–92.

Atwood, H. L., Govind, C. K., & Wu, C. F. (1993). Differential ultrastructure of synaptic terminals on ventral longitudinal abdominal muscles in*Drosophila* larvae. *Journal of neurobiology*, *24*(8), 1008–1024.

Bartles, J. R., Zheng, L., Li, A., Wierda, A., & Chen, B. (1998). Small espin: a third actin-bundling protein and potential forked protein ortholog in brush border microvilli. *The Journal of Cell Biology*, *143*(1), 107–119.

Bartolini, F., Moseley, J. B., Schmoranzer, J., Cassimeris, L., Goode, B. L., & Gundersen, G. G. (2008). The formin mDia2 stabilizes microtubules independently of its actin nucleation activity. *The Journal of Cell Biology*, *181*(3), 523–536.

Barzik, M., Kotova, T. I., Higgs, H. N., Hazelwood, L., Hanein, D., Gertler, F. B., & Schafer, D. A. (2005). Ena/VASP proteins enhance actin polymerization in the presence of barbed end capping proteins. *The Journal of biological chemistry*, *280*(31), 28653–28662.

Bayat, V., Thiffault, I., Jaiswal, M., Tétreault, M., Donti, T., Sasarman, F., Bernard, G., Demers-Lamarche, J., Dicaire, M.-J., Mathieu, J., Vanasse, M., Bouchard, J.-P., Rioux, M.-F., Lourenco, C. M., Li, Z., Haueter, C., Shoubridge, E. A., Graham, B. H., Brais, B., & Bellen, H. J. (2012). Mutations in the mitochondrial methionyl-tRNA synthetase cause a neurodegenerative phenotype in flies and a recessive ataxia (ARSAL) in humans. *PLoS biology*, *10*(3), e1001288.

Bear, J. E., Svitkina, T. M., Krause, M., Schafer, D. A., Loureiro, J. J., Strasser, G. A., Maly, I. V., Chaga, O. Y., Cooper, J. A., Borisy, G. G., & Gertler, F. B. (2002). Antagonism between Ena/VASP proteins and actin filament capping regulates fibroblast motility. *Cell*, *109*(4), 509–521.

Becker, S., Pasca, G., Strumpf, D., Min, L., & Volk, T. (1997). Reciprocal signaling between*Drosophila* epidermal muscle attachment cells and their corresponding muscles. *Development (Cambridge, England)*, *124*(13), 2615–2622.

Bejsovec, A., & Arias, A. M. (1991). Roles of wingless in patterning the larval epidermis of *Drosophila* . *Development (Cambridge, England)*.

Bejsovec, A., & Chao, A. T. (2012). crinkled reveals a new role for Wingless signaling in*Drosophila* denticle formation. *Development (Cambridge, England)*, *139*(4), 690–698.

Bejsovec, A., & Wieschaus, E. F. (1993). Segment polarity gene interactions modulate epidermal patterning in*Drosophila* embryos. *Development (Cambridge, England)*.

Bellaiche, Y., Gho, M., Kaltschmidt, J. A., Brand, A. H., & Schweisguth, F. (2001a). Frizzled regulates localization of cell-fate determinants and mitotic spindle rotation during asymmetric cell division. *Nature Cell Biology*, *3*(1), 50–57.

Bellaiche, Y., Radovic, A., Woods, D. F., Hough, C. D., Parmentier, M. L., O'Kane, C. J., Bryant, P. J., & Schweisguth, F. (2001b). The Partner of Inscuteable/Discs-large complex is required to establish planar polarity during asymmetric cell division in *Drosophila* . *Cell*, *106*(3), 355–366.

Beningo, K. A., Lillie, S. H., & Brown, S. S. (2000). The yeast kinesin-related protein Smy1p exerts its effects on the class V myosin Myo2p via a physical interaction. *Molecular Biology of the Cell*, *11*(2), 691–702.

Bergeland, T., Widerberg, J., Bakke, O., & Nordeng, T. W. (2001). Mitotic partitioning of endosomes and lysosomes. *Current Biology*, *11*(9), 644–651.

Berger, J., Suzuki, T., Senti, K. A., Stubbs, J. L., Schaffner, G., & Dickson, B. J. (2001). Genetic mapping with SNP markers in *Drosophila* . *Nature Genetics*, *29*(4), 475–481.

Bergstralh, D. T., Haack, T., & Johnston, D. S. (2013a). Epithelial polarity and spindle orientation: intersecting pathways. *Philosophical Transactions of the Royal Society B: Biological Sciences*, *368*(1629), 20130291–20130291.

Bergstralh, D. T., Lovegrove, H. E., Kujawiak, I., Dawney, N. S., Zhu, J., Cooper, S., Zhang, R., & St Johnston, D. (2016). Pins is not required for spindle orientation in the*Drosophila* wing disc. *Development (Cambridge, England)*, *143*(14), 2573–2581.

Bergstralh, D. T., Lovegrove, H. E., & St Johnston, D. (2013b). Discs Large Links Spindle Orientation to Apical-Basal Polarity in*Drosophila* Epithelia. *Current Biology*, *23*(17), 1707–1712.

Bertet, C. C., Sulak, L. L., & Lecuit, T. (2004). Myosin-dependent junction remodelling controls planar cell intercalation and axis elongation. *Nature*, *429*(6992), 667–671.

Bieling, P., Telley, I. A., & Surrey, T. (2010). A minimal midzone protein module controls formation and length of antiparallel microtubule overlaps. *Cell*, *142*(3), 420–432.

Bird, A. W., & Hyman, A. A. (2008). Building a spindle of the correct length in human cells requires the interaction between TPX2 and Aurora A. *The Journal of Cell Biology*, *182*(2), 289–300.

Blankenship, J. T., Backovic, S. T., Sanny, J. S. P., Weitz, O., & Zallen, J. A. (2006). Multicellular Rosette Formation Links Planar Cell Polarity to Tissue Morphogenesis. *Developmental Cell*, *11*(4), 459–470.

Bloomington Stock Center (????). Bloomington*Drosophila* Stock Center.
URL `http://flystocks.bio.indiana.edu/`

Bloor, J. W., & Kiehart, D. P. (2001). *zipper* Nonmuscle Myosin-II Functions Downstream of PS2 Integrin in *Drosophila* Myogenesis and Is Necessary for Myofibril Formation. *Developmental biology*, *239*(2), 215–228.

Blumenstiel, J. P., Noll, A. C., Griffiths, J. A., Perera, A. G., Walton, K. N., Gilliland, W. D., Hawley, R. S., & Staehling-Hampton, K. (2009). Identification of EMS-induced mutations in *Drosophila melanogaster* by whole-genome sequencing. *Genetics*, *182*(1), 25–32.

Bolinger, C., Zasadil, L., Rizaldy, R., & Hildebrand, J. D. (2010). Specific isoforms of drosophila shroom define spatial requirements for the induction of apical constriction. *Developmental dynamics : an official publication of the American Association of Anatomists*, *239*(7), 2078–2093.

Bolte, S., & Cordelieres, F. P. (2006). A guided tour into subcellular colocalization analysis in light microscopy. *Journal of Microscopy*, *224*(3), 213–232.

Bosveld, F., Markova, O., Guirao, B., Martin, C. A., Wang, Z., Pierre, A., Balakireva, M., Gaugue, I., Ainslie, A., Christophorou, N., Lubensky, D. K., Minc, N., & Bellaïche, Y. (2016). Epithelial tricellular junctions act as interphase cell shape sensors to orient mitosis. *Nature*, *530*(7591), 495–498.

Bowman, S. K., Neumüller, R. A., Novatchkova, M., Du, Q., & Knoblich, J. A. (2006). The*Drosophila* NuMA Homolog Mud Regulates Spindle Orientation in Asymmetric Cell Division. *Developmental Cell*, *10*(6), 731–742.

Brangwynne, C. P. (2013). Phase transitions and size scaling of membrane-less organelles. *The Journal of Cell Biology*, *203*(6), 875–881.

Brangwynne, C. P., Eckmann, C. R., Courson, D. S., Rybarska, A., Hoege, C., Gharakhani, J., Jülicher, F., & Hyman, A. A. (2009). Germline P granules are liquid droplets that localize by controlled dissolution/condensation. *Science*, *324*(5935), 1729–1732.

Brangwynne, C. P., Mitchison, T. J., & Hyman, A. A. (2011). Active liquid-like behavior of nucleoli determines their size and shape in *Xenopus laevis* oocytes. *Proceedings of the National Academy of Sciences of the USA*, *108*(11), 4334–4339.

Brantl, S., Birch-Hirschfeld, E., & Behnke, D. (1993). RepR protein expression on plasmid pIP501 is controlled by an antisense RNA-mediated transcription attenuation mechanism. *Journal of Bacteriology*, *175*(13), 4052–4061.

Breitsprecher, D., Kiesewetter, A. K., Linkner, J., Urbanke, C., Resch, G. P., Small, J. V., & Faix, J. (2008). Clustering of VASP actively drives processive, WH2 domain-mediated actin filament elongation. *The EMBO Journal*, *27*(22), 2943–2954.

Brown, K. S., Blower, M. D., Maresca, T. J., Grammer, T. C., Harland, R. M., & Heald, R. (2007). Xenopus tropicalisegg extracts provide insight into scaling of the mitotic spindle. *The Journal of Cell Biology*, *176*(6), 765–770.

Brugués, J., Nuzzo, V., Mazur, E., & Needleman, D. J. (2012). Nucleation and Transport Organize Microtubules in Metaphase Spindles. *Cell*, *149*(3), 554–564.

Bruusgaard, J. C. (2006). Distribution of myonuclei and microtubules in live muscle fibers of young, middle-aged, and old mice. *Journal of Applied Physiology*, *100*(6), 2024–2030.

Bryan, J., Edwards, R., Matsudaira, P., Otto, J., & Wulfkuhle, J. (1993). Fascin, an echinoid actin-bundling protein, is a homolog of the*Drosophila* singed gene product. *Proceedings of the National Academy of Sciences of the USA*, *90*(19), 9115–9119.

Bryant, P. J., Huettner, B., Held, L. I., Ryerse, J., & Szidonya, J. (1988). Mutations at the fat locus interfere with cell proliferation control and epithelial morphogenesis in *Drosophila* . *Developmental biology*, *129*(2), 541–554.

Bulgakova, N. A., Grigoriev, I., Yap, A. S., Akhmanova, A., & Brown, N. H. (2013). Dynamic microtubules produce an asymmetric E-cadherin–Bazooka complex to maintain segment boundaries. *The Journal of Cell Biology*, *201*(6), 887–901.

Burakov, A., Nadezhdina, E., Slepchenko, B., & Rodionov, V. (2003). Centrosome positioning in interphase cells. *The Journal of Cell Biology*, *162*(6), 963–969.

Burbank, K. S., Mitchison, T. J., & Fisher, D. S. (2007). Slide-and-cluster models for spindle assembly. *Current Biology*, *17*(16), 1373–1383.

Cant, K. (1994). Drosophila singed, a fascin homolog, is required for actin bundle formation during oogenesis and bristle extension. *The Journal of Cell Biology*, *125*(2), 369–380.

Carvalho, A., Desai, A., & Oegema, K. (2009). Structural Memory in the Contractile Ring Makes the Duration of Cytokinesis Independent of Cell Size. *Cell*, *137*(5), 926–937.

Cate, M.-S., Gajendra, S., Alsbury, S., Raabe, T., Tear, G., & Mitchell, K. J. (2016). Mushroom body defect is required in parallel to Netrin for midline axon guidance in *Drosophila* . *Development (Cambridge, England)*, *143*(6), 972–977.

Celniker, S. E., & Rubin, G. M. (2003). The *Drosophila melanogaster* genome. *Annual review of genomics and human genetics*, *4*, 89–117.

Chan, Y. H. M., & Marshall, W. F. (2012). How Cells Know the Size of Their Organelles. *Science*, *337*(6099), 1186–1189.

Chanut-Delalande, H., Fernandes, I., Roch, F., Payre, F. F., & Plaza, S. (2006). Shavenbaby Couples Patterning to Epidermal Cell Shape Control. *PLoS biology*, *4*(9), e290.

Chanut-Delalande, H., Ferrer, P., Payre, F. F., & Plaza, S. (2012). Effectors of tridimensional cell morphogenesis and their evolution. *Seminars in Cell & Developmental Biology*, *23*(3), 341–349.

Chen, D., Ahlford, A., Schnorrer, F., Kalchhauser, I., Fellner, M., Viràgh, E., Kiss, I., Syvänen, A.-C., & Dickson, B. J. (2008). High-resolution, high-throughput SNP mapping in *Drosophila melanogaster*. *Nature Methods*, *5*(4), 323–329.

Chesarone, M. A., Dupage, A. G., & Goode, B. L. (2010). Unleashing formins to remodel the actin and microtubule cytoskeletons. *Nature Reviews Molecular Cell Biology*, *11*(1), 62–74.

Chesarone-Cataldo, M., Guérin, C., Yu, J. H., Wedlich-Soldner, R., Blanchoin, L., & Goode, B. L. (2011). The myosin passenger protein Smy1 controls actin cable structure and dynamics by acting as a formin damper. *Developmental Cell*, *21*(2), 217–230.

Chou, T. B., & Perrimon, N. (1992). Use of a yeast site-specific recombinase to produce female germline chimeras in *Drosophila* . *Genetics*, *131*(3), 643–653.

Chou, T. B., & Perrimon, N. (1996). The autosomal FLP-DFS technique for generating germline mosaics in *Drosophila melanogaster*. *Genetics*, *144*(4), 1673–1679.

Clohisey, S. M. R., Dzhindzhev, N. S., & Ohkura, H. (2014). Kank Is an EB1 interacting protein that localises to muscle-tendon attachment sites in *Drosophila* . *PloS one*, *9*(9), e106112–e106112.

Colosimo, P. F., & Tolwinski, N. S. (2006). Wnt, Hedgehog and junctional Armadillo/beta-catenin establish planar polarity in the*Drosophila* embryo. *PloS one*, *1*, e9.

Conduit, P. T., Brunk, K., Dobbelaere, J., Dix, C. I., Lucas, E. P., & Raff, J. W. (2010). Centrioles regulate centrosome size by controlling the rate of Cnn incorporation into the PCM. *Current Biology*, *20*(24), 2178–2186.

Conduit, P. T., & Raff, J. W. (2010). Cnn dynamics drive centrosome size asymmetry to ensure daughter centriole retention in*Drosophila* neuroblasts. *Current Biology*, *20*(24), 2187–2192.

Conklin, E. G. (1912). Cell size and nuclear size. *Journal of Experimental Zoology*, *12*(1), 1–98.

Cook, R. K., Deal, M. E., Deal, J. A., Garton, R. D., Brown, C. A., Ward, M. E., Andrade, R. S., Spana, E. P., Kaufman, T. C., & Cook, K. R. (2010). A new resource for characterizing X-linked genes in *Drosophila melanogaster*: systematic coverage and subdivision of the X chromosome with nested, Y-linked duplications. *Genetics*, *186*(4), 1095–1109.

Cunha-Ferreira, I., Bento, I., & Bettencourt-Dias, M. (2009). From zero to many: control of centriole number in development and disease. *Traffic*, *10*(5), 482–498.

Currie, J. D., Stewman, S. F., Schimizzi, G., Slep, K. C., Ma, A., & Rogers, S. L. (2011). The microtubule lattice and plus-end association of*Drosophila* Mini spindles is spatially regulated to fine-tune microtubule dynamics. *Molecular Biology of the Cell*, *22*(22), 4343–4361.

Dai, X., Schonbaum, C. P., Degenstein, L., Bai, W., Mahowald, A. P., & Fuchs, E. (1998). The ovo gene required for cuticle formation and oogenesis in flies is involved in hair formation and spermatogenesis in mice. *Genes & Development*, *12*(21), 3452–3463.

de Belle, J. S., & Heisenberg, M. (1996). Expression of*Drosophila* mushroom body mutations in alternative genetic backgrounds: a case study of the mushroom body miniature gene (mbm). *Proceedings of the National Academy of Sciences of the USA*, *93*(18), 9875–9880.

Decker, M., Jaensch, S., Pozniakovsky, A., Zinke, A., O'Connell, K. F., Zachariae, W., Myers, E. W., & Hyman, A. A. (2011). Limiting amounts of centrosome material set centrosome size in *C. elegans* embryos. *Current Biology*, *21*(15), 1259–1267.

del Solar, G., & Espinosa, M. (2000). Plasmid copy number control: an ever-growing story. *Molecular Microbiology*, *37*(3), 492–500.

Delon, I., Chanut-Delalande, H., & Payre, F. F. (2003). The Ovo/Shavenbaby transcription factor specifies actin remodelling during epidermal differentiation in *Drosophila* . *Mechanisms of development*, *120*(7), 747–758.

Delon, I., & Payre, F. F. (2004). Evolution of larval morphology in flies: get in shape with shavenbaby. *Trends in genetics*, *20*(7), 305–313.

Denef, N., Chen, Y., Weeks, S. D., Barcelo, G., & Schüpbach, T. (2008). Crag regulates epithelial architecture and polarized deposition of basement membrane proteins in *Drosophila* . *Developmental Cell*, *14*(3), 354–364.

Deng, S., Bothe, I., & Baylies, M. K. (2015). The Formin Diaphanous Regulates Myoblast Fusion through Actin Polymerization and Arp2/3 Regulation. *PLoS genetics*, *11*(8), e1005381.

Denk, W., Strickler, J. H., & Webb, W. W. (1990). Two-photon laser scanning fluorescence microscopy. *Science*, *248*(4951), 73–76.

DeRosier, D. J., & Tilney, L. G. (2000). F-Actin Bundles Are Derivatives of Microvilli: What Does This Tell US about How Bundles Might Form? *148*(1), 1–6.

Dewey, E. B., Sanchez, D., & Johnston, C. A. (2015). Warts phosphorylates mud to promote pins-mediated mitotic spindle orientation in *Drosophila* , independent of Yorkie. *Current Biology*, *25*(21), 2751–2762.

Dickinson, W. J., & Thatcher, J. W. (1997). Morphogenesis of denticles and hairs in*Drosophila* embryos: involvement of actin-associated proteins that also affect adult structures. *Cell motility and the cytoskeleton*, *38*(1), 9–21.

Dickinson, W. J., Yang, Y., Schuske, K., & Akam, M. (1993). Conservation of Molecular Prepatterns during the Evolution of Cuticle Morphology in*Drosophila* Larvae. *Evolution*, *47*(5), 1396.

Dilks, S. A. (2010). *Control of Denticle Diversity in the*Drosophila Embryo*.* Ph.D. thesis, University of Pennsylvania.

Dilks, S. A., & DiNardo, S. (2010). Non-cell-autonomous control of denticle diversity in the*Drosophila* embryo. *Development (Cambridge, England)*, *137*(8), 1395–1404.

DiNardo, S., Heemskerk, J., Dougan, S. T., & O'Farrell, P. H. (1994). The making of a maggot: patterning the*Drosophila* embryonic epidermis. *Current opinion in genetics & development*, *4*(4), 529–534.

DiNardo, S., Sher, E., Heemskerk-Jongens, J., Kassis, J. A., & O'Farrell, P. H. (1988). Two-tiered regulation of spatially patterned engrailed gene expression during*Drosophila* embryogenesis. *Nature*, *332*(6165), 604–609.

Dixit, R., Vijayraghavan, K., & Bate, M. (2008). Hox genes and the regulation of movement in *Drosophila* . *Developmental Neurobiology*, *68*(3), 309–316.

Dogterom, M., Kerssemakers, J. W., Romet-Lemonne, G., & Janson, M. E. (2005). Force generation by dynamic microtubules. *Current opinion in cell biology*, *17*(1), 67–74.

Dogterom, M., & Yurke, B. (1997). Measurement of the force-velocity relation for growing microtubules. *Science*, *278*(5339), 856–860.

Doitsidou, M., Poole, R. J., Sarin, S., Bigelow, H., & Hobert, O. (2010). *C. elegans* Mutant Identification with a One-Step Whole-Genome-Sequencing and SNP Mapping Strategy. *PloS one*, *5*(11), e15435.

Donoughe, S., & DiNardo, S. (2011). dachsous and frizzled contribute separately to planar polarity in the*Drosophila* ventral epidermis. *Development (Cambridge, England)*, *138*(13), 2751–2759.

Dougan, S. T., & DiNardo, S. (1992). Drosophila wingless generates cell type diversity among engrailed expressing cells. *Nature*, *360*(6402), 347–350.

Du, F., Ozdowski, E. F., Kotowski, I. K., Marchuk, D. A., & Sherwood, N. T. (2010). Functional conservation of human Spastin in a*Drosophila* model of autosomal dominant-hereditary spastic paraplegia. *Human Molecular Genetics*, *19*(10), 1883–1896.

Du, Q., Taylor, L., Compton, D. A., & Macara, I. G. (2002). LGN Blocks the Ability of NuMA to Bind and Stabilize Microtubules. *Current Biology*, *12*(22), 1928–1933.

Edens, L. J., White, K. H., Jevtic, P., Li, X., & Levy, D. L. (2013). Nuclear size regulation: from single cells to development and disease. *Trends in Cell Biology*, *23*(4), 151–159.

Eom, D. S., Amarnath, S., & Agarwala, S. (2013). Apicobasal polarity and neural tube closure. *Development, Growth & Differentiation*, *55*(1), 164–172.

Eskin, J. A., Rankova, A., Johnston, A. B., Alioto, S. L., & Goode, B. L. (2016). Common formin-regulating sequences in Smy1 and Bud14 are required for the control of actin cable assembly in vivo. *Molecular Biology of the Cell*, *27*(5), 828–837.

Fant, X., Merdes, A., & Haren, L. (2004). Cell and molecular biology of spindle poles and NuMA. *International review of cytology*, *238*, 1–57.

Feric, M., & Brangwynne, C. P. (2013). A nuclear F-actin scaffold stabilizes ribonucleoprotein droplets against gravity in large cells. *Nature Cell Biology*, *15*(10), 1253–1259.

Fernandes, I., Chanut-Delalande, H., Ferrer, P., Latapie, Y., Waltzer, L., Affolter, M., Payre, F. F., & Plaza, S. (2010). Zona Pellucida Domain Proteins Remodel the Apical Compartment for Localized Cell Shape Changes. *Developmental Cell*, *18*(1), 64–76.

Fernandez-Gonzalez, R., Simoes, S. d. M., Röper, J.-C., Eaton, S., & Zallen, J. A. (2009). Myosin II Dynamics Are Regulated by Tension in Intercalating Cells. *Developmental Cell*, *17*(5), 736–743.

Fernandez-Gonzalez, R., & Zallen, J. A. (2011). Oscillatory behaviors and hierarchical assembly of contractile structures in intercalating cells. *Physical Biology*, *8*(4), 045005.

Finkelstein, R., & Perrimon, N. (1990). The orthodenticle gene is regulated by bicoid and torso and specifies*Drosophila* head development. *Nature*, *346*(6283), 485–488.

Finkelstein, R., Smouse, D., Capaci, T. M., Spradling, A. C., & Perrimon, N. (1990). The orthodenticle gene encodes a novel homeo domain protein involved in the development of the*Drosophila* nervous system and ocellar visual structures. *Genes & Development*, *4*(9), 1516–1527.

FlyBase Consortium (2016). FlyBase.
URL `http://flybase.org/`

Folker, E. S., Schulman, V. K., & Baylies, M. K. (2014). Translocating myonuclei have distinct leading and lagging edges that require kinesin and dynein. *Development (Cambridge, England)*, *141*(2), 355–366.

Follain, G., Mercier, L., Osmani, N., Harlepp, S., & Goetz, J. G. (2016). Seeing is believing: multi-scale spatio-temporal imaging towards in vivo cell biology. *Journal of Cell Science*, (p. jcs.189001).

Fortini, M. E., Skupski, M. P., Boguski, M. S., & Hariharan, I. K. (2000). A survey of human disease gene counterparts in the*Drosophila* genome. *The Journal of Cell Biology*, *150*(2), F23–30.

Frankel, N., Erezyilmaz, D. F., McGregor, A. P., Wang, S., Payre, F. F., & Stern, D. L. (2011). Morphological evolution caused by many subtle-effect substitutions in regulatory DNA. *Nature*, *474*(7353), 598–603.

Füger, P., Behrends, L. B., Mertel, S., Sigrist, S. J., & Rasse, T. M. (2007). Live imaging of synapse development and measuring protein dynamics using two-color fluorescence recovery after photo-bleaching at*Drosophila* synapses. *Nature Protocols*, *2*(12), 3285–3298.

Gawad, C., Koh, W., & Quake, S. R. (2016). Single-cell genome sequencing: current state of the science. *Nature reviews Genetics*, *17*(3), 175–188.

Gertler, F. B., Doctor, J. S., & Hoffmann, F. M. (1990). Genetic suppression of mutations in the*Drosophila* abl proto-oncogene homolog. *Science*, *248*(4957), 857–860.

Goehring, N. W., & Hyman, A. A. (2012). Organelle growth control through limiting pools of cytoplasmic components. *Current Biology*, *22*(9), R330–9.

Golembo, M., Raz, E., & Shilo, B. Z. (1996). The*Drosophila* embryonic midline is the site of Spitz processing, and induces activation of the EGF receptor in the ventral ectoderm. *Development (Cambridge, England)*, *122*(11), 3363–3370.

Goley, E. D., & Welch, M. D. (2006). The ARP2/3 complex: an actin nucleator comes of age. *Nature Reviews Molecular Cell Biology*, *7*(10), 713–726.

Golic, K. G., & Lindquist, S. (1989). The FLP recombinase of yeast catalyzes site-specific recombination in the*Drosophila* genome. *Cell*, *59*(3), 499–509.

Gönczy, P., Pichler, S., Kirkham, M., & Hyman, A. A. (1999). Cytoplasmic dynein is required for distinct aspects of MTOC positioning, including centrosome separation, in the one cell stage *Caenorhabditis elegans* embryo. *The Journal of Cell Biology*, *147*(1), 135–150.

Good, M. C., Vahey, M. D., Skandarajah, A., Fletcher, D. A., & Heald, R. (2013). Cytoplasmic volume modulates spindle size during embryogenesis. *Science*, *342*(6160), 856–860.

Goode, B. L., & Eck, M. J. (2007). Mechanism and function of formins in the control of actin assembly. *Annual review of biochemistry*, *76*(1), 593–627.

Goodwin, S. S., & Vale, R. D. (2010). Patronin Regulates the Microtubule Network by Protecting Microtubule Minus Ends. *Cell*, *143*(2), 263–274.

Goshima, G., & Scholey, J. M. (2010). Control of Mitotic Spindle Length. *Annual review of cell and developmental biology*, *26*(1), 21–57.

Greenan, G., Brangwynne, C. P., Jaensch, S., Gharakhani, J., Jülicher, F., & Hyman, A. A. (2010). Centrosome Size Sets Mitotic Spindle Length in *Caenorhabditis elegans* Embryos. *Current Biology*, *20*(4), 353–358.

Greenspan, R. J. (2004). *Fly Pushing*. The Theory and Practice of*Drosophila* Genetics. Cold Spring Harbor, New York: Cold Sprint Harbor Laboratory Press.

Gregory, S. L., & Brown, N. H. (1998). kakapo, a Gene Required for Adhesion Between and Within Cell Layers in *Drosophila* , Encodes a Large Cytoskeletal Linker Protein Related to Plectin and Dystrophin. *The Journal of Cell Biology*, *143*(5), 1271–1282.

Grill, S. W., & Hyman, A. A. (2005). Spindle Positioning by Cortical Pulling Forces. *Developmental Cell*, *8*(4), 461–465.

Gritzan, U., Hatini, V., & DiNardo, S. (1999). Mutual antagonism between signals secreted by adjacent wingless and engrailed cells leads to specification of complementary regions of the*Drosophila* parasegment. *Development (Cambridge, England)*, *126*(18), 4107–4115.

Grueber, W. B., & Sagasti, A. (2010). Self-avoidance and tiling: Mechanisms of dendrite and axon spacing. *Cold Spring Harbor Perspectives in Biology*, *2*(9), a001750–a001750.

Guan, Z., Prado, A., Melzig, J., Heisenberg, M., Nash, H. A., & Raabe, T. (2000). Mushroom body defect, a gene involved in the control of neuroblast proliferation in *Drosophila* , encodes a coiled-coil protein. *Proceedings of the National Academy of Sciences of the USA*, *97*(14), 8122–8127.

Gubb, D., & García-Bellido, A. (1982). A genetic analysis of the determination of cuticular polarity during development in *Drosophila melanogaster*. *Journal of embryology and experimental morphology*, *68*, 37–57.

Guild, G. M. (2005). Actin Filament Bundles in*Drosophila* Wing Hairs: Hairs and Bristles Use Different Strategies for Assembly. *Molecular Biology of the Cell*, *16*(8), 3620–3631.

Gundersen, G. G., & Worman, H. J. (2013). Nuclear positioning. *Cell*, *152*(6), 1376–1389.

Gupta, M. L., Carvalho, P., Roof, D. M., & Pellman, D. (2006). Plus end-specific depolymerase activity of Kip3, a kinesin-8 protein, explains its role in positioning the yeast mitotic spindle. *Nature Cell Biology*, *8*(9), 913–923.

Gupton, S. L., & Gertler, F. B. (2007). Filopodia: the fingers that do the walking. *Science's STKE : signal transduction knowledge environment*, *2007*(400), re5–re5.

Gurtner, G. C., Werner, S., Barrandon, Y., & Longaker, M. T. (2008). Wound repair and regeneration. *Nature*, *453*(7193), 314–321.

Haelterman, N. A., Jiang, L., Li, Y., Bayat, V., Sandoval, H., Ugur, B., Tan, K. L., Zhang, K., Bei, D., Xiong, B., Charng, W.-L., Busby, T., Jawaid, A., David, G., Jaiswal, M., Venken, K. J. T., Yamamoto, S., Chen, R., & Bellen, H. J. (2014). Large-scale identification of chemically induced mutations in *Drosophila melanogaster*. *Genome Research*, *24*(10), 1707–1718.

Haigo, S. L., Hildebrand, J. D., Harland, R. M., & Wallingford, J. B. (2003). Shroom Induces Apical Constriction and Is Required for Hingepoint Formation during Neural Tube Closure. *Current Biology*, *13*(24), 2125–2137.

Hamaguchi, M. S., & Hiramoto, Y. (1986). Analysis of the Role of Astral Rays in Pronuclear Migration in Sand Dollar Eggs by the Colcemid-UV Method. *Development, Growth & Differentiation*, *28*(2), 143–156.

Hammonds, A. S., Bristow, C. A., Fisher, W. W., Weiszmann, R., Wu, S., Hartenstein, V., Kellis, M., Yu, B., Frise, E., & Celniker, S. E. (2013). Spatial expression of transcription factors in*Drosophila* embryonic organ development. - PubMed - NCBI. *Genome Biology*, *14*(12), R140.

Hanahan, D., & Weinberg, R. A. (2011). Hallmarks of cancer: the next generation. *Cell*, *144*(5), 646–674.

Hara, Y., & Kimura, A. (2009). Cell-Size-Dependent Spindle Elongation in the *Caenorhabditis elegans* Early Embryo. *Current Biology*, *19*(18), 1549–1554.

Hara, Y., & Merten, C. A. (2015). Dynein-Based Accumulation of Membranes Regulates Nuclear Expansion in *Xenopus laevis* Egg Extracts. *Developmental Cell*, *33*(5), 562–575.

Haren, L., & Merdes, A. (2002). Direct binding of NuMA to tubulin is mediated by a novel sequence motif in the tail domain that bundles and stabilizes microtubules. *Journal of Cell Science*, *115*(Pt 9), 1815–1824.

Hatini, V., & DiNardo, S. (2001a). Distinct Signals Generate Repeating Striped Pattern in the Embryonic Parasegment. *Molecular Cell*, *7*(1), 151–160.

Hatini, V., & DiNardo, S. (2001b). Divide and conquer: pattern formation in the *Drosophila* embryonic epidermis. *Trends in genetics*, *17*(10), 574–579.

Hazel, J., Krutkramelis, K., Mooney, P., Tomschik, M., Gerow, K., Oakey, J., & Gatlin, J. C. (2013). Changes in cytoplasmic volume are sufficient to drive spindle scaling. *Science*, *342*(6160), 853–856.

He, B., & Adler, P. N. (2002). The genetic control of arista lateral morphogenesis in *Drosophila* . *Development genes and evolution*, *212*(5), 218–229.

Heck, M. M., Pereira, A., Pesavento, P., Yannoni, Y., Spradling, A. C., & Goldstein, L. S. B. (1993). The kinesin-like protein KLP61F is essential for mitosis in *Drosophila* . *The Journal of Cell Biology*, *123*(3), 665–679.

Heemskerk, J., & DiNardo, S. (1994). Drosophila hedgehog acts as a morphogen in cellular patterning. *Cell*, *76*(3), 449–460.

Heemskerk, J., DiNardo, S., Kostriken, R., & O'Farrell, P. H. (1991). Multiple modes of engrailed regulation in the progression towards cell fate determination. *Nature*, *352*(6334), 404–410.

Herman, B., & Albertini, D. F. (1984). A time-lapse video image intensification analysis of cytoplasmic organelle movements during endosome translocation. *The Journal of Cell Biology*, *98*(2), 565–576.

Hidalgo, A., & Ingham, P. (1990). Cell patterning in the*Drosophila* segment: spatial regulation of the segment polarity gene patched. *Development (Cambridge, England)*, *110*(1), 291–301.

Higgs, H. N., Blanchoin, L., & Pollard, T. D. (1999). Influence of the C terminus of Wiskott-Aldrich syndrome protein (WASp) and the Arp2/3 complex on actin polymerization. *Biochemistry*, *38*(46), 15212–15222.

Hildebrand, J. D. (2005). Shroom regulates epithelial cell shape via the apical positioning of an actomyosin network. *Journal of Cell Science*, *118*(22), 5191–5203.

Hildebrand, J. D., & Soriano, P. (1999). Shroom, a PDZ Domain–Containing Actin-Binding Protein, Is Required for Neural Tube Morphogenesis in Mice. *Cell*, *99*(5), 485–497.

Hillman, R., & Lesnik, L. H. (1970). Cuticle formation in the embryo of*Drosophila melanogaster*. *Journal of Morphology*, *131*(4), 383–395.

Hilton, L. K., Gunawardane, K., Kim, J. W., Schwarz, M. C., & Quarmby, L. M. (2013). The kinases LF4 and CNK2 control ciliary length by feedback regulation of assembly and disassembly rates. *Current Biology*, *23*(22), 2208–2214.

Hobert, O. (2010). The impact of whole genome sequencing on model system genetics: get ready for the ride. *Genetics*, *184*(2), 317–319.

Höckendorf, B., Thumberger, T., & Wittbrodt, J. (2012). Quantitative Analysis of Embryogenesis: A Perspective for Light Sheet Microscopy. *Developmental Cell*, *23*(6), 1111–1120.

Hodges, A. R., Bookwalter, C. S., Krementsova, E. B., & Trybus, K. M. (2009). A nonprocessive class V myosin drives cargo processively when a kinesin- related protein is a passenger. *Current Biology*, *19*(24), 2121–2125.

Hough, L. E., Schwabe, A., Glaser, M. A., McIntosh, J. R., & Betterton, M. D. (2009). Microtubule depolymerization by the Kinesin-8 motor Kip3p: a mathematical model. *Biophysical journal*, *96*(8), 3050–3064.

Huisken, J., Swoger, J., Del Bene, F., Wittbrodt, J., & Stelzer, E. H. K. (2004). Optical sectioning deep inside live embryos by selective plane illumination microscopy. *Science*, *305*(5686), 1007–1009.

Iruela-Arispe, M. L., & Beitel, G. J. (2013). Tubulogenesis. *Development (Cambridge, England)*, *140*(14), 2851–2855.

Irvine, K. D., & Wieschaus, E. F. (1994). Cell intercalation during*Drosophila* germband extension and its regulation by pair-rule segmentation genes. *Development (Cambridge, England)*, *120*(4), 827–841.

Ishikawa, H., & Marshall, W. F. (2011). Ciliogenesis: building the cell's antenna. *Nature Reviews Molecular Cell Biology*, *12*(4), 222–234.

Ishikawa, H., & Marshall, W. F. (2014). Mechanobiology of Ciliogenesis. *Bioscience*, *64*(12), 1084–1091.

Izumi, Y., Ohta, N., Hisata, K., Raabe, T., & Matsuzaki, F. (2006). Drosophila Pins-binding protein Mud regulates spindle-polarity coupling and centrosome organization. *Nature Cell Biology*, *8*(6), 586–593.

Jankovics, F., & Brunner, D. (2006). Transiently Reorganized Microtubules Are Essential for Zippering during Dorsal Closure in *Drosophila melanogaster*. *Developmental Cell*, *11*(3), 375–385.

Jevtic, P., Edens, L. J., Li, X., Nguyen, T., Chen, P., & Levy, D. L. (2015). Concentration-Dependent Effects of Nuclear Lamins on Nuclear Size in *Xenopus* and Mammalian Cells. *The Journal of biological chemistry*, (p. jbc.M115.673798).

Johnston, C. A., Hirono, K., Prehoda, K. E., & Doe, C. Q. (2009). Identification of an Aurora-A/PinsLINKER/Dlg Spindle Orientation Pathway using Induced Cell Polarity in S2 Cells. *Cell*, *138*(6), 1150–1163.

Johnston, C. A., Manning, L., Lu, M. S., Golub, O., Doe, C. Q., & Prehoda, K. E. (2013). Formin-mediated actin polymerization cooperates with Mushroom body defect (Mud)-Dynein during Frizzled-Dishevelled spindle orientation. *Journal of Cell Science*, *126*(19), 4436–4444.

Jürgens, G., Wieschaus, E. F., Nüsslein-Volhard, C., & Kluding, H. (1984). *Mutations affecting the pattern of the larval cuticle in Drosophila melanogaster*. II. Zygotic loci on the third chromosome. Zygotic loci on the third . . . .

Kaltschmidt, J. A., Davidson, C. M., Brown, N. H., & Brand, A. H. (2000). Rotation and asymmetry of the mitotic spindle direct asymmetric cell division in the developing central nervous system. *Nature Cell Biology*, *2*(1), 7–12.

Kammermeier, L., Schmied, J., Stierwald, M., Burgunder, J.-M., & Reichert, H. (2003). Identification of the *Drosophila melanogaster* homolog of the human spastin gene. *Development genes and evolution*, *213*(8), 412–415.

Kapitein, L. C., Peterman, E. J. G., Kwok, B. H., Kim, J. H., Kapoor, T. M., & Schmidt, C. F. (2005). The bipolar mitotic kinesin Eg5 moves on both microtubules that it crosslinks. *Nature*, *435*(7038), 114–118.

Karsenti, E., & Vernos, I. (2001). The mitotic spindle: a self-made machine. *Science*, *294*(5542), 543–547.

Kasza, K. E., Farrell, D. L., & Zallen, J. A. (2014). Spatiotemporal control of epithelial remodeling by regulated myosin phosphorylation. *Proceedings of the National Academy of Sciences of the USA*, *111*(32), 11732–11737.

Kato, M., Han, T. W., Xie, S., Shi, K., Du, X., Wu, L. C., Mirzaei, H., Goldsmith, E. J., Longgood, J., Pei, J., Grishin, N. V., Frantz, D. E., Schneider, J. W., Chen, S., Li, L., Sawaya, M. R., Eisenberg, D., Tycko, R., & McKnight, S. L. (2012). Cell-free Formation of RNA Granules: Low Complexity Sequence Domains Form Dynamic Fibers within Hydrogels. *Cell*, *149*(4), 753–767.

Katsura, I. (1987). Determination of bacteriophage lambda tail length by a protein ruler. *Nature*, *327*(6117), 73–75.

Kawasaki, F., Zou, B., Xu, X., & Ordway, R. W. (2004). Active zone localization of presynaptic calcium channels encoded by the cacophony locus of *Drosophila* . *The Journal of neuroscience : the official journal of the Society for Neuroscience*, *24*(1), 282–285.

Kiehart, D. P. (2004). Drosophila crinkled, Mutations of Which Disrupt Morphogenesis and Cause Lethality, Encodes Fly Myosin VIIA. *Genetics*, *168*(3), 1337–1352.

Kimura, A., & Onami, S. (2005). Computer Simulations and Image Processing Reveal Length-Dependent Pulling Force as the Primary Mechanism for *C. elegans* Male Pronuclear Migration. *Developmental Cell*, *8*(5), 765–775.

Kimura, K., & Kimura, A. (2011a). A novel mechanism of microtubule length-dependent force to pull centrosomes toward the cell center. *Bioarchitecture*, *1*(2), 74–79.

Kimura, K., & Kimura, A. (2011b). Intracellular organelles mediate cytoplasmic pulling force for centrosome centration in the *Caenorhabditis elegans* early embryo. *Proceedings of the National Academy of Sciences of the USA*, *108*(1), 137–142.

Kinoshita, K., Habermann, B., & Hyman, A. A. (2002). XMAP215: a key component of the dynamic microtubule cytoskeleton. *Trends in Cell Biology*, *12*(6), 267–273.

Knowles, T. P. J., White, D. A., Abate, A. R., Agresti, J. J., Cohen, S. I. A., Sperling, R. A., De Genst, E. J., Dobson, C. M., & Weitz, D. A. (2011). Observation of spatial propagation of amyloid assembly from single nuclei. *Proceedings of the National Academy of Sciences of the USA*, *108*(36), 14746–14751.

Kollman, J. M., Merdes, A., Mourey, L., & Agard, D. A. (2011). Microtubule nucleation by γ-tubulin complexes. *Nature Reviews Molecular Cell Biology*, *12*(11), 709–721.

Kotak, S., & Gönczy, P. (2013). Mechanisms of spindle positioning: cortical force generators in the limelight. *Current opinion in cell biology*, *25*(6), 741–748.

Kraut, R., Chia, W., Jan, L. Y., Jan, Y. N., & Knoblich, J. A. (1996). Role of inscuteable in orienting asymmetric cell divisions in *Drosophila* . *Nature*, *383*(6595), 50–55.

Kühn, S., & Geyer, M. (2014). Formins as effector proteins of Rho GTPases. *Small GTPases*, *5*(3), e29513.

Lawlor, K. T., Ly, D. C., & DiNardo, S. (2013). Drosophila Dachsous and Fat polarize actin-based protrusions over a restricted domain of the embryonic denticle field. *Developmental biology*, *383*(2), 285–294.

Lawrence, P. A., Casal, J., & Struhl, G. (1999). hedgehog and engrailed: pattern formation and polarity in the*Drosophila* abdomen. *Development (Cambridge, England)*, *126*(11), 2431–2439.

Lécuyer, E., Yoshida, H., Parthasarathy, N., Alm, C., Babak, T., Cerovina, T., Hughes, T. R., Tomancak, P., & Krause, H. M. (2007). Global Analysis of mRNA Localization Reveals a Prominent Role in Organizing Cellular Architecture and Function. *Cell*, *131*(1), 174–187.

Lee, C. F., Brangwynne, C. P., Gharakhani, J., Hyman, A. A., & Jülicher, F. (2013). Spatial Organization of the Cell Cytoplasm by Position-Dependent Phase Separation. *Physical review letters*, *111*(8), 088101.

Lee, H., & Adler, P. N. (2002). The function of the frizzled pathway in the*Drosophila* wing is dependent on inturned and fuzzy. *Genetics*, *160*(4), 1535–1547.

Lee, J. R., Urban, S., Garvey, C. F., & Freeman, M. (2001). Regulated intracellular ligand transport and proteolysis control EGF signal activation in *Drosophila* . *Cell*, *107*(2), 161–171.

Lee, S., Harris, K. L., Whitington, P. M., & Kolodziej, P. A. (2000). short stop is allelic to kakapo, and encodes rod-like cytoskeletal-associated proteins required for axon extension. *The Journal of neuroscience : the official journal of the Society for Neuroscience*, *20*(3), 1096–1108.

Lee, S., & Kolodziej, P. A. (2002). Short Stop provides an essential link between F-actin and microtubules during axon extension. *Development (Cambridge, England)*, *129*(5), 1195–1204.

Lerner, D. W., McCoy, D., Isabella, A. J., Mahowald, A. P., Gerlach, G. F., Chaudhry, T. A., & Horne-Badovinac, S. (2013). A Rab10-Dependent Mechanism for Polarized Basement Membrane Secretion during Organ Morphogenesis. *Developmental Cell*, *24*(2), 159–168.

Lesch, C., Jo, J., Wu, Y., Fish, G. S., & Galko, M. J. (2010). A targeted UAS-RNAi screen in*Drosophila* larvae identifies wound closure genes regulating distinct cellular processes. *Genetics*, *186*(3), 943–957.

Levivier, E., Goud, B., Souchet, M., Calmels, T. P. G., Mornon, J.-P., & Callebaut, I. (2001). uDENN, DENN, and dDENN: Indissociable Domains in Rab and MAP Kinases Signaling Pathways. *Biochemical and biophysical research communications*, *287*(3), 688–695.

Levy, D. L., & Heald, R. (2016). Biological Scaling Problems and Solutions in Amphibians. *Cold Spring Harbor Perspectives in Biology*, *8*(1), a019166.

Lewis, E. B., & Bacher, F. (1968). *Method of feeding ethyl methane sulfonate (EMS) to*Drosophila *males*. Dros. Inf. Serv.

Li, P., Banjade, S., Cheng, H.-C., Kim, S., Chen, B., Guo, L., Llaguno, M., Hollingsworth, J. V., King, D. S., Banani, S. F., Russo, P. S., Jiang, Q.-X., Nixon, B. T., & Rosen, M. K. (2012). Phase transitions in the assembly of multivalent signalling proteins. *Nature*, *483*(7389), 336–340.

Lillie, S. H., & Brown, S. S. (1992). Suppression of a myosin defect by a kinesin-related gene. *Nature*, *356*(6367), 358–361.

Lillie, S. H., & Brown, S. S. (1994). Immunofluorescence localization of the unconventional myosin, Myo2p, and the putative kinesin-related protein, Smy1p, to the same regions of polarized growth in Saccharomyces cerevisiae. *The Journal of Cell Biology*, *125*(4), 825–842.

Lillie, S. H., & Brown, S. S. (1998). Smy1p, a kinesin-related protein that does not require microtubules. *The Journal of Cell Biology*, *140*(4), 873–883.

Lin, C., Schuster, M., Guimaraes, S. C., Ashwin, P., Schrader, M., Metz, J., Hacker, C., Gurr, S. J., & Steinberg, G. (2016). Active diffusion and microtubule-based transport oppose myosin forces to position organelles in cells. *Nature Communications*, *7*, 11814–11814.

Lindsley, D. L., & Zimm, G. G. (1992). *The genome of* Drosophila *melanogaster*. San Diego: San Diego : Academic Press.

Lohs-Schardin, M., Cremer, C., & Nüsslein-Volhard, C. (1979). A fate map for the larval epidermis of*Drosophila melanogaster*: localized cuticle defects following irradiation of the blastoderm with an ultraviolet laser microbeam. *Developmental biology*, *73*(2), 239–255.

Lu, Q., & Adler, P. N. (2015). The diaphanous gene of*Drosophila* interacts antagonistically with multiple wing hairs and plays a key role in wing hair morphogenesis. *PloS one*, *10*(3), e0115623–e0115623.

Lu, Q., Schafer, D. A., & Adler, P. N. (2015). The*Drosophila* planar polarity gene multiple wing hairs directly regulates the actin cytoskeleton. *Development (Cambridge, England)*, *142*(14), 2478–2486.

Lu, Q., Yan, J., & Adler, P. N. (2010). The*Drosophila* Planar Polarity Proteins Inturned and Multiple Wing Hairs Interact Physically and Function Together. *Genetics*, *185*(2), 549–558.

Lubarsky, B., & Krasnow, M. A. (2003). Tube morphogenesis: making and shaping biological tubes. *Cell*, *112*(1), 19–28.

Lucocq, J. M., & Warren, G. (1987). Fragmentation and partitioning of the Golgi apparatus during mitosis in HeLa cells. *The EMBO Journal*, *6*(11), 3239–3246.

Machesky, L. M., & Insall, R. H. (1998). Scar1 and the related Wiskott-Aldrich syndrome protein, WASP, regulate the actin cytoskeleton through the Arp2/3 complex. *Current Biology*, *8*(25), 1347–1356.

Marcinkevicius, E., & Zallen, J. A. (2013). Regulation of cytoskeletal organization and junctional remodeling by the atypical cadherin Fat. *Development (Cambridge, England)*, *140*(2), 433–443.

Marshall, W. F. (2015a). How Cells Measure Length on Subcellular Scales. *Trends in Cell Biology*, *25*(12), 760–768.

Marshall, W. F. (2015b). Subcellular size. *Cold Spring Harbor Perspectives in Biology*, *7*(6), –.

Marshall, W. F. (2016). Cell Geometry: How Cells Count and Measure Size. *Annual Review of Biophysics*, *45*, 49–64.

Marshall, W. F., & Rosenbaum, J. L. (2001). Intraflagellar transport balances continuous turnover of outer doublet microtubules: implications for flagellar length control. *The Journal of Cell Biology*, *155*(3), 405–414.

Martin, P. P., & Parkhurst, S. M. (2004). Parallels between tissue repair and embryo morphogenesis. *Development (Cambridge, England)*, *131*(13), 3021–3034.

Martin, S. G., Dobi, K. C., & St Johnston, D. (2001). A rapid method to map mutations in *Drosophila* . *Genome Biology*, *2*(9), RESEARCH0036.

Martínez-Arias, A., Baker, N. E., & Ingham, P. W. (1988). Role of segment polarity genes in the definition and maintenance of cell states in the*Drosophila* embryo. *Development (Cambridge, England)*, *103*(1), 157–170.

Mauser, J. F., & Prehoda, K. E. (2012). Inscuteable Regulates the Pins-Mud Spindle Orientation Pathway. *PloS one*, *7*(1), e29611.

McGregor, A. P., Orgogozo, V., Delon, I., Zanet, J., Srinivasan, D. G., Payre, F. F., & Stern, D. L. (2007). Morphological evolution through multiple cis-regulatory mutations at a single gene. *Nature*, *448*(7153), 587–590.

McNally, F. J. (2013). Mechanisms of spindle positioning. *The Journal of Cell Biology*, *200*(2), 131–140.

Merdes, A., Ramyar, K., Vechio, J. D., & Cleveland, D. W. (1996). A complex of NuMA and cytoplasmic dynein is essential for mitotic spindle assembly. *Cell*, *87*(3), 447–458.

Metzger, R. J., Klein, O. D., Martin, G. R., & Krasnow, M. A. (2008). The branching programme of mouse lung development. *Nature*, *453*(7196), 745–750.

Metzger, T., Gache, V., Xu, M., Cadot, B., Folker, E. S., Richardson, B. E., Gomes, E. R., & Baylies, M. K. (2012). MAP and kinesin-dependent nuclear positioning is required for skeletal muscle function. *Nature*, *484*(7392), 120–124.

Metzker, M. L. (2010). Sequencing technologies - the next generation. *Nature reviews Genetics*, *11*(1), 31–46.

Mével-Ninio, M., Terracol, R., & Kafatos, F. C. (1991). The ovo gene of*Drosophila* encodes a zinc finger protein required for female germ line development. *The EMBO Journal*, *10*(8), 2259–2266.

Minc, N., Burgess, D. R., & Chang, F. (2011). Influence of Cell Geometry on Division-Plane Positioning. *Cell*, *144*(3), 414–426.

Minevich, G., Park, D. S., Blankenberg, D., Poole, R. J., & Hobert, O. (2012). CloudMap: A Cloud-Based Pipeline for Analysis of Mutant Genome Sequences. *Genetics*, *192*(4), 1249–1269.

Mitchison, T. J., Maddox, P. S., Gaetz, J., Groen, A. C., Shirasu, M., Desai, A., Salmon, E. D., & Kapoor, T. M. (2005). Roles of polymerization dynamics, opposed motors, and a tensile element in governing the length of *Xenopus* extract meiotic spindles. *Molecular Biology of the Cell*, *16*(6), 3064–3076.

Miyamoto, D. T., Perlman, Z. E., Burbank, K. S., Groen, A. C., & Mitchison, T. J. (2004). The kinesin Eg5 drives poleward microtubule flux in *Xenopus laevis* egg extract spindles. *The Journal of Cell Biology*, *167*(5), 813–818.

modENCODE Consortium, Roy, S., Ernst, J., Kharchenko, P. V., Kheradpour, P., Negre, N., Eaton, M. L., Landolin, J. M., Bristow, C. A., Ma, L., Lin, M. F., Washietl, S., Arshinoff, B. I., Ay, F., Meyer, P. E., Robine, N., Washington, N. L., Di Stefano, L., Berezikov, E., Brown, C. D., Candeias, R., Carlson, J. W., Carr, A., Jungreis, I., Marbach, D., Sealfon, R., Tolstorukov, M. Y., Will, S., Alekseyenko, A. A., Artieri, C., Booth, B. W., Brooks, A. N., Dai, Q., Davis, C. A., Duff, M. O., Feng, X., Gorchakov, A. A., Gu, T., Henikoff, J. G., Kapranov, P., Li, R., MacAlpine, H. K., Malone, J., Minoda, A., Nordman, J., Okamura, K., Perry, M., Powell, S. K., Riddle, N. C., Sakai, A., Samsonova, A., Sandler, J. E., Schwartz, Y. B., Sher, N., Spokony, R. R., Sturgill, D., van Baren, M., Wan, K. H., Yang, L., Yu, C., Feingold, E., Good, P., Guyer, M., Lowdon, R., Ahmad, K., Andrews, J., Berger, B., Brenner, S. E., Brent, M. R., Cherbas, L., Elgin, S. C. R., Gingeras, T. R., Grossman, R., Hoskins, R. A., Kaufman, T. C., Kent, W., Kuroda, M. I., Orr-Weaver, T., Perrimon, N., Pirrotta, V., Posakony, J. W., Ren, B., Russell, S., Cherbas, P., Graveley, B. R., Lewis, S., Micklem, G., Oliver, B., Park, P. J., Celniker, S. E., Henikoff, S., Karpen, G. H., Lai, E. C., MacAlpine, D. M., Stein, L. D., White, K. P., & Kellis, M. (2010). Identification of functional elements and regulatory circuits by*Drosophila* modENCODE. *Science*, *330*(6012), 1787–1797.

Mogensen, M. M., Tucker, J. B., Mackie, J. B., Prescott, A. R., & Näthke, I. S. (2002). The adenomatous polyposis coli protein unambiguously localizes to microtubule plus ends and is involved in establishing parallel arrays of microtubule bundles in highly polarized epithelial cells. *The Journal of Cell Biology*, *157*(6), 1041–1048.

Mohan, S., Rizaldy, R., Das, D., Bauer, R. J., Heroux, A., Trakselis, M. A., Hildebrand, J. D., & VanDemark, A. P. (2012). Structure of Shroom domain 2 reveals a three-segmented coiled-coil required for dimerization, Rock binding, and apical constriction. *Molecular Biology of the Cell*, *23*(11), 2131–2142.

Mohapatra, L., Goode, B. L., & Kondev, J. (2015). Antenna Mechanism of Length Control of Actin Cables. *PLoS computational biology*, *11*(6), e1004160.

Morin, X., & Bellaïche, Y. (2011). Mitotic spindle orientation in asymmetric and symmetric cell divisions during animal development. *Developmental Cell*, *21*(1), 102–119.

Moussian, B. B. (2010). Recent advances in understanding mechanisms of insect cuticle differentiation. *Insect biochemistry and molecular biology*, *40*(5), 363–375.

Moussian, B. B., Seifarth, C., Müller, U., Berger, J., & Schwarz, H. (2006). Cuticle differentiation during*Drosophila* embryogenesis. *Arthropod Structure & Development*, *35*(3), 137–152.

Mukherji, S., & O'Shea, E. K. (2014). Mechanisms of organelle biogenesis govern stochastic fluctuations in organelle abundance. *eLife*, *3*, e02678–e02678.

Muller, H. J. (1918). Genetic Variability, Twin Hybrids and Constant Hybrids, in a Case of Balanced Lethal Factors. *Genetics*, *3*(5), 422–499.

Mullins, R. D., Heuser, J. A., & Pollard, T. D. (1998). The interaction of Arp2/3 complex with actin: nucleation, high affinity pointed end capping, and formation of branching networks of filaments. *Proceedings of the National Academy of Sciences of the USA*, *95*(11), 6181–6186.

Näthke, I. (2004). APC at a glance. *Journal of Cell Science*, *117*(21), 4873–4875.

Neely, G. G., Hess, A., Costigan, M., Keene, A. C., Goulas, S., Langeslag, M., Griffin, R. S., Belfer, I., Dai, F., Smith, S. B., Diatchenko, L., Gupta, V., Xia, C.-P., Amann, S., Kreitz, S., Heindl-Erdmann, C., Wolz, S., Ly, C. V., Arora, S., Sarangi, R., Dan, D., Novatchkova, M., Rosenzweig, M., Gibson, D. G., Truong, D., Schramek, D., Zoranovic, T., Cronin, S. J. F., Angjeli, B., Brune, K., Dietzl, G., Maixner, W., Meixner, A., Thomas, W., Pospisilik, J. A., Alenius, M., Kress, M., Subramaniam, S., Garrity, P. A., Bellen, H. J., Woolf, C. J., & Penninger, J. M. (2010). A genome-wide*Drosophila* screen for heat nociception identifies $\alpha 2\delta 3$ as an evolutionarily conserved pain gene. *Cell*, *143*(4), 628–638.

Ni, J.-Q., Zhou, R., Czech, B., Liu, L.-P., Holderbaum, L., Yang-Zhou, D., Shim, H.-S., Tao, R., Handler, D., Karpowicz, P., Binari, R., Booker, M., Brennecke, J., Perkins, L. A., Hannon, G. J., & Perrimon, N. (2011). A genome-scale shRNA resource for transgenic RNAi in *Drosophila* . *Nature Methods*, *8*(5), 405–407.

Nishimura, T., & Takeichi, M. (2008). Shroom3-mediated recruitment of Rho kinases to the apical cell junctions regulates epithelial and neuroepithelial planar remodeling. *Development (Cambridge, England)*, *135*(8), 1493–1502.

Noatynska, A., Tavernier, N., Gotta, M., & Pintard, L. (2013). Coordinating cell polarity and cell cycle progression: what can we learn from flies and worms? *Open Biology*, *3*(8), 130083–130083.

Noordermeer, J., Johnston, P., Rijsewijk, F., Nusse, R., & Lawrence, P. A. (1992). The consequences of ubiquitous expression of the wingless gene in the*Drosophila* embryo. *Development (Cambridge, England)*, *116*(3), 711–719.

Nüsslein-Volhard, C. (1996). The Identification of Genes Controlling Development in Flies and Fishes (Nobel Lecture). *Angewandte Chemie International Edition*, *35*(19), 2176–2187.

Nüsslein-Volhard, C., Frohnhöfer, H. G., & Lehmann, R. (1987). Determination of anteroposterior polarity in *Drosophila* . *Science*, *238*(4834), 1675–1681.

Nüsslein-Volhard, C., & Wieschaus, E. F. (1980). Mutations affecting segment number and polarity in *Drosophila* . *Nature*, *287*(5785), 795–801.

Nüsslein-Volhard, C., Wieschaus, E. F., & Kluding, H. (1984). Mutations affecting the pattern of the larval cuticle in *Drosophila melanogaster*. *Wilhelm Roux's archives of developmental biology*, *193*(5), 267–282.

Obholzer, N., Swinburne, I. A., Schwab, E., Nechiporuk, A. V., Nicolson, T., & Megason, S. G. (2012). Rapid positional cloning of zebrafish mutations by linkage and homozygosity mapping using whole-genome sequencing. *Development (Cambridge, England)*, *139*(22), 4280–4290.

Oda, H., & Tsukita, S. (2001). Real-time imaging of cell-cell adherens junctions reveals that*Drosophila* mesoderm invagination begins with two phases of apical constriction of cells. *Journal of Cell Science*, *114*(Pt 3), 493–501.

O'Keefe, L., Dougan, S. T., Gabay, L., Raz, E., Shilo, B. Z., & DiNardo, S. (1997). Spitz and Wingless, emanating from distinct borders, cooperate to establish cell fate across the Engrailed domain in the*Drosophila* epidermis. *Development (Cambridge, England)*, *124*(23), 4837–4845.

Palazzo, A. F., Cook, T. A., Alberts, A. S., & Gundersen, G. G. (2001). mDia mediates Rho-regulated formation and orientation of stable microtubules. *Nature Cell Biology*, *3*(8), 723–729.

Pandey, U. B., & Nichols, C. D. (2011). Human disease models in *Drosophila melanogaster* and the role of the fly in therapeutic drug discovery. *Pharmacological Reviews*, *63*(2), 411–436.

Parker, J. (2006). Control of Compartment Size by an EGF Ligand from Neighboring Cells. *Current Biology*, *16*(20), 2058–2065.

Parks, A. L., Cook, K. R., Belvin, M., Dompe, N. A., Fawcett, R., Huppert, K., Tan, L. R., Winter, C. G., Bogart, K. P., Deal, J. E., Deal-Herr, M. E., Grant, D., Marcinko, M., Miyazaki, W. Y., Robertson, S., Shaw, K. J., Tabios, M., Vysotskaia, V., Zhao, L., Andrade, R. S., Edgar, K. A., Howie, E., Killpack, K., Milash, B., Norton, A., Thao, D., Whittaker, K., Winner, M. A., Friedman, L., Margolis, J., Singer, M. A., Kopczynski, C., Curtis, D., Kaufman, T. C., Plowman, G. D., Duyk, G., & Francis-Lang, H. L. (2004). Systematic generation of high-resolution deletion coverage of the *Drosophila melanogaster* genome. *Nature Genetics*, *36*(3), 288–292.

Pasic, L., Kotova, T., & Schafer, D. A. (2008). Ena/VASP proteins capture actin filament barbed ends. *The Journal of biological chemistry*, *283*(15), 9814–9819.

Pastink, A., Heemskerk, E., Nivard, M. J. M., van Vliet, C. J., & Vogel, E. W. (1991). Mutational specificity of ethyl methanesulfonate in excision-repair-proficient and -deficient strains of *Drosophila melanogaster*. *Molecular & general genetics : MGG*, *229*(2), 213–218.

Payre, F. F. (2004). Genetic control of epidermis differentiation in *Drosophila* . *The International journal of developmental biology*, *48*(2-3), 207–215.

Payre, F. F., Vincent, A., & Carreno, S. (1999). ovo/svb integrates Wingless and DER pathways to control epidermis differentiation. *Nature*, *400*(6741), 271–275.

Peng, Y., Clark, K. J., Campbell, J. M., Panetta, M. R., Guo, Y., & Ekker, S. C. (2014). Making designer mutants in model organisms. *Development (Cambridge, England)*, *141*(21), 4042–4054.

Perkins, L. A., Holderbaum, L., Tao, R., Hu, Y., Sopko, R., McCall, K., Yang-Zhou, D., Flockhart, I., Binari, R., Shim, H.-S., Miller, A., Housden, A., Foos, M., Randkelv, S., Kelley, C., Namgyal, P., Villalta, C., Liu, L.-P., Jiang, X., Huan-Huan, Q., Wang, X., Fujiyama, A., Toyoda, A., Ayers, K., Blum, A., Czech, B., Neumuller, R., Yan, D., Cavallaro, A., Hibbard, K., Hall, D., Cooley, L., Hannon, G. J., Lehmann, R., Parks, A., Mohr, S. E., Ueda, R., Kondo, S., Ni, J.-Q., & Perrimon, N. (2015). The Transgenic RNAi Project at Harvard Medical School: Resources and Validation. *Genetics*, *201*(3), 843–852.

Perrimon, N. (1984). Clonal Analysis of Dominant Female-Sterile, Germline-Dependent Mutations in DROSOPHILA MELANOGASTER. *Genetics*, *108*(4), 927–939.

Perrimon, N., Engstrom, L., & Mahowald, A. P. (1989). Zygotic lethals with specific maternal effect phenotypes in *Drosophila melanogaster*. I. Loci on the X chromosome. *Genetics*, *121*(2), 333–352.

Perrimon, N., Lanjuin, A., Arnold, C., & Noll, E. (1996). Zygotic lethal mutations with maternal effect phenotypes in *Drosophila melanogaster*. II. Loci on the second and third chromosomes identified by P-element-induced mutations. *Genetics*, *144*(4), 1681–1692.

Perrimon, N., Mohler, D., Engstrom, L., & Mahowald, A. P. (1986). X-linked female-sterile loci in *Drosophila melanogaster*. *Genetics*, *113*(3), 695–712.

Port, F., Chen, H.-M., Lee, T., & Bullock, S. L. (2014). Optimized CRISPR/Cas tools for efficient germline and somatic genome engineering in *Drosophila* . *Proceedings of the National Academy of Sciences of the USA*, *111*(29), E2967–E2976.

Price, M. H., Roberts, D. M., McCartney, B. M., Jezuit, E., & Peifer, M. (2006). Cytoskeletal dynamics and cell signaling during planar polarity establishment in the*Drosophila* embryonic denticle. *Journal of Cell Science*, *119*(Pt 3), 403–415.

Rafelski, S. M., & Marshall, W. F. (2008). Building the cell: design principles of cellular architecture. *Nature Reviews Molecular Cell Biology*, *9*(8), 593–602.

Rafelski, S. M., Viana, M. P., Zhang, Y., Chan, Y.-H. M., Thorn, K. S., Yam, P., Fung, J. C., Li, H., da F Costa, L., & Marshall, W. F. (2012). Mitochondrial Network Size Scaling in Budding Yeast. *Science*, *338*(6108), 822–824.

Rauzi, M. M., Lenne, P.-F., & Lecuit, T. (2010). Planar polarized actomyosin contractile flows control epithelial junction remodelling. *Nature*, *468*(7327), 1110–1114.

Razzell, W., Wood, W., & Martin, P. P. (2011). Swatting flies: modelling wound healing and inflammation in *Drosophila* . *Disease Models & Mechanisms*, *4*(5), 569–574.

Reber, S. B., Baumgart, J., Widlund, P. O., Pozniakovsky, A., Howard, J., Hyman, A. A., & Jülicher, F. (2013). XMAP215 activity sets spindle length by controlling the total mass of spindle microtubules. *Nature Cell Biology*, *15*(9), 1116–1122.

Reber, S. B., & Goehring, N. W. (2015). Intracellular Scaling Mechanisms. *Cold Spring Harbor Perspectives in Biology*, *7*(12), a019067.

Reinsch, S., & Gönczy, P. (1998). Mechanisms of nuclear positioning. *Journal of Cell Science*, *111 (Pt 16)*, 2283–2295.

Reiter, L. T., Potocki, L., Chien, S., Gribskov, M., & Bier, E. (2001). A systematic analysis of human disease-associated gene sequences in *Drosophila melanogaster*. *Genome Research*, *11*(6), 1114–1125.

Ren, N., He, B., Stone, D., Kirakodu, S., & Adler, P. N. (2006). The shavenoid gene of*Drosophila* encodes a novel actin cytoskeleton interacting protein that promotes wing hair morphogenesis. *Genetics*, *172*(3), 1643–1653.

Repiso, A., Saavedra, P., Casal, J., & Lawrence, P. A. (2010). Planar cell polarity: the orientation of larval denticles in*Drosophila* appears to depend on gradients of Dachsous and Fat. *Development (Cambridge, England)*, *137*(20), 3411–3415.

Revenu, C., Athman, R., Robine, S., & Louvard, D. (2004). The co-workers of actin filaments: from cell structures to signals. *Nature Reviews Molecular Cell Biology*, *5*(8), 635–646.

Roch, F. (2003). Drosophila miniature and dusky encode ZP proteins required for cytoskeletal reorganisation during wing morphogenesis. *Journal of Cell Science*, *116*(7), 1199–1207.

Roper, K. (2002). The 'Spectraplakins': cytoskeletal giants with characteristics of both spectrin and plakin families. *Journal of Cell Science*, *115*(22), 4215–4225.

Röper, K., & Brown, N. H. (2004). A Spectraplakin Is Enriched on the Fusome and Organizes Microtubules during Oocyte Specification in *Drosophila* . *Current Biology*, *14*(2), 99–110.

Rosin-Arbesfeld, R., Ihrke, G., & Bienz, M. (2001). Actin-dependent membrane association of the APC tumour suppressor in polarized mammalian epithelial cells. *The EMBO Journal*, *20*(21), 5929–5939.

Rubin, G. M., & Lewis, E. B. (2000). A brief history of *Drosophila* 's contributions to genome research. *Science*, *287*(5461), 2216–2218.

Rubin, G. M., Yandell, M. D., Wortman, J. R., Gabor Miklos, G. L., Nelson, C. R., Hariharan, I. K., Fortini, M. E., Li, P. W., Apweiler, R., Fleischmann, W., Cherry, J. M., Henikoff, S., Skupski, M. P., Misra, S., Ashburner, M., Birney, E., Boguski, M. S., Brody, T., Brokstein, P., Celniker, S. E., Chervitz, S. A., Coates, D., Cravchik, A., Gabrielian, A., Galle, R. F., Gelbart, W. M., George, R. A., Goldstein, L. S. B., Gong, F., Guan, P., Harris, N. L., Hay, B. A., Hoskins, R. A., Li, J., Li, Z., Hynes, R. O., Jones, S. J., Kuehl, P. M., Lemaitre, B., Littleton, J. T., Morrison, D. K., Mungall, C., O'Farrell, P. H., Pickeral, O. K., Shue, C., Vosshall, L. B., Zhang, J., Zhao, Q., Zheng, X. H., & Lewis, S. (2000). Comparative genomics of the eukaryotes. *Science*, *287*(5461), 2204–2215.

Ryder, E. (2004). The DrosDel Collection: A Set of P-Element Insertions for Generating Custom Chromosomal Aberrations in *Drosophila melanogaster*. *Genetics*, *167*(2), 797–813.

Rzadzinska, A. K., Schneider, M. E., Davies, C., Riordan, G. P., & Kachar, B. (2004). An actin molecular treadmill and myosins maintain stereocilia functional architecture and self-renewal. *The Journal of Cell Biology*, *164*(6), 887–897.

Saavedra, P., Brittle, A. L., Palacios, I. M., Strutt, D., Casal, J., & Lawrence, P. A. (2016). Planar cell polarity: the Dachsous/Fat system contributes differently to the embryonic and larval stages of *Drosophila* . *Biology open*, *5*(4), 397–408.

Saavedra, P., Vincent, J.-P., Palacios, I. M., Lawrence, P. A., & Casal, J. (2014). Plasticity of both planar cell polarity and cell identity during the development of *Drosophila* . *eLife*, *3*, 5689.

Sanson, B. (2001). Generating patterns from fields of cells. *EMBO reports*, *2*(12), 1083–1088.

Sanson, B., Alexandre, C., Fascetti, N., & Vincent, J.-P. (1999). Engrailed and Hedgehog Make the Range of Wingless Asymmetric in*Drosophila* Embryos. *Cell*, *98*(2), 207–216.

Sarin, S., Bertrand, V., Bigelow, H., Boyanov, A., Doitsidou, M., Poole, R. J., Narula, S., & Hobert, O. (2010). Analysis of multiple ethyl methanesulfonate-mutagenized *Caenorhabditis elegans* strains by whole-genome sequencing. *Genetics*, *185*(2), 417–430.

Sarin, S., Prabhu, S., O'Meara, M. M., Pe'er, I., & Hobert, O. (2008). *Caenorhabditis elegans* mutant allele identification by whole-genome sequencing. *Nature Methods*, *5*(10), 865–867.

Savage, D. F., Afonso, B., Chen, A. H., & Silver, P. A. (2010). Spatially Ordered Dynamics of the Bacterial Carbon Fixation Machinery. *Science*, *327*(5970), 1258–1261.

Schneider, C. A., Rasband, W. S., & Eliceiri, K. W. (2012). NIH Image to ImageJ: 25 years of image analysis. *Nature Methods*, *9*(7), 671–675.

Schnorrer, F., Ahlford, A., Chen, D., Milani, L., & Syvänen, A.-C. (2008). Positional cloning by fast-track SNP-mapping in *Drosophila melanogaster*. *Nature Protocols*, *3*(11), 1751–1765.

Schober, M., Schaefer, M., & Knoblich, J. A. (1999). Bazooka recruits Inscuteable to orient asymmetric cell divisions in*Drosophila* neuroblasts. *Nature*, *402*(6761), 548–551.

Schott, D., Ho, J., Pruyne, D., & Bretscher, A. (1999). The COOH-terminal domain of Myo2p, a yeast myosin V, has a direct role in secretory vesicle targeting. *The Journal of Cell Biology*, *147*(4), 791–808.

Schüpbach, T., & Wieschaus, E. F. (1986a). Germline autonomy of maternal-effect mutations altering the embryonic body pattern of *Drosophila* . *Developmental biology*, *113*(2), 443–448.

Schüpbach, T., & Wieschaus, E. F. (1986b). Maternal-effect mutations altering the anterior-posterior pattern of the*Drosophila* embryo. *Roux's Archives of Developmental Biology*, *195*(5), 302–317.

Schüpbach, T., & Wieschaus, E. F. (1989). Female sterile mutations on the second chromosome of *Drosophila melanogaster*. I. Maternal effect mutations. *Genetics*, *121*(1), 101–117.

Schwartz, S. L., Cao, C., Pylypenko, O., Rak, A., & Wandinger-Ness, A. (2007). Rab GTPases at a glance. *Journal of Cell Science*, *120*(Pt 22), 3905–3910.

Schweitzer, R., Shaharabany, M., Seger, R., & Shilo, B. Z. (1995). Secreted Spitz triggers the DER signaling pathway and is a limiting component in embryonic ventral ectoderm determination. *Genes & Development*, *9*(12), 1518–1529.

Segalen, M., Johnston, C. A., Martin, C. A., Dumortier, J. G., Prehoda, K. E., David, N. B., Doe, C. Q., & Bellaïche, Y. (2010). The Fz-Dsh Planar Cell Polarity Pathway Induces Oriented Cell Division via Mud/NuMA in*Drosophila* and Zebrafish. *Developmental Cell*, *19*(5), 740–752.

Semova, N., Kapanadze, B., Corcoran, M., Kutsenko, A., Baranova, A., & Semov, A. (2003). Molecular cloning, structural analysis, and expression of a human IRLB, MYC promoter-binding protein: new DENN domain-containing protein family emerges. *Genomics*, *82*(3), 343–354.

Sharp, D. J., McDonald, K. L., & Brown, H. M. (1999a). The bipolar kinesin, KLP61F, cross-links microtubules within interpolar microtubule bundles of*Drosophila* embryonic mitotic spindles. *The Journal of cell . . . .*

Sharp, D. J., Yu, K. R., Sisson, J. C., Sullivan, W., & Scholey, J. M. (1999b). Antagonistic microtubule-sliding motors position mitotic centrosomes in*Drosophila* early embryos. *Nature Cell Biology*, *1*(1), 51–54.

Shaw, S. L., Yeh, E., Maddox, P. S., Salmon, E. D., & Bloom, K. (1997). Astral microtubule dynamics in yeast: a microtubule-based searching mechanism for spindle orientation and nuclear migration into the bud. *The Journal of Cell Biology*, *139*(4), 985–994.

Shirasu-Hiza, M., Perlman, Z. E., Wittmann, T., Karsenti, E., & Mitchison, T. J. (2004). Eg5 Causes Elongation of Meiotic Spindles When Flux-Associated Microtubule Depolymerization Is Blocked. *Current Biology*, *14*(21), 1941–1945.

Siegrist, S. E., & Doe, C. Q. (2005). Microtubule-induced Pins/Galphai cortical polarity in*Drosophila* neuroblasts. *Cell*, *123*(7), 1323–1335.

Siller, K. H., Cabernard, C., & Doe, C. Q. (2006). The NuMA-related Mud protein binds Pins and regulates spindle orientation in*Drosophila* neuroblasts. *Nature Cell Biology*, *8*(6), 594–600.

Siller, K. H., & Doe, C. Q. (2009). Spindle orientation during asymmetric cell division. *Nature Cell Biology*, *11*(4), 365–374.

Siller, K. H., Serr, M., Steward, R., Hays, T. S., & Doe, C. Q. (2005). Live imaging of*Drosophila* brain neuroblasts reveals a role for Lis1/dynactin in spindle assembly and mitotic checkpoint control. *Molecular Biology of the Cell*, *16*(11), 5127–5140.

Simoes, S. d. M., Mainieri, A., & Zallen, J. A. (2014). Rho GTPase and Shroom direct planar polarized actomyosin contractility during convergent extension. *The Journal of Cell Biology*, *204*(4), 575–589.

Simone, R. P., & DiNardo, S. (2010). Actomyosin contractility and Discs large contribute to junctional conversion in guiding cell alignment within the*Drosophila* embryonic epithelium. *Development (Cambridge, England)*, *137*(8), 1385–1394.

Soares e Silva, M., Depken, M. M., Stuhrmann, B., Korsten, M. M., MacKintosh, F. C., & Koenderink, G. H. G. (2011). Active multistage coarsening of actin networks driven by myosin motors. *Proceedings of the National Academy of Sciences of the USA*, *108*(23), 9408–9413.

St Johnston, D. (2002). The art and design of genetic screens: *Drosophila melanogaster*. *Nature reviews Genetics*, *3*(3), 176–188.

Stenmark, H. (2009). Rab GTPases as coordinators of vesicle traffic. *Nature Reviews Molecular Cell Biology*, *10*(8), 513–525.

Strome, S., & Wood, W. B. (1983). Generation of asymmetry and segregation of germ-line granules in early *C. elegans* embryos. *Cell*, *35*(1), 15–25.

Strutt, D., & Warrington, S. J. (2008). Planar polarity genes in the*Drosophila* wing regulate the localisation of the FH3-domain protein Multiple Wing Hairs to control the site of hair production. *Development (Cambridge, England)*, *135*(18), 3103–3111.

Stumpff, J., von Dassow, G., Wagenbach, M., Asbury, C., & Wordeman, L. (2008). The kinesin-8 motor Kif18A suppresses kinetochore movements to control mitotic chromosome alignment. *Developmental Cell*, *14*(2), 252–262.

Subramanian, A., Prokop, A., Yamamoto, M., Sugimura, K., Uemura, T., Betschinger, J., Knoblich, J. A., & Volk, T. (2003). Shortstop Recruits EB1/APC1 and Promotes Microtubule Assembly at the Muscle-Tendon Junction. *Current Biology*, *13*(13), 1086–1095.

Subramanian, R., Ti, S.-C., Tan, L., Darst, S. A., & Kapoor, T. M. (2013). Marking and measuring single microtubules by PRC1 and kinesin-4. *Cell*, *154*(2), 377–390.

Szüts, D., Eresh, S., & Bienz, M. (1998). Functional intertwining of Dpp and EGFR signaling during*Drosophila* endoderm induction. *Genes & Development*, *12*(13), 2022–2035.

Szüts, D., Freeman, M., & Bienz, M. (1997). Antagonism between EGFR and Wingless signalling in the larval cuticle of *Drosophila* . *Development (Cambridge, England)*, *124*(16), 3209–3219.

Tabata, T., Eaton, S., & Kornberg, T. B. (1992). The*Drosophila* hedgehog gene is expressed specifically in posterior compartment cells and is a target of engrailed regulation. *Genes & Development*, *6*(12b), 2635–2645.

Tadros, W., & Lipshitz, H. D. (2005). Setting the stage for development: mRNA translation and stability during oocyte maturation and egg activation in *Drosophila* . *Developmental dynamics : an official publication of the American Association of Anatomists*, *232*(3), 593–608.

Tadros, W., & Lipshitz, H. D. (2009). The maternal-to-zygotic transition: a play in two acts. *Development (Cambridge, England)*, *136*(18), 3033–3042.

Taylor, A. B. (2006). Dendrites Contain a Spacing Pattern. *The Journal of neuroscience : the official journal of the Society for Neuroscience*, *26*(4), 1154–1163.

Thérond, P. P., Limbourg Bouchon, B., Gallet, A., Dussilol, F., Pietri, T., van den Heuvel, M., & Tricoire, H. (1999). Differential requirements of the fused kinase for hedgehog signalling in the*Drosophila* embryo. *Development (Cambridge, England)*, *126*(18), 4039–4051.

Thoresen, T., Lenz, M., & Gardel, M. L. (2011). Reconstitution of Contractile Actomyosin Bundles. *Biophysical journal*, *100*(11), 2698–2705.

Tilney, L. G. (1995). F actin bundles in*Drosophila* bristles. I. Two filament cross-links are involved in bundling. *The Journal of Cell Biology*, *130*(3), 629–638.

Tilney, L. G. (1996). F-actin bundles in*Drosophila* bristles are assembled from modules composed of short filaments. *The Journal of Cell Biology*, *135*(5), 1291–1308.

Tilney, L. G., Connelly, P. S., Vranich, K. A., Shaw, M. K., & Guild, G. M. (1998). Why Are Two Different Cross-linkers Necessary for Actin Bundle Formation In Vivo and What Does Each Cross-link Contribute? *The Journal of Cell Biology*, *143*(1), 121–133.

Tomizawa, J., & Itoh, T. (1981). Plasmid ColE1 incompatibility determined by interaction of RNA I with primer transcript. *Proceedings of the National Academy of Sciences of the USA*, *78*(10), 6096–6100.

Tran, P. T., Marsh, L., Doye, V., Inoué, S., & Chang, F. (2001). A mechanism for nuclear positioning in fission yeast based on microtubule pushing. *The Journal of Cell Biology*, *153*(2), 397–411.

Truebestein, L., Elsner, D. J., Fuchs, E., & Leonard, T. A. (2015). A molecular ruler regulates cytoskeletal remodelling by the Rho kinases. *Nature Communications*, *6*, 10029–10029.

Tsruya, R., Schlesinger, A., Reich, A., Gabay, L., Sapir, A., & Shilo, B.-Z. (2002). Intracellular trafficking by Star regulates cleavage of the*Drosophila* EGF receptor ligand Spitz. *Genes & Development*, *16*(2), 222–234.

Tsruya, R., Wojtalla, A., Carmon, S., Yogev, S., Reich, A., Bibi, E., Merdes, G., Schejter, E., & Shilo, B.-Z. (2007). Rhomboid cleaves Star to regulate the levels of secreted Spitz. *The EMBO Journal*, *26*(5), 1211–1220.

Turner, C. M., & Adler, P. N. (1998). Distinct roles for the actin and microtubule cytoskeletons in the morphogenesis of epidermal hairs during wing development in *Drosophila* . *Mechanisms of development*, *70*(1-2), 181–192.

Tyler, D. M., & Baker, N. E. (2007). Expanded and fat regulate growth and differentiation in the*Drosophila* eye through multiple signaling pathways. *Developmental biology*, *305*(1), 187–201.

Tyska, M. J., & Mooseker, M. S. (2002). MYO1A (brush border myosin I) dynamics in the brush border of LLC-PK1-CL4 cells. *Biophysical journal*, *82*(4), 1869–1883.

Uv, A. E., & Moussian, B. B. (2010). The apical plasma membrane of*Drosophila* embryonic epithelia. *European Journal of Cell Biology*, *89*(2-3), 208–211.

Varga, V., Helenius, J., Tanaka, K., Hyman, A. A., Tanaka, T. U., & Howard, J. (2006). Yeast kinesin-8 depolymerizes microtubules in a length-dependent manner. *Nature Cell Biology*, *8*(9), 957–962.

Varga, V., Leduc, C., Bormuth, V., Diez, S., & Howard, J. (2009). Kinesin-8 motors act cooperatively to mediate length-dependent microtubule depolymerization. *Cell*, *138*(6), 1174–1183.

Venken, K. J. T., He, Y., Hoskins, R. A., & Bellen, H. J. (2006). P[acman]: A BAC Transgenic Platform for Targeted Insertion of Large DNA Fragments in D. melanogaster. *Science*, *314*(5806), 1747–1751.

Venken, K. J. T., Popodi, E., Holtzman, S. L., Schulze, K. L., Park, S., Carlson, J. W., Hoskins, R. A., Bellen, H. J., & Kaufman, T. C. (2010). A Molecularly Defined Duplication Set for the X Chromosome of *Drosophila melanogaster*. *Genetics*, *186*(4), 1111–1125.

Vichas, A., Laurie, M. T., & Zallen, J. A. (2015). The Ski2-family helicase Obelus regulates Crumbs alternative splicing and cell polarity. *The Journal of Cell Biology*, *211*(5), 1011–1024.

Wallingford, J. B., & Mitchell, B. J. (2011). Strange as it may seem: the many links between Wnt signaling, planar cell polarity, and cilia. *Genes & Development*, *25*(3), 201–213.

Walter, H., & Brooks, D. E. (1995). Phase separation in cytoplasm, due to macromolecular crowding, is the basis for microcompartmentation. *FEBS letters*, *361*(2-3), 135–139.

Walters, J. W., Dilks, S. A., & DiNardo, S. (2006). Planar polarization of the denticle field in the*Drosophila* embryo: Roles for Myosin II (Zipper) and Fringe. *Developmental biology*, *297*(2), 323–339.

Walters, J. W., Muñoz, C., Paaby, A. B., & DiNardo, S. (2005). Serrate–Notch signaling defines the scope of the initial denticle field by modulating EGFR activation. *Developmental biology*, *286*(2), 415–426.

Wang, C., Li, S., Januschke, J., Rossi, F., Izumi, Y., Garcia-Alvarez, G., Gwee, S. S. L., Soon, S. B., Sidhu, H. K., Yu, F., Matsuzaki, F., Gonzalez, C., & Wang, H. (2011). An ana2/ctp/mud complex regulates spindle orientation in*Drosophila* neuroblasts. *Developmental Cell*, *21*(3), 520–533.

Wang, H., Brust-Mascher, I., & Scholey, J. M. (2015). The microtubule cross-linker Feo controls the midzone stability, motor composition, and elongation of the anaphase B spindle in*Drosophila* embryos. - PubMed - NCBI. *Molecular Biology of the Cell*, *26*(8), 1452–1462.

Webb, R. L., Zhou, M. N., & McCartney, B. M. (2009). A novel role for an APC2-Diaphanous complex in regulating actin organization in *Drosophila* . *Development (Cambridge, England)*, *136*(8), 1283–1293.

Weber, S. C., & Brangwynne, C. P. (2015). Inverse Size Scaling of the Nucleolus by a Concentration-Dependent Phase Transition. *Current Biology*, *25*(5), 641–646.

Wee, B., Johnston, C. A., Prehoda, K. E., & Doe, C. Q. (2011). Canoe binds RanGTP to promote Pins TPR/Mud-mediated spindle orientation. *The Journal of Cell Biology*, *195*(3), 369–376.

Wiellette, E. L., & McGinnis, W. (1999). Hox genes differentially regulate Serrate to generate segment-specific structures. *Development (Cambridge, England)*, *126*(9), 1985–1995.

Wieschaus, E. F. (1996a). Embryonic transcription and the control of developmental pathways. *Genetics*, *142*(1), 5–10.

Wieschaus, E. F. (1996b). From molecular patterns to morphogenesis—the lessons from studies on the fruit fly*Drosophila* (Nobel lecture). *Angewandte Chemie International Edition in . . .*, *35*(19), 2188–2194.

Wieschaus, E. F., & Nüsslein-Volhard, C. (2016). The Heidelberg Screen for Pattern Mutants of *Drosophila* : A Personal Account. *Annual review of cell and developmental biology*, *32*(1), annurev–cellbio–113015–023138.

Wieschaus, E. F., Nüsslein-Volhard, C., & Jürgens, G. (1984). Mutations affecting the pattern of the larval cuticle in *Drosophila melanogaster*. *Wilhelm Roux's archives of developmental biology*, *193*(5), 296–307.

Winkelman, J. D., Bilancia, C. G., Peifer, M., & Kovar, D. R. (2014). Ena/VASP Enabled is a highly processive actin polymerase tailored to self-assemble parallel-bundled F-actin networks with Fascin. - PubMed - NCBI. *Proceedings of the National Academy of Sciences of the USA*, *111*(11), 4121–4126.

Winslow, G. M., Carroll, S. B., & Scott, M. P. (1988). Maternal-effect genes that alter the fate map of the*Drosophila* blastoderm embryo. *Developmental biology*, *129*(1), 72–83.

Winter, C. G., Wang, B., Ballew, A., Royou, A., Karess, R., Axelrod, J. D., & Luo, L. (2001). Drosophila Rho-Associated Kinase (Drok) Links Frizzled-Mediated Planar Cell Polarity Signaling to the Actin Cytoskeleton. *Cell*, *105*(1), 81–91.

Wippich, F., Bodenmiller, B., Trajkovska, M. G., Wanka, S., Aebersold, R., & Pelkmans, L. (2013). Dual specificity kinase DYRK3 couples stress granule condensation/dissolution to mTORC1 signaling. *Cell*, *152*(4), 791–805.

Wodarz, A., & Näthke, I. (2007). Cell polarity in development and cancer. *Nature Cell Biology*, *9*(9), 1016–1024.

Wodarz, A., Ramrath, A., Kuchinke, U., & Knust, E. (1999). Bazooka provides an apical cue for Inscuteable localization in*Drosophila* neuroblasts. *Nature*, *402*(6761), 544–547.

Wong, L. L., & Adler, P. N. (1993). Tissue polarity genes of*Drosophila* regulate the subcellular location for prehair initiation in pupal wing cells. *The Journal of Cell Biology*, *123*(1), 209–221.

Wühr, M., Chen, Y., Dumont, S., Groen, A. C., Needleman, D. J., Salic, A., & Mitchison, T. J. (2008). Evidence for an Upper Limit to Mitotic Spindle Length. *Current Biology*, *18*(16), 1256–1261.

Wühr, M., Dumont, S., Groen, A. C., Needleman, D. J., & Mitchison, T. J. (2014). How does a millimeter-sized cell find its center? *Cell cycle (Georgetown, Tex.)*, *8*(8), 1115–1121.

Wühr, M., Tan, E. S., Parker, S. K., Detrich, H. W., & Mitchison, T. J. (2010). A model for cleavage plane determination in early amphibian and fish embryos. *Current Biology*, *20*(22), 2040–2045.

Xiong, B., Bayat, V., Jaiswal, M., Zhang, K., Sandoval, H., Charng, W.-L., Li, T., David, G., Duraine, L., Lin, Y.-Q., Neely, G. G., Yamamoto, S., & Bellen, H. J. (2012). Crag Is a GEF for Rab11 Required for Rhodopsin Trafficking and Maintenance of Adult Photoreceptor Cells. *PLoS biology*, *10*(12), e1001438.

Xu, K., Zhong, G., & Zhuang, X. (2013). Actin, spectrin, and associated proteins form a periodic cytoskeletal structure in axons. *Science*, *339*(6118), 452–456.

Xu, X. Z. S., Wes, P. D., Chen, H., Li, H. S., Yu, M. H., Morgan, S., Liu, Y., & Montell, C. (1998). Retinal Targets for Calmodulin Include Proteins Implicated in Synaptic Transmission. *The Journal of biological chemistry*, *273*(47), 31297–31307.

Yamamoto, S., Charng, W. L., Rana, N. A., Kakuda, S., Jaiswal, M., Bayat, V., Xiong, B., Zhang, K., Sandoval, H., David, G., Wang, H., Haltiwanger, R. S., & Bellen, H. J. (2012). A Mutation in EGF Repeat-8 of Notch Discriminates Between Serrate/Jagged and Delta Family Ligands. *Science*, *338*(6111), 1229–1232.

Yamamoto, S., Jaiswal, M., Charng, W.-L., Gambin, T., Karaca, E., Mirzaa, G., Wiszniewski, W., Sandoval, H., Haelterman, N. A., Xiong, B., Zhang, K., Bayat, V., David, G., Li, T., Chen, K., Gala, U., Harel, T., Pehlivan, D., Penney, S., Vissers, L. E. L. M., de Ligt, J., Jhangiani, S. N., Xie, Y., Tsang, S. H., Parman, Y., Sivaci, M., Battaloglu, E., Muzny, D., Wan, Y.-W., Liu, Z., Lin-Moore, A. T., Clark, R. D., Curry, C. J., Link, N., Schulze, K. L., Boerwinkle, E., Dobyns, W. B., Allikmets, R., Gibbs, R. A., Chen, R., Lupski, J. R., Wangler, M. F., & Bellen, H. J. (2014). A*Drosophila* Genetic Resource of Mutants to Study Mechanisms Underlying Human Genetic Diseases. *Cell*, *159*(1), 200–214.

Yan, J., Huen, D., Morely, T., Johnson, G., Gubb, D., Roote, J., & Adler, P. N. (2008). The multiple-wing-hairs Gene Encodes a Novel GBD-FH3 Domain-Containing Protein That Functions Both Prior to and After Wing Hair Initiation. *Genetics*, *180*(1), 219–228.

Yang, C., & Svitkina, T. (2011). Filopodia initiation: focus on the Arp2/3 complex and formins. *Cell adhesion & migration*, *5*(5), 402–408.

Yang, C.-F., Tsai, W.-Y., Chen, W.-A., Liang, K.-W., Pan, C.-J., Lai, P.-L., Yang, P.-C., & Huang, H.-C. (2016). Kinesin-5 Contributes to Spindle-length Scaling in the Evolution of Cancer toward Metastasis. *Scientific Reports*, *6*, 35767.

Yasuda, G. K., Schubiger, G., & Wakimoto, B. T. (1995). Genetic characterization of ms (3) K81, a paternal effect gene of *Drosophila melanogaster*. *Genetics*, *140*(1), 219–229.

Yu, F., Morin, X., Cai, Y., Yang, X., & Chia, W. (2000). Analysis of partner of inscuteable, a novel player of*Drosophila* asymmetric divisions, reveals two distinct steps in inscuteable apical localization. *Cell*, *100*(4), 399–409.

Yu, J. X., Guan, Z., & Nash, H. A. (2006). The mushroom body defect gene product is an essential component of the meiosis II spindle apparatus in*Drosophila* oocytes. *Genetics*, *173*(1), 243–253.

Zallen, J. A. (2007). Planar Polarity and Tissue Morphogenesis. *Cell*, *129*(6), 1051–1063.

Zallen, J. A., & Wieschaus, E. F. (2004). Patterned Gene Expression Directs Bipolar Planar Polarity in *Drosophila* . *Developmental Cell*, *6*(3), 343–355.

Zhai, R. G., Hiesinger, P. R., Koh, T. W., Verstreken, P., Schulze, K. L., Cao, Y., Jafar-Nejad, H., Norga, K. K., Pan, H., Bayat, V., Greenbaum, M. P., & Bellen, H. J. (2011). Mapping*Drosophila* mutations with molecularly defined P element insertions. *Proceedings of the National Academy of Sciences of the USA*, *100*(19), 10860–10865.

Zhao, T., Graham, O. S., Raposo, A., & St Johnston, D. (2012). Growing microtubules push the oocyte nucleus to polarize the*Drosophila* dorsal-ventral axis. *Science*, *336*(6084), 999–1003.

Zink, D., Fischer, A. H., & Nickerson, J. A. (2004). Nuclear structure in cancer cells. *Nature reviews Cancer*, *4*(9), 677–687.